Advancing sustainable gravel road construction through innovative nano-emulsion treatment of a micaceous gravel

by

Nathan Ntanda Chilukwa

(220018011)

Thesis submitted in fulfilment of the requirements for the degree of

Doctor of Philosophy (Civil Engineering)

College of Agriculture, Engineering and Science

School of Engineering

Durban

Supervisor

Prof MMH Mostafa

2024

Supervisor Agreement:

As the candidate's Supervisor, I agree to the submission of this thesis.

Signed: [redacted]

Prof MMH Mostafa

DECLARATION 1 - PLAGIARISM

Candidate:

I, Chilukwa Nathan Ntanda, declare that

1. The research reported in this thesis, except where otherwise indicated, is my original research.

2. This thesis has not been submitted for any degree or examination at any other university.

3. This thesis does not contain other persons' data, pictures, graphs or other information, unless specifically acknowledged as being sourced from other persons.

4. This thesis does not contain other persons' writing, unless specifically acknowledged as being sourced from other researchers. Where other written sources have been quoted, then:
   a. Their words have been re-written but the general information attributed to them has been referenced
   b. Where their exact words have been used, then their writing has been placed in italics and inside quotation marks, and referenced.

5. This thesis does not contain text, graphics or tables copied and pasted from the Internet, unless specifically acknowledged, and the source being detailed in the thesis and in the References sections.

Signed: 

DECLARATION 2 - PUBLICATIONS

DETAILS OF CONTRIBUTION TO PUBLICATIONS that form part and/or include research presented in this thesis (including publications in preparation, submitted, *in press* and published)

Publication 1: Chilukwa, N. N., & Mostafa, M. M. H. (2024). An investigation of the efficacy of nanoemulsions as alternative treatment for a marginal quality pavement material. Road Materials and Pavement Design, 1–14. https://doi.org/10.1080/14680629.2023.2297717

Publication 2: S. Okem, E., N. Chilukwa, N., & M.H. Mostafa, M. (2024). Strengthening Substandard Road Materials with Nanoemulsion-Based Stabilisation: An Experimental Study. IntechOpen. doi: 10.5772/intechopen.1004313

Publication 3: Chilukwa N.N. and Mostafa M.M.H. 2023. Investigating the behavioural properties and characteristics of nano-emulsion stabilised gravel material for use in constructing structural layers of road pavements. [Under Review]

Publication 4: Chilukwa N.N. and Mostafa M.M.H. 2023. Pavement modelling and structure analysis of a gravel road incorporating Nano Modified Emulsion Stabilised Materials (NMESMs). [Under Preparation]

Signed:

ACKNOWLEDGEMENTS

This has been a long and arduous journey beginning at the peak of the covid pandemic and navigating through all its offshoots. It is only through the support received from various persons and institutions that this work has come to fruition. Be it through resources or just a word of encouragement, I wish to express my gratitude to everyone that supported this work, some of whom I may not be able to mention.

Firstly, thanks to God Almighty for keeping me healthy and sane, and giving me the strength I needed to get to the finish line. I would also like to thank the under listed;

- My supervisor, Prof Mostafa, for the support, guidance and mentorship,
- My employers, Copperbelt University, for sponsorship,
- Johann McLeod and John Young from Soilform, Martin Murphy from Ge-nano and Chris Harburn from Giba Gorge for material provision and technical assistance,
- Wynand van Niekerk from BSM laboratories for assistance with material testing,
- All the technical and administrative staff at UKZN, including Ishaan, Ooma, Sjah and Logon for all the support and assistance rendered,
- Family, for the support and encouragement,
- Friends and other colleagues, for the interactions, support and encouragement.

ABSTRACT

Materials used for road construction play a critical role in the performance of the pavement structure. Winning and haulage of virgin materials have been highlighted as factors that contribute significantly to the increased construction cost and environmental degradation. In the quest to achieve sustainability, it has been recognised that functionalising locally available materials is one of the ways of tackling the challenge highlighted above. Such materials are enhanced through stabilisation traditionally using products such as cement and lime. However, these (cement and lime) have limitations and various products have been developed and marketed as viable alternatives for material enhancement.

This study evaluated the efficacy of Nano-Modified Emulsion (NME), a relatively new product, for stabilisation of gravel materials, particularly for use as a gravel road-wearing course. NME comprises of Conventional Bitumen Emulsion (CBE) modified with an organofunctional nanosilane. Therefore, the product (NME) draws on the properties of nanotechnology to functionalise and improve properties of materials traditionally considered of marginal quality. Previous studies show that this product has great potential in this regard. However, it is recognised that current knowledge of the product is limited and further research is required on the fundamental properties and behavioural traits of NME stabilised materials (NMESMs) to streamline concepts, understanding, leading to the development of design guidelines of the materials.

A marginal quality micaceous gravel material was chosen as a suitable candidate to demonstrate the efficacy of the NME. The material, stabilised with varying NME applications from 0.7% to 1.5%, was evaluated for various engineering properties, including mechanical strength, stiffness and deformation characteristics. Results of tests for mechanical strengths conducted through California Bearing Ratio (CBR), Unconfined Compressive Strength (UCS), Indirect Tensile Strength (ITS) and Static Triaxial Tests (STT) showed improved material properties by more than 70%. It was observed that minimal applications of NME are required to achieve specified strengths and that increasing the application dosage does not significantly improve material strength. The NME is also shown to impart hydrophobic properties on the gravel material such that increased applications of NME increase the gravel's resistance to moisture damage as determined by the Moisture-Induced Damage Ratio (MDR).

The STT results demonstrate that the NME improves the shear strength of materials by increasing the cohesion parameter by up to 54% while the angle of friction remains virtually unchanged. The resilient modulus of NMESMs exhibits a combination of stress-dependent and -independent behaviour and it was determined that the parabolic model suitably represents this behaviour. Results of plastic strain tests also show that NMESMs provide better performance with regard to resisting deformation.

Modelling and pavement structure analysis was implemented using a Finite Element (FE) based software, ANSYS 2022 R2. This was done to simulate the performance of the material in an actual pavement structure. It was determined that incorporating a NMESM layer as a wearing course on a gravel road pavement structure improves pavement responses to loading i.e. strain and deflection by up to 14% and 28%, respectively. The use of NMESM also reduces the thickness of the layer, resulting in a saving on materials.

Additional studies are recommended for Life-Cycle Cost Analysis (LCCA) to help in quantifying cost-benefit ratios of implementing NMEs in industry.

TABLE OF CONTENTS

TABLE OF TABLES

TABLE OF FIGURES

ABBREVIATIONS AND ACRONYMS

BSM – Bitumen Stabilised Materials

CBE - Conventional Bitumen Emulsion

CBR - California Bearing Ratio

CSIR – Council of Scientific and Industrial Research

DCP-DN - Laboratory Dynamic Cone Penetration

DSR – Deviator Stress Ratio

GM – Grading Modulus

ITS – Indirect Tensile Strength

LS – Linear Shrinkage

LVR – Low Volume Roads

MDD – Maximum Dry Density

MDR – Moisture Induced Damage Ratio

M_R - Resilient Modulus

NDPS - NME Draft Project Specifications

NME - Nano Modified Emulsion

NMESM - Nano Modified Emulsion Stabilised Materials

OMC – Optimum Moisture Content

PD - Permanent Deformation

PSD - Particle Size Distribution

RDm = Maximum Theoretical Relative Density

RDv = Bulk Relative Density

RCS – Retained Compressive Strength

RLT (RLTT) - Repeated Load Triaxial (RLT) tests

RTS – Retained Tensile Strength

SA - South Africa

SANRAL - South African National Roads Agency Limited

SDG – Sustainable Development Goals

SEM – Scanning Electron Microscopy

SR – Stress Ratio

STT - Static Triaxial Tests

TD – Treated Dry

TW – Treated Wet

UCS – Unconfined Compressive Strength

UT - Untreated

XRD – X-Ray Diffraction

ε_p - Plastic strain

μ – Poisson's ratio

1 INTRODUCTION

1.1 Background

The South African (SA) Government recognises transport as one of five main priority areas for socio-economic development. The vision of the Government is for a transport system that “provides safe, reliable, effective, efficient and fully integrated transport operations and infrastructure which best meets the needs of freight and passenger customers at improving levels of service and cost in a fashion which supports Government strategies for economic and social development whilst being environmentally and economically sustainable” (RSA, 1996). This vision also resonates with Sustainable Development Goal (SDG) number 11, which calls for sustainable cities and communities.

Roads are a crucial component of transport systems. A road provides a means of travel by some form of conveyance, e.g. vehicle, bicycle, ox-cart, or even on foot, to access important services. Fraissard (2012) describes roads as the wealth of nations, a tool for social inclusion, economic development and environmental sustainability. Chakwizira and Mashiri (2009) add that improved conditions of roads bring immediate benefits for communities through better access to basic amenities like hospitals, schools, and markets, greater comfort, speed, and safety and lower vehicle operating costs. Worldwide, there is a large dependence on road transport infrastructure.

In SA, more than 77% of land freight is hauled on its roads, accounting for 73.8% of total land freight income. Therefore, the condition of the roads directly affects the ease of movement of goods and people and is a basis for a thriving market and social environment (Transport, 2019). The SA Government needs help to meet the cost of road infrastructure development. South African National Roads Agency Limited (SANRAL) reports that financing to the road sector has been consistently lower than planned for the past few years as indicated in Figure 1-1. This has resulted in a substantial backlog for strengthening (rehabilitation) and expansion of roads.

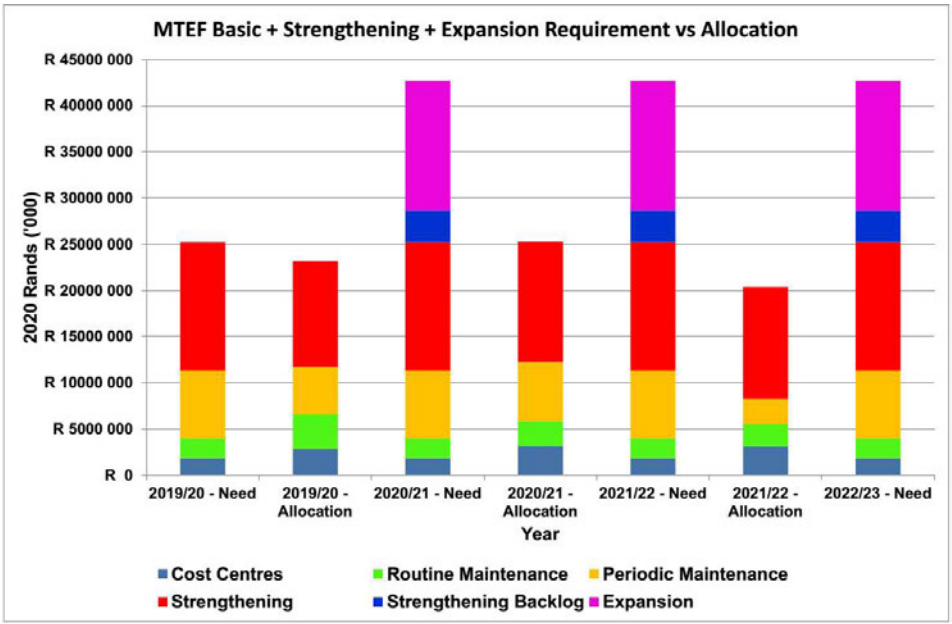

Figure 1-1: Road Financing (SANRAL, 2020)

1.2 Sustainability of the road sector

The long-term strategy for the road sector is anchored on ensuring sustainability in the provision of roads (SANRAL, 2020). Sustainability is premised on achieving intergenerational equity and is reflected in mainly three dimensions, i.e. the environmental, economic and social dimension. In the road sector, sustainability essentially entails meeting specific engineering requirements with the least amount of energy consumption, reduced greenhouse gas emissions, reduced pollution of air, water, land and noise, improved health, safety and risk prevention and ensuring a high level of user comfort (Maher et al. 2006; FHWA, 2014; SANRAL, 2020). Thus, so long as performance is not adversely affected, the key to successful implementation of sustainability best practices is to identify opportunities for reducing costs over the life cycle of the project through effective management of resources.

Materials is one such resource that is the subject of much interest and studies (Toole et al, 2018). Henderson and van Zyl (2017) illustrate the current strategies (Figure 1-2) to reduce the demand for virgin (standard) material and to extend the time to total depletion of materials. It is shown that standard materials have a short lifespan (in quantity terms) and that there is need to employ alternative strategies to reduce demand. Also, that reclaimed, non-standard and waste materials can meet demand over a longer period. Henning et al. (2008) affirm that non-standard and reclaimed

materials may be fit for purpose and function successfully in particular road environments despite not complying with strict material specifications.

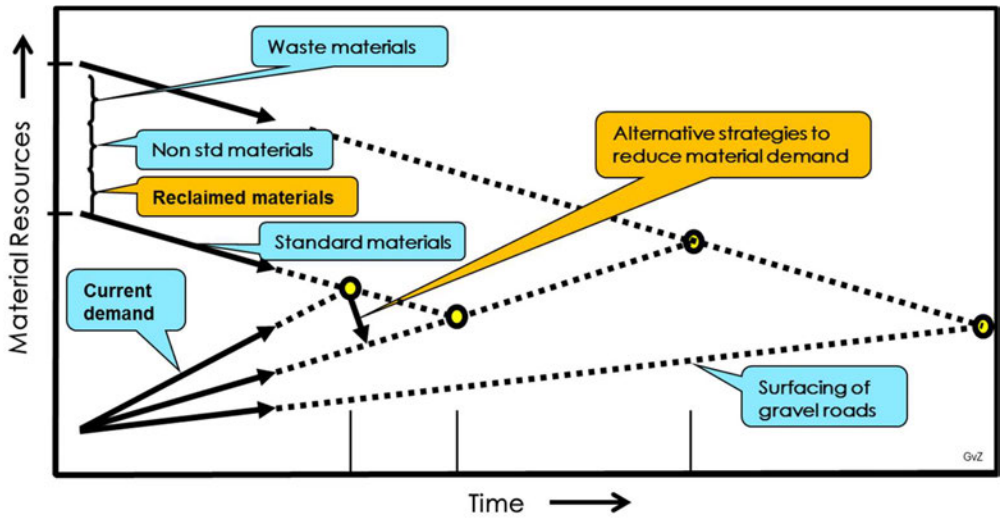

Figure 1-2: Strategies to extend the time towards depletion of materials (Henderson and van Zyl, 2017)

1.3 Gravel roads

Close to 80% of SA's 750, 000 km of road network is comprised of unsealed roads (DoT, 2023). This is an important class of roads and is not only prevalent in rural areas but forms a large proportion of the urban network, with some roads carrying up to 1,000 vehicles per day (vpd) (Paige-Green and Hongve, 2003). Many stakeholders have bemoaned the condition of these roads. According to Ross (cited by Obuseng, 2019), it is estimated that 77.5% of the unsealed road network in SA is in a poor to very poor condition and more than ZAR 500 billion is required for functional maintenance and technical needs to bring the infrastructure to acceptable standards.

The 2022 South African Institution of Civil Engineering (SAICE) infrastructure report card also gives a damning report on unsealed roads, stating that their condition is exposing the public to health and safety hazards and requires immediate action.

The highest class of unsealed roads, gravel roads, are the focus of this study. They (gravel roads) typically comprise a designed bound or unbound aggregate surface layer placed over the natural subgrade soil. Imported or native materials meeting Particle Size Distribution (PSD) requirements and plasticity are used to construct the surfacing to specified standards, to provide all-weather access.

Gravel roads are a viable option for road transport provision (and will continue to be so for the foreseeable future) due to the limited resource pocket of most countries. According to Ferry (1998) and Mwaipungu and Allopi (2014), gravel roads must coexist with sealed roads for intergenerational equity and the conservation of non-renewable resources used for constructing and maintaining sealed roads. In some cases, gravel roads are preferred over sealed roads for aesthetic reasons e.g., in rural communities, in the countryside, national parks and game reserves, as they fit better with the environment and ecosystems. Mwaipungu and Allopi (2014) outline additional advantages of gravel roads including lower construction and maintenance costs, ease of maintenance, and less equipment and labour requirements. They are frequently constructed using locally available natural materials, which lessens their impact on global warming. Less waste is generated during construction and subsequent maintenance activities than sealed roads and because traffic speeds are often lower, they are comparatively safer.

Gravel roads deteriorate relatively quickly compared to paved roads. Moloisane and Visser (2014) identify poor riding quality, impassability in wet weather and traffic safety concerns resulting from dust emissions as common problems with gravel roads. The authors explain that all gravel roads, when dry, suffer from surface abrasion resulting in loss of material because the adhesion between the particles is reduced. Material (gravel) loss is, arguably, the most important factor with regard to gravel roads. The loss of gravel surface material leads to the loss of shape and the formation of other defects including ruts, corrugations (washboards) and potholes (van Wijk et al., 2019). Subsequently water collects on the surface and this decreases the natural durability and strength properties of the road system, making the road uncomfortable and dangerous to drive on.

Over 30 million cubic metres of gravel material is estimated to be lost annually from gravel roads in SA through dust, erosion and traffic (Ross and Field, 2007). Re-gravelling is the costliest maintenance operation for gravel roads, accounting for between 40% and 60% in some cases (Deepa et al., 2019; Henning et al., 2008; LRRB, 2005; Verhaenghe et al., 2010). Therefore, to ensure sustainability, the design and construction of gravel roads should aim to limit gravel loss. Henning et al. (2008) explain that limiting gravel loss can have significant benefits in lowering maintenance

costs and placing less demand on winning gravel, less surface ravelling, better ride qualities and improved road safety.

1.4 Innovative material treatment

Gravel loss can be reduced by, among other methods, selecting suitable material (Kassa, 2015; TRH20, 1990; van Zyl et al., 2007). However, such materials may not always be available near the construction site. Bennet et al. (2002), Henderson and van Zyl (2017) and Paige-Green and Hongve (2003) all highlight shortages of suitable gravel materials for road construction in various regions of SA. Various contributing factors have been advanced, including lack of cooperation by landowners, the need to avoid restricted areas containing endangered indigenous vegetation, nature reserves, national parks and high value agricultural areas, and poor underlying geology (Henderson and van Zyl, 2017). The alternative of hauling suitable materials from distant areas contributes significantly to the high cost of road construction. Gourley and Greening (1999) add that the continued sourcing and extraction of new gravel material has far-reaching impacts on the environment, including permanent loss of natural resources, morphological damage, habitat fragmentation and dust pollution.

Reclamation of existing materials and sourcing of locally available marginal quality gravels are often the last options for road construction. Such materials are modified and enhanced through stabilisation with various products, the most common being cement, lime and bitumen. However, these products pose significant challenges for particular conditions including; increased material rigidity, proneness to cracking, incompatibility with certain materials, susceptibility to particular environmental conditions (e.g. water or temperature) and deterioration with use (Akhalwaya and Rust, 2018; Steyn, 2009). Furthermore, changes in construction equipment and techniques, available raw materials, effects of climate change and the need for rapid construction have resulted in updating some construction practices for these products (Paige-Green, 2008). Against this background, alternative (non-standard) products are being sought, which can be used to improve available in-situ materials to reduce losses and enable them to fulfil the required specifications. One such category of products that has been receiving greater consideration in SA is nanomaterials.

Nanomaterials are defined as materials possessing, at minimum, one external dimension measuring in nanometres (Nagarajan and Hatton, 2008). It is a rapidly emerging technology with enormous potential to create new materials and products (with unique properties) for numerous applications. They are characterised by their extremely small sizes (compared to their bulk states) which means they have a much greater specific surface area. The small size of particles also means a greater proportion of the particle's atoms are found at the surface where chemical reactions occur. Thus, a small quantity of nanomaterial can significantly improve reactivity properties between intermixed materials. For this reason, nanomaterials have found use in the pavement engineering industry although this has mainly been limited to improving binders for asphaltic materials (Jordaan and Steyn, 2021a; Rust et al., 2020).

The current study considers an innovative nanotechnology-based product, Nano Modified Emulsion (NME), for the stabilisation of a naturally available micaceous gravel to be used as a gravel road-wearing course. The NME considered for this study comprises of Conventional Bitumen Emulsion (CBE) modified with a compatible organofunctional nanosilane. Studies by Akhalwaya and Rust (2018), Jordaan et al. (2017a, 2017b), Jordaan and Steyn (2021a, 2021b, 2021c), Kidgell et al. (2019) and Rust et al. (2019, 2020) show that this product has the potential to improve the stability and hydrophobicity characteristics of most gravel materials. NME is distinguished from the standard bitumen stabilisation (foamed or emulsion) practice by the lack (non-addition) of an active filler.

1.5 Problem statement

The adoption of NME in the road industry has the potential to reduce construction costs by up to 50 per cent or more by maximising the use of materials recycled from within the pavement structure or found in the vicinity of the construction site (Jordaan and Steyn, 2021b; Rust et al., 2020). This would be a significant step towards the provision of sustainable road infrastructure. However, current knowledge of the product is limited, leading to inertia in its adoption by the industry. On-going efforts to streamline concepts, understand, and develop design guidelines of NME stabilised materials (NMESMs) require further research into these materials' fundamental

properties and behaviour. Therefore, experimental based research is proposed to demonstrate and extend the knowledge on the efficacy of NME stabilisation.

NME Draft Project Specifications (NDPS), included in TRH24 (2022), propose material mixing and evaluation procedures for NMESMs for various material categories. The evaluation procedures are mainly based on results of Indirect Tensile Strength (ITS) and Unconfined Compressive Strength (UCS) laboratory tests. The procedures provide an avenue for further testing and understanding of the behaviour of NMESMs. By incorporating advanced test methods such as triaxial testing, fundamental material engineering properties that better characterise the strengths and behaviour of NMESMs can be obtained. The results of these tests also provide critical inputs in applications that simulate and predict the materials' performance through pavement responses in structure analysis procedures such as those deployed in mechanistic-empirical pavement designs.

1.6 Aim and objectives

The aim of this study is to investigate the efficacy of NME for gravel material stabilisation by characterising and evaluating the engineering strength and durability properties of NMESMs in the laboratory. Thus, advancing sustainable gravel road construction through innovative nano-emulsion treatment of a micaceous gravel. The study objectives are to:

i. Evaluate characteristics of the mechanical strength and load bearing capacity of NMESMs,
ii. Evaluate stiffness and deformation characteristics of NMESMs,
iii. Determine durability and moisture susceptibility characteristics of NMESMs,
iv. Determine the permeability and void characteristics,
v. Evaluate changes in phase composition and microstructure,
vi. Model and analyse pavement responses of a gravel road structure incorporating NME stabilised layers.

1.7 Significance of the study

A large proportion of the road network in SA is already established, thus, the demand is mostly for maintenance and rehabilitation activities. The focus is therefore on

increasing the durability of the established roads, through rehabilitation, so that they can last longer and reduce maintenance requirements (Steyn, 2008). However, the continued use of traditional road rehabilitation methods (against the backdrop of limited resources) has brought about challenges in the industry leading to a backlog of rehabilitation projects. Furthermore, rehabilitation practices such as re-gravelling, aim at repairing damage after it occurs rather than minimizing or preventing its occurrence in the first place (Li, 2016). This leads to a reduced life cycle of these roads and means more resources are required for maintenance and rehabilitation activities.

The use of new and innovative technologies, such as NME, is targeted at breaking the cycle of hauling good quality materials by functionalising recycled material from within the pavement structure or locally available in the vicinity of the road project. This study broadens the understanding of the engineering properties of NMESMs. These properties are crucial for predicting performance and allowing for informed decisions on the use of the material. The study also contributes to the ongoing development of design standards and the drive for eventual acceptance and adoption of the technology by the pavement industry. Potential savings that would be realised from the implementation of NMEs would significantly minimise the challenges faced by the industry.

1.8 Scope and limitations of the study

The characteristic behaviour and performance of stabilised material mixes are influenced, to a large extent, by the individual constituent materials, i.e. the NME binder and the gravel material in this case. Due to limitations of time and resources, only one gravel material type and one NME binder type were considered for this study. The NME binder is a proprietary material provided by a local vendor (in SA). A micaceous gravel material was chosen as a suitable candidate for demonstrating the effectiveness of NME due to its problematic nature. The fundamental mixing procedures contained in NDPS (TRH24, 2022) were adopted and used to produce the mix.

This study is limited to laboratory testing to assess the behavioural characteristics of the mix (of the two materials) by identifying patterns and trends in the measured engineering properties at varied NME application levels. Other factors that may

influence the behaviour and performance of NMESM, such as grading and density were not assessed but kept constant to minimise their influence.

Routine tests including, Laboratory Dynamic Cone Penetration (DCP-DN), California Bearing Ratio (CBR), Unconfined Compressive Strength (UCS), and Indirect Tensile Strength (ITS) were supplemented by advanced tests i.e. Static Triaxial Tests (STT) and Repeated Load Triaxial (RLT) tests for Resilient Modulus (M_R) and plastic strain (ε_p). The durability of the mix was evaluated in terms of its resistance to moisture damage through the Moisture-Induced Damage Ratio (MDR). The study did not consider an economic analysis or life cycle assessment of the product (NME).

1.9 Thesis structure

The layout of the remainder of the thesis is as follows:

Chapter 2: The literature review is discussed. It details the broad context of the development of NME and the compatibility requirements in applying the product to gravel materials. The principles of nanotechnology, its applications and the policy framework to advance research and development in this field in SA are also discussed.

Chapter 3: Presents the research approach and experimental design procedure. Materials used in the research are itemised, and the standard test methods used for classification and material property tests. The adopted mixing and evaluation procedure is also presented.

Chapter 4: Provides the results of material characterisation tests and the mix procedure. The gravel material is classified based on index tests in applicable material standards. In addition, the aggregate mineralogy is presented based on X-Ray Diffraction (XRD) test results.

Chapter 5: Details main results of the study. The results of load-bearing capacity tests, mechanical strength tests, stiffness and resilient modulus tests, Etc., are discussed. Patterns and trends are identified and benchmarked against available standards and recent research.

Chapter 6: Discusses the development of a pavement structure model to simulate the behaviour of the NMESM. Pavement responses are analysed and benchmarked against equivalent unstabilised material layers.

Chapter 7: This Chapter concludes the research. Major findings are summarised in line with the objectives. The findings of the laboratory test results are linked to the performance of NME stabilised materials to improve current design methods. Recommendations are made for implementation and further research.

2 LITERATURE REVIEW

2.1 Introduction

Materials play a significant role in the performance of gravel roads. The choice of materials for construction of gravel roads depends on, among other factors, availability, cost and environmental factors. Additionally, functional requirements of the road dictate that the materials meet specified requirements including;

a) Stiffness – required to quantify the load carrying capacity,
b) Resilience - ability to recover after release of load,
c) Strength - defined by limits of the stress-strain relationship,
d) Retained strength after exposure to particular climatic conditions (moisture, temperature),
e) Durability - cumulative distress during pavement service-life and susceptibility to weathering action.

The extent to which materials meet these requirements is dependent on the materials' inherent properties, qualities of the individual particles in the materials and the means by which they are held together (PDM, 2013). Various stabilisation technologies are available to bind material particles and enhance performance properties of particularly low-quality materials that do not meet these functional requirements. The efficacy and suitability of these binders for use with a particular material is evaluated through laboratory-based characterisation and strength tests.

This Chapter reviews literature on the potential of NME, a relatively new technology, for material stabilisation. NME offers the promise of the construction of sustainable roads by taking advantage of the unique properties of nanotechnology. The review begins with an overview of a gravel road pavement structure. Nanotechnology applications, the state and framework for advancement of the technology in the SA road industry are discussed. The constituents of NME, i.e. nanomaterial and CBE are explored, and the process leading to the production of NME. Further, the properties of materials for road construction are highlighted with regard to compatibility requirements for stabilisation with NME. The last part of the review centres on the

fundamental behavioural properties of NMESM and laboratory test properties that exemplify this behaviour as depicted in Figure 2-1.

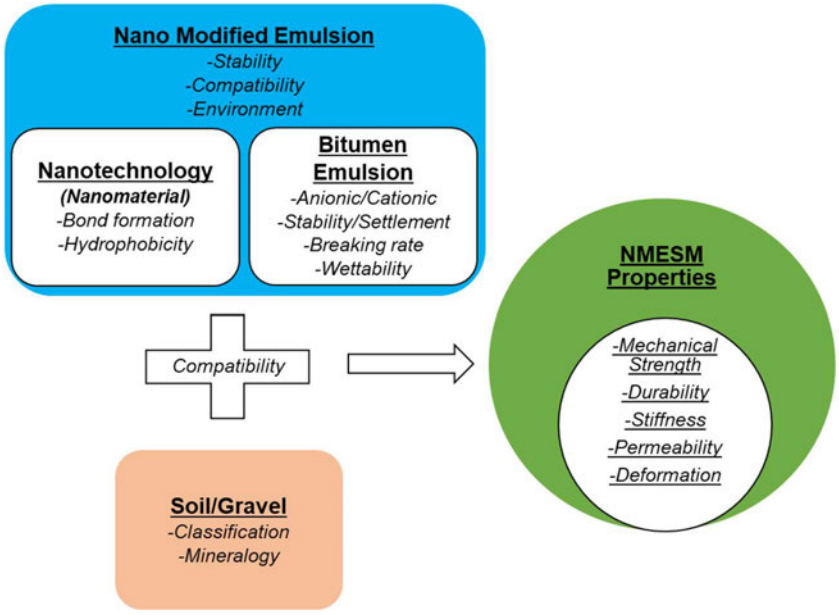

Figure 2-1: Depiction of the formulation of NME stabilised materials

2.2 Gravel road structure

A gravel road consists of designed layers of imported gravel to form a wearing course and a structural layer (base) which covers the in-situ material (Figure 2-2). The wearing course, which is directly in contact with traffic, is designed considering the loss of surface material due to traffic and effects of the environment (e.g. rain). The base course is designed to protect the subgrade from excessive compressive stress (Pinard et al. 2019). However, in many cases, the same material is used for both the structural layer and the wearing course thus forming one upper layer – the surfacing. According to Toole et al (2018), the surfacing of most gravel roads is typically 100 mm to 300 mm thick and provides sufficient structural strength and cover thickness to distribute the applied traffic loads to the roadbed material. Most design guidelines, including TRH20 (1990), stipulate that to provide all-weather access, the minimum thickness of the surfacing should be maintained in service by replenishing the gravel material throughout the design life of the road.

Material selection is a critical aspect for gravel road construction. The best quality gravel material should be selected to ensure adequate performance and durability.

According to Henning et al., (2008), an ideal material should have properties which result in an even, tight, relatively impermeable, erosion-resistant and wear-resistant surface. Often, the selection of materials is a compromise between achieving the desired properties with available funds. Environmental factors may eliminate some sources of material.

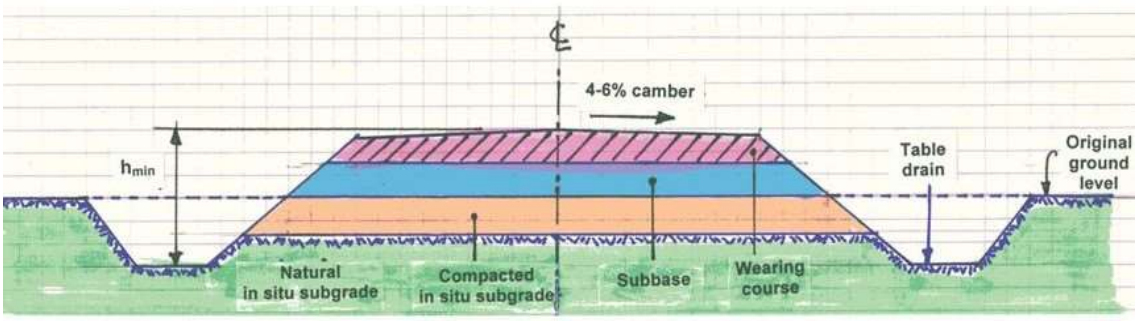

Figure 2-2: Typical cross section of gravel road (Pinard et al. 2019)

2.3 Nanotechnology

The term “Nanotechnology” was coined by Taniguchi, a Japanese scientist, in 1974. In the paper, “On the Basic Concept of Nanotechnology”, Taniguchi describes nanotechnology as mainly consisting of the processing, separation, consolidation and deformation of materials by one atom or one molecule (Taniguchi, 1974). According to Bayda et al., (2019), "nano" is a Greek prefix that means dwarf or extremely small.

Many authors have attempted to describe nanotechnology in the modern era. What is evident from the definitions is the broad context in which the technology is applicable. Tolochko (2009), for instance, asserts that it is a broad term covering a wide spectrum of technologies based on various types of physical, chemical and biological processes realised at nanometre level. Papadimitropoulos et al. (2018) add that it is not just a science that deals with materials in minute dimensions, but a science that exploits the unique physical, chemical, mechanical and optical properties of materials on this scale. Saidi and Douglas (2017) also describe it as a microcosm of the innovation system, covering the creation of nanomaterials through to their application. The authors assert that the technology has a ubiquitous influence on the whole manufacturing industry and a propensity to spur complementary innovations that span the full breadth of the field of science and engineering.

The application of nanotechnology and nanomaterials can be traced as far back as the fourth century AD (Bayda et al., 2019). The Lycurgus Cup, a typical example of nanotechnology from the ancient world, exhibits peculiar optical properties. It appears red in transmitted light or green in reflected light due to the dichroic (two colours) glass it was made of. In 1990, the cup was analysed using a Transmission Electron Microscope (TEM). The observed dichroism was determined to be due to nanoparticles, 50–100 nm in diameter, (Bayda et al. 2019; Leon et al. 2020). Similar and other nano-products and discoveries made throughout the 19th century are accounted for in various literature including, Bayda et al. (2019).

Nevertheless, purposely created and applied technological processes and means of manipulating matter at the nanoscale, subsequently termed nanotechnology, is relatively new, conceptualised by Richard Feynman in 1959 (Bayda et al., 2019; Leon et al., 2020; Tolochko, 2009). Delivering a lecture dubbed “There is a lot of space down there” at a session of the American Physics Society, the possibility of creating nano-sized products with the use of atoms as building blocks was considered for the first time. In the 1980s to the early 1990s, several discoveries and inventions were made, which impacted the further development of nanotechnology (Tolochko, 2009). One such development was the invention of the Scanning Tunnelling Microscope (STM) by IBM researchers; Gerd Binnig and Heinrich Rohrer in 1981. It allowed scientists and engineers the ability not only to image atoms but also to manipulate atoms and clusters with a precision equal to that of a chemical bond (Goddard et al., 2003).

Materials and structures developed through nanotechnology perform tasks that are not possible using the materials in their typical macroscopic form (Steyn, 2008). For this reason, the technology has found use in almost all aspects of modern life. Kumar et al. (2011) depict the broad range of sectors where nanotechnology applications are being explored as shown in Figure 2-3.

Figure 2-3: Schematic representation of nanomaterials and their applications (Kumar et al. 2011)

Marr (2020) and Nanowerk (2020) also list some products, incorporating nanotechnology-based materials or processes, currently on the market and in daily use;

a) Cosmetics; sunscreen, moisturisers and hair care products,
b) Sports equipment; baseball bats, tennis and badminton racquets, hockey sticks, racing bicycles, golf balls/clubs, skis, etc.
c) Clothing; sports clothing, protective garments for workers involved in emergency services, etc.
d) Furniture; particle boards, high scratch resistant lacquers, antibacterial, self-cleaning or easy-to-clean coatings and ultra-strong concrete material for kitchen and street furniture applications
e) Coatings; corrosion, water and ice protection and friction reduction
f) Automotive equipment; fuel cells, batteries, wear-resistant tires, lighter but stronger materials, etc.

2.4 Dimensional aspects

Nanomaterials are defined as materials characterised at least in one of three measurements by the nanometre (nm) scale. A nanometre is a billionth of a metre (10^{-9}m), that is, about 1/80,000 of the diameter of a human hair or 10 times the diameter

of a hydrogen atom (SANI, 2003). Therefore, nanomaterials are too small to be seen with the naked eye and even with conventional laboratory microscopes. Typically, the dimensions that are considered to be at the nanoscale range up to several hundred nm (NNI, 2021). However, Boverhof et al. (2015) explain that while the size limits are somewhat arbitrary, there is a general agreement that any unique nano-specific phenomena of particulates are most likely to occur between 1 and 100 nm.

The surface of an object becomes increasingly important as its size decreases because the surface area increases significantly with size reduction. This is exemplified by Bell (2006) in Figure 2-4. It is shown that the surface area of a cubic centimetre of a solid material is six square centimetres but if the same cube is pulverised into 1-nm particles, the total surface area of the cube in an ultrafine powder form is 60 million square centimetres.

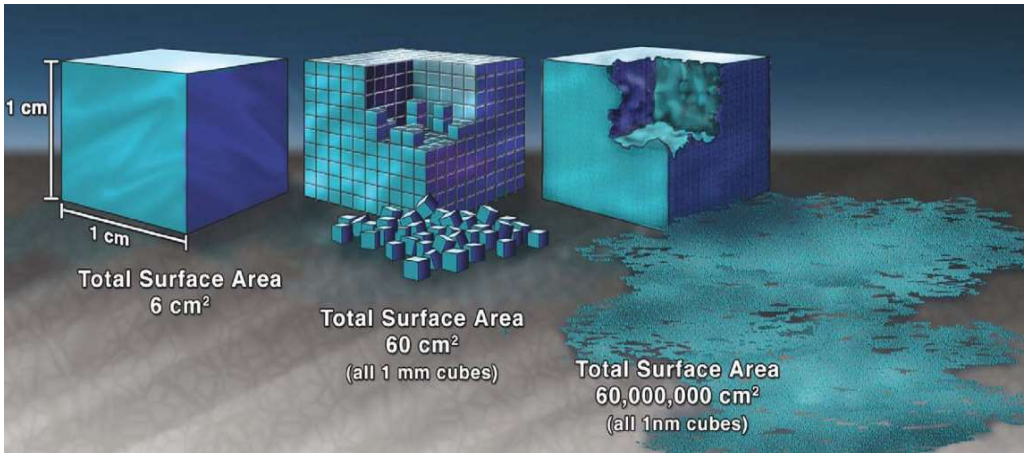

Figure 2-4: Surface Area Coverage (Bell, 2006)

The surface area of nanomaterials is of significance because most chemical reactions involving solids happen at the surfaces, where chemical bonds are incomplete. Therefore, a larger surface provides more area for reactions and the chemical activity of a material increases drastically. For this reason, nanomaterials exhibit unique features, characteristics and properties compared to commonly used materials (Papadimitropoulos et al., 2018). Majeed and Taha (2013) itemise some of the properties brought on by the transition to nanoscale level;

- The greater surface area to volume ratio results in a higher cation exchange capacity. Because of this, nanomaterials interact very actively with other

particles and solutions such that even very minute amounts can significantly influence the physico-chemical behaviour and engineering properties.

- Movement and interactions are dominated by electromagnetic forces rather than gravity forces.
- Instead of classical mechanics, quantum mechanical models are utilized for describing movement and energy at the nanoscale.
- Random molecular movements are of higher significance at the nanoscale

2.5 Nanotechnology in SA

SA is one of the countries that has realised the potential of nanotechnology and moved to adopt it with the aim of enhancing global competitiveness and sustainable economic growth. A number of SA research institutions, universities, science councils and industrial companies are actively researching in nanotechnology. In 2002, the SA Nanotechnology Initiative (SANI) was formed as a collaborative effort between universities and industrial companies. In 2003, the SA government commissioned SANI to develop the National Nanotechnology Strategy (SANI, 2003). The strategy was developed and approved in 2005 with the objectives to;

i. Support long-term nanoscience research,
ii. Support the creation of new and novel devices for applications in various areas,
iii. Develop the required resources; human and supporting infrastructure,
iv. Stimulate new developments in technology missions such as nano-bio materials for biotechnology, precious metal-based nanoparticles for resource-based industries, and advanced materials for information and communication technologies.

The strategy also aims to contribute, directly or indirectly to other national strategies in line with the broad development goals of economic growth, poverty reduction and enhancing quality of life.

2.6 Nanotechnology in road construction

In the early 1990s, the construction industry was one of the first industries to identify nanotechnology as one of the emerging technologies with potential to contribute to its

development. However, it is only since the early 2000s that significant advancements have been made in research and development in the broad area of construction (Zhu et al., 2004).

In pavement engineering and road construction, most of the early research on nanotechnology has been concentrated on asphalt materials through modification of binders with the main research areas depicted by Partl et al. (2004) in Figure 2-5. However, studies in many parts of the world demonstrate the potential of this technology for improving natural gravels and soils used in structural layers of road pavements. Alireza et al. (2013) report on the increased CBR strength after the addition of up to 3% nano-silica and 5% lime to a mixture of a weak local soil. However, it was observed that increased nano-silica up to 5% had the opposite effect on the material. Gallagher and Mitchell (2002), Kodaka et al. (2005) and Persoff et al. (1999), report improved material properties including, UCS, permeability, cyclic shear strength and liquefaction, on application of various percentages of colloidal silica to different soil types. Ugwu et al. (2013) also showed that the stabilization of laterite and clay soils with nanomaterial improves the CBR strength, Liquid Limit (LL), Plastic Limit (PL), Shrinkage Index (SI) and hydrophobic properties. The nanomaterial also improved the hydrophobic properties of black soil but not the strength.

In SA, Jordaan and Kilian (2016) and Jordaan et al. (2017a) report that a scientifically based programme to prove the viability of nanotechnology on roads was embarked on in 2014 after it was identified as a potential game changer in delivery of cost-effective roads. Suitable roads to demonstrate the applicability of the technology were identified and rehabilitated, incorporating NMEs. Jordaan et al. (2017a) reports that initial results at design stage and through Accelerated Pavement Testing (APT) with a Heavy Vehicle Simulator (HVS) showed good promise, prompting more research in the area.

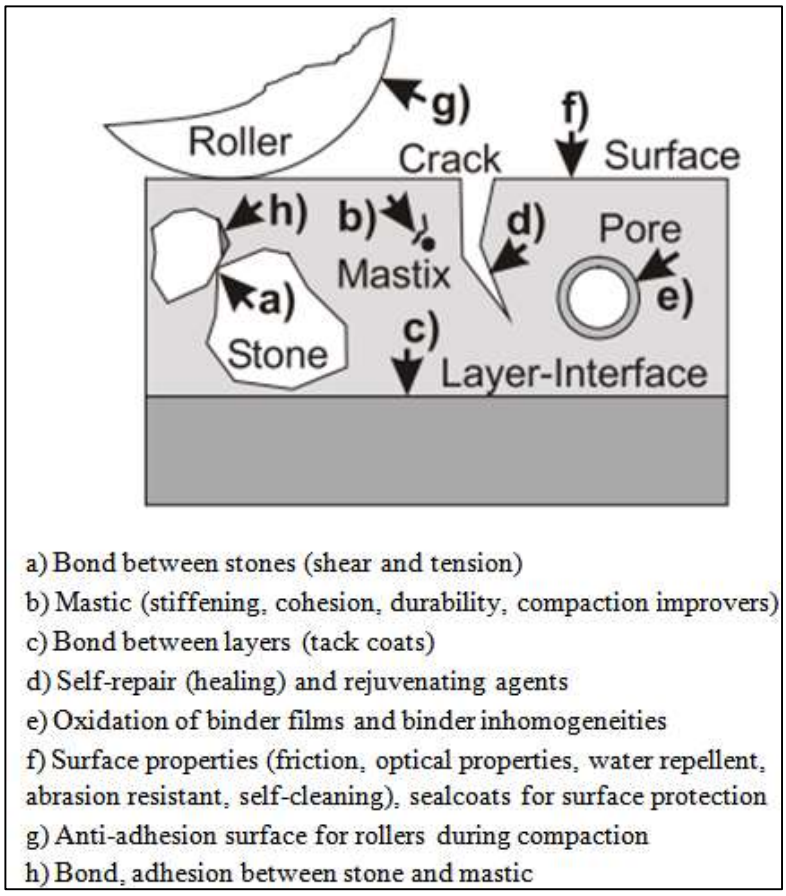

Figure 2-5: Schema of focus areas for nanotechnology development in asphaltic materials (Partl et al. 2004)

2.7 Synthesis and characterisation of nanomaterials

Nanomaterials exist in nature and can also be created from a variety of products and minerals such as carbon, silicon, silver etc. They can be synthesised in different morphologies depending on the required properties for the desired application (Jeevanandam et al., 2018). Nagarajan and Hatton (2008) discuss the methods for the synthesis of nanomaterials listed below;

- Mechanical processes of size reduction such as grinding, milling and alloying.
- Gas phase processes - flame pyrolysis, high temperature evaporation and plasma synthesis, microwave irradiation, physical and chemical vapor deposition synthesis.
- Colloidal or liquid phase methods - chemical reactions in solvents leading to the formation of colloids.
- Molecular self-assembly

Nagarajan and Hatton (2008) also explain that the synthesis of material to nano-sizes renders them chemically very reactive and/or physically aggregative. Thus, the synthesised nanoparticles have to be surface modified in most cases, for the purposes of passivating a very reactive nanoparticle, stabilizing a very aggregative nanoparticle in a medium (such as a solvent or polymer) where the nanoparticles are to be dispersed, functionalising the nanoparticle for applications such as molecular recognition or promoting the assembly of nanoparticles. Most commonly used surface modification methods include grafting thiolated surfactants or polymers, adsorption of charged surfactants, charged ligands or polymer brushes, attachment of biological molecules or coating a continuous polymer film on nanoparticles.

Based on the method of synthesis and characteristic material nature, nanomaterials can be organized into four categories (Jeevanandam et al., 2018);

- Carbon-based nanomaterials: Generally, these nanomaterials contain carbon, and are found in morphologies such as hollow tubes, ellipsoids or spheres. Fullerenes (C60), carbon nanotubes (CNTs), carbon nanofibers, carbon black, graphene (Gr), and carbon onions are included under the carbon-based nanomaterials category. Laser ablation, arc discharge, and chemical vapor deposition (CVD) are the important production methods for these carbon-based materials fabrication (except carbon black).
- Inorganic-based nanomaterials: These nanomaterials include metal and metal oxides. These nanomaterials can be synthesized into metals such as Gold (Au) or Silver (Ag) nanoparticles, metal oxides such as TiO_2 and ZnO nanoparticles, and semiconductors such as silicon and ceramics.
- Organic-based nanomaterials: These include nanomaterials made mostly from organic matter. The utilization of noncovalent (weak) interactions for the self-assembly and design of molecules helps to transform the organic nanomaterials into desired structures such as dendrimers, micelles, liposomes and polymer nanoparticles.
- Composite-based nanomaterials: Composite nanomaterials are multiphase with one phase on the nanoscale dimension. They can either be a combination of nanoparticles with other nanoparticles or nanoparticles with larger or bulk-type materials (e.g., hybrid nanofibers) or more complicated structures, such as

metal-organic frameworks. The composites may be any combinations of carbon-based, metal-based, or organic-based nanomaterials with any form of metal, ceramic, or polymer bulk materials.

2.8 Silanes

For centuries scientists experimented on various products to protect and preserve stone material for art work, buildings and other works against ageing and the effects of the environment. Around the mid-1800s, with the synthesis of various silicon-based compounds, it was recognised that silanes could be used for this purpose (Wheeler, 2005).

Silanes are compounds that contain monomeric silicon structures (Jerez et al. 2018; Materne et al. 2012). The root name, silane (SiH_4) is derived by analogy with methane (CH_4). Each hydrogen atom in the compound may be replaced by other elements or groups, for example, replacement by one, two, three or four chlorine atoms yields the names chlorosilane ($ClSiH_3$), dichlorosilane (Cl_2SiH_2) trichlorosilane (Cl_3SiH) and tetrachlorosilane ($SiCl_4$), the latter more often called silicon tetrachloride (Wheeler, 2005). When the hydrogen atoms in the Si-H bond in the silane are replaced with alkoxy (alkyl + oxygen) groups, the silanes are known as alkoxysilanes and when there is at least one carbon-silicon bond (Si-C) structure, they are known as an organosilanes (Jerez et al., 2018; Materne et al., 2012; Xu et al., 2019).

A typical silane compound, depicted in Figure 2-6, contains;

- R – a non-hydrolysable organic moiety; This moiety can be reactive towards another chemical (e.g., amino, epoxy, vinyl, methacrylate, sulfur) or non-reactive (e.g., alkyl).
- OR – a hydrolysable group; like an alkoxy group (e.g., methoxy (CH_3O) or ethoxy (CH_3CH_2O)) or an acetoxy group

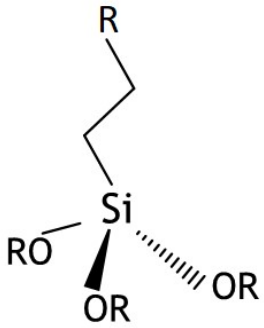

Figure 2-6: Silane Molecule (BRB, 2021)

Silane compounds are distinguishable by the nature of the hydrolysable groups attached to the silicon. They exhibit unique chemical reactivity and, in the presence of moisture, form siloxane bonds (Materne et al., 2012). The ability to form siloxane bonds is one of the major reasons why silanes are used in stone preservation – soil/aggregate stabilisation.

The formation of siloxane bonds with substrates such as soil happens through a four-stage process (Arkles, 2006; Materne et al., 2012; Wheeler, 2005). First, the hydrolysable groups in the silane molecule are hydrolysed i.e. react with atmospheric or absorbed water on a surface to form silanol, Si-OH (Figure 2-7).

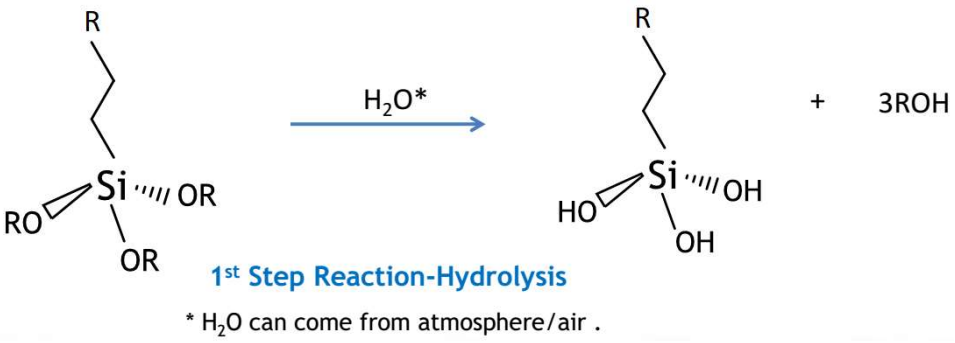

Figure 2-7: Hydrolysis of Silane molecule (BRB, 2021)

In the second step, oligomers (molecule consisting of a few repeating units) are formed through a condensation process. The oligomers hydrogen bond with hydroxide (OH) groups of soils (substrate), in the third step, and finally during drying or curing, covalent bonds - siloxane (-Si-O-Si) bonds - are formed with the soil, with concomitant loss of water. Figure 2-8 provides a summary of the process.

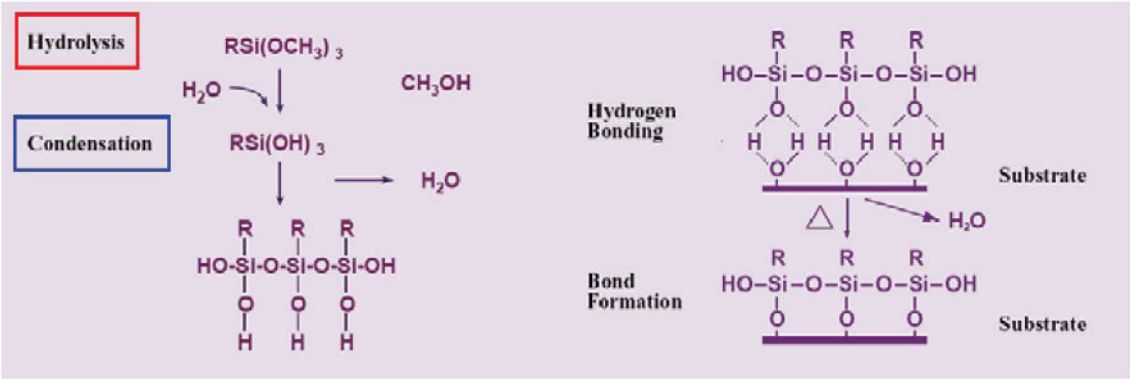

Figure 2-8: The mechanism of hydrolysis, condensation and bonding of silanes to Inorganic surface (Materne et al., 2012)

Usually only one bond is formed from each silicon to the interface with the substrate. The two remaining silanol groups are present either in condensed or free form. The R group remains available for covalent reaction or physical interaction with other phases (Arkles, 2006).

2.8.1 Properties of silanes

The siloxane bonds have many properties that are beneficial to soil. They (siloxane bonds) are one of the strongest bonds established in nature (see Table 2-1). They have good weathering resistibility, possess thermal and oxidative stability and resist cleavage by ultraviolet solar radiation. This is exemplified by the abundance and long life of rain- and sun-drenched silicate minerals in the earth's crust (Wheeler, 2005; Xu et al. 2019).

Table 2-1: Chemical Bond Strengths (Wheeler, 2005)

Bond Strengths in kcal/mol	
Si-O	108
C-H	99
C-C	83
C-O	86
C=C	148
C=O	169

Mealey and Thomas (2006) and Wacker (2015) further explain that silanes are hybrid compounds that combine the functionality of a reactive organic group and an inorganic group in a single molecule. For this reason, they are called organofunctional silanes. They have dual reactivity and work by forming molecular bridges between inorganic substrates (soils) and organic/polymeric matrices as shown in Figure 2-9. This unique dual reactivity differentiates silanes from other treatments.

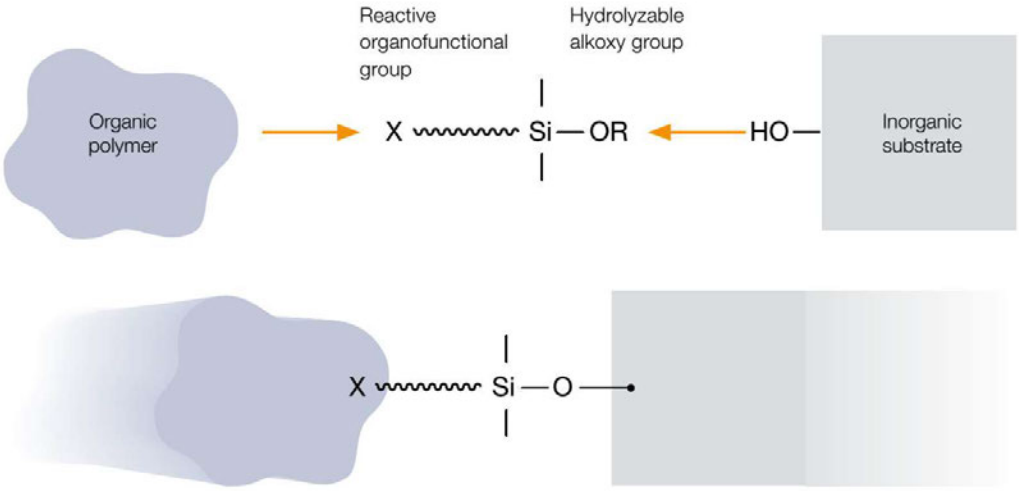

Figure 2-9: Organofunctional silanes act as molecular bridges between organic polymers and inorganic materials (Wacker, 2015)

Arkles (2006), Fonseca et al. (2018) and Wheeler (2005) add that silanes are relatively easy to apply and have low viscosities. The low viscosities make for mobile liquids that easily penetrate the intergranular network of substrates (soils). No harmful by-products are produced during the formation of the siloxane bonds and it does not compromise aggregate strength nor form hardened/brittle layers due to over-consolidation.

Brinker and Scherer (1990) demonstrate that silanes are hydrophobic. Hydrophobicity is the ability of a material to repel water. The hydrophobicity of silanes is imparted onto the surfaces of stabilised soil/aggregates such that the surfaces tend not to absorb or be wetted by water. This is demonstrated in Figure 2-10 (Jordaan et al., 2021b). This is an important property as road materials are adversely affected by water through loss of bearing strength, leading to manifestation of pavement defects and serviceability loss.

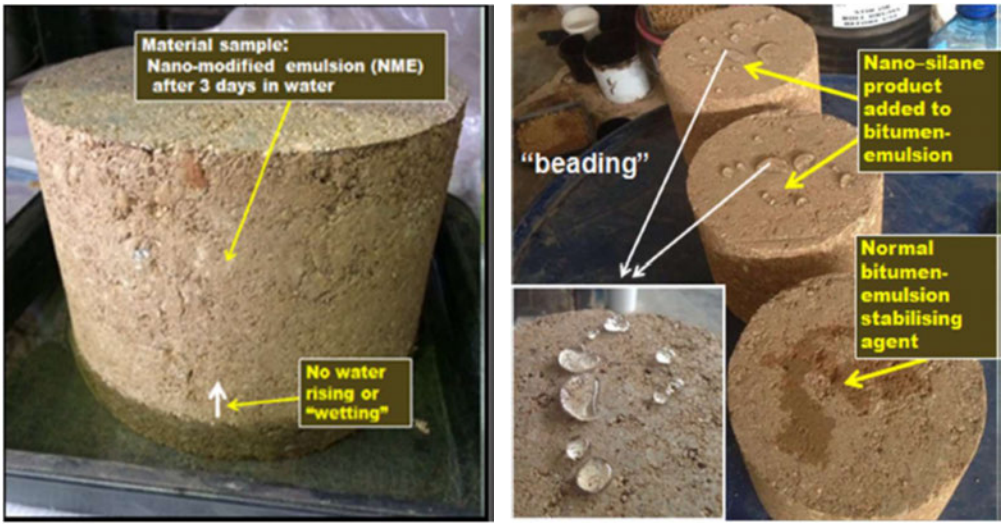

Figure 2-10: Illustration of hydrophobicity of stabilised materials (Jordaan et al., 2021b)

However, not all silanes can be used for stabilisation of material, bringing about the benefits of hydrophobicity among other properties. According to Wheeler (2005), to function as a consolidant the silane compound must have the ability to form three-dimensional networks and so must have a minimum of three reactive groups. Therefore, only tri- and tetra-functional silicon compounds form gels to bind soils. All difunctional compounds that form only linear polymers are eliminated. Additionally, some silanes produce harmful by-products such as hydrogen gas and hydrochloric acid on hydrolysis. This is discussed further in Section 2.11.6. Such compounds are avoided as they cause environmental and human health problems. Vapour pressure and reactivity rate are two other factors considered. Silanes with high vapour pressure are likely to evaporate before consolidation occurs. This may be exacerbated by high temperature and/or low humidity. Slow acting volatile stabilisers also stand the risk of evaporative loss. On the other hand, stabilisers that react too rapidly may not be able to penetrate deep into the soil/aggregate before gelation occurs.

Brinker and Scherer (1990) and Wypych et al. (2018) explain how steric and inductive effects also come into play in silane reactivity. Steric effects (or steric hindrance) is the crowding or blocking of the central silicon atom by larger or geometrically more complicated alkyl or alkoxy groups. Steric hindrance can also happen when reactive groups on the polymer chains do not match positions of the reactive sites on mineral surfaces. Thus, few (if any) covalent bonds are formed due to reduced rates of hydrolysis and condensation. Inductive effects refer to the effect on electron density in

one portion of a molecule due to electron-withdrawing or electron-donating groups elsewhere in the molecule. In silanes, this may result from substituting alkyl for alkoxy groups. For example, replacing a methoxy group on tetramethoxysilane with an 'electron-donating' methyl group (transforming it into methyltrimethoxysilane (MTMOS)) increases the electron density on the silicon atom and, under acid conditions, increases the rate of hydrolysis. However, for base conditions, the alkyl-for-alkoxy trade decreases the rate of hydrolysis. Reduced hydrolysis rate means reduced condensation and therefore reduced gelation.

2.8.2 Nanosilanes

Nanosilanes are derivatives of silanes, and may be produced through one of the processes discussed in Section 2.7. According to Nagarajan and Hatton (2008), the molecular self-condensation method is a particularly effective method for the production of polymeric nanoparticles. Thermodynamically stable nanoparticles can be produced whose size and shape can be controlled by the self-assembly conditions. Figure 2-11 illustrates the production of liquid phase nanosilanes through the process of self-condensation.

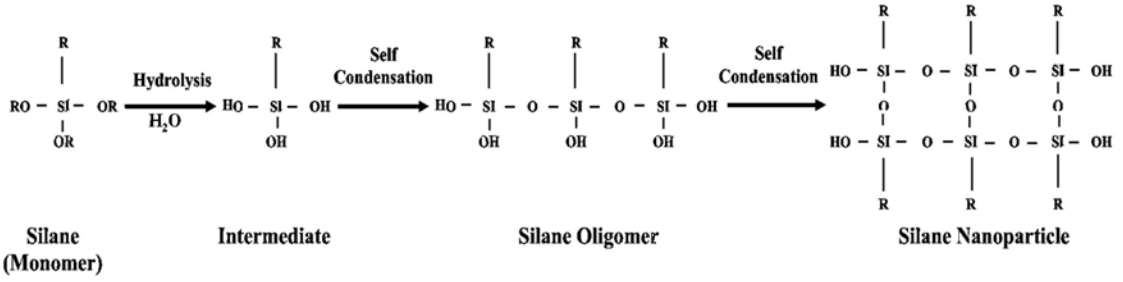

Figure 2-11: Production of silane nanoparticle through self-condensation (Feng et al. 2016)

Feng et al. (2016) explain that the process begins with the formation of silane oligomers through the first condensation process. Further condensation of oligomers leads to the formation of nanosilanes consisting of thousands of repeating silane units.

Nanosilanes offer additional advantages for use in soil stabilisation due to their characteristically small molecular size (nano size). They are particularly suited for deep penetration into the intergranular network of soils (Feng et al. 2016; Jordaan et al. 2017a; Kidgell et al., 2019). This is aided by their low viscosity and high mobility. In addition, they have high molecular weight and low vapour pressure and, thus, are less

likely to evaporate (Feng et al. 2016; Wheeler, 2005). Further, nanosilanes, with more repeating silane units, have more RO groups available for condensation and bond formation with soils. Due to size, the siloxane bonds are formed at the molecular level of a mineral soil or aggregate (Jordaan et al. 2017a). This means more surface area covered and hence higher (molecular) level hydrophobicity on a treated surface.

However, Wendler et al. (1999) and Wheeler (2005) point out that nanosilanes cannot be singly used to bridge gaps and bind together aggregates/soil particles used in road construction. The (small) sizes of nanosilanes means that when applied to a soil, the gels formed can only bridge pore sizes of up to 60 µm. Such pore sizes are only possible for a maximum aggregate size of about 4mm while soils and aggregates used in road construction currently vary in size from less than 0.075mm to about 63mm. It is for this reason that in many studies (Alireza et al. 2013; Ugwu et al. 2013; Hussain, 2016; Rosales et al, 2020), nanomaterials are added to other binders (of larger molecules) to aid the bridging effect required to bind aggregates. Cement, lime and water have all been used to pair the nanomaterial.

2.9 Bitumen Emulsions

Emulsions are heterogeneous systems with two or more liquid phases, i.e. a continuous liquid phase and at least a second liquid phase dispersed in the former as fine droplets. Thus, bitumen emulsions consist mainly of two immiscible liquids, bitumen and water. The bitumen is dispersed throughout the continuous water phase in the form of discrete globules and is referred to as Oil in Water (O/W) emulsion. The water is referred to as the dispersing phase and the bitumen as the dispersed phase. Bitumen emulsions are widely used for cold paving technologies and material stabilisation (Lesueur, 2011). It offers many advantages including environmental friendliness, better safety profile and ease of application. Heating of emulsions during storage or application is not required, avoiding short-term ageing of the binder.

2.9.1 Manufacturing method

There are a number of methods for manufacturing bitumen emulsions, one of which is by colloid mill. Using this method, bitumen, heated to between 120 to 180 ℃ with a viscosity of about 0.2 Pa.s and water (at a temperature between 40 and 65 °C) is

mixed by forcing the two mediums through small openings (<1 mm) of a colloid mill. The mixing process is achieved under high shear conditions of around 1000 to 6,000 rotations per minute. The amount of bitumen added ranges from 40 to 70%, depending on the nature of use of the bitumen emulsion. Above this range, very large droplets are formed and the emulsions have little storage stability (Al-Mohammedawi and Mollenhauer, 2022; Lesueur et al., 2008; Murphy et al., 2019; Rahman, 2021). A schematic of the manufacturing process is depicted in Figure 2-12.

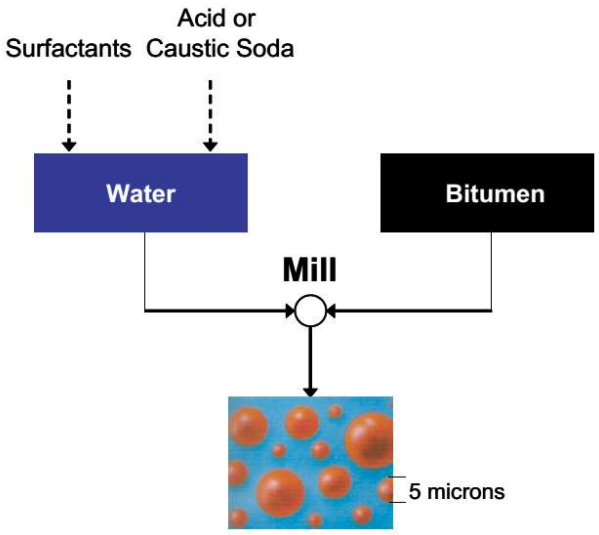

Figure 2-12: Manufacture of Bitumen Emulsion (TG2, 2009)

Chemical emulsifying agents are used to facilitate the mixing of the two mediums, bitumen and water, which otherwise do not mix. These are surface-active agents (surfactants) that act to reduce the interfacial energy between the water and the bitumen, promoting the stable distribution of bitumen droplets in the dispersing (aqueous) phase. Additionally, they control bitumen emulsion properties such as viscosity, breaking, and adhesivity (Abdullin and Emelyanycheva, 2019; Al-Mohammedawi and Mollenhauer, 2022).

A surfactant molecule has two parts, a hydrophilic (head) part and hydrophobic (tail) part and are thus called amphiphilic. The hydrophilic heads of surfactant molecules typically have positive and negative charge areas (polar) and therefore are attracted by the molecules of polar solvents such as water. The tail consists of a long chain organic group (such as a hydrocarbon) that is not soluble in water but is soluble in other organic materials e.g. bitumen. Thus, an emulsifying agent is one molecule with

both hydrophilic and lipophilic (oil-loving) ends (commonly referred to as “Janus” particle; from the Greek mythology meaning “two-faced”) (Bitumina, 2014; Kopeliovich, 2013; Murphy et al., 2019). In a bitumen emulsion, the hydrophilic end of the surfactant molecule orients towards the water phase and the lipophilic end towards the bitumen. Thus, each bitumen droplet is similarly charged and will repel each other in continuous water phase, thereby form a stable solution as depicted in Figure 2-13.

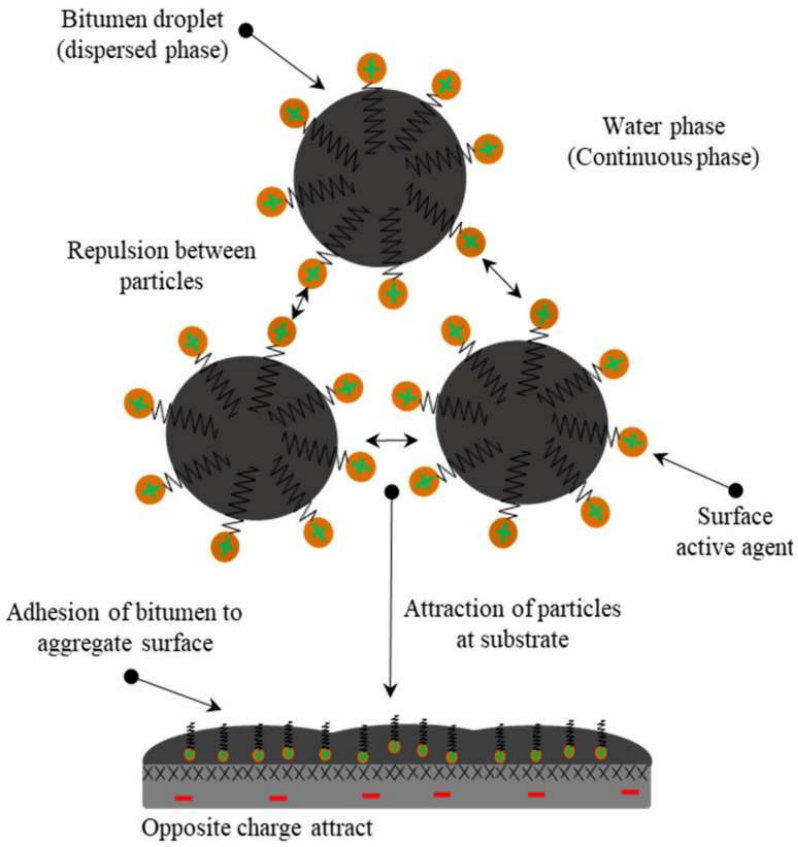

Figure 2-13: An illustration of an emulsifier stabilised bitumen droplet (Al-Mohammedawi and Mollenhauer, 2022)

2.9.2 Classification

Emulsions are classified as anionic, cationic and non-ionic depending on the charge their head groups adopt in water (James, 2006). Franklin and Zhou (2018) explain that in anionic bitumen emulsions, generally the non-polar tails of the anionic emulsifier align inward toward the bitumen material to form a bitumen emulsion particle having a generally negative charge due to the outward-facing negatively charged polar heads surrounding the bitumen particle. In cationic bitumen emulsions, the non-polar tails of the cationic emulsifier align inward toward the bitumen material to form a bitumen

emulsion particle having a generally positive charge due to the outward-facing positively charged polar heads surrounding the bitumen particle.

The bituminous properties of bitumen emulsions are obtained after the emulsion breaks (when it comes into contact with aggregates) and droplets of bitumen coalesce and adhere to the aggregate and the water is expelled. The rate of this breaking depends on, among other factors, the amount of emulsifier, temperature, the reactivity of the emulsion and the surface properties and reactivity of the aggregates (Al-Mohammedawi and Mollenhauer, 2022; Manual 30, 2011). The breaking rate of emulsions can be controlled depending on final application, to be either rapid, medium or slow. Thus, bitumen emulsions are also classified as Rapid-Setting (RS), Medium-Setting (MS) and Slow-Setting (SS) (Franklin and Zhou, 2018, Ignatavicius et al., 2021). RS emulsions are reactive and set quickly in contact with unreactive clean aggregates (of low-surface area). MS emulsions set sufficiently less quickly that they can be mixed with aggregates of low surface area. SS emulsions are unreactive and mix with reactive aggregates of high surface area (James, 2006). The actual breaking and curing time in the field depends on the mixing techniques, materials used as well as the environmental conditions.

2.9.3 Properties of bitumen emulsions

Al-Mohammedawi and Mollenhauer (2022) and Murphy et al. (2019) explain that most of the emulsion properties are determined by various factors of the manufacturing process including, properties of bitumen used, properties of the surfactant, the pressure under which the bitumen emulsion is manufactured as well as the applied shear during mixing with water. Thus, through the manufacturing process, the emulsion can be tailored to the application. Some properties of bitumen emulsions, particularly relevant to this study, are discussed below (Bahia et al., 2008; Kashaya, 2013; Hunter et al., 2015; Murphy et al., 2019; TG2, 2020).

a) Physical stability: Stability refers to the ability of bitumen droplets to stay dispersed throughout the continuous phase for a prolonged period. During storage, bitumen droplets in an emulsion tend to approach one another, a phenomenon called flocculation. Coalescence occurs if the surfactant layer between the droplets is compromised, allowing the droplets to contact one

another. The surfactant can be compromised by lack of agitation, flow of the emulsion caused by pumping, heating (convection currents) or transportation. Some emulsifiers also have a tendency to foam, which may cause coalescence because bitumen particles in the thin film of a bubble are subjected to the forces of surface tension. Coalescence of bitumen emulsion also depends on formulation, i.e. bitumen grade, temperature and surfactant type.

b) Chemical stability: Jordaan and Steyn (2021d) explain that in terms of chemical stability, bond strengths between the various atoms in the emulsifying agent play a major role in the stability of the emulsion. The authors submit that bond strengths between the elements comprising an anionic emulsifying agent are considerably stronger than the bond strengths comprising typical cationic emulsifying agents. Thus, anionic bitumen emulsions are characteristically more stable than their cationic counterparts and will normally have a longer shelf life, an important factor in practice.

c) Settlement: Settlement or sedimentation is the end-result of instability of emulsions as depicted in Figure 2-14. Bitumen emulsions with low viscosity and low bitumen content as well as those with densities of bitumen higher than that of the aqueous phase of the emulsion are prone to sedimentation. The bitumen droplets tend to fall through the aqueous phase, resulting in a bitumen-rich lower layer and a bitumen-deficient upper layer. Other factors that influence settlement are the amount of emulsifier and storage temperature. Settlement can be reduced by equalising the densities of the two phases, reducing either the mean particle size or the range of particle sizes present in the mix and/or increasing the viscosity of the aqueous phase. For a stable emulsion, gentle agitation restores its original quality after settlement.

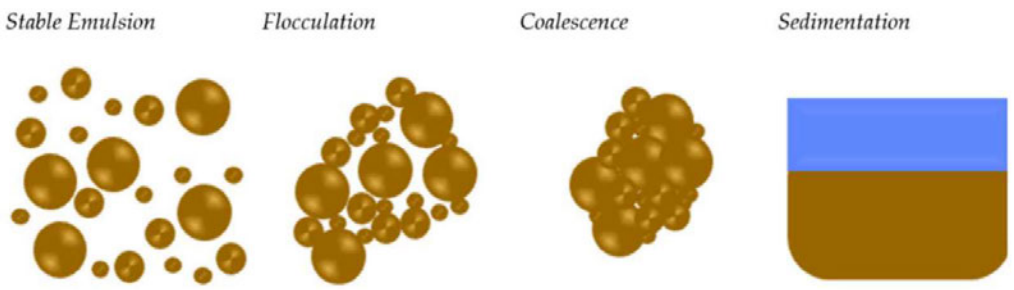

Figure 2-14: Sedimentation process of bitumen emulsion (James, 2006)

d) Breaking/setting rate: This is the time it takes the bitumen to separate from the water phase (through flocculation) and coalesce to produce films of bitumen on the aggregate. In the process, the emulsion changes from a liquid to a continuous film of bitumen, turning from a brown to a black colouration. Breaking is differentiated from curing, which is the displacement of water and subsequent increase in stiffness and tensile strength. Factors that influence breaking and curing include bitumen content, type and dosage of emulsifier, pH, the type of aggregate and particle size distribution, moisture content, environmental conditions, mineralogical composition of aggregate and mechanical action such as compaction or trafficking.

e) Viscosity: Emulsion viscosity is a key performance factor of bitumen emulsions. Highly viscous emulsions may not distribute well in the material whereas low viscosity emulsions may affect the aggregate/binder adhesion evolution, which in turn affects the gaining of the mechanical strength. According to Al-Mohammedawi and Mollenhauer (2022), viscosity is affected by factors such as emulsion particle size and particle size distribution, the bitumen to water ratio and the surfactant type.

f) Wettability: The bitumen in the emulsion needs to 'wet' the aggregate to create the maximum effective contact area. This is called wettability. The potential wettability of a substrate is indicated by the contact angle which is the angle the liquid makes on a solid interface as explained in Section 2.8.1. A lower contact angle is associated with increased wettability. Wettability is dependent on the solid surface (tension) free energy which must be high enough to ensure that the bitumen spreads easily over the surface of the aggregate. The resultant adhesion should generally exceed the cohesion of the bitumen, to avoid ravelling failure. Poor wettability can be caused by premature coalescence occurring away from the emulsion-aggregate interface or presence of water or dust at the interface.

g) Granulometry: The granulometry of an emulsion can be characterised as a function of mass, volume and surface of droplets, though the mean average size is the most commonly used definition (Al-Mohammedawi and Mollenhauer, 2022). Emulsions are classified into two types, based on droplet size, macro-

emulsions and micro-emulsions. Macro-emulsions have particle sizes measurable in micrometres (μm), and are thermodynamically unstable whereas micro-emulsions are in the size range of nanometres (nm) and are characterised by thermodynamic stability. Additionally, the droplet size also influences the emulsion's rheological characteristics as explained in Section 2.10.

2.9.4 Modification of bitumen emulsion

Bitumen emulsions have a limited application range as not all (emulsions) meet requirements for particular applications (Lesueur, 2011). Factors like traffic volume, deflection bowls, crack activity and environmental conditions may preclude the use of conventional bitumen emulsions (TRH7, 1994). Al-Mohammedawi and Mollenhauer (2022) add that low early mechanical performances, such as low bearing capacity and adhesion, are some of the main obstacles that stands against the vast usage of bitumen emulsions. There is a continuing need for improvements in bituminous emulsions and for optimizing compositions for various applications (Franklin and Zhou, 2018). As such, bitumen emulsion may be modified to improve its performance and meet specific requirements for its intended use and the environment in which it is to be used. The modification is done to improve the emulsion's properties during storage, shipping and application. Through the years, several additives have been developed as modifiers to bitumen emulsions. Murphy et al. (2019) identify some of them and their functions;

- Calcium chloride - reduce the osmosis of water into the bitumen and reduce the risk of an increase in viscosity during storage,
- Sodium tripolyphosphate - acts as a water "softener" and improves the emulsion quality,
- Bitumen peptizers - improve adhesion properties, promote smaller particles and reduce the risk of settlement and higher viscosities,
- Latex polymer modifications - improve the bitumen characteristics in terms of crack resistance at low temperatures or resistance against deformation and flow at high temperatures (the type of latex need to be compatible with the type of emulsion used with control of pH balances to ensure that latex is added successfully to the emulsion and create a stable mix),

- Fisher-Tropsch (FT) wax modifications - used to improve the bitumen characteristics in terms of low temperature crack propagation and high temperature deformation
- Emulsion thickeners - introduced to the mix to increase the viscosity to reduce emulsion run-off (these products could also negatively affect the breaking and adhesion of the emulsion), and
- Adhesion promoters - added to the bitumen or the emulsion to improve the adhesion characteristics of the emulsion – (similar restrictions in compactability as related to the addition of latex modifications apply).

2.10 Nano Modified Emulsion (NME)

The advent of nanotechnology means that nano-additives can now be incorporated into bitumen emulsions so that the bituminous residue obtained after curing behaves in the manner of nano-composites, which are generally more durable than unmodified residues. These additives can be incorporated into the bituminous emulsions during formulation, by post-addition of the additive into bituminous emulsions after the emulsions have been formed or by use of bitumen materials already modified with nano-additives (Franklin and Zhou, 2018).

For this study, CBE is modified with an organofunctional nanosilane through an emulsification process, at high shear to ensure even distribution throughout the emulsion (Jordaan and Steyn, 2021d). The organic group of the organofunctional silane reacts with a functional group of the bitumen emulsion to create a chemical bond between the emulsion and the nano-additive while the hydrolysable group is left free to bond with inorganic substrates such as soils/aggregates.

However, as was discussed in Section 2.8.1, not all silanes that form siloxane bonds are useful for consolidating soil/aggregates. Only tri- and tetra-functional silicon compounds can act as consolidants and of these, few have the correct balance of volatility and reactivity and are safe for the environment and soil/aggregate. In the same vein, not all nanosilanes react with bitumen emulsions to form a stable, low risk NME with a long shelf life and the desirable properties, usable for soil stabilisation. The nanosilane must be compatible with the bitumen emulsion for the two to attach firmly and achieve successful mixing and stability of NMEs. According to Jordaan and

Steyn (2021b), compatibility and short- or medium-term stability are influenced by basic properties such as the condition of materials. The authors submit that compatibility is achievable by pairing/modifying anionic or cationic emulsions with appropriate anionic or cationic nanosilane modifiers. Mkhize (2022) demonstrates this in Figure 2-15. It is shown that unstable, non-homogenous solutions are obtainable when an anionic nanosilane is used to modify a cationic bitumen emulsion and conversely, a cationic silane used to modify an anionic emulsion. Similar findings are reported by Qacha (2022).

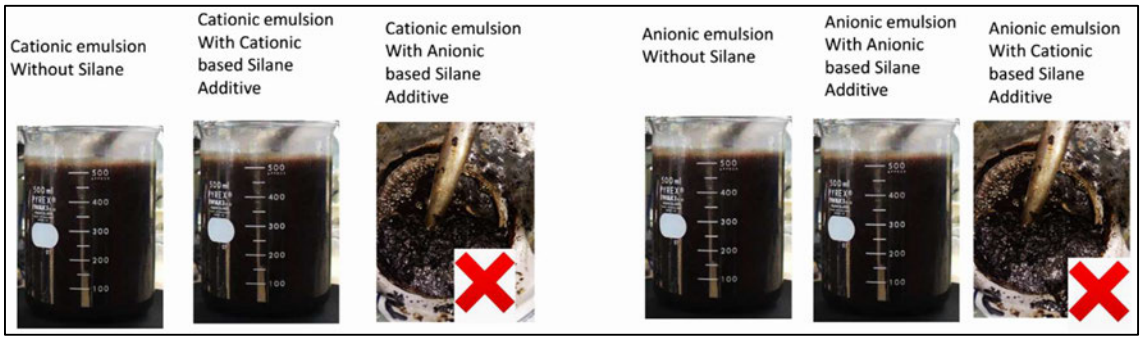

Figure 2-15: Stability of bitumen emulsions modified with silane nano-additives (Mkhize, 2022)

2.10.1 Properties

It was explained in the preceding section that the nanosilane is incorporated into the bitumen emulsion through an emulsification process. Thus, to produce the NME, the bitumen undergoes two emulsification processes. The bitumen droplets obtained from the first emulsification process are classified as macro-emulsions and are of sizes, 1-10 µm. They have relatively high surface tension characteristics and can almost be made out due to the effect of Van der Waal forces (Jordaan, 2019). Macro-emulsions are also considered to be thermodynamically unstable, have relatively high settlement and break down over time due to various physicochemical destabilizing factors including, gravitational separation, coalescence, flocculation, inversion and Ostwald ripening (Engmana et al. 2000; Solà, 2013; Aswathanarayan and Vittal, 2019; Kiihnl, 2020). The modification of the bitumen emulsion by the introduction of another emulsifier (nanosilane) in a second emulsification process results in increased concentration of the emulsifier and the further reduction of bitumen droplet sizes. Thus,

a bitumen emulsion with effectively separated nano-sized molecules is obtained (NME) (James, 2006; Jordaan, 2019; Yaacob et al. 2013).

The NME produced is characterised by thermodynamic metastability and kinetic stability. Due to the weaker attraction forces between the small sized bitumen droplets, there is no gravitational separation and droplet aggregation. Movement is governed by Brownian forces as demonstrated in Figure 2-16 (Jordaan and Steyn, 2021b). These unique qualities mean that the NME can be transported and stored for many months, a great advantage in the road construction industry.

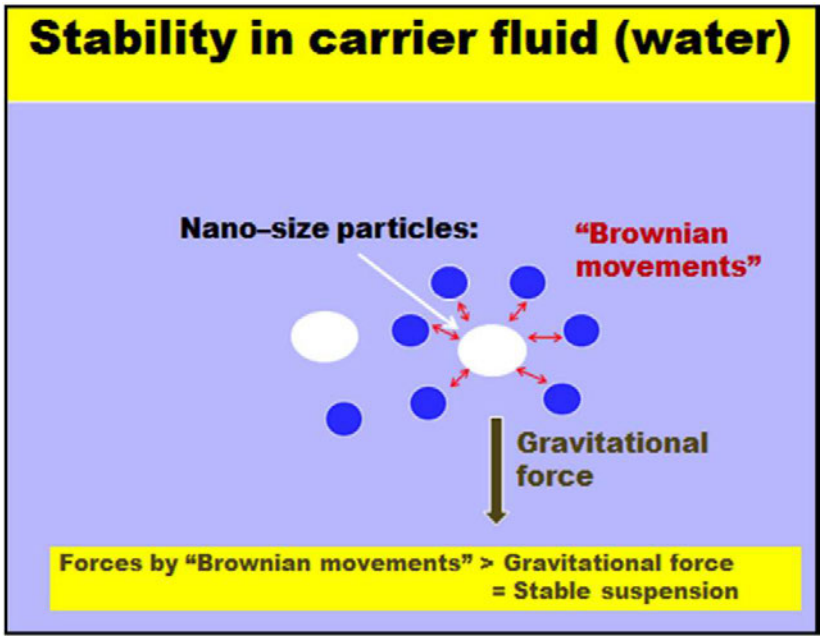

Figure 2-16: Demonstration of the stability of nano-scale technologies in a water carrier fluid (Jordaan and Steyn, 2021b)

The droplet size of NMEs also influences its rheological properties and release behaviour (Aswathanarayan and Vittal, 2019; Goodarzi and Zendehboudi, 2018). Engmana et al. (2000) show that emulsions with smaller average particle size have higher viscosities (Figure 2-17). The authors also explain that the size of the droplets directly affects their mobility towards the surface of the aggregate under the influence of the surface charge, since smaller particles move faster. Better penetration power in substrates is also expected with smaller bitumen droplets.

Thus, the distribution, coverage and consequently, stabilisation properties of bitumen emulsions are considerably enhanced by modification with organofunctional

nanosilanes. Due to the increased performance qualities, just a minimal amount of residue bitumen is needed to meet design strength requirements. The imparted hydrophobicity is aided by the encapsulation and immobilisation of finer particles of the material by the binder. Additionally, the organofunctional properties of the nanosilane promote the polar attraction between the emulsion and aggregates. Thus, the nanosilane acts as an adhesion promoter, enabling the increased adhesion of the residue bitumen with the aggregate during stabilisation.

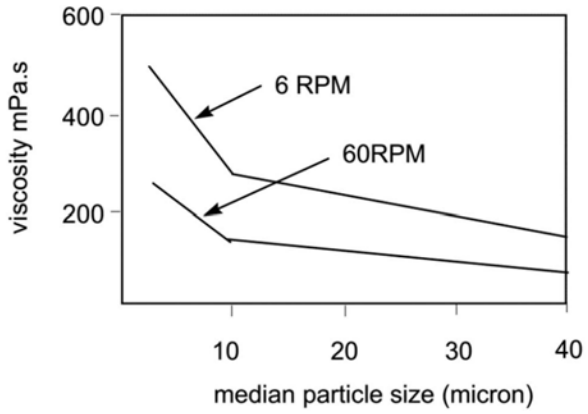

Figure 2-17: Effect of emulsion particle size on emulsion viscosity (Engmana et al. 2000)

2.11 Nano Modified Emulsions Stabilised Materials (NMESM)

NMESMs are composed of NME and aggregates/soil, with the latter making up the majority - more than 98%. The two ingredients have to be evaluated individually and optimally combined to produce a NMESM that provides reliable performance for specific application. Having discussed the properties of NMEs in the preceding sections, this section begins by addressing particular aggregate properties that have been proved to influence the engineering properties of the composite product. According to TG2 (2020), bituminous materials with less than 2% added binder behave in much the same way as granular materials, therefore, the properties of the aggregate/soils are expected to significantly influence the fundamental behaviour and performance of NMESMs.

2.11.1 Aggregate properties

Aggregate properties play a crucial role in interactions with binders. While the mineralogy of the aggregates and soils have been promulgated as the primary

consideration for determining the suitability for NME treatment (Jordaan et al. 2017b; Jordaan and Steyn, 2021a), other properties including material type, gradation and plasticity are equally important and form the basis for the different classification of NMESMs, as discussed in Section 2.11.6.

2.11.1.1 Material type

Based on SA standards, road construction materials are classified as G1 to G10 depending on the source, maximum aggregate size, relative compaction density, CBR and plasticity of fines, among other factors (TRH14, 1985). Therefore, reference to material type is mostly based on this classification. G1 to G3 are high quality materials sourced from crushing of rock and usually do not require stabilisation for use in pavement construction. G4 to G6 are natural, modified or processed gravels of medium to low quality and G7 to G10 are gravel soils of low quality. Gravels and gravel soils may require chemical or mechanical stabilisation depending on the particular application.

Current guidelines for BSMs restrict the use of the stabilisation technology to G5 and higher quality materials. NME stabilisation is targeted at lower quality materials (G5 to G7) (Jordaan and Kilian, 2016). These materials offer a comparative advantage as they are readily available at least cost as indicated in Figure 2-18.

2.11.1.2 Particle Size Distribution (PSD)

Generally, a refined continuous PSD targeted at providing the lowest Voids in the Mineral Aggregate (VMA) produces the most desirable mix properties of materials including, density and permeability requirements (TG2, 2020). For lower quality materials, TRH14 (1985) classifies the PSD requirements based on the Grading Modulus (GM). The GM gives an indication of the coarseness or fineness of a material based on a delineated scale of 3 (for coarse material) to 0 (for fine material) (Paige-Green, 1999). The GM of G5 to G7 materials range from 0.75 to 1.5 (TRH14, 1985). Rolt et al. (2020) submit that the GM is one of the most crucial elements for the functionality and effective performance of gravel roads.

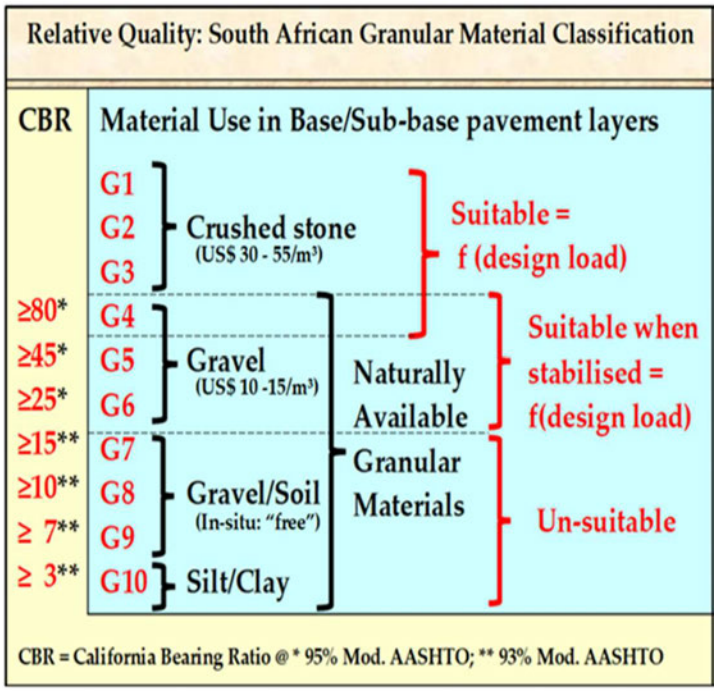

Figure 2-18: Typical material costs based on South African experience (Jordaan and Steyn, 2022)

An important consideration of the PSD of material is the quantity of filler (i.e. fraction passing the 0.075 mm sieve). The amount of filler has an impact of the achievable density, moisture sensitivity and permeability characteristics of the material. The filler also has an impact on how the materials react to moisture, and by extension, to colloid based binders. Fillers present a greater specific surface area than medium and coarse aggregates, leading to an increased demand for the binder needed for stabilisation.

2.11.1.3 Plasticity

Plasticity is one of the major concerns regarding use of naturally available (marginal quality) materials. The chemical decomposition of materials results in the release of secondary minerals (such as clays) which are associated with high plasticity, typified by a high Plasticity Index (PI). This leads to a reduction in the strength and bearing capacity of the materials. According to TG2 (2020) materials with a high PI (more than 6%) are not suitable for bituminous stabilisation.

Kidgell et al. (2019) studied the effectiveness of NME on the properties of dolomite, a material particularly prone to chemical weathering. Results show that application of up to 1.2% NME improved the properties of the dolomite by reducing the plasticity and

moisture sensitivity of the material. The PI of the material reduced by 90% and 85% for fractions passing the 0.425 mm and 0.075 mm sieves respectively, as shown in Figure 2-19.

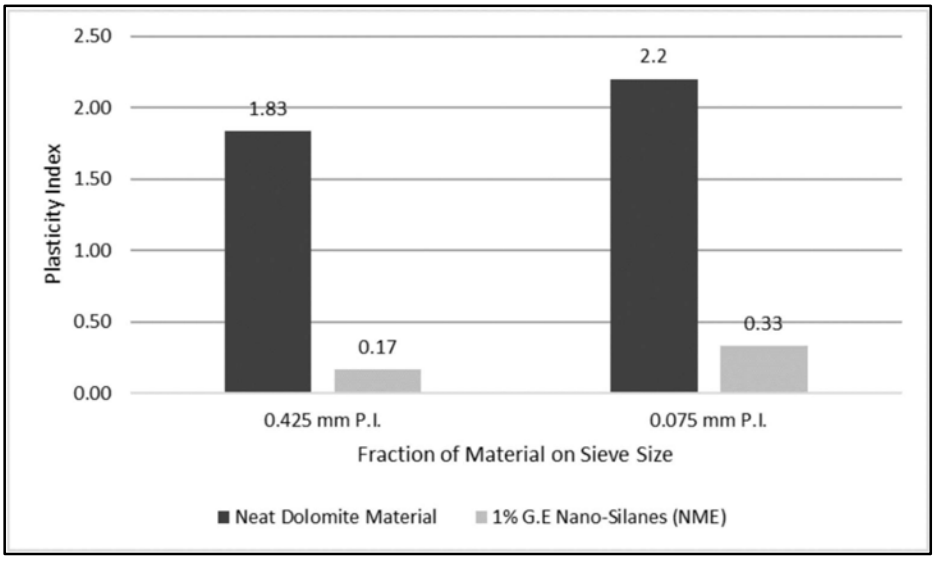

Figure 2-19: Effect of NME on PI of Dolomite (Kidgell et al., 2019)

Ugwu et al. (2013) also treated native materials labelled Mfamosing and Nru with nanomaterial diluted in water to ratios, 1:500 down to 1:150. Results obtained (Figure 2-20) show improvements in all the material properties with the PI reducing by as much as 74% at concentrations of 1:150.

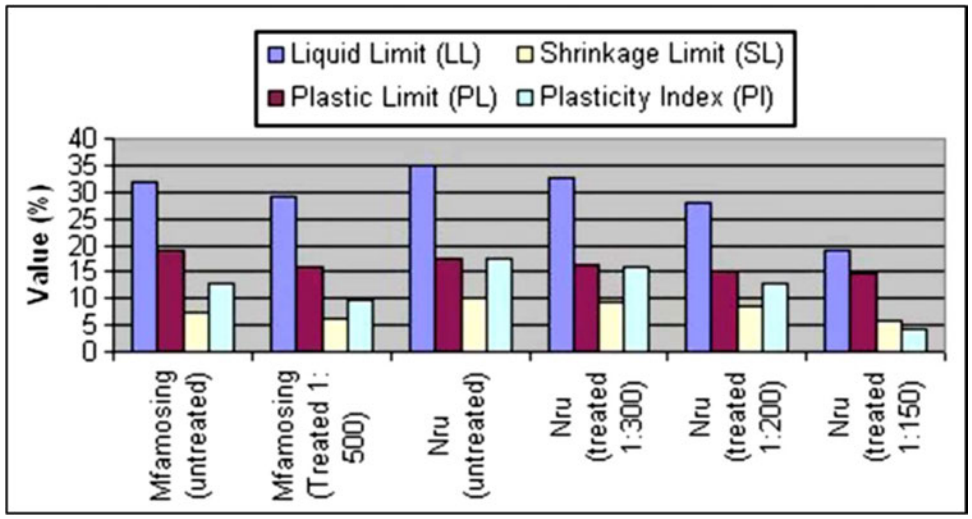

Figure 2-20: Atterberg limit tests for Mfamosing and Nru soils (Ugwu et al. 2013)

Another study by Ugwu et al. (2018), using an organosilane to stabilise an active soil at concentration ratios of up to 1:50 (with water), made the following observations; Increase of Plastic Limit (PL) by more than 15% and decreases of Liquid Limit (LL) by 24%, PI by 45%, Shrinkage Limit (SL) by 29% and Activity Index (AI) by 7.4%. Ugwu et al. (2018) attributed the findings to cation exchange reactions in the material, brought on by the organosilane, resulting in the flocculation and agglomeration of the clay particles, lowering the PI and the Optimum Moisture Content (OMC) because of the decrease in surface area.

2.11.1.4 Density

Density is probably the single most important property for the structural performance of materials. Aggregate shape and texture, PI, moisture content, PSD and compaction method are among factors that influence the achievable density. The introduction of a binder in the material might influence the density by affecting the frictional contact between particles or changing the material PSD. Kidgell et al.'s (2019) study of the effect of NME on dolomite showed that the OMC and Maximum Dry Density (MDD) of the material remain unaffected after stabilisation with up to 1.2% NME. This is in contrast to Ugwu et al.'s (2018) findings that the OMC is reduced. The difference between the two findings can be attributed to the different carrier fluids. Nonetheless, Kidgell et al. (2019) show that the NME reduces the sensitivity of the material to moisture changes as shown in Figure 2-21.

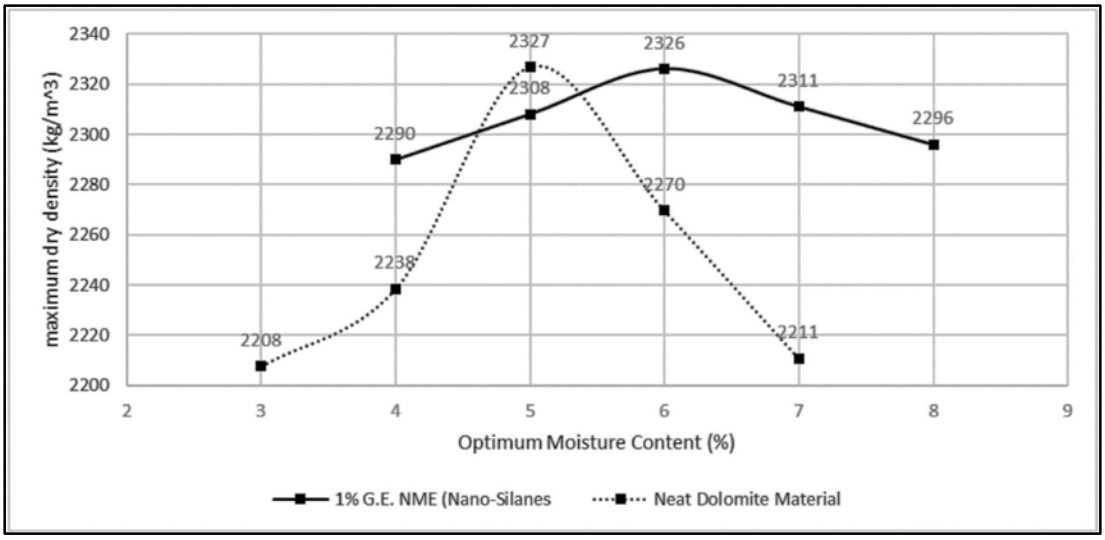

Figure 2-21: Effect of NME on MDD and OMC of Dolomite (Kidgell et al. 2019)

2.11.1.5 Surface free energy

Aggregates are composed of an assemblage of one or more minerals that have definite chemical compositions and order of atomic arrangement as discussed in the succeeding section. The arrangement of the minerals in the atomic lattice is such that each atom is bound by neighbouring atoms through electrostatic coordination bonds (Mitchell, 1993). When aggregates are crushed or cleaved in the quarry, during construction, or while in-service, some of these coordination bonds are broken, leaving new, unbalanced atoms at the surface. These (surface) atoms seek to repair the damaged coordination bonds by creating new ones, thus, a surface charge is created (surface free energy) (Tarrer and Wagh, 1991; Twagira, 2010). This surface free energy is responsible for the materials' surface adsorption and desorption characteristics and interactions with binders (during stabilisation), which in turn affects the strength and durability of soils and aggregates. Higher surface free energy is required to have strong attraction (adhesion) forces of the material.

2.11.1.6 Mineralogy

Figure 2-22 shows some of the most common rock-forming minerals. It is observed that Silicon (Si) and Oxygen (O) elements occur abundantly in most of the minerals. In fact, the earth's crust is composed mostly of these two elements (accounting for more than 74 percent), largely in the form of silica (SiO_2). Hence, materials are generally categorised as silicate and non-silicate materials (Jordaan and Steyn, 2021a; Twagira, 2010; Wheeler, 2005). Minerals such as quartz, feldspar, mica, amphibole, pyroxene and olivine are all examples of silicate minerals. These are characteristic components of igneous and certain metamorphic rocks and the rocks composed of these minerals are called crystalline rocks. With the exception of quartz, these minerals are susceptible to decomposition i.e. they may undergo chemical weathering and give rise to the development of secondary minerals, particularly clay (Weinert, 1980).

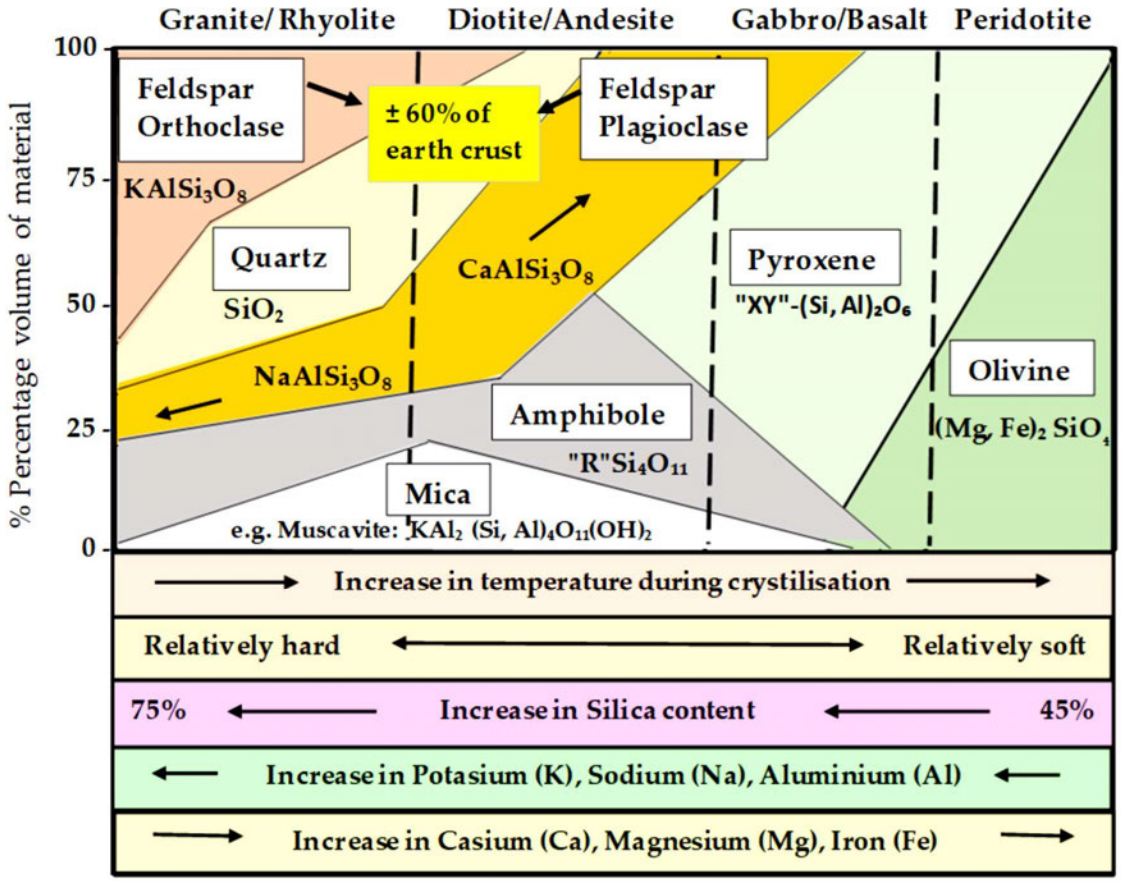

Figure 2-22: Chemical composition and mineral content of aggregates (Jordaan and Steyn, 2021a)

The building block of silicate minerals is the silica tetrahedron shown in Figure 2-23. The silica tetrahedron is a combination of four oxygen atoms and one silicon atom that form a four-sided pyramid shape with O at each corner and Si in the middle. These tetrahedra are arranged and linked together in a variety of ways, from single units to chains, rings and more complex frameworks. The bonds in a silica tetrahedron have some of the properties of covalent bonds and some of the properties of ionic bonds. The hardness of quartz and the fact that it breaks irregularly and not along smooth planes result from the strong covalent/ionic bonds characteristic of the silica tetrahedron (Klein and Hurlbut, 1993).

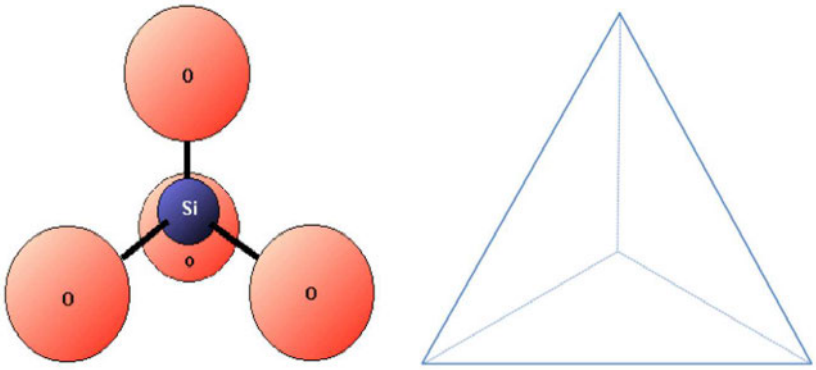

Figure 2-23: The Silica Tetrahedron (McGoldrick, 2020)

When a silicate-based aggregate is fractured, unsatisfied charges are created on the surface as illustrated in Figure 2-24. When water adsorbs, a hydration process occurs and H_2O is dissociated into H^+ and OH^- in response to the unsatisfied charges (Twagira, 2010). The H^+ and OH^- attach themselves to the aggregate and OH groups are created on the surface of aggregate. These OH groups are available to hydrogen bond with oligomers of silanes (or other agents) as explained in Section 2.8.

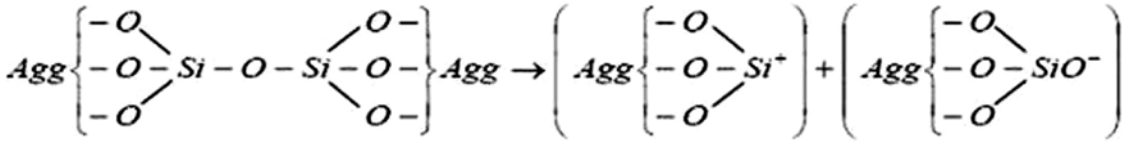

Figure 2-24: Elemental composition and break up of silicate mineral (agg – bulk aggregate structure) (Twagira, 2010)

2.11.2 Compatibility

The preceding section highlights factors that affect the interactions between binders and aggregates. It follows therefore, that not all aggregates and soil materials have the right conditions required for stabilisation with NME. The two media have to be compatible to produce a composite product with the required benefits.

Section 2.8.1 discusses a number of reasons why only a few nanosilanes are able to function as soil/aggregate consolidants. Arkles (2006) and Jordaan and Steyn (2021b) extend the discussion by explaining that some nanosilanes can only react effectively with soils with large quantities of silica and appropriate surface free energies. This is necessary to form strong and significant number of Si-O-Si bonds. In this regard,

Arkles (2006) delineates substrates in order of their recipiency for silane modification in Figure 2-25.

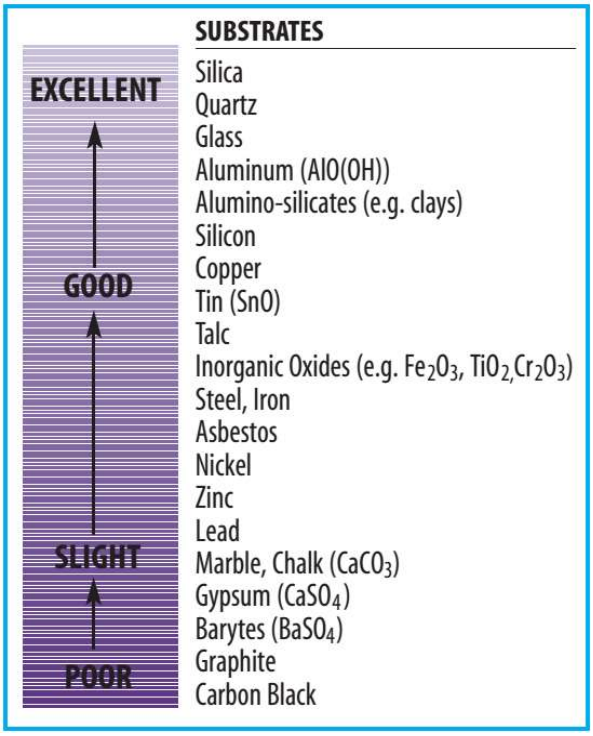

Figure 2-25: Silane effectiveness on Inorganics (Arkles, 2006)

Another consideration for compatibility between nanosilanes and soils is the type and concentration of OH groups, which vary widely depending on soil type. Some soil types have few OH groups with which silanes can react quickly to form bonds. For instance, the reaction of MTMOS with calcite is so slow that most of the MTMOS ends up evaporating (Arkles, 2006; Wheeler, 2005). However, Weiss et al. (2000) explains that it is possible to chemically change the surface of some soils to produce more OH groups via a procedure known as Hydroxy Conversion Treatment (HCT), enabling the production of siloxane linkages. However, this is not part of the scope of the current work. Additionally, Arkles (2006) explains that hydrogen bonded vicinal silanols react more readily with silane compared to isolated or free OH groups.

The bond formed between the soil and the nanosilane has to be hydrolytically stable to be effective. Some bonds are susceptible to chemical decomposition in the presence of significant amounts of physically adsorbed water (Arkles, 2006). This leads to loss of durability of the material and is undesirable especially for gravel roads.

Silanes have a penchant for materials with corresponding pH conditions. This has been documented since the early 1900s when Laurie (1926) observed that the application of silicic-ester to an acidic material resulted in the formation of preservative layer within the pores and on the surface. However, the opposite occurred with an alkaline-stratum, forming a soft gelatinous precipitate, useless as a preservative layer. According to Ignatavicius et al. (2021), materials with high silica content are considered acidic (low pH) while materials with high carbonate and metallic oxide contents are alkaline (high pH).

Ignatavicius et al. (2021) reports that a premise was put forward in 1950s that aggregates possess surface charges, such that acidic aggregates generally possess an electro-negative charge while basic aggregates have an electro-positive charge. Based on this premise, bitumen emulsions, cationic or anionic, have been rationally intuited to be best suited for stabilisation of aggregates and soils of opposite electro surface charge. However, this premise has been disputed by some researchers including, Dybaiski (1976) who argued that all aggregates have negative surface charges. Therefore, the adsorption and breaking of emulsions on aggregates is influenced by other factors including evaporation and mechanical action of compaction or traffic. Plotnikova (1993) also points out that the adsorption rates of cationic and anionic emulsifiers onto wet or dry aggregates are different. Ignatavicius et al., (2021) submit that this could explain why slow set (stable grade) anionic bitumen emulsions are almost exclusively used for stabilisation of all material types in SA.

The state or condition of the soil/aggregate is another consideration with regard to compatibility. According to Jordaan and Steyn (2021b), the presence of secondary minerals produced as a result of chemical weathering and decomposition, can be used to quantify the condition of the soil. Secondary minerals have detrimental effects when used for road construction in an unstabilised state and react adversely with particular stabilising agents. Therefore, the identification of these (secondary) minerals is a necessary step in the design process to aid the selection and quantification of appropriate nanosilane modifiers that work to neutralise and/or counteract their negative effects. Jordaan and Steyn (2019) identify some of these (secondary) minerals;

- Clay minerals such as smectite (e.g. montmorillonite), kaolinite, illite, etc., Clay minerals often cause difficulties in construction due to their low strength and stiffness and tendency to soften and liquefy in the presence of water. The crystals of clay particles are smaller than 1 nm in size and the amount of clay in the percentage of sample passing the 0.075 mm sieve can be crucial to the amount of nanosilane required to effectively protect against the negative impact of these minerals.
- Mica minerals (e.g. muscovite) - present in most metamorphic, sedimentary or igneous rocks such as granites, shales, etc. Free mica (especially muscovite) tend to absorb and retain water, resulting in heaving and rutting failures. Miskovsky (2004) also claims that mica absorbs low molecular bitumen phases resulting in the rapid ageing of bitumen while Mshali and Viser (2014) demonstrate that, stabilisation with cement causes significant decrease in material strength.
- Others include calcretes, sulphide and iron minerals, soluble salts and organic materials.

2.11.2.1 Mineralogy Testing

The preceding section highlights the need to identify primary and secondary minerals contained in materials. Jordaan et al. (2017a) state that this is necessary to optimise design aspects with regard to the chemical interaction of the binder with the various mineral components of materials. Various methods exist for the determination of mineralogy of materials, broadly classified under the following categories (Jordaan et al. 2017a; Platypus, 2022);

- Microscopic analyses: Microscopes employ a variety of techniques to generate magnified images of objects and surfaces. Optical microscopes produce a magnified image with visible light by employing a combination of lenses and mirrors. Electron microscopes use beams of electrons instead of light beams to conduct material characterisation. Other varieties of microscopies include, Atomic Force Microscopy (AFM), Ultraviolet (UV) Microscopy, X-Ray Microscopy and Scanning Electron Microscope (SEM).
- Spectroscopy: Spectroscopy is the investigation and measurement of response produced by material to electromagnetic radiation. Depending on the chosen

technique, material characterization can be determined by the measurement of absorption, emission, impedance or reflection of incident energy by a sample. Some of the most commonly used techniques for spectroscopy include infrared (IR) spectroscopy, nuclear magnetic resonance spectroscopy (NMR), Raman spectroscopy and X-Ray Diffraction spectroscopy (XRD).

The XRD and Scanning Electron Microscope (SEM) are discussed here because they are pertinent to this study.

XRD uses x-ray radiation to identify minerals, measure crystallite size, determine thicknesses of atomic layers, recognise deformation of crystals and other phenomena of crystalline organic and inorganic samples. The x-rays are diffracted in a pattern determined by the position, arrangement, and size of the constituents of the crystal. Scattered photons lead to a characteristic diffraction pattern, which is specific to the crystalline powder and may serve as its fingerprint, allowing it to be defined (Tamiri and Zitrin, 2013).

A SEM projects a focused stream of electrons over a surface to produce detailed, magnified images of an object. The electrons in the beam interact with the sample, thereby producing various signals that can be used to obtain information about the surface's topography and features. In combination with the Energy-Dispersive X-Ray Spectroscopy (EDX), it also provides detailed elemental analysis that can be targeted at particular points on the magnified sample image (Kambole, 2018).

2.11.3 Mixing procedure

The mix design process of bituminous materials requires the optimisation of compatibility, volumetrics and workability (TG2, 2020). The optimisation of volumetrics and workability is critical to ensure the proper construction and performance of materials. Factors such as void volume and binder content are important in this regard. The determination of compatibility between the two materials, NME and aggregate, is achieved by conducting XRD tests to determine the primary and secondary minerals in the material as explained in the preceding sections. Jordaan and Steyn (2019) explain that primary minerals are determined by testing the bulk sample of the material while secondary minerals are identified by testing of the fraction of material passing the 0.075 mm sieve.

Figure 2-26 shows the discrimination of materials as silicate and non-silicate based on the primary minerals contained therein, while the combined quantity of secondary minerals determines the particle size of the NME. The quantity of NME needed for stabilisation, in the second step, is determined by the quantity of the fraction passing the 0.075 mm sieve and the secondary minerals contained therein, as exemplified in Section 4.4. Evaluation of engineering properties and durability is then used to optimise material constituents by checking for compliance with set requirements.

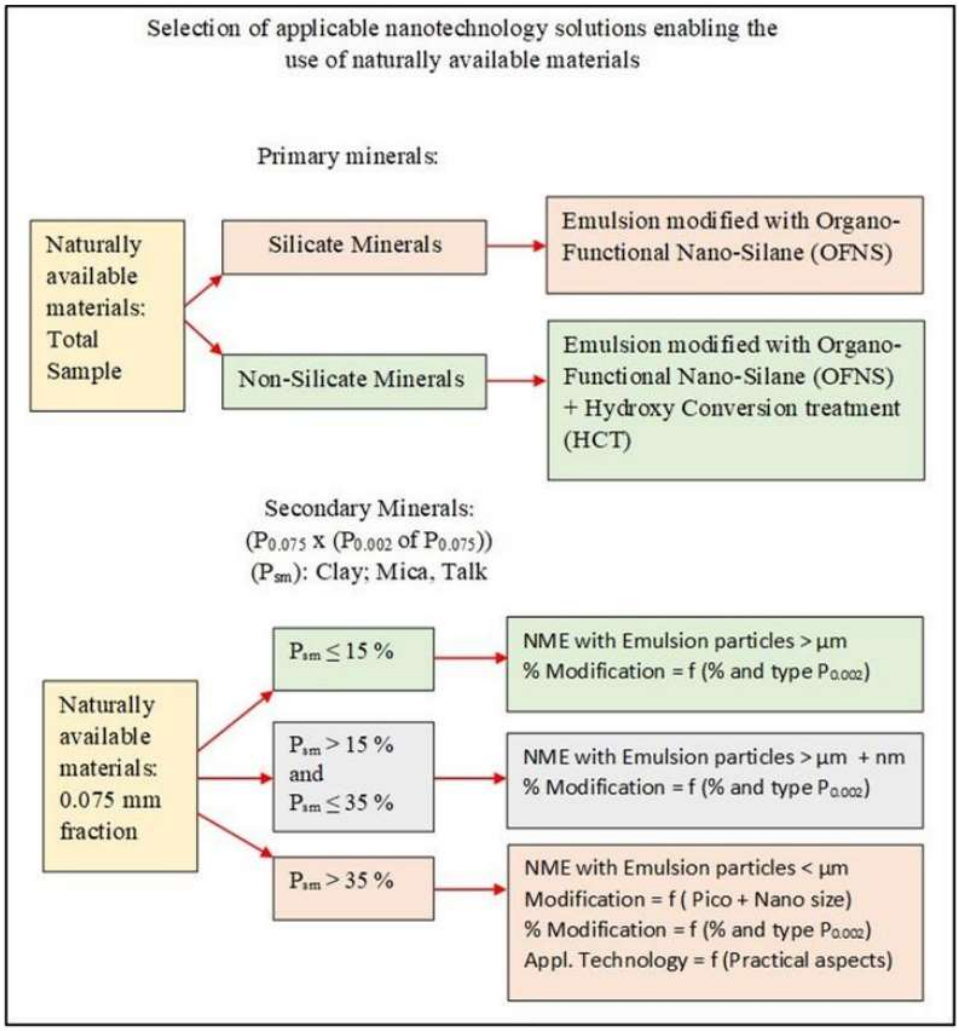

Figure 2-26: Input to the selection of a material compatible NME (Jordaan and Steyn, 2021a)

2.11.4 Characteristic behaviour of NMESMs

NMESMs are differentiated from BSMs by the lack of active filler in the mix. According to TG2 (2020), the purpose of incorporating active fillers in BSMs is to:

- Improve adhesion of the bitumen to the aggregate,
- Improve dispersion of the bitumen in the mix,
- Modify the plasticity of the natural materials (reduce PI),
- Increase the stiffness of the mix and rate of strength gain,
- Accelerate curing of the compacted mix.

Organofunctional nanosilanes in NMEs have been reported to perform similar functions. The organofunctional purpose promotes adhesion between the residue bitumen and the aggregate while the nano-size improves the dispersion of the NME. It has also been shown that the NME reduces the plasticity of soils, thereby reducing the effect of moisture variations. The siloxane bonds formed with aggregates are also expected to improve the stiffness and strength of NMESMs. Therefore, NMESMs are expected to behave in a manner comparable to BSMs in most respects. Figure 2-27 depicts the position of NMESM in relation to other pavement materials.

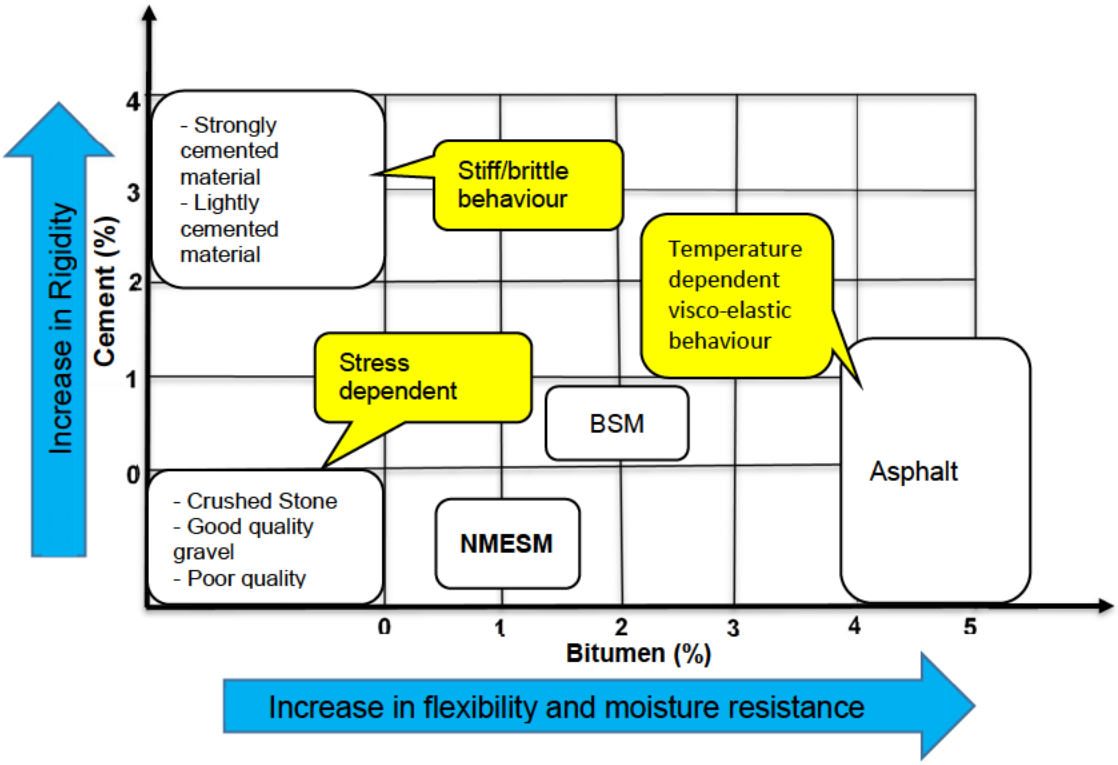

Figure 2-27: Conceptual behaviour of NMESM (modified from TG2, 2020)

It has been demonstrated for bituminous stabilisation that the binder disperses among the fine particles, immobilizing them and creating a bitumen-rich mortar between the coarse particles. The action of the bitumen residue and the hydrophobicity of the

siloxane bonds in NME are expected to combine to prevent moisture from accessing the fines, reducing chances of secondary chemical weathering and moisture damage to the material. The bound fines also reduce chances of pumping failure when subjected to load under saturated conditions. Additionally, according to TG2, (2020), bituminous materials are relatively thermally insensitive due to the non-continuity of the bitumen phase.

The stiffness of NMESM is expected to be stress dependent and deformation rather than fatigue cracking should be the primary mode of failure. The stiffness of NMESM is likely to be much less than BSMs due to the action and quantity of the filler in the latter. Nonetheless, similar to BSMs, the stiffness of NMESM is expected to be influenced by (TG2, 2020);

- The inherent quality of the untreated material.
- The density of the material in the layer (a function of packing).
- The dispersion of the binder throughout the mixed material.
- The local climate,
- The stiffness of the underlying support.

2.11.5 Engineering evaluation

The development and introduction of new materials for road construction requires that the materials are adequately defined in terms of behaviour and engineering properties. Several practical tests exist for the engineering evaluation of NMESM. Most are based on empirical derivations and only provide indicative material behaviours. Nonetheless, these tests find extensive usage in practice due to availability and lower associated costs. Coupling these with fundamental tests such as triaxial testing (i.e. resilient modulus, permanent deformation, and shear property) augments evidence of the material behavioural traits (Twagira, 2010). These tests are even more essential as they provide input parameters for mechanistic design techniques. UP (n.d) provides an example of the required definition of materials for incorporation in the SA Mechanistic Design Method (SAMDM);

- The behaviour of the material should be properly defined in terms of resilience, strength and performance characteristics.

- Representative input parameters should be defined, representing behavioural pattern and failure mechanism
- Performance model should be developed, relating calculated stress or strain condition to structural performance and terminal condition level.

The next few sections discuss laboratory-based tests available for evaluating bituminous materials particularly pertinent to this study.

2.11.5.1 Permeability

Permeability is one of the critical factors that influence the performance and durability of gravel roads. It is defined by SABITA (2014) as a measure of the penetration of the material by air, water or water vapour. According to Saha and Ksabaiti (2017), permeability (also called hydraulic conductivity) is one of the primary causes of deterioration of gravel roads due to stagnation of water on the surface as the road loses shape. The stagnant water ingresses the wearing course to the underlying road layers, compromising their strength and bearing capacity, leading to various distresses including deformation and potholes. A study by Qacha (2022) found that NME can reduce the permeability of material by more than 220%. Alsharef et al. (2016) and Liu et al. (2021) report similar results with different nanomaterials. However, due to the differences in carrier fluids of the nanomaterials and methods of test used, this property remains worthy of further investigations.

2.11.5.2 California Bearing Ratio (CBR) and Laboratory DCP-DN

The laboratory test for CBR was developed in the early 1930's for the testing of material strengths in the laboratory for the design of pavements. Most early pavement design procedures are based on the CBR method where the CBR values of the subgrade and structural layers are used to determine the required thickness of imported necessary material (Paige-Green and Du Plessis, 2009). This test remains relevant today for differentiation of different material classes and selection and design of unbound material layers as provided for in various technical guidelines (SATCC, 1998; TRH4, 1996).

The DCP is a hand-operated tool that has been an important part of pavement evaluation for many years. The test is simple, almost non-destructive and inexpensive.

It was standardised in the 1970s and guidelines for its interpretation and application included in the national code of practice on pavement rehabilitation investigation and design (Netterberg, 2018; TRH 12, 1997). Previous use for pavement design was based on various correlation models with CBR and other pavement strength parameters. The test has since been developed into a full-fledged method for the structural design of Low Volume Roads (LVRs) that avoids the use of correlations by utilising the cone penetration rate (DN value) directly as a design parameter (ReCAP, 2023). A laboratory version of the test is used for the evaluation and classification of laboratory compacted materials through the procedure detailed in Section 3.4.1.

No tests for CBR and DCP-DN for NMESMs could be found in the literature. However, the NDPS (TRH24, 2022) proposes limiting values for these properties, most likely based on comparable material test findings.

2.11.5.3 Tensile and compressive strength

UCS and ITS tests are proposed for compressive strength and tensile strength respectively, of NMESMs and durability using standard test procedures for the measurement of MDR (Jordaan and Steyn, 2019). Numerous researchers have employed these tests for evaluating NMESMs. Jordaan et al. (2017a, 2017b), Akhalwaya and Rust (2018), Kidgell et al. (2019), Rust et al. (2019, 2020) and Murphy et al. (2019), all report improved material strengths of more than 15% based on UCS and ITS tests. Jordaan and Steyn (2021b) compared results of stabilising a G8 material with NME and regular BSM (bitumen emulsion at 1.5% and cement at 1%) and reported UCS results of NME stabilisation to be within 80% of BSM results while the ITS results of NME were more than 70% of BSM's. Qacha (2022) investigated the effect of adding an active filler (hydrated lime) to NMESMs and reported another intriguing result. ITS results showed that lime additive does not increase the strength of NMESMs; on the contrary, increased lime content had the reverse effect of decreasing the strength of the material. Similar findings are reported by Alireza et al. (2013), highlighted in Section 2.6.

These two test methods remain the most useful for practical applications, as indicator tests for initial evaluation, screening and optimisation of constituent materials before

deployment of fundamental testing such as STT. The two tests provide the best avenue for continual research to refine the NMESM specifications.

2.11.5.4 Static Triaxial Test

STT for shear strength provides a measure of the soil's resistance to deformation by continuous displacement of its individual soil particles. This resistance is influenced by material gradation, moisture and density, maximum particle size, amount and plasticity of fines, geometric properties and confining pressure (Mulusa, 2009). According to TG2 (2020), the shear strength of bituminous materials is influenced by two components; the cohesive strength, which is determined mainly by the mastic and the frictional strength provided by inter-particle contact. When compressed, the cohesive and frictional components together define the stiffness and shear strength of the material while when in tension, material particles are not in contact and the stiffness and shear strength are determined mainly by the cohesive element.

According to Jenkins et al. (2007), shear parameters, cohesion (C) and internal friction angle (φ), used to define the shear strength of materials, provide a point of reference to analyse relative damage resulting from repeated loading at lower stress states. The shear strength of material is defined using a Mohr-Coulomb failure criterion. According to the criterion, shear strength increases with increasing normal stress on the failure plane as indicated in Equation 2-1.

$$\tau_f = C + \sigma_f . tan\,\varphi \qquad \text{Equation 2-1}$$

Where;

τ_f = shear strength,

C = cohesion,

σ_f = major principal stress at failure, and

φ = angle of internal friction.

The stress conditions at which shear failure occurs can be represented by means of Mohr-Coulomb circles (Mohr Circles). A tangent line (represented by Equation 2-1) between two Mohr circles of stress, obtained from two STTs at different confining stresses, is used to approximate the failure of the material. A third test, conducted at

a different confining pressure, provides more reliability to define the tangent line. Shear parameters, C and φ, are as defined in Figure 2-28.

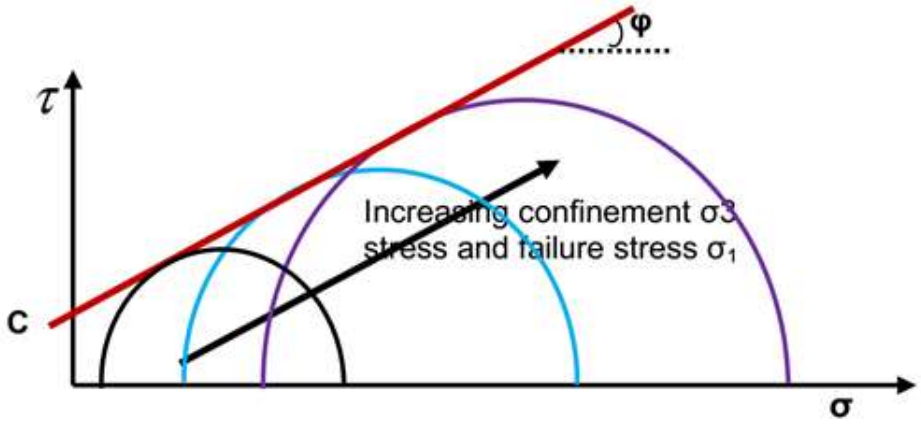

Figure 2-28: Mohr-Coulomb circles at failure and determination of shear parameters (Twagira, 2010)

The major principal stress at which failure occurs σ_{1f} is defined geometrically using a relationship between the failure parameters, C and φ, and the minor principal (confining) stress σ_3 as shown in Equation 2-2.

$$\sigma_{1f} = \frac{(1+sin\,\varphi).\sigma_3 + 2.C.cos\varphi}{(1-sin\quad)} \qquad \text{Equation 2-2}$$

Smit et al. (2021) conducted a study on the shear strength properties of NMESMs. A G5 material stabilised with 0.7% NME showed an increase in the cohesion parameter of more than 400% while the friction angle remained relatively unchanged as shown in Table 2-2. More studies are required to understand the shear strength properties of NMESMs and to develop limiting values, usable as input parameters in design of pavement structures.

Table 2-2: Static triaxial tests results (Smit et al. 2021)

	Cohesion C (kPa)	Friction angle φ (º)	Saturation (%)	Relative density (%)
Untreated	31.3	49.7	71	81
NME-treated	181	50.9	74	82

2.11.5.5 Resilient modulus and plastic strain

NMESMs are expected to behave in a manner comparable to granular materials and thus can be examined by their response to elastic and plastic deformations under repetitive loads. Figure 2-29 illustrates the typical material response, resilient and plastic strain (deformation) under loading and unloading cycles. The Resilient Modulus (M_R) defines the elastic properties of materials under dynamic (repetitive) loads, which is a key input parameter in pavement design systems. Plastic strain characterises the rutting potential of materials, the primary distress mode of granular materials layers (Jayakody et al., 2019).

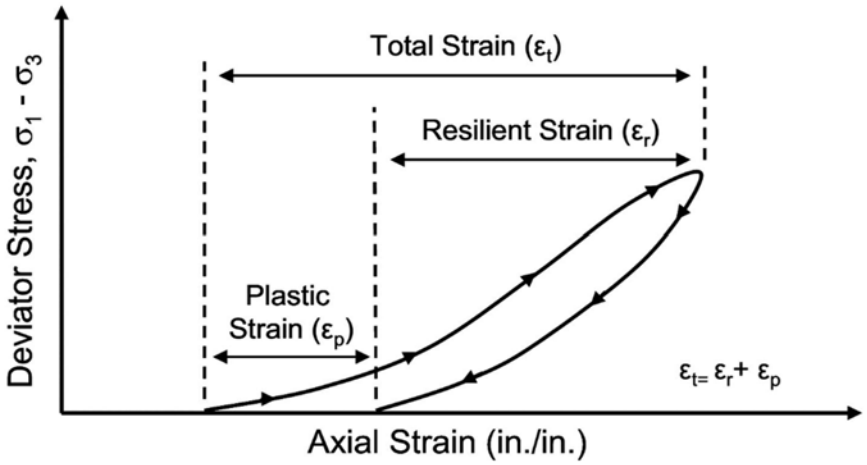

Figure 2-29: Typical material response during axial loading (Buchanan, 2007)

2.11.5.5a Resilient Modulus (M_R)

M_R is described as the ratio of applied deviator stress to recoverable or resilient strain. It is a measure of material stiffness, reflected by the deviator stress-resilient strain relation, which is typically nonlinear and stress-dependent in nature (Buchanan, 2007; Wang et al., 2022). M_R is used to characterise pavement materials under loading conditions that will not result in failure of the pavement system (Buchanan, 2007) and provides a better representation of the pavement behaviour under traffic loads and three-dimensional stress state (Sağlik and Gungor, 2012).

A number of factors affect the M_R of granular materials including, stress history, moisture content, density, aggregate properties (type, angularity, texture), gradation, and fines content (Ba et al.,2011; Ebels, 2008). Ekblad (2007) reports that greater M_R

values are obtained for aggregate specimens containing coarser particles compared to specimens containing finer particles. Equally, angular aggregates with rough surfaces exhibit a higher M_R than round aggregates with smooth surfaces (Barskale, 1989). Li et al. (2021) and Gu et al. (2020) also report that M_R increases with increased loading frequency and amplitude of deviator stress. According to Hicks and Monismith (1972), the single most primary factor influencing M_R is the state of stress. M_R can therefore be related to the confining pressure, σ_3, or to the bulk stress, θ. Generally, M_R increases with increase in stress. However, Ebels (2008) asserts that it is not uncommon for a material to exhibit the following phenomena concurrently:

- An increase in M_R (stiffening) with increasing confinement (σ_3) at constant deviator stress (σ_d) and
- A decrease in M_R (softening) with increasing deviator stress (σ_d) at a constant confinement (σ_3).

Since M_R is determined as a function of the stress condition, it is possible to fit models to allow the M_R to be predicted at any imposed stress condition within the tested range of stress conditions. Several models have been developed and are available that project the resilient behaviour of granular materials. Various researchers, including Jenkins (2000), van Niekerk (2002), Ebels (2008) and Qacha (2022) have demonstrated that the M_R models developed for granular material can also be used to describe the behaviour of bituminous materials such as NMESMs. Table 2-3 provides a summary of models considered in the current study. The models, developed by various researchers, estimate the M_R based on the influence of various factors including, bulk stress, confining and deviator stresses and principal and deviator stress ratios and regression constants, k_1, k_2, etc.

Table 2-3: Selected MR models

No.	Name	Formula	Source
1	M_R-θ	$M_R = k_1\theta^{k_2}$	Jenkins (2000), Ebels (2008)
2	Uzan Model	$M_R = k_1\theta^{k_2}{\sigma_d}^{k_3}$	Uzan (1985)
3	Universal	$M_R = k_1 P_a\left(\frac{\theta}{P_a}\right)^{k_2}\left(\frac{\tau_{oct}}{P_a}+1\right)^{k_3}$	Wang et al. (2022)
4	Superpave	$M_R = k_1 P_a\left(\frac{\theta-3k_4}{P_a}\right)^{k_2}\left(\frac{\tau_{oct}}{P_a}\right)^{k_3}$	Hopkins et al. (2001), Wang et al. (2022)
5	M_R-θ-σ_d/σ_{df}	$M_R = k_1\theta^{k_2}\left(1-k_3\left(\frac{\sigma_d}{\sigma_{df}}\right)^{k_4}\right)$	Jenkins (2000), Kotzé (2022)
6	Parabolic M_R-σ_3-σ_d	$M_R = k_1{\sigma_3}^{k_2}\left(k_3\left(\frac{\sigma_d}{\sigma_{df}}\right)^2+k_4\left(\frac{\sigma_d}{\sigma_{df}}\right)+k_5\right)$	van Niekerk (2002)
7	M_R-θ-σ_1/σ_{1f}	$M_R = k_1\theta^{k_2}\left(1-k_3\left(\frac{\sigma_1}{\sigma_{1f}}\right)^{k_4}\right)$	Jenkins (2000), Kotzé (2022)
8	TU Delft M_R-σ_3- σ_1/σ_{1f}	$M_R = k_1{\sigma_3}^{k_2}\left(1-k_3\left(\frac{\sigma_1}{\sigma_{1f}}\right)^{k_4}\right)$	Jenkins (2000), Kotzé (2022)
9	M_R-σ_3- σ_d/σ_{df}	$M_R = k_1{\sigma_3}^{k_2}\left(1-k_3\left(\frac{\sigma_d}{\sigma_{df}}\right)^{k_4}\right)$	Jenkins (2000), Kotzé (2022)

Where;

θ = bulk stress = $\sigma_1 + \sigma_2 + \sigma_3$

σ_3 = confining stress,

σ_{df} = deviator stress at failure

σ_d = deviator stress

P_a = atmospheric pressure (i.e. 100 kPa)

τ_{oct} = Octahedral shear stress $= \frac{1}{3}\sqrt{(\sigma_1-\sigma_2)^2+(\sigma_1-\sigma_3)^2+(\sigma_2-\sigma_3)^2}$

2.11.5.5b Plastic strain (ε_p)

ε_p or Permanent Deformation (PD) accumulated in base, subbase or subgrade layers contribute to surface rutting and deformation, which can result in functional and serviceability failure of a pavement (Puppala et al., 2005). ε_p is characterised for

granular materials using the triaxial set-up by means of repeated load applications for a controlled stress ratio. According to Puppala et al. (2005) and Jenkins et al. (2007), it is possible to determine ε_p from RLT tests for M_R; however, this is not accurate for most soils. Therefore, separate ε_p measurements are conducted for better characterisation of soils in flexible pavement design.

According to Jenkins et al. (2007), the accumulation of ε_p for most materials follow two model forms;

- Hyperbolic Linear (HL), which is applicable to ε_p results with a two-phase structure i.e. a primary phase at a fast rate followed by a secondary phase of stabilised deformation (either plateau or constant rate),
- Double Exponential (DE), which includes the same two phases as HL but is followed by third phase, the tertiary flow, defined by accelerated deformation.

The three phases typical of DE are depicted in Figure 2-30. Dal Ben (2014) explains that the primary phase, the accumulation of permanent deformation, occurs fairly quickly and is attributed to bedding-in, seating of the loading plates and densification. The secondary phase is characterised by a constant rate of deformation. The accumulation of permanent deformation is somewhat linear with respect to load repetitions. The tertiary phase is characterised by an accelerated accumulation of ε_p due to tertiary flow. The tertiary phase begins at a point called the flow-point and the material may be considered to be failing in shear under repeated loading. van Niekerk et al. (2000) provides a mathematical formulation, Equation 2-3, describing the DE model form;

$$\varepsilon_p = A.\left(\frac{N}{1000}\right)^B + C.\left(e^{D\frac{N}{1000}} - 1\right) \qquad \text{Equation 2-3}$$

Where;

N = Number of applied load cycles,

$A = a_1.\left(\frac{\sigma_1}{\sigma_{1.f}}\right)^{a_2}$; B= $b_1.\left(\frac{\sigma_1}{\sigma_{1.f}}\right)^{b_2}$; $C = c_1.\left(\frac{\sigma_1}{\sigma_{1.f}}\right)^{c_2}$; $D = d_1.\left(\frac{\sigma_1}{\sigma_{1.f}}\right)^{d_2}$

σ_1 = major principal stress,

$\sigma_{1,f}$ = major principal stress at failure,

$a_1, a_2, \ldots, d_2$ = model coefficients

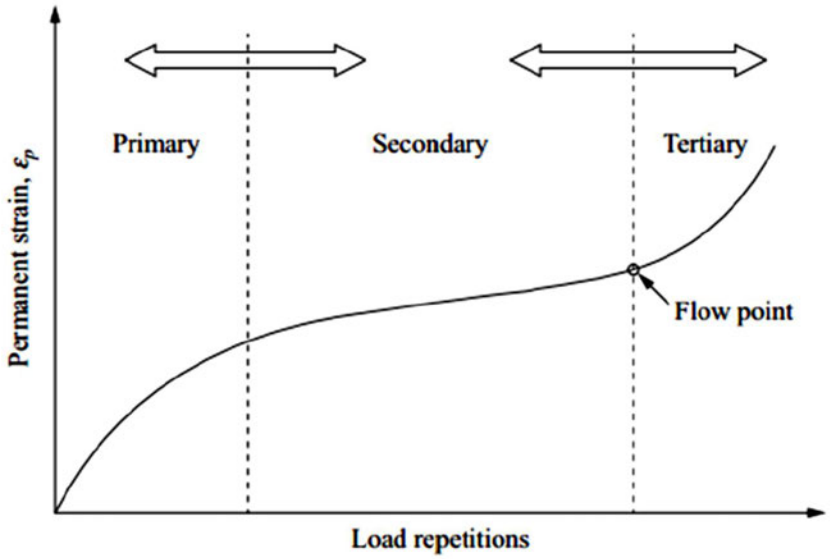

Figure 2-30: Typical material permanent deformation behaviour (Alzaidy and Albayati, 2021)

2.11.5.6 Susceptibility to moisture damage

The susceptibility of bituminous materials, including NMESMs, to moisture damage has been discussed. The MDR is a widely used approach for quantifying moisture damage to a material (Twagira, 2010). In this approach, moisture (wet) conditioned specimens are tested for the same parameters as dry specimens and the ratio of the wet to dry specimen is quantified as the retained strength of the material. Moisture conditioning simulates the detrimental effect of exposure of the material layer to moisture in the field. The appropriate period of exposure to moisture in the laboratory may be different for different materials, but it is agreeable that a longer period, subject to time and test constraints, is desirable. In this regard it is noted that standards specify up to twenty-four hours for BSMs (TG2, 2020) and four hours for NMESMs (TRH24, 2022).

2.11.6 Classification of NMESMs

Jordaan et al. (2017b) proposed material categories and specifications to aid testing and further studies on NMESMs. Five classes were proposed ranging from NME1 to NM-EG5 based on the inherent quality of the aggregate/soil and expected performance properties of the mix as shown in Table 2-4. Materials are classified based on traditional tests i.e. plasticity, grading and strength and the performance parameters are based on mechanical strength tests, DCP-DN, ITS and UCS. Limits of

elastic moduli are also provided, probably based on the performance limits of equivalent materials. The material categories are defined as follows;

i). NME1 - Highest quality naturally available materials - stabilised with a compatible NME. Suitable for use in upper layers of pavement structures capable of withstanding high axle loadings under conditions of high tyre pressures without durability problems. Can be compared to a typical G1 or C1 equivalent material,

ii). NME2 – High quality naturally available materials - stabilised with a compatible NME. Capable of withstanding relatively high traffic loadings and tyre pressures without durability problems; can be compared to a typical G2 or C2 equivalent material,

iii). NME3 – Medium quality naturally available materials - stabilised with a compatible NME. Capable of withstanding traffic loadings of medium impact. Can be compared to a typical G3 of C3 equivalent material,

iv). NME4 – Relatively low quality naturally available materials, normally rejected for use in pavement layers using current criteria - stabilised with a compatible NME. The NME stabilisation will enable these materials to be utilised successfully within the pavement structure, and

v). NM-EG5 – Lower quality material (quality less than that of a G5 material) - modified with a suitable NME to become water repellent and an improved bearing capacity of a minimum CBR of 45 at 95% Mod AASHTO. Usable as wearing course for gravel roads.

Akhalwaya and Rust (2018) recognise the need for more studies and tests to refine these material classes. The authors observed that results of tests conducted on particular materials sometimes fall in a class, different from what is defined in the proposed specifications. Additionally, the presumed material properties need to be verified and the limits of material performance characteristics need to be expanded to include fundamental property parameters.

Table 2-4: Classification of NMESMs (Jordaan et al., 2017b)

Test or Indicator	Material[1]	Material classification			
		NME1	NME2	NME3	NME4
Minimum material requirements before stabilisation and/or treatment (Natural materials)					
Material spec.(minimum) Unstabilised material: Soaked CBR (%) (Mod AASHTO)	NG /(CS)	> 45(95%) and ACV < 30% or 10% FACT >110 kN	>45 or >35 (95%) and ACV< 30% or 10% FACT >110 kN	> 25 (95%)	> 10 (93%)
Plasticity Index (PI)	CS	< 10	< 10	-	-
	NG	< 12	< 12	< 16	< 16
	GS	-	< 12	< 16	< 16
	SSSC	-	-	-	< 16
PI - 0.075 fraction (test when OMC >8% and/or % passing 0.075 mm sieve >10%)	CS	< 15	< 15	-	-
	NG	< 20	< 20	< 25	< 40
	GS	-	< 20	< 25	< 30
	SSSC	-	-	-	< 30
Grading modulus	NG	> 2.0 (G4 Grading)	> 1.5	> 1.2	> 0.45
	GS	-	>1.5	> 1.2	> 0.75
DCP DN (mm/blow) (Material compacted to spec. before stabilisation)		< 3.6	< 5.7	< 9.0	< 18.6
Material specifications after stabilisation and/or treatment					
Mod AASHTO density		> 100%	> 98%	> 97%	> 95 %
DCP DN (mm/blow) Material compacted to spec. (after stabilisation)		< 1.1	< 1.6	< 2.6	< 3.4
UCS (wet) (rapid curing method: 24h at ambient temp (30°C) + 48h at 40°C - 45°C + 24h cooling + 4h water soaking) (kPa)	150mm Φ Sample	> 2 000	> 1 200	> 700	> 450
UCS (dry) (rapid curing method: No soaking in water) (kPa)	150mm Φ Sample	> 2 500	> 1 700	> 1 000	> 750
ITS* (wet) (kPa) (rapid curing as per UCS method)	150mm Φ Sample	> 140	> 100	> 80	> 60
ITS* (dry) (kPa) (rapid curing as per UCS) (no soaking in water)	150mm Φ Sample	> 175	> 140	> 100	> 80
Retained Cohesion: ITS: Wet/Dry (%)	All	> 80	> 70	> 65	> 60
Typical Effective Elastic Moduli for pavement design (MPa)**		600 - 300	400 - 250	300 - 200	220 - 180

[1]CS – crushed stone; NG – natural gravel; GS – gravel soil, and SSSC – sand, silty sand, silt, clay.

2.11.7 Safety, Health and Environment (SHE)

Despite the obvious benefits of nanotechnology, concerns exist regarding how it may affect human life and the environment and whether the benefits outweigh the potential risks associated with the technology. Therefore, it is critical to understand the form and response of nanoparticles during service and after undergoing degradation so that

any undesirable effects can be addressed or avoided (Ray et al., 2009). For instance, Smita et al. (2010) point out that most of the engineered nanomaterials that are made up of carbon, silicon, metal or metal oxides are believed to adversely affect the environment and human health directly or indirectly.

The incorporation of nanomaterials in road construction brings about three major areas of concern (Steyn, 2009; Jordaan and Steyn, 2021b);

- Release of materials into airways (e.g. through the generation of dust on unpaved roads),
- Exposure to potentially harmful materials during construction and maintenance operations
- Leaching of materials and contamination of groundwater,

According to Jordaan and Steyn (2021b), two chemical processes are usually applicable with the use of nanosilanes in pavement engineering i.e., a process of hydrolysis when mixing with the carrying fluid (e.g., water) and condensation during construction, when the product attaches to the material during treatment or stabilisation. Some nanomaterials produce toxic by-products during the two processes, harmful to life forms and to the environment (Wheeler, 2005). For instance, silanes such as SiH_4 are toxic, volatile and generate hydrogen gas during hydrolysis as shown in Equation 2-4.

$$SiH_4 + 4H_2O \Rightarrow Si(OH)_4 + 4H_2 \qquad \text{Equation 2-4}$$

Tri- and tetra-functional chloro- and fluoro-silanes (silicon halides) form volatile and dangerous acids under hydrolysis, such as hydrochloric (Equation 2-5) and hydrofluoric acids (Equation 2-6) that are also detrimental to the various mineral groups of aggregates and are not suitable to be used as consolidants (Wheeler, 2005).

$$SiCl_4 + 4H_2O \Rightarrow Si(OH)_4 + 4HCL \qquad \text{Equation 2-5}$$

$$SiF_4 + 4H_2O \Rightarrow Si(OH)_4 + 4HF \qquad \text{Equation 2-6}$$

Jordaan and Steyn (2021b) also add that carbon (C), in combination with reactive groups containing chlorine (Cl), can produce chloroform ($CHCl_3$) as a by-product during hydrolysis or during the consolidation process. This is a volatile material that

quickly evaporates to gas and is typically difficult to detect. It is harmful and even fatal when applied in confined areas or under conditions with low or no wind-speeds. It is important that such products are excluded from use.

Organofunctional nanosilanes fit the bill of products suitable for material stabilisation because of their low vapour pressures and the fact that they do not produce toxic gases or acids during hydrolysis, but instead produce water as a by-product or, in the worst-case, a non-corrosive alcohol (Wheeler, 2005).

The benefits of employing bitumen emulsion as a carrier fluid in NME is outlined in TG2 (2020). Bitumen emulsion is regarded as a non-hazardous material, can be handled at considerably low temperatures and does not emit any significant fumes or vapour that could be harmful if inhaled by humans. Jordaan and Steyn (2021b) add that the functionality of the nanosilanes in NME as adhesion promoters ensures the firm attachment of the residue bitumen to the soil/aggregate through permanent bonds, preventing detachment and eliminating the risk of leaching or contamination.

2.12 Summary

This Chapter reviewed literature related to NME stabilisation of gravel materials for use in road construction. It is highlighted that various nanomaterials exist in nature and can be engineered for various purposes. One such material, organofunctional nanosilane (with sizes down to 5 nm), readily available in SA and worldwide, has been found useful for stabilisation of gravel material for use in road construction. The nanosilane is incorporated into conventional bitumen emulsion to produce NME. The potential of NME is premised on its capacity to improve performance of low-quality gravel materials, normally available near the site of construction, thus, reducing costs associated with hauling good quality material from distant places.

Various researchers have indicated the positive impact of NME on various low-quality materials, improving them to meet required specifications for use in pavement structural layers. The ability of the NMESMs to resist moisture damage is also exemplified by MDR, which accounts for loss in material strength after a specified period of exposure to water. It is also highlighted that the material is relatively safe, does not produce harmful by products and is not likely to contaminate the environment.

The need for further studies on the material has been recognised and include, the need for continued development of design standards and test protocols, the need to include advanced, fundamental testing methods to better characterise material behaviour and the need to build confidence in the efficacy of the material, which will lead to its adoption and greater usage.

3 EXPERIMENTAL DESIGN

3.1 Introduction

This Chapter provides the methodology implemented to achieve the objectives of the study. Proposed tests are based on material test procedures contained in relevant SA standards. The methodology begins by identifying and classifying the gravel material used, necessary to select a compatible Nano Modified Emulsion (NME). The mixes (NMESMs) are evaluated for engineering properties pertinent to performance prediction. The key steps of the methodology are shown in the schematic in Figure 3-1;

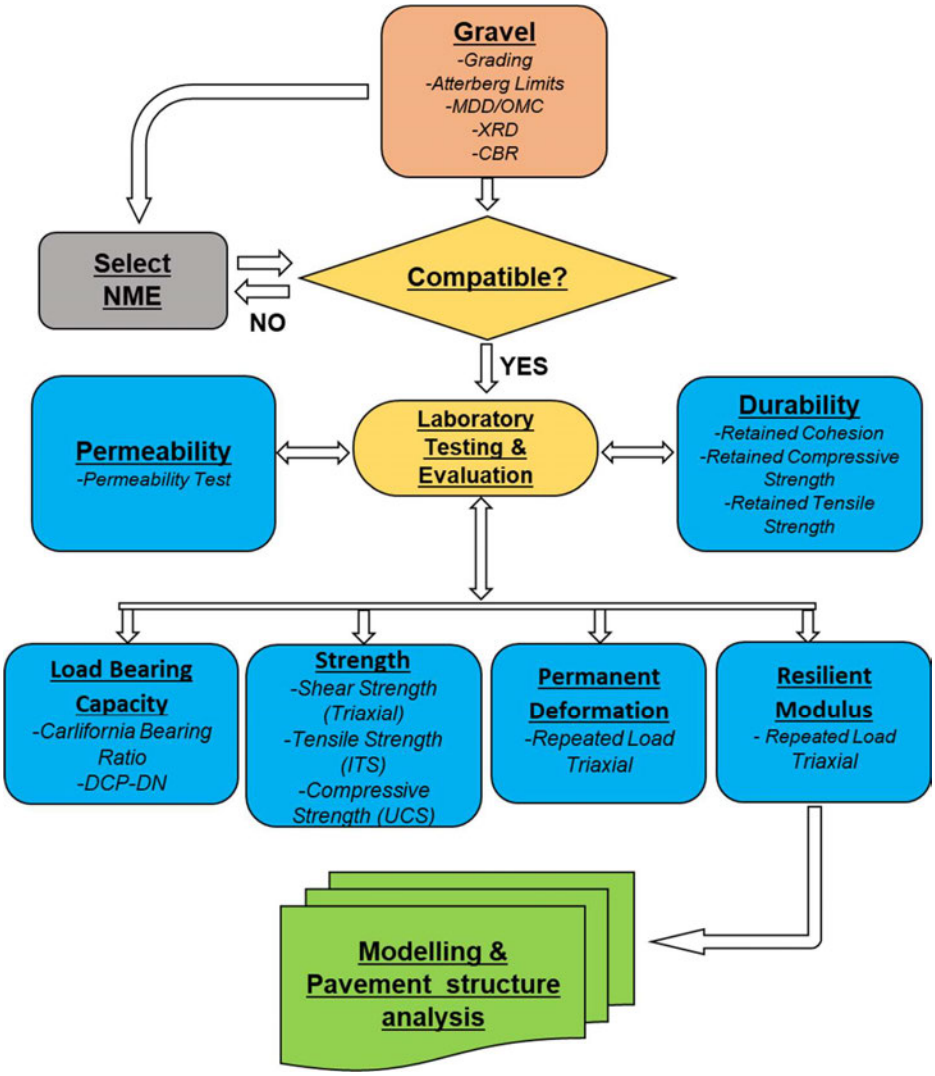

Figure 3-1: Research design process

3.2 Materials

3.2.1 Description

Table 3-1 provides the description and visual images of the two materials, the gravel and NME. The NME is a proprietary material provided by a local vendor while the gravel was obtained from Stockville Quarry in Pinetown, Eastern SA.

Table 3-1: Material description and source

	Gravel Material	Nano Modified Emulsion
Description	Weathered ferruginous granite	Thick milky brown colloid
Picture		

3.2.2 Characterisation of materials

3.2.2.1 Gravel Material

Classification tests conducted on the gravel material including motivation and standards used are itemised in Table 3-2. The XRD test, though not part of traditional material classification tests, is included and the principle of the test discussed in the succeeding Section. The results of the tests are given in Chapter 4.

Table 3-2: Material Characterisation tests

Test	**Objective**	**Test Method**
Grading	Tests to determine nature and class of material	TMH1 Method A1
Atterberg Limits		TMH1 Method A3
Max Dry Density		TMH1 Method A7
CBR		TMH1 Method A8
XRD Tests	Test to determine mineralogy of the material	-

3.2.2.1a XRD test description and procedure

Figure 3-2 depicts the principle method of the XRD test, explained by Chacha (2014); a fixed wavelength X-ray source is used to irradiate a powdered sample, producing a diffracted beam that is recorded with a detector as depicted in Figure 3-2. The angle and intensity of the diffracted beam forms a diffraction pattern, called a diffractogram, which provides information about the crystalline phases of the sample. Each crystalline phase has a unique diffraction pattern whose 'fingerprint' can be matched against a database of recorded phases. If parallel planes of atoms of a crystal are struck at the same angle, coherent (additive) intensity is detected and recorded as a peak.

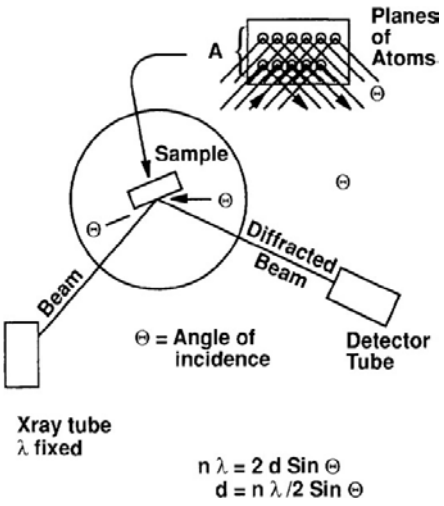

Figure 3-2: Principle of XRD (AAPG WIKI, 2014)

The procedure followed in conducting the test is outlined below;

1. A 500g representative sample of the gravel was collected and split into two as shown in Plate 3-1.

Plate 3-1: Sample splitting

2. One of the samples was sieved for the fraction passing the 0.075 mm sieve, while the other (bulk) sample was milled in a chrome steel milling pot

Plate 3-2: Sample sieving and milling

3. About 5 g of each of the two samples were then placed on zero background holders and prepared for XRD scanning (Plate 3-3).

Plate 3-3: Prepared specimen for XRD testing

4. The two samples were scanned and a Malvern Panalytical Aeris diffractometer with PIXcel detector was used to obtain the diffractogram. The X'Pert Highscore plus software was used to identify the phases in the scans.

3.2.2.2 NME

The NME used for this study is based on a SS60 anionic bitumen emulsion modified with a compatible organofunctional nanosilane. No chemical analysis tests were conducted on the NME, as it is a proprietary product bound by copyright ownership. However, the manufacturer provides a description of the chemical composition of the product; a water-based dispersion of a polyvinyl acetate homopolymer and a mixture of heavy hydrocarbons, high molecular weight organic compounds that are obtained from processing residue streams from the refining of Petroleum crude oils. Physical properties of the material are provided in Table 3-3.

Table 3-3: Physical Properties of the NME

Properties	**NME**
Appearance	Thick milky brown
Odour	Slight
pH	10 - 11
Density	1.01g/cm^3
Boiling Point	100 ºC
Specific gravity	> 1.0
Vapour pressure	As per water
Water solubility	Fully miscible
Environment	Environmentally friendly

3.3 Material mixing

3.3.1 Compatibility and determination of NME quantity

The method of determining the compatibility and quantity of NME required for stabilising a particular gravel material espoused by Jordaan and Steyn (2021a) was adopted. Figure 3-3 shows a flow chart that was used to quantify the NME required for stabilisation. The first input, the CBR of the gravel material is used to reference to traditional material classification tests. The second input is an adjustment based on the quantity of material passing the 0.075 mm sieve. The third and last input is the quantity of the secondary minerals present in the 0.075 mm sieve as determined from the XRD test. The quantity of NME for laboratory evaluation is selected depending on Zones 1, 2, 3A and 3B as exemplified in Section 4.4.

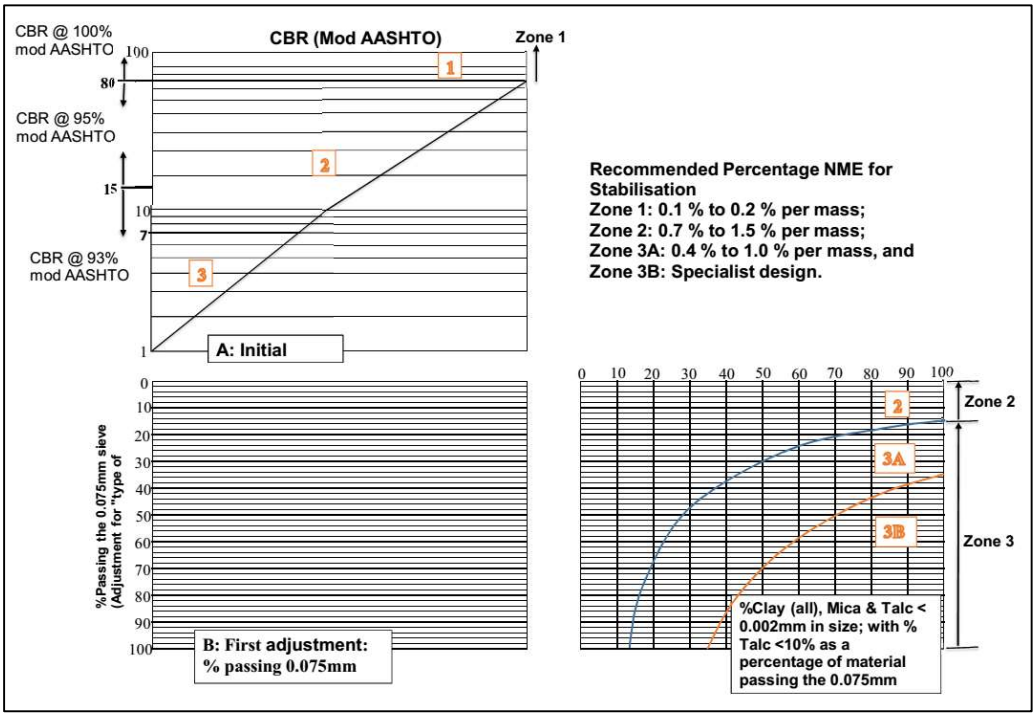

Figure 3-3: Material input information required for the selection of NME (Adapted from Jordaan and Steyn, 2021a)

3.3.2 Preparation of test specimens

The procedure for material preparation recommended in NDPS (TRH24, 2022) was followed in preparing specimens for evaluation. Mixing was achieved using a vertical shaft mixer, shown in Plate 3-4, as recommended by various standards including TG2 (2020). Relatively small material samples were mixed at a time, to ensure a shorter duration between mixing and compaction. Longer mixing times have been known to affect specimen quality by impairing bond formation during compaction.

The specimens were prepared at OMC and rapid cured using a forced draft oven. The NDPS proposes a curing period of 48 hours at ± 45 ℃ after an initial 24-hour settling period at 30 ℃. However, repeat tests with this procedure produced less than satisfactory results. It was determined that this curing period was not adequate to ensure sufficiently dry specimens as moisture content differences of up to 50% would be recorded when the curing period is extended by a further 24 hours. Greenwood and Norris (1999) assert that curing periods that do not allow sufficient time for drying can produce misleading results. Reeb and Milota (1999) also indicate that at low oven temperatures, the relative humidity of the ambient air may influence the relative

humidity in the oven, affecting the extent to which specimens in the oven dry and the equilibrium moisture content attained. Taking this into account, the procedure for production of test specimens set out, includes an adjustment to the material curing procedure as indicated in steps number 5 and 6 below;

Plate 3-4: Material mixing

1. The MDD and OMC of the material was determined according to TMH1 Method A7.

2. NME stabilised samples were prepared at OMC by mixing the NME with water. For example, if the OMC of the material determined in (1) is 5.8% and 0.7% of the NME stabiliser is to be added, then 5.1 per cent water (less the materials' hygroscopic moisture) is added to achieve OMC.

3. The NME was added to the water to ensure a good dispersion of the NME in the material.

4. Briquettes, such as those shown in Plate 3-5, were prepared depending on the tests to be conducted as indicated in Section 3.4.

5. Each briquette was weighed and placed in the oven for 24 hours at a temperature of 30 °C before being subjected to a rapid curing process for 48 hours at 45 °C. (Note: The temperature should not be allowed to exceed 50 °C as some polymers are known to degrade at such temperatures (Jordaan et al.,

2017b) and limiting the temperature (to < 50 °C) also ensures that excessive softening of the bitumen residue is avoided.

Plate 3-5: Briquettes prepared for ITS and UCS Tests

6. After 48 hours, each specimen was weighed to the nearest 1 g and returned in the oven. The specimens were reweighed after a further 4 hours in the oven. If the specimen weights differ by more than 10 g, the specimen were returned in the oven for a further 24 hours. This was repeated until there was a consistency in weight.

7. After the rapid curing, the temperature was reduced back to 30 °C to allow the samples to cool off for 24 hours.

8. Six briquettes were prepared for each test, with three tested in a dry state immediately after curing while the other three were tested after wet conditioning. Wet conditioning was done for a stipulated period (depending on the test) by submerging in water at 25 °C, ensuring the specimens are completely submerged by up to 25 mm of water.

3.4 Laboratory evaluation tests

3.4.1 Dynamic Cone Penetration (DCP-DN) Test

The DCP test is a non-destructive indicator test used in the assessment of pavement structures. The test is performed by driving a standard metal cone into the pavement by repeatedly striking it with an 8 kg weight dropped from a distance of 575 mm. The rate of penetration and change in the penetration rate of the cone into pavement layers is used to indicate layer thickness and to derive in-situ material strengths. This is an important test particularly for gravel roads due to its simplicity and relatively low cost.

A laboratory version of the test, DCP-DN, was used to determine the cone penetration rate of moulded, laboratory compacted specimens. The procedure of the test is similar to that of the CBR test except that a DCP cone is used instead of the CBR plunger as shown in Plate 3-6. The test was used to evaluate the strength characteristics and behavioural patterns of material stabilised with varying percentages of NME compared to an unstabilised, control specimen. The test specimens were cured, re-moulded and soaked in water for four days in the CBR mould, before testing according to the procedure detailed by Pinard et al. (2020), summarised below;

1. The CBR mould with the sample was placed on a level floor with the annular weight on top.

2. An empty CBR mould was placed upside down next to the full mould, as shown in Plate 3-6, to support the base of the DCP ruler.

3. The DCP cone was positioned in the middle of the CBR mould and held in a vertical position. It (DCP) was knocked down slightly until the top of the 3 mm shoulder of the cone was level with the top of the sample and the zero-reading recorded.

4. Two to three blows (depending on the material strength) were applied to the DCP and the reading on the ruler, recorded. This is continued until just before the tip of the cone touches the base plate in order to avoid blunting the cone.

5. The obtained data was analysed using the Laboratory Module of the ReCAP LVR DCP Software (a freeware).

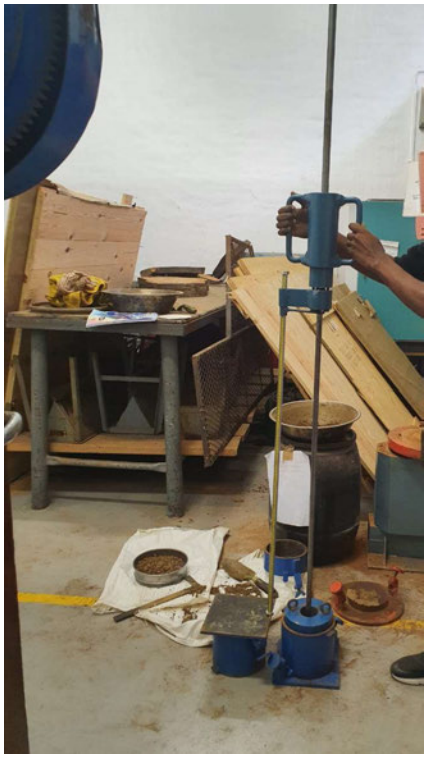

Plate 3-6: Laboratory DCP-DN Test

3.4.2 California Bearing Ratio

The CBR test was developed by the California Department of Transportation to measure the strength of materials used in road construction. It is defined as the ratio of force per unit area required to penetrate a soil mass with a standard circular plunger of 1 935 mm^2 at the rate of 1.27 mm/min, expressed as a percentage of standard values of a California crushed limestone. The method of the test, as detailed in TMH1-Method A8, specifies penetration depths of 2.54 mm, 5.08 mm and 7.62 mm and standard forces, 13.3 kN, 20.0 kN and 25.4 kN, respectively.

The test was used to assess the performance of NME stabilised samples against an unstabilised, control sample. The tests were performed on remoulded cured samples, soaked for four days. The test specimens were also checked for swell as shown in Plate 3-7.

.

Plate 3-7: Specimen soaking and preparation for CBR test

3.4.3 Indirect Tensile Strength (ITS) test

ITS is the stress at failure generated by the load required to split a cylindrical specimen. The test is performed according to TMH1 Method A14. A cylindrical specimen of height, 127 mm and diameter, 152 mm, is loaded on its diametrical axis at a steady rate of 50 ± 5 mm/min as depicted in Plate 3-8. The ITS is determined according to Equation 3 -1.

$$ITS = \frac{2 \times P}{\pi \times d \times h} \times 10^6 \qquad \text{Equation 3-1}$$

Where;

ITS - indirect tensile strength [kPa]

P - applied force [kN]

d - specimen diameter [mm]

h - specimen height [mm]

ITS tests were conducted on the NME stabilised samples. A set of three specimens were tested for each of the dry and wet conditioned tests at each of the NME contents from 0.7% to 1.5%. A neat (unstabilised) sample was also tested as a control.

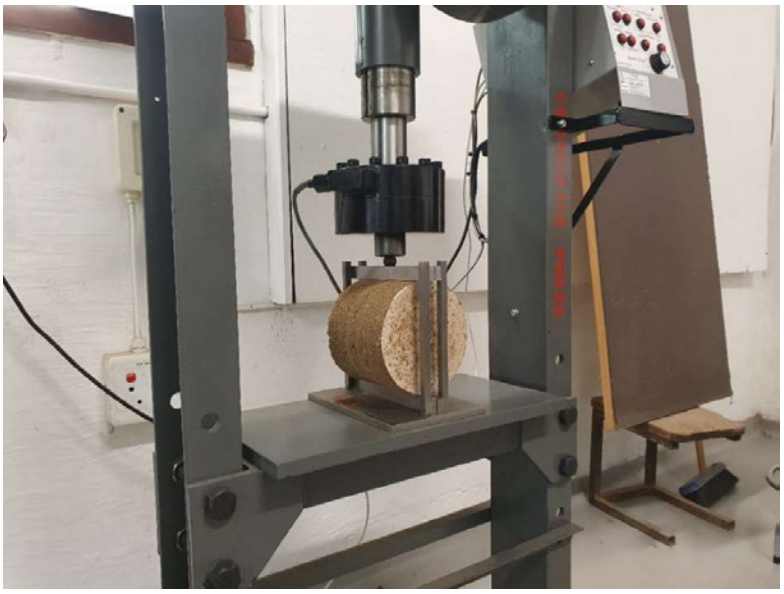

Plate 3-8: ITS Test setup

3.4.4 Unconfined Compressive Strength (UCS) test

UCS tests were performed according to TMH1 Method A16T. Cylindrical specimens measuring 127 mm in height and 152mm in diameter were crushed to total failure in a compression testing machine that applies load at a rate of 153 kN/min as shown in Plate 3-9. The maximum force required to crush the specimen was recorded and the UCS determined according to Equation 3-2.

$$UCS = 1000\ \frac{P}{\pi r^2} \qquad \text{Equation 3-2}$$

Where:

UCS – Unconfined Compressive Strength [MPa]

P - applied force [kN]

r – radius of specimen [mm]

UCS tests were conducted on the NMESM. Similar to ITS, a set of three specimens were tested for both the dry and wet conditioned tests at NME contents from 0.7% to 1.5%, with a neat (unstabilised) sample used as a control.

Plate 3-9: UCS Test Setup

3.4.5 Triaxial Testing

Three types of triaxial tests were performed i.e., the STT and RLTT for resilient modulus and plastic strain.

3.4.5.1 Static Triaxial Tests

The method of the STT is detailed in TG2 (2020). Test specimens, 150 mm in diameter and 300 mm high, were prepared using the vibratory hammer compaction method and tested by compression testing in a triaxial cell. The test was conducted by applying a vertical load at a constant rate of 3 mm/min at four confining pressures, i.e. 0 kPa, 50 kPa, 100 kPa and 200 kPa at each of the NME contents from 0.7% to 1.5% until the load reaches a maximum and starts to reduce. The control test (0% NME) was tested at three confining stresses, i.e. 50 kPa, 100 kPa and 200 kPa. Readings of maximum load (fi) and displacement (Δi) were taken and a sample of the specimen was collected after the test for moisture determination. For each test, plots of applied stress versus the induced displacement (strain) were produced as depicted in Figure 3-4.

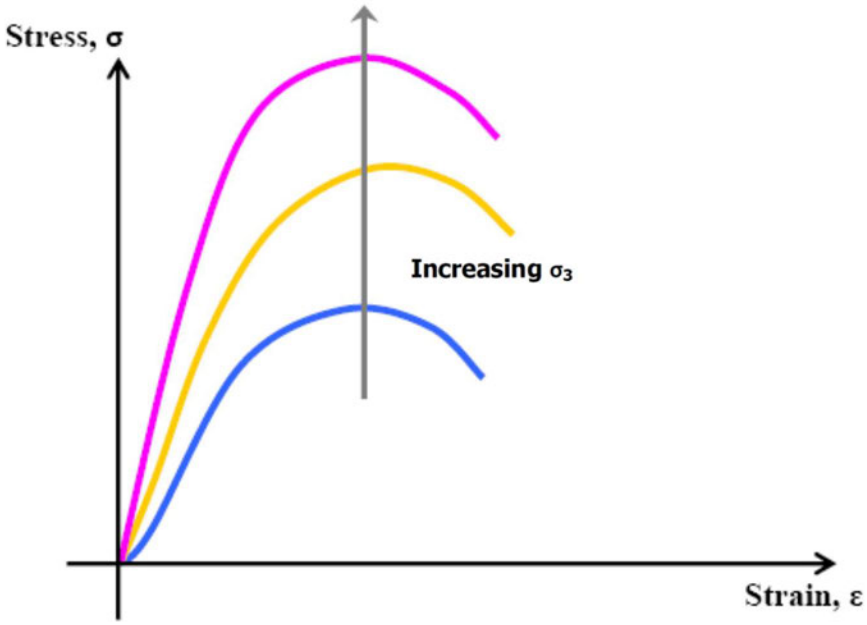

Figure 3-4: Plots of stress vs strain from STT (adapted from Mulusa, 2009)

Two specimens were tested at each confining stress and for each of the dry and wet conditions except for the unstabilised specimens, which were tested in the dry condition only. Therefore, a total of seventy tests were conducted. Plate 3-10 to Plate 3-13 show preparation for testing of specimens for STT.

Plate 3-10: Measurement of specimen after compaction

Plate 3-11: Specimens ready for curing

Plate 3-12: Mounting of STT specimen

Plate 3-13: Static triaxial testing

The tests were conducted at 25 ˚C. The Mohr-Coulomb criterion was used to determine the shear strength parameters of the material.

3.4.5.2 Repeated Load Triaxial Tests (M_R)

M_R is determined in the laboratory through RLTT by applying a series of combinations of confining and deviator stresses. Repeated axial cyclic stresses of fixed magnitude, load duration and cyclic duration are applied to a test specimen, while subjected to a static confining stress provided by a triaxial pressure chamber. Low stresses are applied creating low strains so that the elastic range of materials is not exceeded. The total resilient axial deformation response of the specimen is measured and used to calculate the M_R using Equation 3-3;

$$M_R = \frac{\sigma_d}{\varepsilon_r} \qquad \text{Equation 3-3}$$

Where,

M_R is the resilient modulus,

σ_d is the deviator stress,

ε_r is the resilient (recovered) axial strain due to σ_d

The Council for Scientific and Industrial Research (CSIR) protocol was used for the M_R test. The protocol is based on the Long-Term Pavement Performance (LTPP) Protocol P46 (FHWA, 1996) with in-country specific modifications. Due to resource limitations, the tests were conducted on a single NME application rate (i.e. 1.5%) for both the wet and dry conditions. The test on unstabilised specimens were used as control. Variables of the tests included;

- Temperature = 25 ºC.
- Stress Ratio = 20% to 60% (in 10 % increments)
- Confining pressure = 20 kPa, 50 kPa, 100 kPa, 150 kPa and 200 kPa.
- Load waveform = haversine
- Load duration = 0.2s load and 0.8s rest

Up to 1000 conditioning cycles were applied at axial deviator stress of 45% of the deviator stress at failure, with a confining pressure of 200 kPa. The deformation was measured by two Linear Variable Displacement Transducers (LVDT's) installed on the specimen.

3.4.5.3 Repeated Load Triaxial Tests (Plastic Strain)

The long duration RLTT is used to assess the potential of a material for plastic strain. This is done by measuring the irrecoverable strain responses, recorded by LVDTs, to the application of several thousand repeated cyclic loads, which correspond to a certain SR.

RLTT were performed on 1.5% NME stabilised (dry and wet conditioned) specimens as well as on the neat specimen to compare and establish the plastic strain behaviour of the mixes. The selected variables for the tests included;

- Loading waveform = haversine
- Frequency = 2.5Hz
- Temperature = 25 ºC
- Stress ratio = 20%

- Confining pressure = 100kPa
- Cycles = 80,000 (as per CSIR protocol).

3.4.6 Voids analysis

The void content of bituminous material mixes is important as it influences various factors including, stability, deformability, permeability and durability. Therefore, the determination of the void content is critical for the characterisation of the material mixes.

The void content of the NMESMs were evaluated according to TMH1 methods C3 and C4 by carrying out tests for the Bulk Relative Density (RDv) and Maximum Theoretical Relative Density (RDm). Equation 3-4 was used to determine the void content.

$$Voids\ \% = \frac{RDm - RDv}{RDm}\ x\ 100 \qquad \text{Equation 3-4}$$

Where;

RDm = maximum theoretical relative density

RDv = bulk relative density

The determination of the RDv of the unstabilised specimens was practically impossible, as the specimens would disintegrate before the stipulated minimum of 3 minutes immersion in water. Therefore, the void content of the unstabilised specimen is based on secondary data sources, in particular Geotechdata (2013).

3.4.7 Permeability test

Permeability is critical especially for gravel roads as it influences the bearing strengths of materials. It is crucial that the gravel-wearing course limits the ingression of water through to the subgrade to maintain road performance.

The falling head permeability test method was used to determine the permeability of a material mixed with 1% NME. This was gauged against an unstabilised specimen. The test involves flow of water through a soil sample of height (i) connected to a standpipe which provides the water head and also allows the measurement of the

volume of water passing through the sample. A schematic of the falling head test is shown in Figure 3-5.

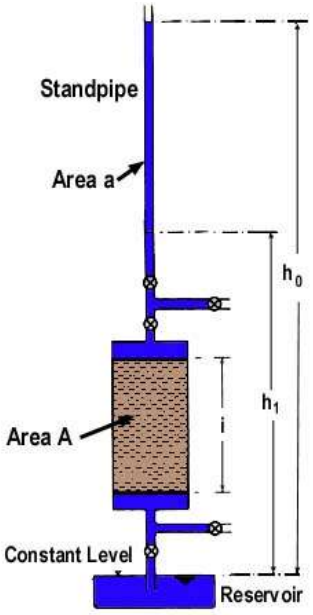

Figure 3-5: Schematic of falling head permeability test (adapted from CIVCAL, 2023)

Where;

a = area of standpipe,

i = height of the sample,

A = area of sample

t = time for water level to drop from h_0 to h_1

h_0 = initial water level

h_1 = final water level.

The time required for the water in the standpipe to drop from predefined heights h_0 to h_1 was recorded. Three readings were taken for sensitivity analysis and statistical significance. The average of the three results was used to calculate the permeability (k) using Equation 3-5.

$$k = \frac{2.3a \times i}{A \times t} ln\left(\frac{h_0}{h_1}\right) \quad \text{Equation 3-5}$$

3.4.8 Scanning Electron Microscopy (SEM)

SEM testing is another good method for characterising stabilised specimens as it allows for the observation of the dispersion of the binder in the gravel material, validating (or disapproving) some of the presumptions made with regards to NMEs. EDX analysis also aids in the determination of the mineralogy (and changes thereof) of the composite material resulting from the stabilisation.

SEM tests were conducted on NMESMs stabilised at 1.2% and 1.5% NME contents as well as on a control test. The two were considered due to the relatively higher binder contents. The procedure of the tests, done at the Microscopy and Microanalysis Unit (MMU) of UKZN, is detailed below;

1. Small pieces of the sample (<10 mm) were carefully cut from the compacted specimen, ensuring that they do not disintegrate.

2. The samples were mounted onto aluminium SEM stubs with double-sided adhesive carbon tape as shown in Plate 3-14.

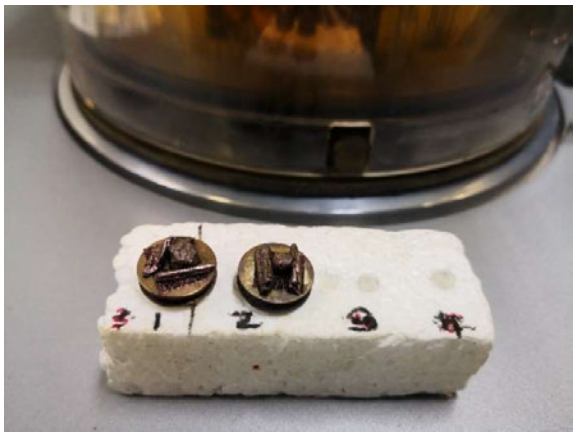

Plate 3-14: Specimens mounted on SEM stubs

3. The stubs were gold sputter coated with a Quorum K 150 RES sputter coater. This prevents charge build-up on the specimen surface.

4. The samples were imaged with a Zeiss Ultra Plus FEG SEM (Plate 3-15),

5. EDX data was obtained with the Oxford X-Max EDX detector.

Plate 3-15: Zeiss Ultra Plus FEG SEM

3.5 Modelling

Modelling was employed as part of the analytical procedure to provide the predictive performance of NMESMs in a pavement structure. Results from the laboratory testing were used as input parameters in a Finite Element (FE) based software, ANSYS 2022 R2, to model a pavement structure incorporating a NME stabilised gravel-wearing course, contrasted against a corresponding structure without the stabilised layer. The pavement structure modelled was based on Ingweni road, a gravel road in Pinetown area of Eastern SA, constructed and maintained using the same gravel material as used in this study. Chapter 6 provides details of the modelling.

3.6 Summary

This Chapter provides the methodology used for the study. The methodology is designed in line with the objective to characterise and evaluate the engineering behavioural traits of NMESMs in the laboratory. The gravel material classification is based on traditional classification tests, extended to include mineralogy tests using XRD. This is critical to the selection and quantification of a compatible NME that adequately binds the material as well as provide the level of hydrophobicity required.

Procedures proposed in the NDPS (TRH24, 2022) for material preparation and mixing are followed with the only point of departure being the curing period. The curing procedure was adjusted somewhat after diagnostic assessments revealed a considerable effect on the results of mechanical tests as explained in Section 3.3.2.

The NMESM mixes are proposed to be evaluated for mechanical strength properties through traditional strength characterisation tests including, DCP-DN, CBR, ITS and

UCS. The tests are conducted at four NME contents; 0.7%, 1%, 1.2% and 1.5%, to observe trends in performance of the materials. Tests on the neat (unstabilised) specimens are also performed as control tests. Advanced testing, through STT and RLTT is also detailed. These tests provide fundamental material properties that more accurately represent the performance of material in the pavement structure. The tests consider the dry and wet conditions, to evaluate the retained strengths of NMESM after soaking, indicative of the durability of the material. Other tests proposed include voids analysis and permeability, performed to determine the extent to which NME stabilised layers protect underlying layers (subgrade) from water ingress and SEM, proposed to evaluate the dispersion of the NME in the material and establish the chemical changes resulting from the stabilisation.

Finally, modelling using a Finite Element (FE) based platform is proposed to provide the predictive performance of structural layers of NMESMs and contrasted against a corresponding unstabilised layer.

4 MATERIAL CHARACTERISATION

4.1 Introduction

The structural capacity of a pavement structure is a function of the ability of the different layers to distribute loads, which is determined by the engineering properties of the materials in each particular pavement layer that are in turn dependent on the materials' intrinsic properties (RA, 2014). Paige-Green (2008) submits that materials' range of intrinsic properties such as strength, gradation, density, moisture content and resistance to deformation reflect the impact of physical, chemical and environmental factors on the materials over time.

The essence of material characterisation is to determine the intrinsic properties and behavioural characteristics of materials to enable their usage for specific purposes. Some materials, capable of high performance, are usable in construction of particular pavement layers without the need for further enhancements whilst others, of marginal or low quality, may require enhancement through mechanical and/or chemical stabilisation to improve their engineering properties and performance. The suitability of a material for stabilisation with a particular technology is also determined through material characterisation. Therefore, this Chapter discusses the results of characterisation tests conducted on the gravel material used in this study. Based on the results of laboratory tests, the material is classified by referencing to appropriate SA material standards. This Chapter also presents results of mineralogy tests conducted on the material and how the mineralogy is used together with results of the characterisation tests to select a compatible NME to be used in the mix design to produce the composite, NMESM.

4.2 Gravel material classification

4.2.1 Particle Size Distribution (PSD)

Dry sieving of a representative sample of the material was carried out according to TMH1 Method A1(b). This is in line with the recommendation by TG2 (2020) as wet sieving may indicate a high percentage of filler material (fraction passing the 0.075 mm sieve) than would be available during full-scale mixing. Figure 4-1 presents the PSD of the material resulting from the sieve analysis.

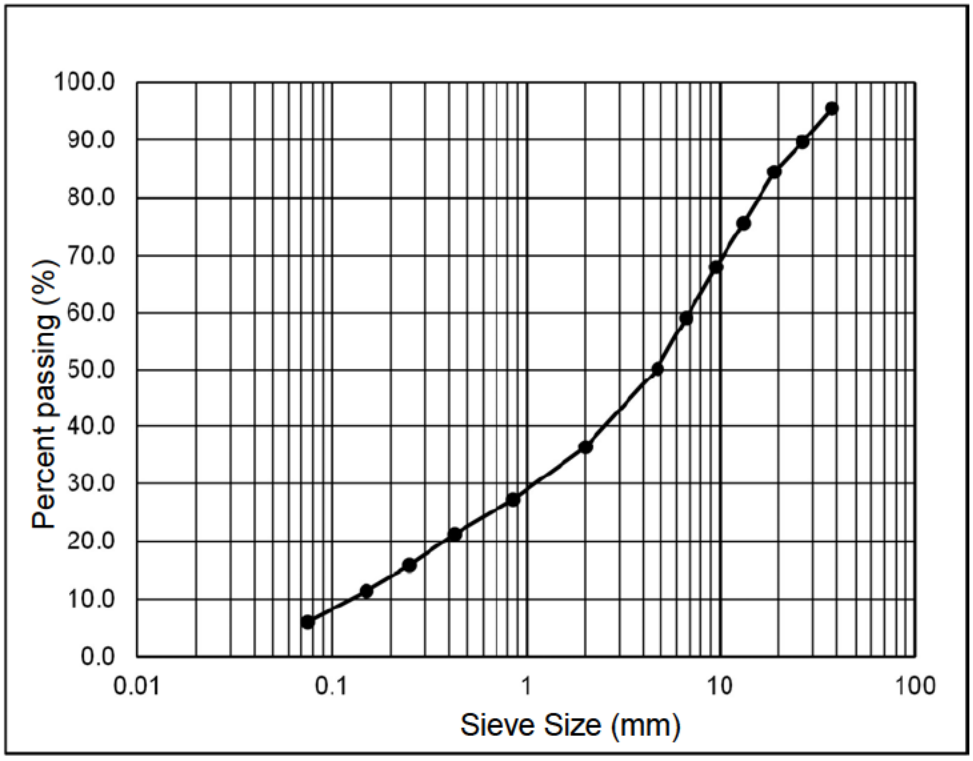

Figure 4-1: Material PSD

The results show that the soil material has a continuous grading with the majority coarse fraction (49.7%) and minority fine fraction (44.2%). The material is therefore classified as gravel according to COTO (2020). The maximum aggregate size is 37.5 mm and the filler content is 6.1%.

The PSD influences various material properties that determine performance including achievable density, permeability and strength. Recommended material gradings limits (envelopes) are provided in applicable standards for high quality material while for low quality materials, factors such as the GM and Grading Coefficient (Gc) are used to define material gradings. GM quantifies the PSD of the material by indicating whether the material is considered a coarse or fine material and ranges from 0 to 3, with 0 for fine material and 3 for coarse material as indicated in Section 2.11.1.2. The GM of the gravel material was determined from the results of sieve analysis using Equation 4-1 as 2.3. This indicates a generally coarse graded material. The NDPS recommends a minimum GM of 0.45 for natural gravel material to be stabilised with NME and used as a gravel-wearing course therefore, this material qualifies on this score.

$$GM = \frac{(P2.00\ mm + P0.425\ mm + P0.075\ mm)}{100} \quad \text{Equation 4-1}$$

Where;

GM = Grading Modulus

P2.00 mm etc. = Percentage retained on the indicated sieve

The Gc indicates the percentage of fine and medium gravel in a material. It ranges from 0 (all particles smaller than 2 mm) to 100 (gravel with all particles larger than 4.75 mm and smaller than 26.5 mm) (Paige-Green, 1999). It was calculated as 26.8 from Equation 4-2 and meets requirements set out by COTO (2020), which recommends a Gc between 15 and 35 for material to be used for rural and urban gravel roads.

$$Gc = \frac{((\%\ pass\ 26.5\ mm - \%\ pass\ 2.00\ mm)\ x\ (\%\ pass\ 4.75\ mm))}{100} \quad \text{Equation 4-2}$$

The influence of the filler content of materials is discussed in Section 2.11.1.2. Accordingly, the amount of filler influences the optimum quantity of the NME binder that is effective for the treatment of the material. The filler fraction of the material also influences the material properties such as the maximum density achievable. The results show that the material meets requirements set out by TG2 (2020), which recommends a filler content between 6 and 10% for bituminous stabilisation.

4.2.2 Plasticity characteristics

The results of tests conducted for Atterberg limits of the material are provided in Table 4-1. The PI of the material (i.e. the difference between the LL and PL) is 4%. Based on the LL and PI, the fine fraction of the material is classified as low plastic silt according to the Unified Soil Classification System (USCS) as shown in Figure 4-2. According to Sherwood (1993), silty materials are sensitive to small changes in moisture and, therefore, may present difficulties with some stabilisation technologies.

Plasticity of a soil is an important characteristic that indicates the materials' sensitivity to moisture and its ability to undergo deformation without cracking. Highly plastic materials used for gravel wearing courses lead to cracking of the surface while materials with low plasticity may ravel, leading to material losses. Increase in plasticity

also results in reduced density and shear strength properties of gravel materials. The NDPS (TRH24, 2022) specifies a PI of less than 16% for gravel wearing course.

Table 4-1: Atterberg Limits

Atterberg Limits	
Liquid Limit (LL) (%)	30.1
Plastic Limit (PL) (%)	26.1
PI (%)	4
Linear Shrinkage (LS) (%)	0

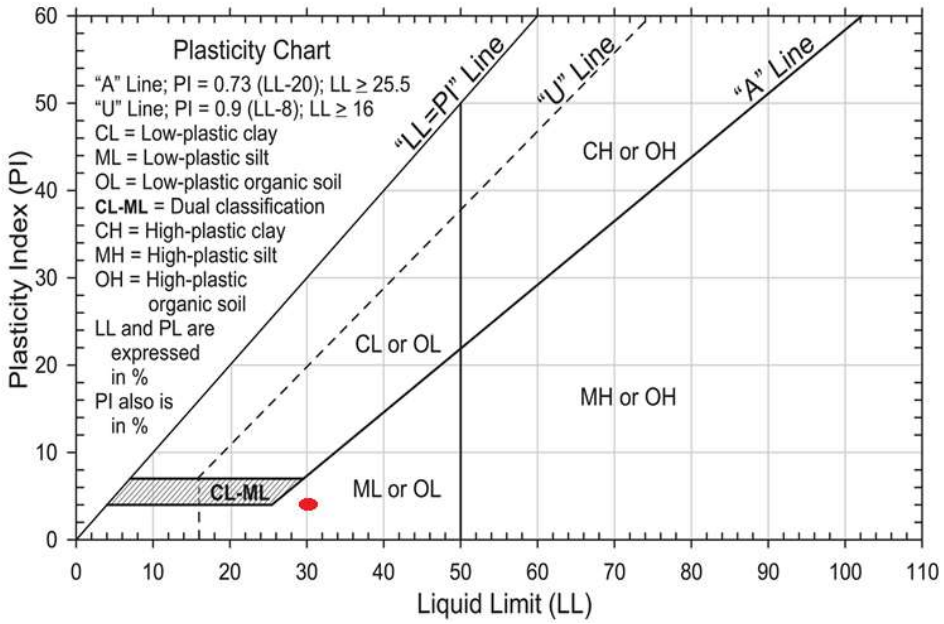

Figure 4-2: Material plasticity chart

The Shrinkage product (Sp) is another property that is particularly useful for materials used for construction of gravel roads. It is the product of the percentage of material passing the 0.425 mm sieve and the material's LS. It has been established that the right combination of Gc and Sp results in a generally good gravel road wearing course with adequate strength to resist potholing when effectively maintained, indicated as Zone E of Figure 4-3.

The LS of the material was determined to be 0 thus, the Sp is 0. With a Gc of 26.8, it is shown that the material lies in Zone B of Figure 4-3. Accordingly, this material generally lacks cohesion (low PI) and is highly susceptible to the formation of loose material (ravelling) and corrugations. A visual assessment of Ingweni road, a gravel

road section constructed using this gravel material confirmed the occurrence of wide spread corrugations and presence of loose materials as shown in Plate 4-1. The road is said to be maintenance intensive.

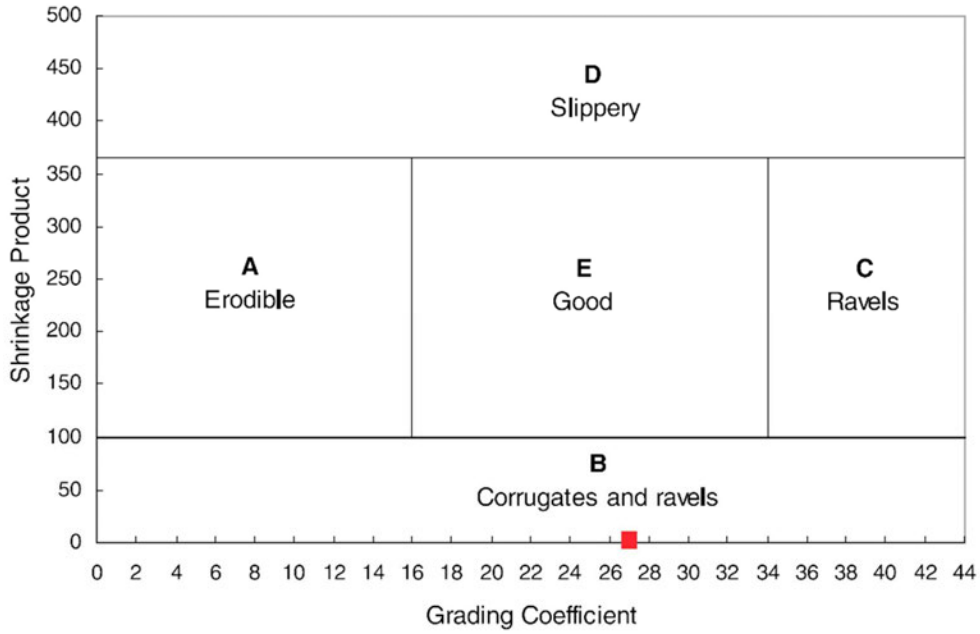

Figure 4-3: Diagrammatic indication of expected performance of gravel road wearing course (Adapted from Paige-Green, 2007)

Plate 4-1: Section of Ingweni road in Pinetown, SA showing corrugation failures

4.2.3 Density-Moisture content relationship

The density-moisture content relationship was established through compaction tests according to the Mod AASHTO method espoused in TMH1 Method A7. The results, provided in Figure 4-4, show the MDD to be 2093 kg/m^3 and the OMC, 5.8%.

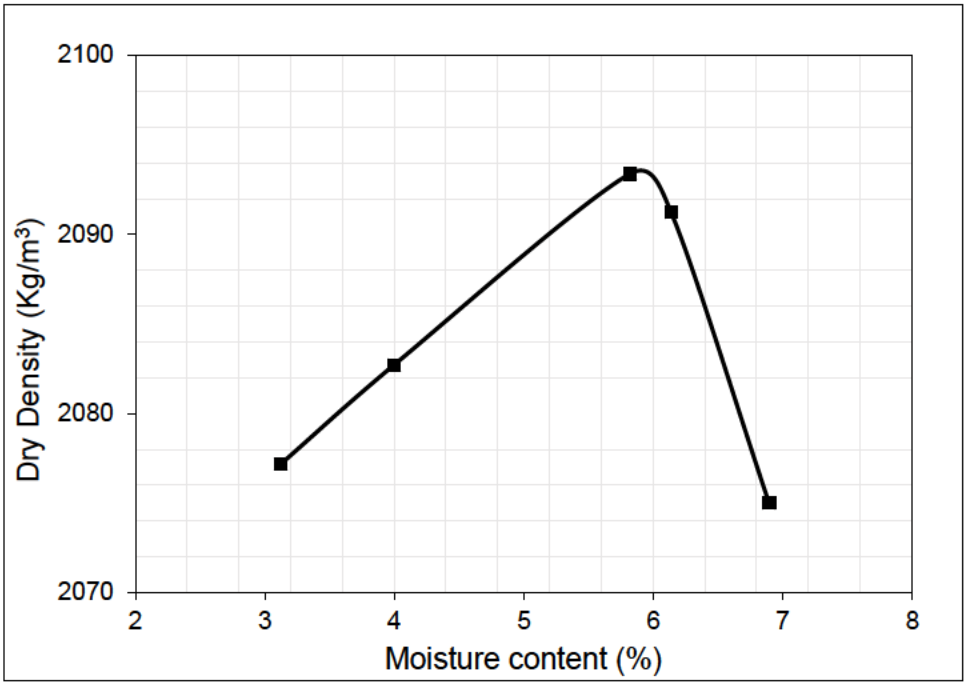

Figure 4-4: Maximum Dry Density-Moisture content relationship

The density-moisture content relationship of a material is one of the most important properties that influence performance and engineering behaviour of material. It reflects the material's ability to function as a structural support and influences the shear strength properties and permeability characteristics. It is for this reason that material strength tests are referenced to particular relative densities. The density is influenced by several factors including, closeness of packing, size, shape and distribution of aggregates and method of compaction.

4.2.4 California Bearing Ratio

The CBR test of the neat material was conducted as part of the classification of the material as well as for strength determination of NMESMs as discussed in Section 5.3. Soaked CBR results were obtained at three compactive efforts as outlined in TMH1 Method A8. Graphs of plunger load vs penetration were obtained and are included as

part of the appendices indicated (in Section 5.3). Ideally, the CBR computed at 2.54 mm should be used in the analysis, however, repeated tests consistently demonstrated that this CBR is lower than that at 5.08 mm penetration. Therefore, the CBR computed at 5.08 mm penetration was used in the analysis.

The densities obtained at the three compactive efforts were compared to that from the MDD/OMC test and the Relative Compactions (RC) were calculated. A CBR-RC curve was plotted and the CBR at 95% of Mod AASHTO density was obtained as 42.5% as shown in Figure 4-5.

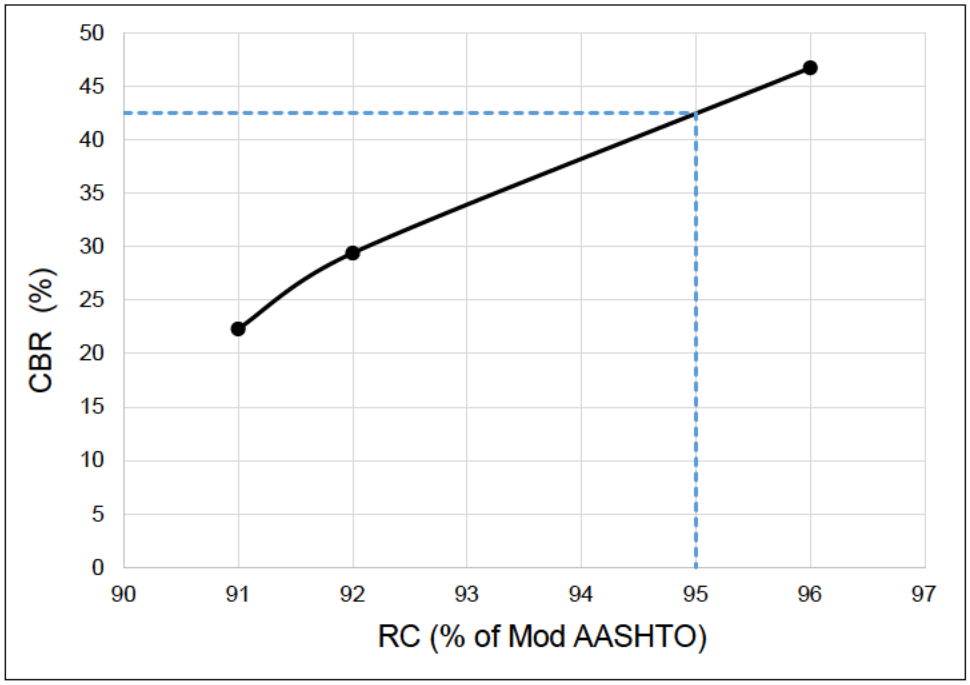

Figure 4-5: CBR-RC curve

According to COTO (2020), the minimum required CBR for rural and urban gravel roads is 15% at 95% Mod AASHTO density. This is also the specified minimum for consideration of material for NME stabilisation according to NDPS (TRH24, 2022) therefore, this material qualifies for NME stabilisation and use as a gravel-wearing course on this account.

4.2.5 Material class

The soil material has been identified as a low plastic silty gravel, based on the USCS. In SA, TRH14 (1985) and COTO (2020) are used as guidelines for classifying soil

material. The guidelines are based on the specification method. According to the method, the material is assigned a class based on it meeting specified limits given in standard specifications for the material properties. These are essentially one-fail-all-fail type criteria, and if any one test fails the criterion for the material class, then the material cannot be assigned to that class. Based on the specifications provided in the two guidelines and the results of classification tests conducted, the material is classified as a G6 material. Material property descriptions and limits for a G6 material are provided in Table 4-2.

Table 4-2: Material property limits for a G6

Property	TRH14 (1985)	COTO (2020)	Material Parameters
Material Description	Natural gravel or a mixture of natural gravels and boulders which may require crushing	Natural gravel or natural gravel and boulders which may need crushing or crushed rock	Natural gravel
Nominal Max. Size	2/3 compacted layer or 63mm whichever is smaller	Uncrushed: 2/3 compacted layer. Crushed: 63mm before compaction	37.5mm
Grading Modulus	> 1.2	2.6 ≥ GM ≥ 1.2	2.3
PI (-0.425mm fraction)	< 3GM + 10	< 12 or < 3GM + 10	4.1
Strength (CBR)	> 25% at 93% of Mod AASHTO	> 25% at 95% of Mod AASHTO	42.5% at 95% of Mod AASHTO
Swell (Max.)	< 1%	< 1%	0%

G6 materials are described as relatively poor-quality natural gravel materials, usually only considered for use in pavement construction after stabilisation. This material is generally considered unsuitable for the conventional bituminous stabilisation provided for in TG2 (2020). Successful stabilisation with NME would provide a great alternative in this regard, enabling the materials' use in road construction.

4.2.6 X-Ray Diffraction Test

The mineralogy of the materials was identified using XRD tests. The tests were conducted on the bulk sample and the sample of the fraction passing the 0.075 mm

sieve as explained in Section 3.2.2.1. The XRD patterns of the two samples are shown in Figure 4-6 while Table 4-3 presents the main mineralogy phases of the gravel material samples.

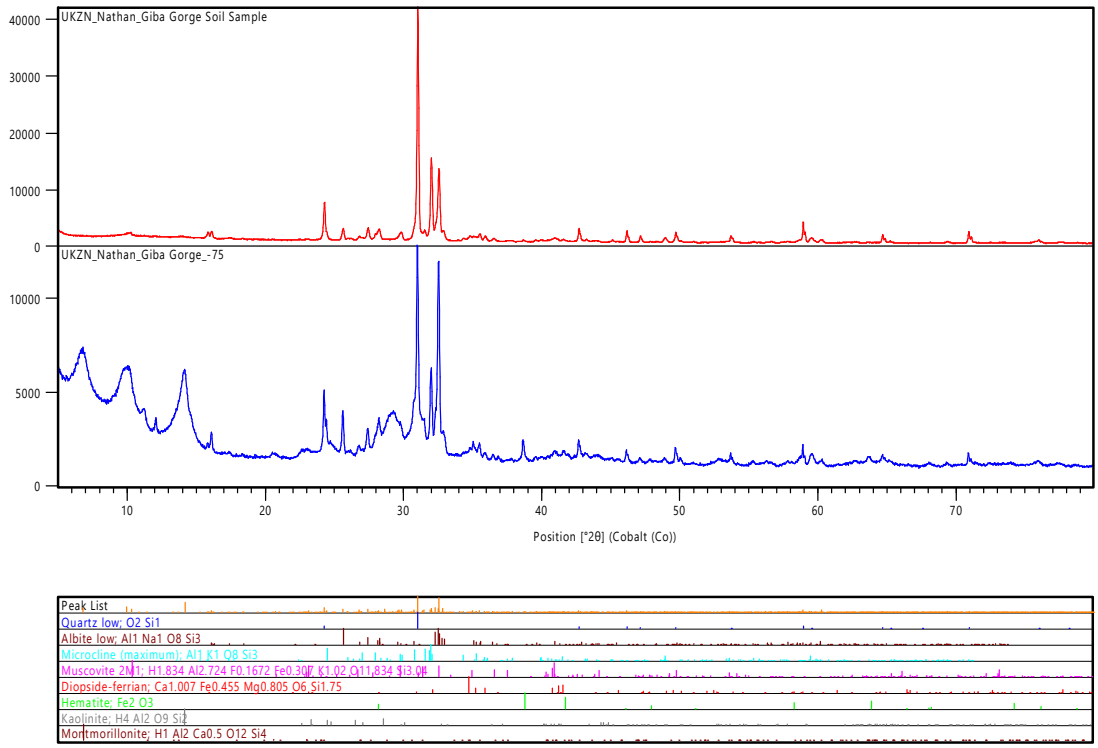

Figure 4-6: XRD test results of gravel samples

It is observed that the material is mainly comprised of quartz (58%), a continuous network of silica tetrahedron. The silica (containing silicon and oxygen) is essential for the formation of siloxane bonds. The larger the quantity of silica, the more siloxane bonds that can be formed. The results also show that the material weathers down to Mica (Muscovite) at 7.7%. Mica is a deleterious mineral that has the tendency to absorb and retain moisture as explained in Section 2.11.2. In base or subbase layers of road pavements, the retention of moisture may cause heaving and rutting failures and reduction in bearing capacity. It also reacts adversely to bitumen or cement treatment. COTO (2020) recommends that aggregates should not contain more than 4% free mica, especially muscovite.

Table 4-3: Main mineralogy phases

	Bulk Sample		0.075mm Fraction	
Mineral Groups	**Individual**	**Combined total**	**Individual**	**Combined total**
Primary - Not subject to weathering				
Quartz	58		20.4	
		58		**20.4**
Primary - Subject to weathering				
Plagioclase	20.1		17.8	
Microline	20.6		16.9	
Diopside	0.1		0	
Hematite	0		0.7	
		40.8		**35.4**
Mica				
Muscovite	1		7.7	
		1		**7.7**
Clay Minerals				
Kaolinite	0.2		23.9	
Smectite	12.6		12.6	
		12.8		**36.5**

The results also show clay minerals (Kaolinite and Smectite) at 36.5% in the fraction passing the 0.075 mm sieve. Clay minerals are problematic for road construction due to their low strength, high compressibility and high level of volumetric changes. The swell-shrinkage behaviour of clays in reaction to changes in moisture content may cause heaving or settlement of layers, undesirable in roads. COTO (2020) advises that the most careful assessment of durability be conducted on materials containing clay minerals especially in areas with low Weinert N values.

The combined quantity of the deleterious minerals (mica and clay) is used to determine the quantity of NME required for stabilisation and consideration of laboratory evaluations.

4.3 Compatible NME

The results show that the gravel material is silicate-based, with the silica-based mineral, quartz, accounting for more than 50% of the material's mineralogy content. Based on the first consideration in compatibility requirements explained in Section 2.11.3, it was determined that a bitumen emulsion modified with an organofunctional nanosilane is compatible and could be used for treatment of the gravel material without

the need for any conversion treatments. In this regard, the NME was obtained with the properties provided in Section 3.2.2.2.

4.4 Quantifying NME

The second stage of the design process is the quantification of the NME recommended for evaluation of the material. This is established based on the surface area of the material to be covered by the NME stabilising agent. Therefore, the process involves primarily adjusting the NME for the fraction of material passing the 0.075 mm sieve and the quantity of clay minerals and mica present in this fraction of materials as shown in Figure 4-7.

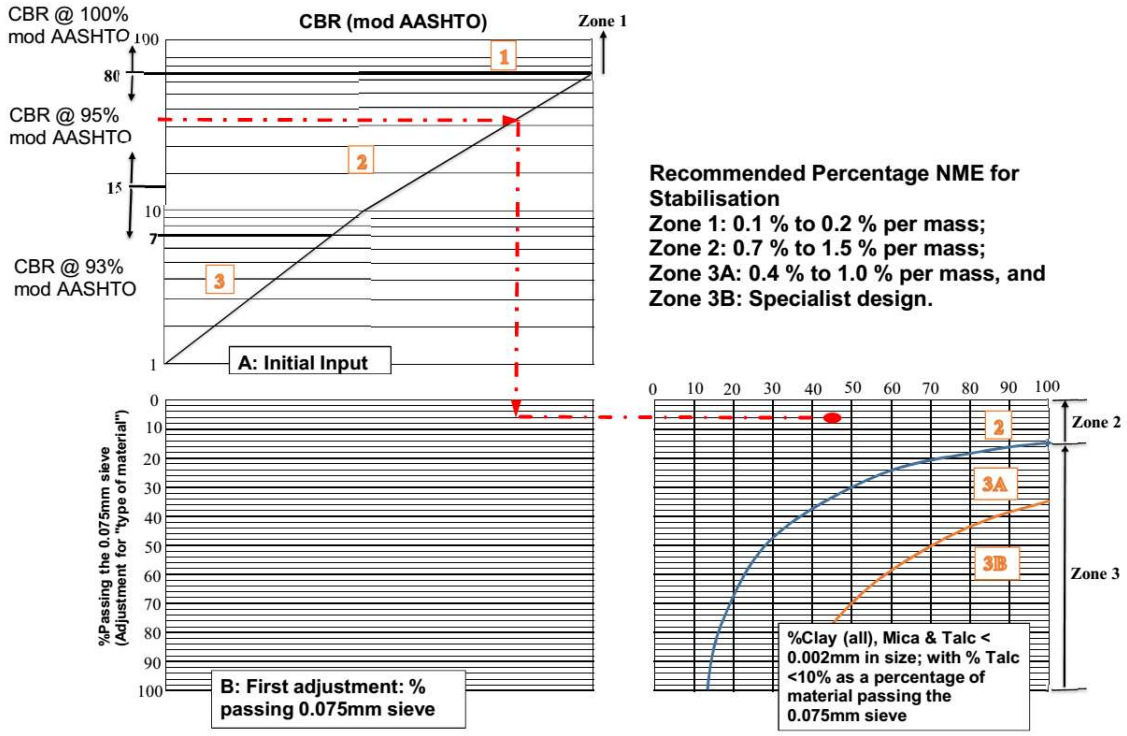

Figure 4-7: Recommended quantity of NME for stabilisation of material (modified from Jordaan and Steyn, 2021a)

Based on the results obtained, the CBR of the gravel material was determined to be 42.5% (at 95% of Mod AASHTO density). The grading analysis shows that 6.1% of the material passes the 0.075 mm sieve and from the XRD tests, the total combined percentage of mica and clay minerals is 44.2%. Plotting these values as shown in Figure 4-7, it was determined that the material lies in delineated Zone 2. This means

the optimum NME required for stabilisation is between 0.7% and 1.5%. This is what was used for laboratory evaluation and strength tests.

4.5 Summary

This Chapter presents results of tests conducted for gravel material characterisation. Traditional material characterisation tests contained in the relevant TMH1 standards including; sieve analysis, Atterberg limits, MDD/OMC and CBR, were conducted on the material. The results of the tests were compared against specified material classes to identify the gravel material as a G6, based on SA material standards.

G6 materials are low quality natural gravels usually only considered for use in pavement construction after stabilisation. The material is however not suitable for conventional bituminous stabilisation practised in SA. XRD tests of the fraction of material passing the 0.075 mm sieve shows that it contains deleterious minerals, among other minerals, and may be unsuitable for most stabilisation technologies. The mineralogy results however indicate that it contains enough quantities of the silica mineral required for NME stabilisation. Thus, a compatible NME was selected for stabilisation of the material with recommended applications rates between 0.7% and 1.5%.

5 LABORATORY EVALUATION OF NMESM MIXES

5.1 Introduction

This Chapter provides results of the laboratory evaluation of NMESMs. Although this study focuses on gravels roads, it is recognised that NMESMs have the potential for use across the entire road class range, from low-end rural access roads (e.g. gravel roads) to major urban access roads (surface roads), thus, the laboratory tests conducted take this into account. Mechanical strength tests conducted can be classed at three levels, i.e. low-reliability – (DCP-DN and CBR), medium-reliability – (ITS and UCS) and high-reliable – (STT and RLTT). This corresponds to the design requirements and reliability levels required of different categories of roads. Additional tests are incorporated to supplement the characterisation of the material performance.

A number of factors including, material density, moisture, particle strength, grading and plasticity are known to influence results of laboratory tests for load bearing, mechanical and shear strength and durability properties of compacted soil specimens. Therefore, to evaluate the effect of NME on material strength, it is critical that these parameters are maintained relatively constant. To this end, measures were taken to limit the influence of the aforementioned factors by ensuring consistency in the material sampling, handling and testing procedures highlighted in Chapter 3.

5.2 Influence of NME on DCP-DN

The DCP-DN laboratory test is a critical part of the DCP-DN pavement design method that is widely been promoted as a simple yet appropriate LVR design method especially for developing countries. The test was used to evaluate NMESM mixes after four days soaking, stabilised at NME applications from 0.7% to 1.5%. Tests on the unstabilised specimens were conducted as control tests. An attempt was made to test at least three specimens per NME application. However, sometimes, refusal was encountered and, in such cases, the results were excluded. The recorded penetration data was analysed using the ReCAP LVR-DCP freeware provided by CSIR and results appended in Appendix A. Figure 5-1 provides extracted results of the tests.

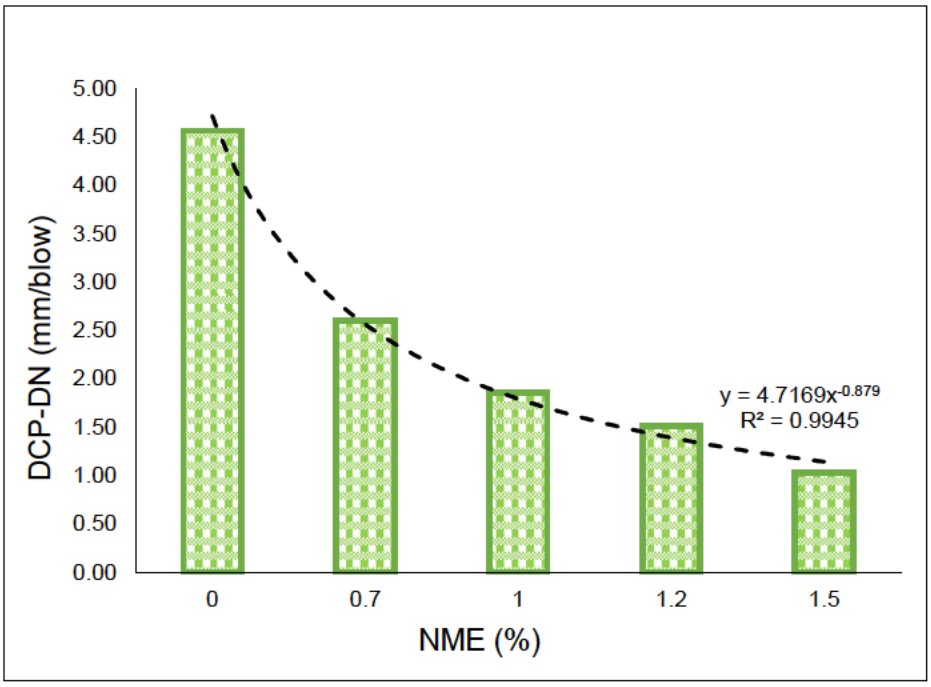

Figure 5-1: Laboratory DCP-DN Results

The results show that the penetration rate (DCP-DN) decreases with increase in NME application. A reduction in the penetration rate signifies improvement in the strength of the material such that it resists the penetration of the DCP. On application of 0.7% NME, the DCP-DN improves by 75% compared to the control (unstabilised) sample. From 0.7% to 1.5% the improvement is gradual averaging around 37%. The 1.03 mm/blow obtained at 1.5% NME represents an improvement of more than 340% on the unstabilised material. It is shown that the variation of the DCP-DN relative to the applied NME can be best described by a power function with a coefficient of determination (R^2) of 0.9832 as shown in Equation 5-1.

$$DCP - DN = 4.7169NME^{-0.879} \qquad \text{Equation 5-1}$$

Table 5-1 is an extract from the proposed NMESM material classification provided in TRH24 (2022), indicating limits of DCP-DN for material classes from NME1 to NM-EG5. Based on these classes and considering a minimum NME application level of 0.7%, the 2.61 mm/blow obtained for the material evaluated, places it in class NME4 although it is just at the boundary with NME3. NME4 class of materials are described as materials derived from stabilising relatively low-quality natural gravels that otherwise would not be considered for use in pavement construction (TRH24, 2022).

It is also observed that at 1.5% NME application, the penetration rate of 1.03 mm/blow obtained for the material, meets requirements for class NME1, notwithstanding the higher compaction requirements.

Table 5-1: DCP-DN limits for NMESM classes (TRH24, 2022)

Property	Material classes				
	NME1	NME2	NME3	NME4	NME-EG5
Mod AASHTO Density	>100%	>98%	>97%	>95%	>95%
DCP-DN (Unstabilised)	<3.6	<5.7	<9.0	<18.6	<13.5
DCP-DN (Stabilised)	<1.1	<1.6	<2.6	<3.4	<3.4

Based on limits provided for cement stabilised materials by SAPEM (2013) and Pinard et al. (2020), the range of DCP penetration rates from 2.6 mm/blow to 1.03 mm/blow meet requirements equivalent to lightly cemented materials C3 to C4 (based on SA standards) adequate to sustain up to 0.7 million Equivalent Standard Axle Loads (ESAL).

The penetration rate measured using the DCP is an indicator of the shear strength of the material. It is sensitive to density, moisture content, particle strength, grading and plasticity (TG2, 2020) and in a soaked condition, measures the cohesive strength component of the shear strength of materials. The specimens in this study were prepared and tested under similar conditions, thus, the recorded improvements in strength of the material can be attributed to the action of the NME in material bonding and resistance to moisture damage, even after four days of soaking.

5.3 Influence of NME on CBR

Soaked CBR tests were conducted on the NMESMs at NME applications from 0% to 1.5%. The CBR of the unstabilised specimen was used as the control test as explained in Section 4.2.4. Graphs of plunger load vs penetration depth were obtained and are appended in Appendix B. The CBRs were computed and are provided in Table 5-2 and illustrated in Figure 5-2 for better perception of the trends.

Table 5-2: Results of tests for CBR

NME (%)	0	0.7	1	1.2	1.5
Ave. Density (kg/m^3)	1989	2002	1990	2020	2036
RC (%)	95	95.7	95.1	96.5	97.3
Soaked CBR (%)	42.5	72.6	91.9	126.2	126.6
Swell (%)	0	0	0	0	0

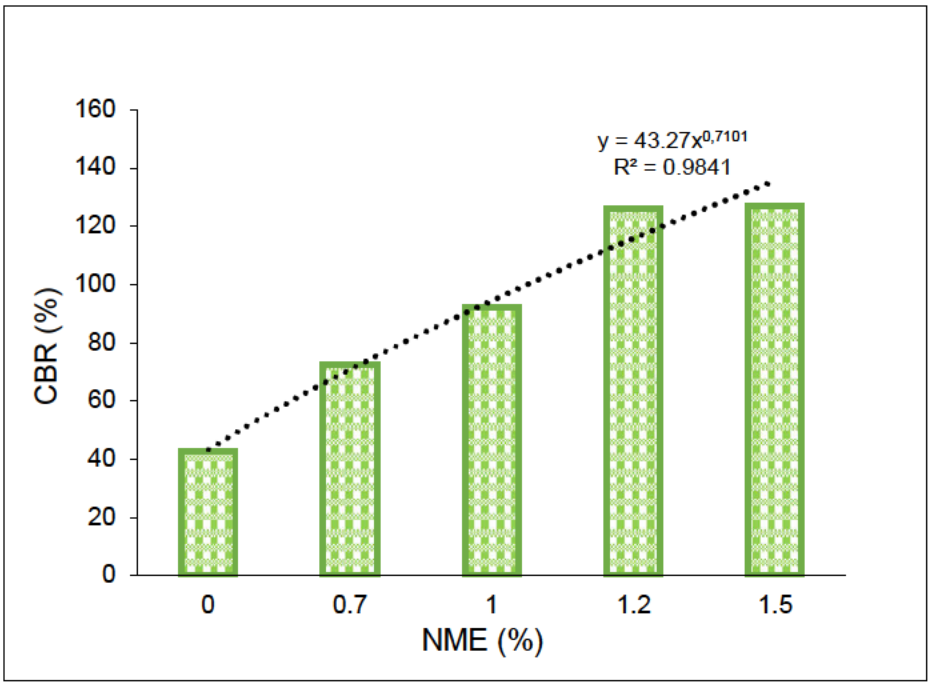

Figure 5-2: Soaked CBR Test Results

The results show that the NME has a significant impact on the soaked CBR of the material. A 71% increase in CBR strength is recorded on application of 0.7% NME, increasing to 116% and 197% at 1 and 1.2% NME applications, respectively. The increase in CBR strength from 1.2% to 1.5% NME is negligible, indicating that the strength reaches a plateau and that 1.2% is the optimum NME application level for CBR strength for this material.

Figure 5-2 also shows that the increase in CBR, relative to the applied NME, is best described by a power function with a $R^2 = 0.9841$ as indicated in Equation 5-2.

$$CBR = 43.27NME^{0.7101} \qquad \text{Equation 5-2}$$

The CBR test has been used as a basis for most road design methods, since its development in the late 1950s, due to its simplicity and familiarity. According to

Caicedo and Mendoza (2015), CBR is essentially a bearing capacity test working in a different strain range than the strains created within materials by moving loads. Thus, the test is more related to the strength characteristics of the material (friction angle and cohesion) than its stiffness (Young's modulus and Poisson's ratio (μ)).

COTO (2020) specifies minimum CBR requirements for granular materials to be used as base and subbase layers of flexible pavements at 80% and 30%, respectively. The CBR specifications for gravel roads, which are ideally meant to carry low volume traffic, is quite low at a minimum of 15% (COTO, 2020). The results show that at 0.7% NME application, the material meets requirements for use as a gravel-wearing course for gravel roads and subbase layer for surfaced flexible pavements. The material can also be used as a base layer on application of at least 1% NME.

Due to the large proportion and extensiveness of the gravel road network in most countries, SA included, it is inevitable that heavy vehicles use these roads. The higher CBR values would thus be advantageous and would contribute to the durability of the roads and cost savings stemming from reduced maintenance requirements.

5.4 Influence of NME on UCS results

The UCS test was used to evaluate the strength characteristics of NMESM mixes with NME application levels from 0% to 1.5%. Plots of load vs time (typical graph shown in Figure 5-3) were obtained for the wet and dry tests and are appended in Appendix C. Three tests were conducted for each test condition as part of sensitivity analysis and the average of the peak loads at which failure occurred, used to calculate the UCS as explained in Section 3.4.4. The results of the tests are shown in Figure 5-4.

The results show that the application of 0.7% NME to the material results in a 33% increase in UCS strength of the dry test (UCS_d). The strength appears to plateau thereafter up to 1.5% NME. This is shown in Figure 5-5, where a linear function (R^2 = 0.665) is used to represent the variation of UCS_d relative to the NME application levels from 0.7% to 1.5%.

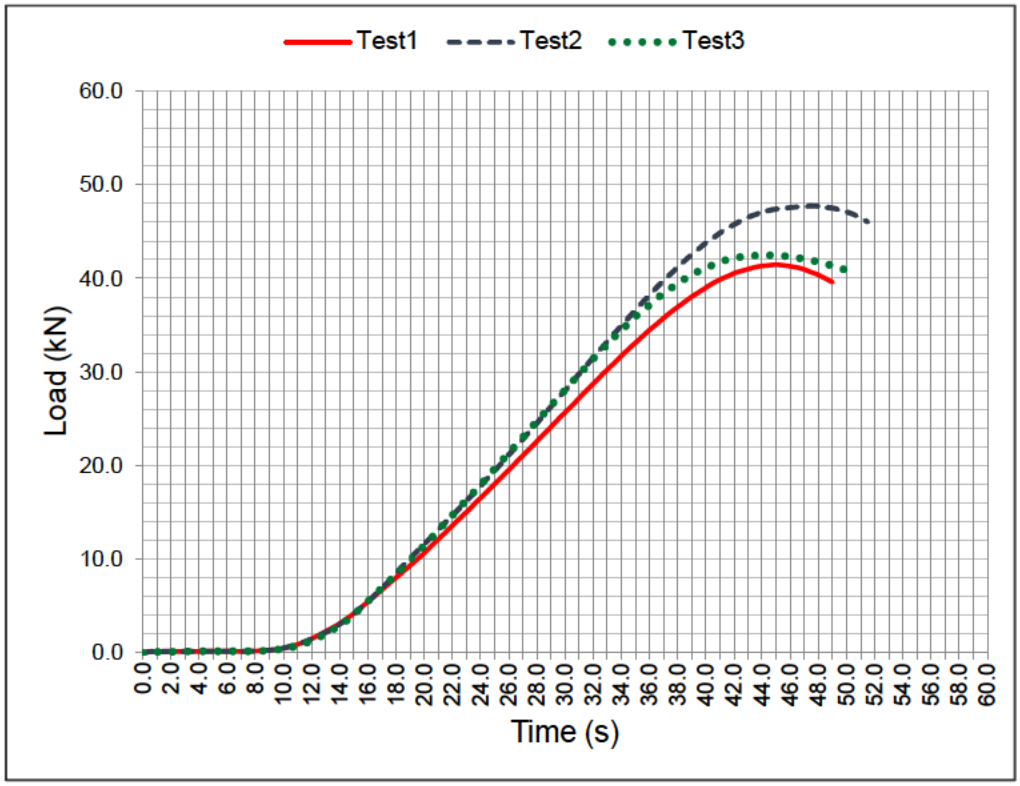

Figure 5-3: Typical Load vs time plots from UCS test

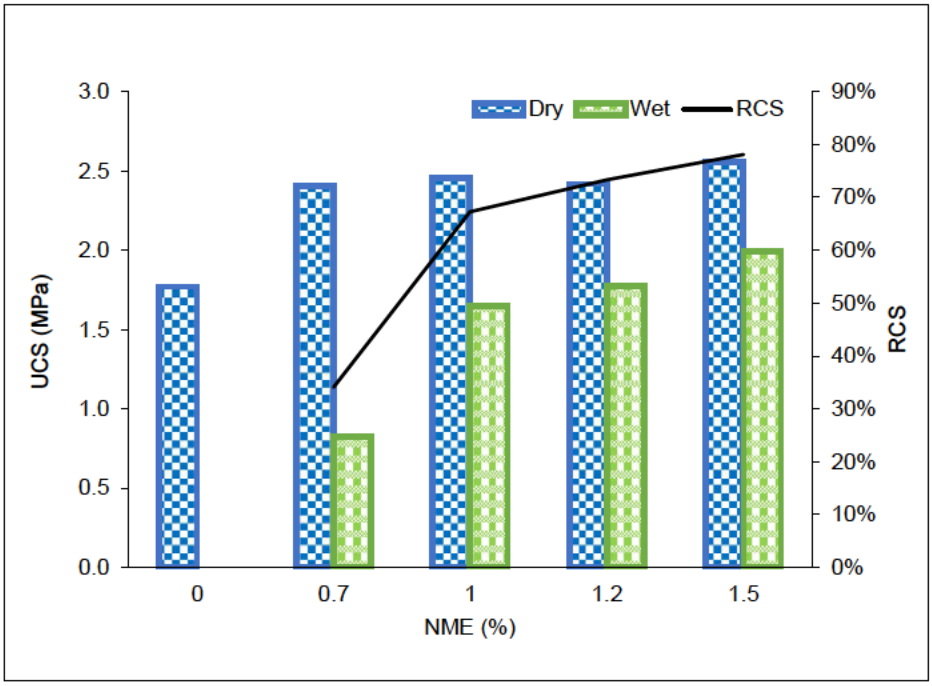

Figure 5-4: UCS Test Results

The wet test (UCS_w) was conducted from 0.7% NME. The 1.6 MPa recorded at 1.0% NME represents a 100% improvement in UCS strength on that recorded at 0.7% NME (0.8 MPa). The improvements taper off thereafter with 12.5% and 11% increases recorded on increased NME applications from 1% to 1.2% and 1.2% to 1.5%, respectively. Figure 5-5 shows that the behaviour of the UCS_w results is best represented by a polynomial equation of the second order with $R^2 = 0.9828$.

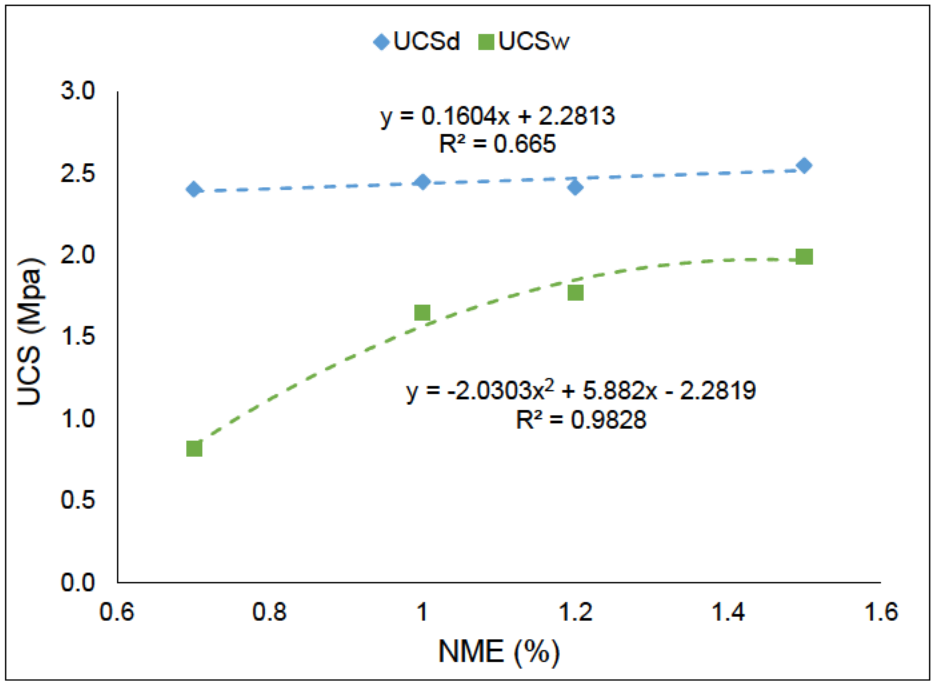

Figure 5-5: UCS strength characteristics

The Retained Compressive Strength (RCS) represents the proportion of retained strength after soaking of the specimen in water (for four hours). It provides an indication of the materials' durability and is calculated from Equation 5-3 below;

$$RCS = \frac{UCS_w}{UCS_d} \; x \; 100 \qquad \text{Equation 5-3}$$

The RCS, shown in Figure 5-4, increases from 34% at 0.7% NME to 78% at 1.5% NME, with the percentage moisture gain reducing from average 0.83% to 0.31%. This shows that increased NME application results in a material mix that is more resistant to moisture damage. The NDPS (TRH24, 2022) recommends a RCS >75% for gravel road wearing courses. On this basis, it is shown that 1.5% NME is the optimal

application level for achieving the required residual UCS of the material to be used as a gravel-wearing course.

For most requirements in the built environment, the UCS test is a suitable indicator of the mechanical strength of material and provides a measure of the shear strength and the stress-strain relationship. However, the test is highly influenced by the stone type in the material and thus it is not considered very useful in evaluation of bituminous stabilised materials and it is omitted from the TG2 (2020) guide. This notwithstanding, Jordaan and Steyn (2021b) submit that the RCS, derived from the ratio of UCS_w and UCS_d, is an indicator of the future behaviour of the pavement structure and the potential for formation of potholes when exposed to water. The residual strength is also an indicator of the materials durability and resistance to secondary weathering effects. The results show that increasing NME applications above the minimum 0.7% does not increase the UCS_d strength of the material but increases the UCS_w and thus the RCS of the material. The plateauing of the UCS_d is attributable to the depletion of the surface free energy and unsatisfied charges necessary for the formation of siloxane bonds described in Sections 2.11.1.5 and 2.11.1.6. It is supposed that once all the siloxane bonds are formed, further addition of the binder does not result in the formation of new bonds but only adds to the hydrophobicity of the material.

The results obtained at 1.5% NME meet requirements for a NME1 class material (TRH24, 2022) and by extension, requirements for a gravel-wearing course material. NME1 materials are described as high-quality material, capable of withstanding high traffic loadings and tyre pressures. The material is likened to a G1 crushed stone material or C1 cement stabilised material (COTO, 2020), usable as a base layer in a heavily trafficked road.

5.5 Influence of NME on ITS results

ITS tests were conducted as explained in Section 3.4.3. Similar to UCS test results, graphs of load vs time were obtained (and appended in Appendix D) from which the average peak load was determined and used to calculate the ITS. The results for both the dry test (ITS_d) and wet test (ITS_w) are provided in Figure 5-6.

The results show an increase in ITS_d of more than 16% on application of 0.7% NME to the neat material. Thereafter, the ITS remains relatively constant despite increased

NME applications up to 1.5%. ITS_w results show a somewhat steady increase up to 1.2% NME application after which it levels off, similar to the ITS_d results. The increase in ITS_w on application of 1% NME from 0.7% NME is 43% and this reduces to 28% upon increasing NME to 1.2% (from 1%) and just over 1.0% between 1.2% to 1.5% NME.

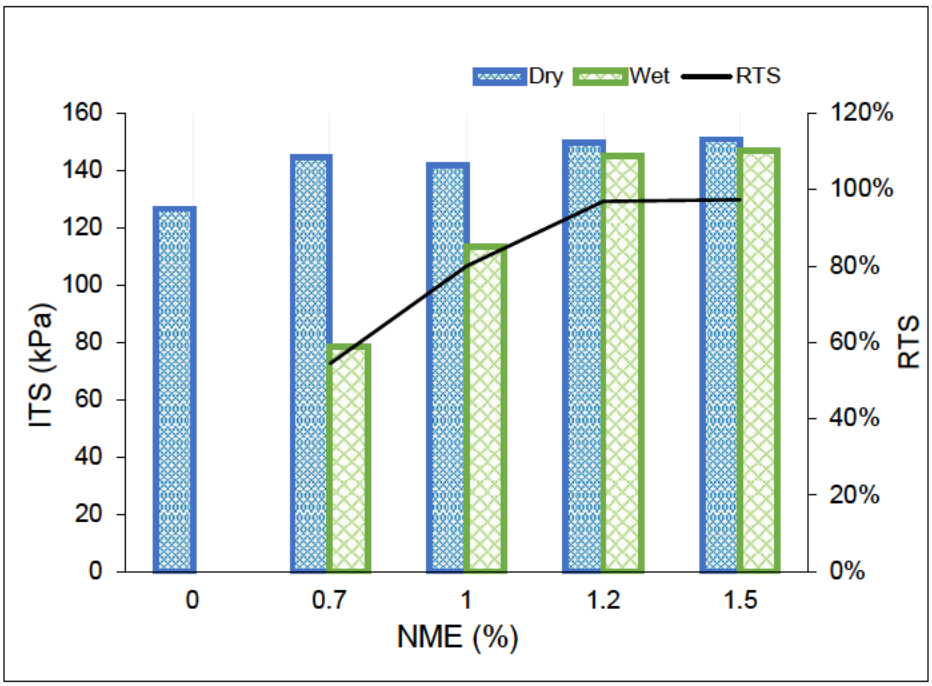

Figure 5-6: ITS test results

Figure 5-7 shows the derived relationships prescribing the variation of ITS in relation to the NME. It is shown that the results of ITS_d can be represented by a linear function with $R^2 = 0.6071$. The ITS_w results, on the other hand, are represented by a second order polynomial function with a very good fit, $R^2 = 0.9683$.

The Retained Tensile Strength (RTS) is used to indicate the moisture susceptibility of the mix. It is a ratio of the wet and dry tests and represents the retained strength after soaking of the specimen for four hours. It is calculated from Equation 5-4.

$$\mathrm{RTS} = \frac{\mathrm{ITS_{wet}}}{\mathrm{ITS_{dry}}} \times 100 \qquad \text{Equation 5-4}$$

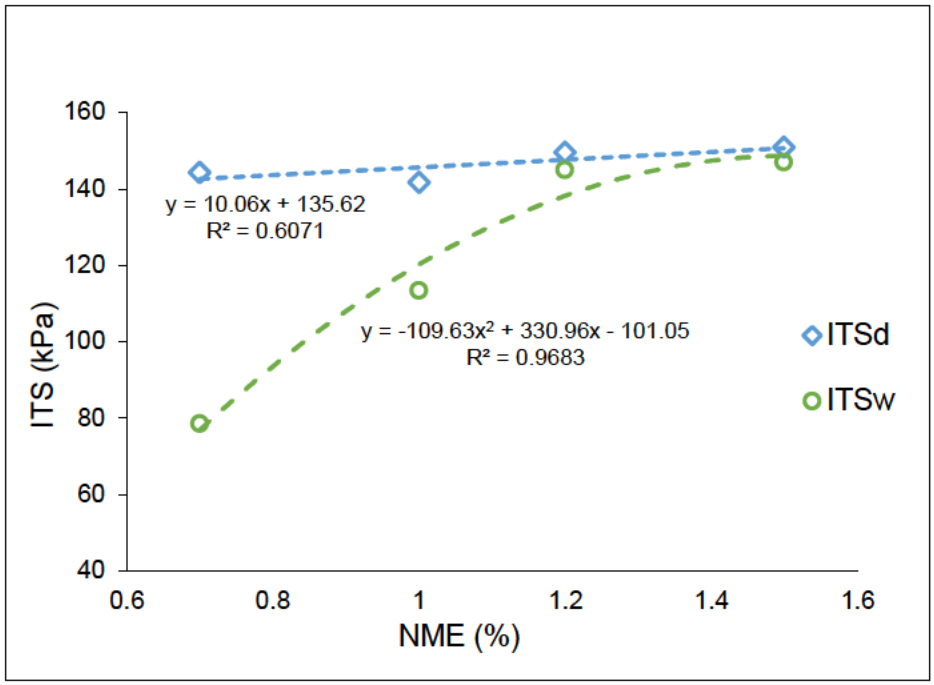

Figure 5-7: ITS strength characteristics

The RTS, as shown in Figure 5-6, increases from 53% at 0.7% NME to 97% at 1.2% NME. Moisture content determinations indicate average moisture absorption reducing from 0.98% to 0.29%. According to the NDPS (TRH24, 2022), a minimum RTS of 60% is recommended for material to be used as gravel road wearing course and lower-level material class (NME4). Based on this, the results show that 1.0% is the optimal NME application level. At 1% NME, the NMESM meets requirements for class NME2 material, a high-quality material comparable to a G2 or C2 (refer to SA material specifications, COTO, 2020), used as base layer in flexible pavements of major and inter-urban collector roads and, by extension, meets requirements for a gravel wearing course.

The ITS test is the recommended test for elemental evaluation of bituminous mixtures, used for screening and optimisation of binder quantities (TG2, 2020). It is highlighted in Chapter 2 that the organofunctional nanosilane in NME acts to promote the adhesion of the residue bitumen to inorganic substrates. Thus, it is only rational that the competence of the bonds that provide the adhesion are evaluated by a test that verges on the tensile properties of the material mix.

Table 5-3 provides limits of ITS tests for material categorised as BSM1 and BSM2 in TG2 (2020). It is notable that the limit of ITS_d for BSM2 (>175 kPa) is higher than the proposed limit for NME2 (>140 kPa) while the ITS_w for BSM2 is the same as for NME2. The results show that, at 1.5% NME, the 151 kPa recorded for the ITS_d falls short of the BSM2 limit of 175 kPa while the 147kPa recorded for the ITS_w is well within the range of BSM2.

Table 5-3: BSM ITS test limits (TG2, 2020)

Class	ITS Limits	
	ITS_{DRY} (kPa)	ITS_{WET} (kPa)
BSM1	> 225	> 125
BSM2	> 175	> 100

It should be noted that BSMs are almost exclusively for major (high-end) roads and the limits provided are for material of classes, G5 or better with added filler, so the comparison may not be valid or fair. However, it does provide a very good appreciation of the potential of NMESMs and the effect of NME especially with regard to resistance to moisture damage.

5.6 ITS-UCS relationship

The establishment of a relationship between ITS and UCS would be useful for practical purposes, whereby one of the parameters can be estimated based on the results of the other. A similar relationship is suggested for cement stabilised materials (TRH13, 1986) such that the ITS is related to UCS using a material coefficient, a, as indicated in Equation 5-5;

$$ITS = aUCS \qquad \text{Equation 5-5}$$

Accordingly, the material coefficient is the ratio between ITS and UCS. Various factors influence such a relationship including, compaction density, moulding moisture and curing conditions, all of which are controllable. However, one uncontrollable factor is the difference in measurement configuration. Therefore, a large data set is required to develop a reliable correlation. Nonetheless, based on the data collected in this study, a correlation was ventured by plotting a linear function between the results of the two parameters for both the wet and dry tests as shown in Figure 5-8.

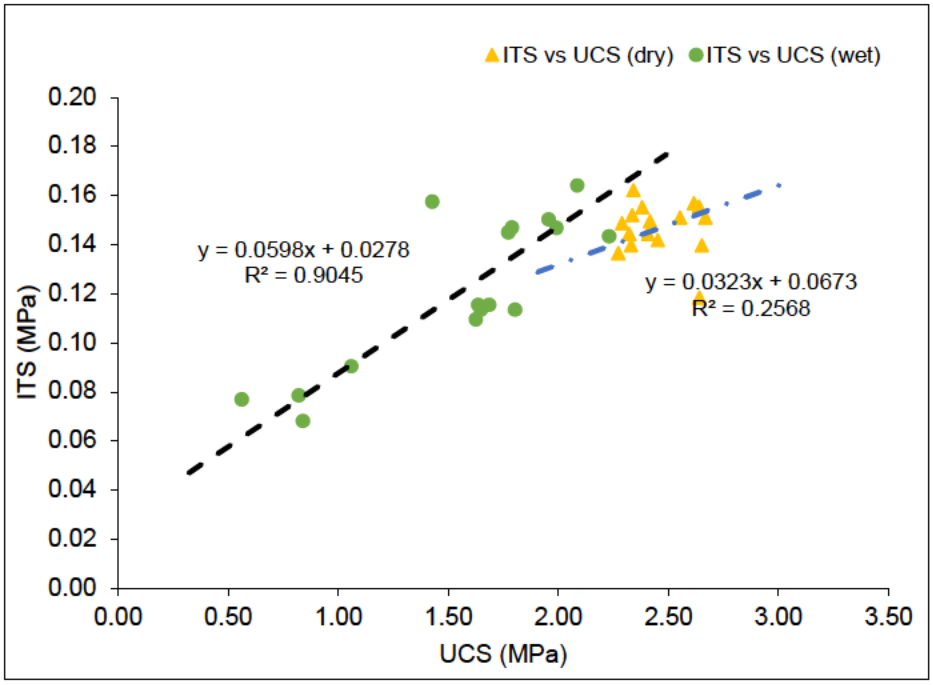

Figure 5-8: ITS-UCS relationship

The results show a linear function with a very good coefficient of determination (0.9044) for the wet tests and a poor one (R^2 = 0.2419) for the dry test. It can be concluded from these results that the ITS represents anything between 3 and 6% of UCS results. However, this is subject to verification and refinement with studies involving a larger dataset.

5.7 Effect of moisture conditioning on NMESMs

The evaluation of the retained strengths of laboratory prepared specimens after soaking (conditioning) in water for a stipulated period simulates the worst condition of a road pavement layer i.e. the event that the layer is exposed to moisture and the resulting damage, thence. While indications are that NME provides great resistance to moisture damage, the NDPS (TRH24, 2022) proposes MDRs evaluated after a conditioning period of four hours compared to twenty-four hours provided for similar materials. Therefore, the retained strength of NMESMs after conditioning was evaluated further. ITS and UCS tests were conducted on NMESM stabilised with 1.5% NME and conditioned for four, twelve and twenty-four hours and compared with the dry (unconditioned) specimens to establish loss of strength over the conditioning time. The results of the twelve- and twenty-four-hour tests are appended in Appendix E

while those for four and unconditioned are appended in respective ITS and UCS results indicated above. Extracted results are presented in Figure 5-9.

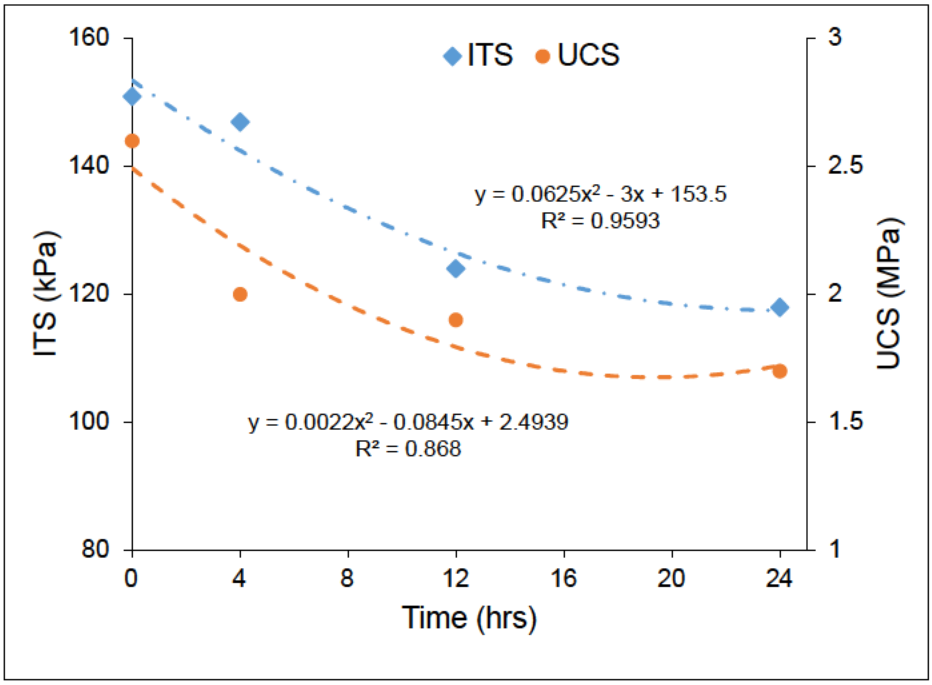

Figure 5-9: Effect of Soaking Time on ITS and UCS

The ITS results show that the strength reduces by 3%, 22% and 28% after four, twelve and twenty-four hours of conditioning, respectively. The reductions in strength of the UCS were relatively larger at 30%, 36%, 53% after the same time periods. The RTS is recorded at 78% after twenty-four hours and is still above the 60% minimum proposed in the NDPS while the RCS of 65% recorded after twenty-four hours of conditioning is slightly lower than the 75% specified in the NDPS. It is notable that the limits proposed in the NDPS are conservative and based on a four-hour conditioning period. It would therefore be rational to reconsider the limits if a longer conditioning period is proposed.

Figure 5-9 shows that the reduction in strength of both ITS and UCS tests are best represented by second order polynomials with relatively good coefficients of determination. Therefore, It appears that strength loss is reduced as the conditioning period increases, suggesting the attainment of equilibrium in terms of hydrophobicity of the material. The results therefore show that it is possible to extend the conditioning period of laboratory prepared NME stabilised specimens. Increased conditioning to

twenty-four hours would provide MDRs with higher-level certainty, particularly invaluable for gravel roads due to their susceptibility to moisture damage.

5.8 NME vs CBE

The impact of NME was compared to CBE to appreciate the unique effect of the Nano modification. An anionic SS60 bitumen emulsion was obtained and applied to the gravel at 1.5% and tested for ITS and UCS for both dry and wet conditioned cases. The results (appended in Appendix F) were compared to equivalent results of NME stabilised specimens. Extracted results for UCS and ITS are presented in Figure 5-10 and Figure 5-11, respectively.

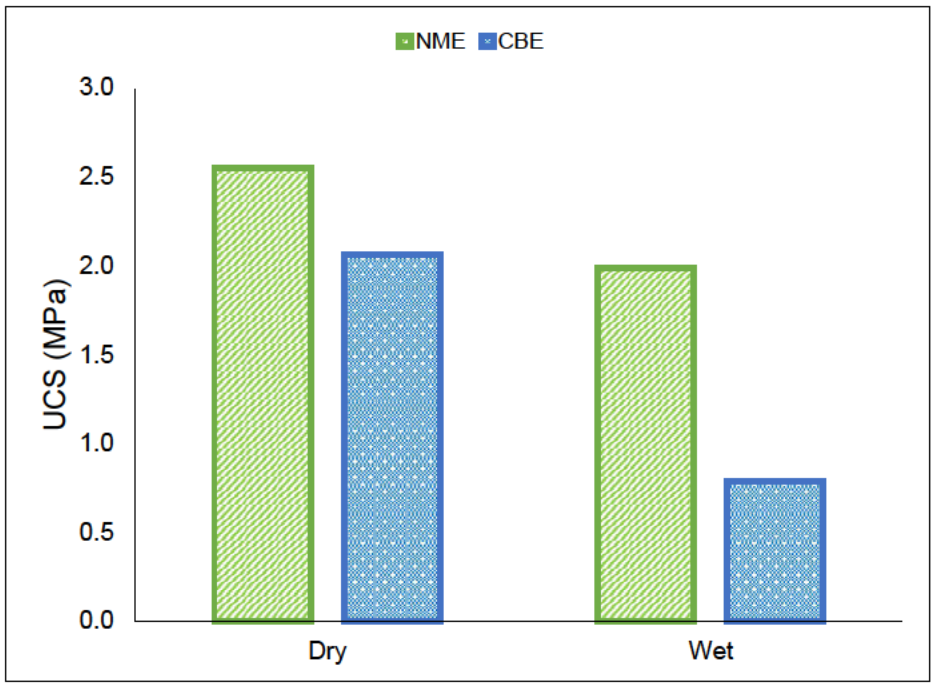

Figure 5-10: UCS Results (NME vs CBE)

The UCS results show that the NME stabilised specimens perform better in both the dry and wet conditioned cases. The dry test shows a difference of 24% between the NME and CBE stabilised specimens while the difference in the wet test is significantly higher, at 150%. It is apparent that the conditioning of the specimens in water compromises the frictional resistance component of the shear strength of CBE stabilised materials. The NME in NMESMs prevents this from happening by limiting moisture ingress and ensuring that the material retains its shear strength. This signifies the influence of NME on the material based on the UCS test.

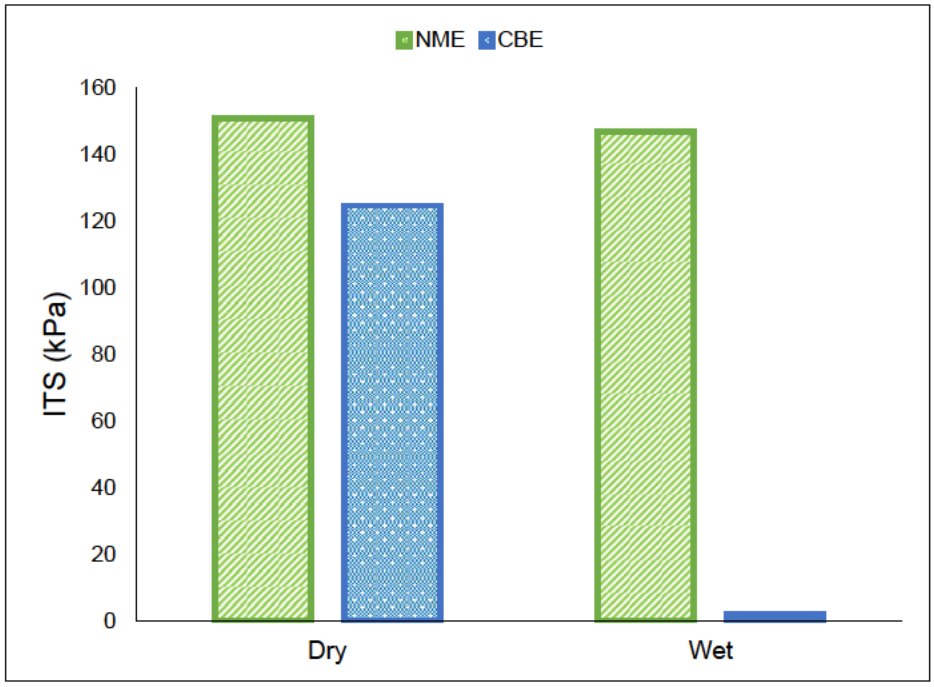

Figure 5-11: ITS Results (NME Vs CBE)

The ITS_d test results show that 21% higher strength is obtainable with NME compared to CBE. For the wet test, the CBE specimen could not withstand the conditioning and disintegrated in the water. This is consistent with the findings of Akhalwaya and Rust (2018) and provides further evidence of the extent of NME in influencing resistance to moisture damage.

Plate 5-1 shows images of some of the specimens after moisture conditioning; (A) shows CBE stabilised specimens after four hours of conditioning and (B) shows NMESMs after twenty-four hours of conditioning. The CBE stabilised specimens were observed to be completely moistened and would easily crumble and disintegrate while the NME samples showed almost complete dryness especially in the mid-section of the specimens. Moisture contents of 4.6% and 1.1% were recorded for the CBE and NME stabilised specimens, respectively.

It is noted that the CBE used for the test was not obtained from the same source as the one used for modification to NME. However, this is not expected to significantly influence the outcomes especially for the wet conditioned tests and the resistance to moisture damage thereof.

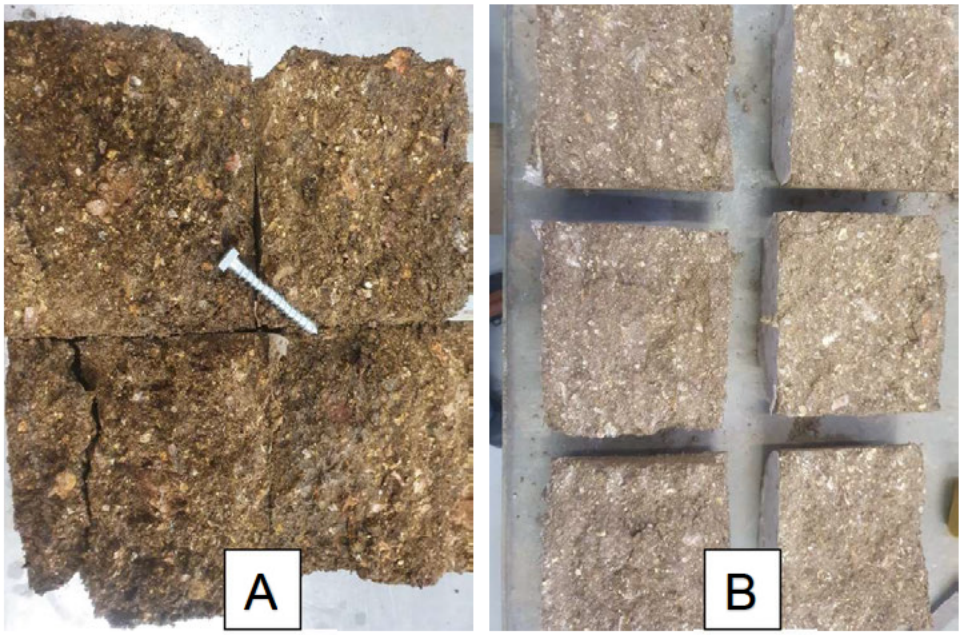

Plate 5-1: (A) CBE stabilised specimen after 4 hours soak (B) NME stabilised specimen after 24 hours soak

5.9 Influence of NME on shear strength properties

Shear strength properties of NMESMs stabilised at varying levels of NME from 0% to 1.5% were determined as explained in Section 3.4.5.1. Stress-Strain diagrams for both dry and wet conditioned tests were obtained and are appended in Appendix G. Figure 5-12 presents selected results for comparison purposes.

A number of observations can be made from the stress-strain diagrams. The peak stress of specimens increase with increase in confinement. This is attributable to the increased density of the specimens. It is also observed that the peak stress of the wet conditioned specimens are characteristically lower than their corresponding dry test results, indicating that the NMESM sustains less load in a wet condition. No discernible pattern in peak stress or strain is observable among the dry specimens while for the wet specimens, the peak stresses appear to increase with increased NME application.

The deformation to failure is not abrupt but rather drawn out as the material is loaded, clearly suggesting a flexible (non-brittle) material. It is also observed that both the stress-at-failure and strain-at-failure increase with increased confinement stress, indicative of the stress dependent behaviour of the material. This is clearly shown in Figure 5-13 for the strain-at-failure, with a few outliers excluded.

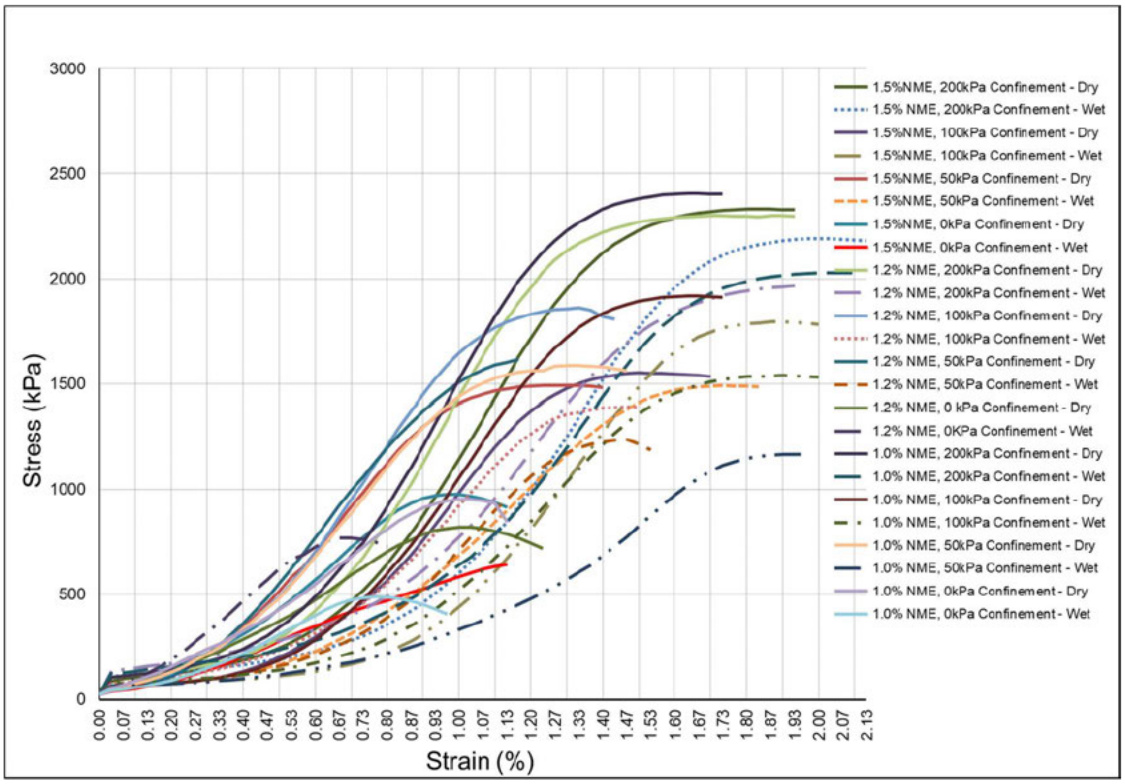

Figure 5-12: Typical stress-strain diagrams

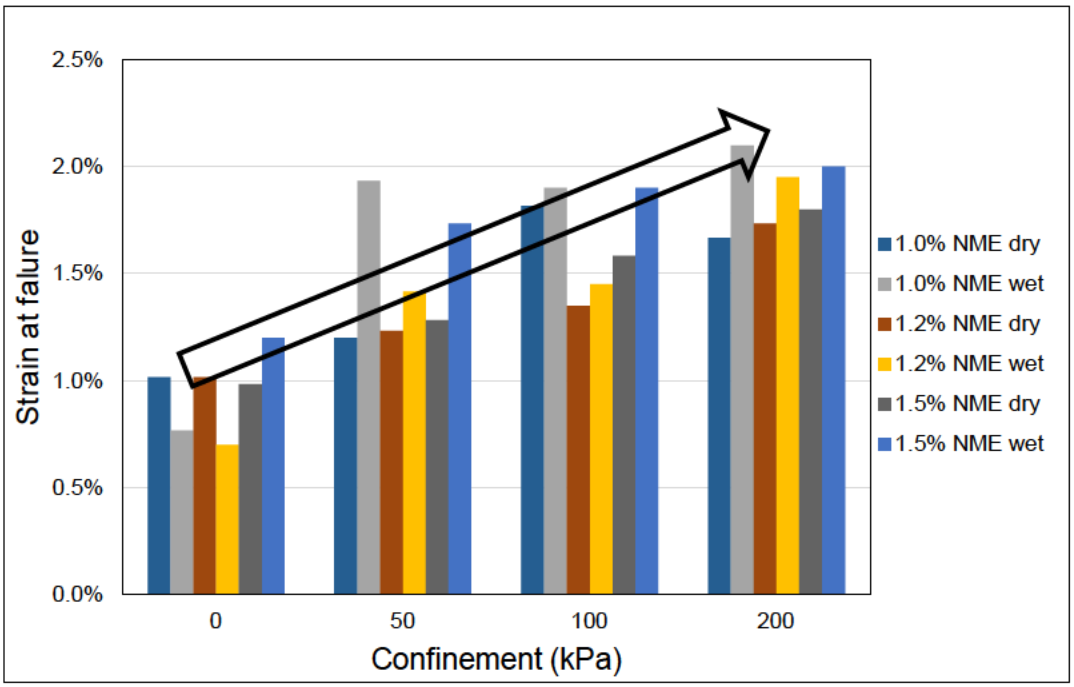

Figure 5-13: Strain-at-failure vs confinement stress

Figure 5-13 also show that generally, the strain-at-failure increases with increase in NME content and with wet material condition. This suggests that the two factors have

a lubricating effect on the material, making it more flexible. A minimum strain of 0.7% is recorded before failure at 0 kPa confinement. This strain level appears to be a threshold, below which shear failure does not occur under static loading, although this could be a conservative value as materials in a pavement structure are rarely in a situation of zero confinement.

5.9.1 Mohr-Coulomb plots

Mohr circle plots of the STT results were developed to determine the shear parameters, cohesion and angle of friction of the material. The plots for the unstabilised and 0.7% NME stabilised, for both dry and wet conditioned specimens, are shown in Figure 5-14 and Figure 5-15 respectively, while plots for 1.0%, 1.2% and 1.5% NME applications are appended in Appendix G.

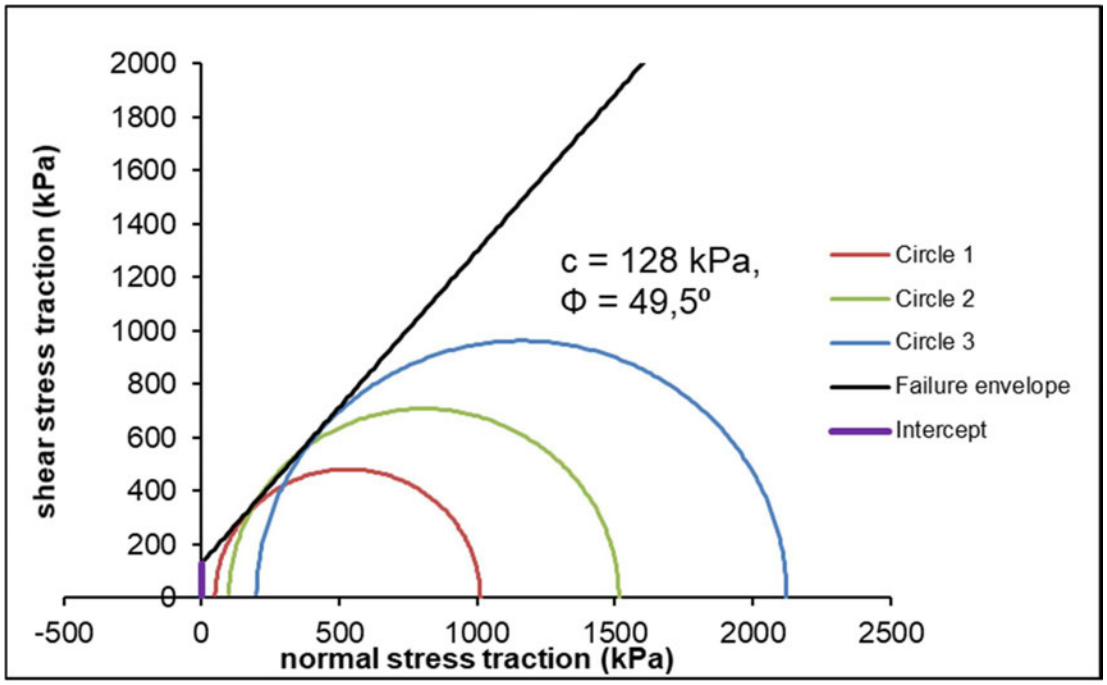

Figure 5-14: Mohr-Coulomb circles – Unstabilised

Table 5-4 provides a summary of the results and the shear parameters. The linear function analysis used to derive the Mohr-Coulomb failure envelope lines produced good coefficients of determination in excess of 0.99. This demonstrates the consistency of the results for ultimate strengths obtained at the various confinement levels.

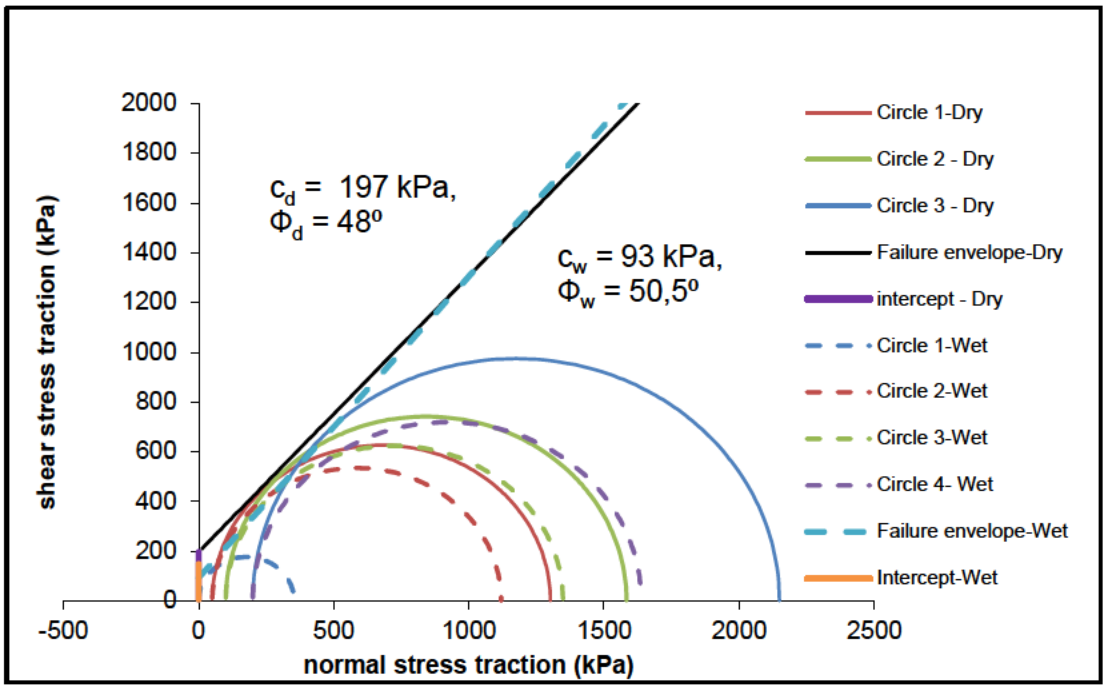

Figure 5-15: Mohr-Coulomb circles – 0.7%NME

Table 5-4: Summary of STT results

NME (%)	Condition	Cohesion (kPa)	Friction Angle (°)	R^2
0	Dry	128	49.5	0.999
0.7	Dry	197	47.6	0.997
	Wet	93	50.5	0.990
1	Dry	184	51.5	0.997
	Wet	102	52.6	0.997
1.2	Dry	168	52.2	0.993
	Wet	152	48.2	0.999
1.5	Dry	185	49.4	0.998
	Wet	135	53.1	0.994

5.9.2 Cohesion

The cohesion of the unstabilised material was determined to be 128 kPa. This is an apparent cohesion, as granular materials do not exhibit true cohesion. Jenkins et al. (2007) explain that apparent cohesion of untreated granular materials is likely to be the result of capillary forces due to interstitial moisture forming small bonds between particles. The authors indicate that it generally does not exceed 150 kPa. Theyse (2008) provides typical ranges of cohesion and angle of friction for a G5/6 granular material proposed for use in SAMDM. Cohesion values of up to 125 kPa are proposed for material in dry condition, reducing to 100 kPa in the moderate (wet) condition as

indicated in Table 5-5. Therefore, the obtained cohesion is clearly within the acceptable limits.

Table 5-5: Shear strength properties for unbound granular materials (Theyse, 2008)

	Material Class	Saturation level	Cohesion (kPa)	Angle of Friction (°)
Subbase Coarse material GM: 1.7 - 2.3 Max. size: 26.5 - 37.5	G5/6	Dry	100 - 125	45 - 49
		Moderate	50 - 100	41 - 45

The results of the dry tests show that the cohesion increases by between 31% and 54% for NME applications up to 1.5% (Table 5-4). The wet conditioned test results range from 93 kPa to 152 kPa and are consistently lower than their corresponding dry test results. This is consistent with the findings of Smit et al. (2021). Figure 5-16 shows the characteristic variations of the cohesive strength at the NME applications (from 0.7% to 1.5%). The dry cohesive strength results show a relatively linear trend, slightly distorted by the high cohesion obtained at 0.7% NME, attributable to experimental errors. The cohesive strength (wet test) shows the variation of the cohesion is represented by a polynomial of the second order, a trend similar to ITS and UCS results.

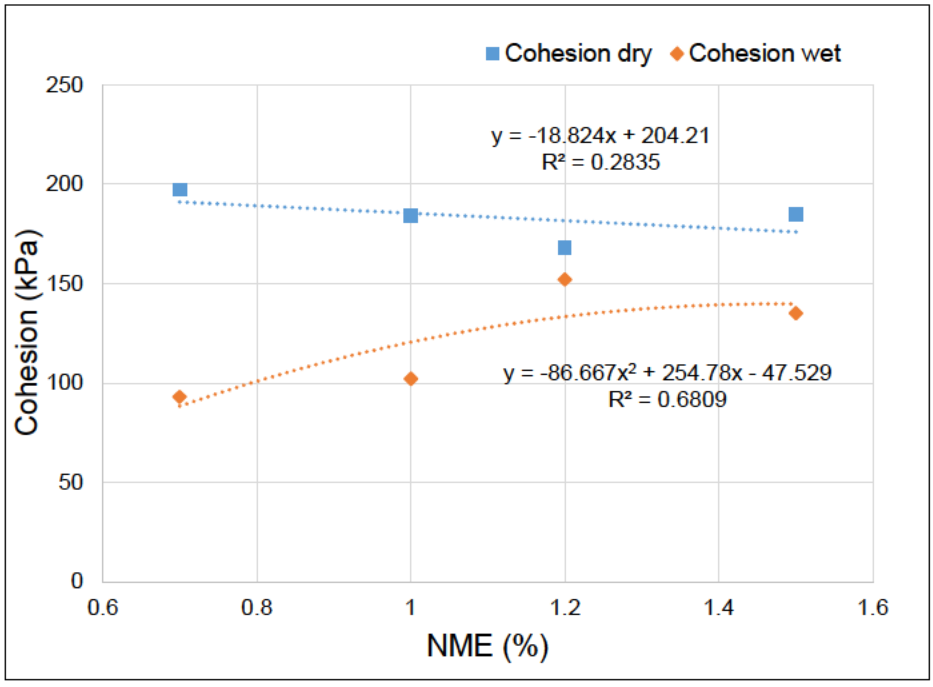

Figure 5-16: Cohesion strength characteristics

The Retained Cohesion (RetC) is defined as the percentage of residual cohesion of the NMESM after moisture exposure. It provides an indication of the durability of the material and is defined by Equation 5-6 (TG2, 2020);

$$RetC = \frac{\sigma_{1WE\ ,F} - \sigma_3}{\sigma_{1EQUIL,F} - \sigma_3} \times 100 \qquad \text{Equation 5-6}$$

Where;

RetC = retained cohesion after soaking, expressed as a percentage;

σ_3 = confining pressure in kPa

$\sigma_{1WET,F}$ = conditioned applied peak stress at confining pressure σ_3, in kPa

$\sigma_{1EQUIL,F}$ = dry peak stress read from the best fit line at confining pressure (σ_3) in kPa.

RetC is calculated at a confining stress (σ_3) of 100 kPa at each of the NME applications from 0.7% to 1.5%. The results are provided in Table 5-6. It is shown that a minimum RetC of 75% is obtained at 0.7% NME application. This increases up to 99% at 1.5% NME, indicating increased hydrophobicity with increase in NME application. TG2 (2020) defines a RetC threshold of 65%, above which materials are considered relatively moisture insensitive or less susceptible to moisture damage. Therefore, the minimum 0.7% NME is adequate and optimum, based on this requirement.

Table 5-6: Retained Cohesion

NME (%)	RetC (%)
0.7	75
1	78
1.2	78
1.5	99

5.9.3 Angle of Friction

The angle of friction component of the shear strength is mobilised through particle contact when compressive stresses force the particles together. It is influenced by material grading and other aggregate properties including angularity and texture. Table 5-5 provides typical range of values of angle of friction for a G5/6 material.

Figure 5-17 depicts the results of angle of friction for both dry and wet conditioned tests shown in Table 5-4. It is observed that the measured angles of friction for the treated materials (for both wet and dry material conditions) do not vary significantly from that of the unstabilised nor from each other. This is consistent with the findings

of Smit et al. (2021). Therefore, it can be concluded that neither the NME nor the four-hour conditioning of specimens have a significant influence on the angle of friction of NMESMs.

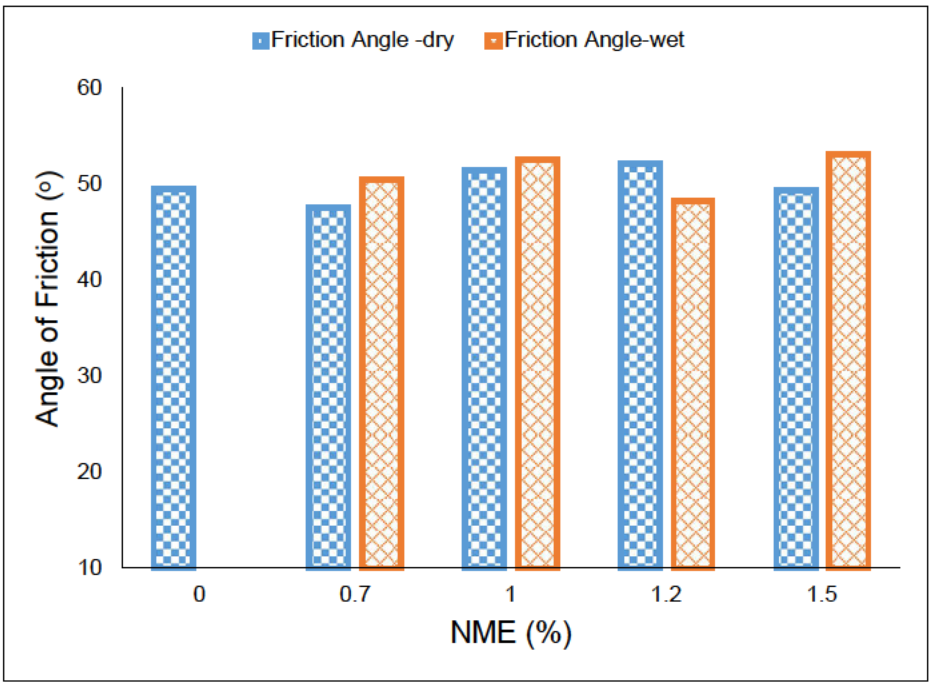

Figure 5-17: Angle of Friction of NMESM

5.9.4 Shear stress

The determination of the maximum shear stress that a material can support is ultimately the most important factor with regard to the determination of shear strength properties of materials. The maximum shear stress of the material is determined by the shear parameters C and angle of friction and is represented as the shear strength envelopes of the respective Mohr circles. Figure 5-18 and Figure 5-19 compare the shear strength envelopes of dry and wet conditioned NME stabilised materials, at varying levels from 0.7 to 1.5%, against the neat (UT) material.

The results show that the envelopes of the 0.7% NME, both dry and wet conditioned, do not significantly depart from the UT envelopes. Considerable shifts are observed after 1.0% NME particularly for the dry conditioned specimens. This indicates the improvement in the shear strength of the material. The wet test envelopes are also observed to generally show improvement compared to the dry test. The minor

differences in the angle of friction are observed to cause overlaps of the failure envelopes.

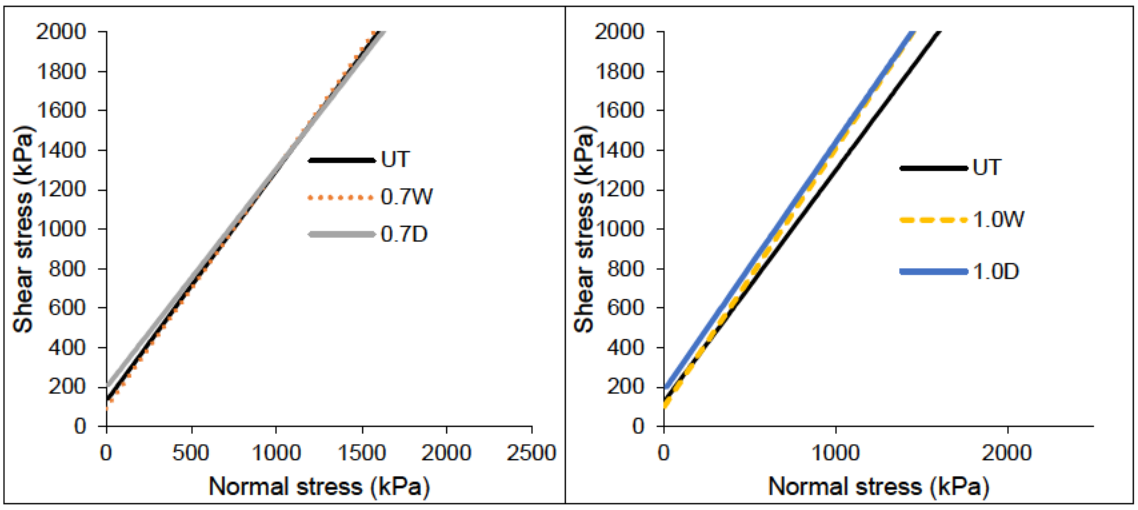

Figure 5-18: Comparison of maximum shear stress (0.7 and 1.0% NME)

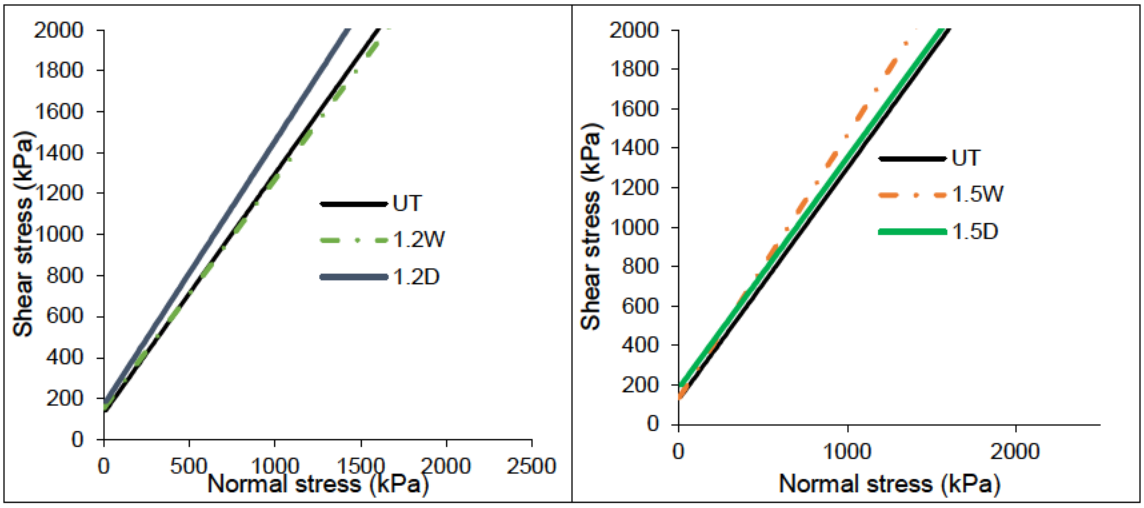

Figure 5-19: Comparison of maximum shear stress (1.2 and 1.5% NME)

5.9.5 Compressive and tensile strengths

It is possible to estimate the compressive and tensile strengths of the NMESMs based on the results of shear strength tests and failure envelope thereof. According to Ebels (2008), the compressive strength is estimated for the case when $\sigma_3 = 0$ while the tensile strength is estimated when $\sigma_1 = 0$ as shown in Figure 5-20. The two stresses are determined from Equation 2-2 reproduced below. The results of the determinations are provided in Table 5-7 and Figure 5-21 for better perception of the trends

$$\sigma_{1f} = \frac{(1 + \sin\varphi).\sigma_3 + 2.C.\cos\varphi}{(1 - \sin\varphi)}$$

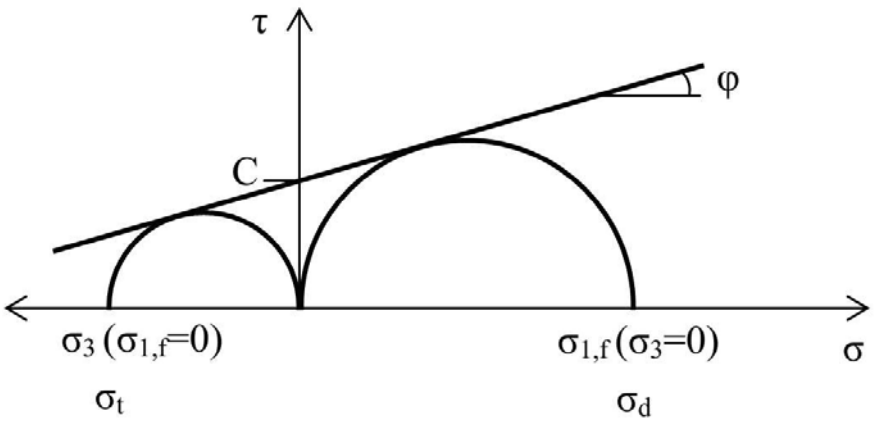

Figure 5-20: Mohr Coulomb diagram for determination of compressive and tensile strength (Ebels, 2008)

Table 5-7: Estimated compressive and tensile strengths

NME (%)	Condition	Estimated compressive strength (kPa)	Estimated tensile strength (kPa)
0	Dry	694	94
0.7	Dry	1016	153
	Wet	518	67
1	Dry	1054	128
	Wet	603	69
1.2	Dry	981	115
	Wet	796	116
1.5	Dry	1000	137
	Wet	809	90

The results show that the estimated compressive strength of the material increases by an average of 46% upon stabilisation (dry condition). Thereafter, not much difference is observed between 0.7 to 1.5% NME applications. For the wet conditioned materials, the compressive strength is observed to increase uniformly between 0.7% and 1.2% NME and plateaus up to 1.5%. A similar pattern is observed with the tensile strength. The average increase on NME application to the material is 42% (dry condition). In the wet condition, the tensile strength is relatively constant between 0.7 and 1.0%, increasing at 1.2% before decreasing again.

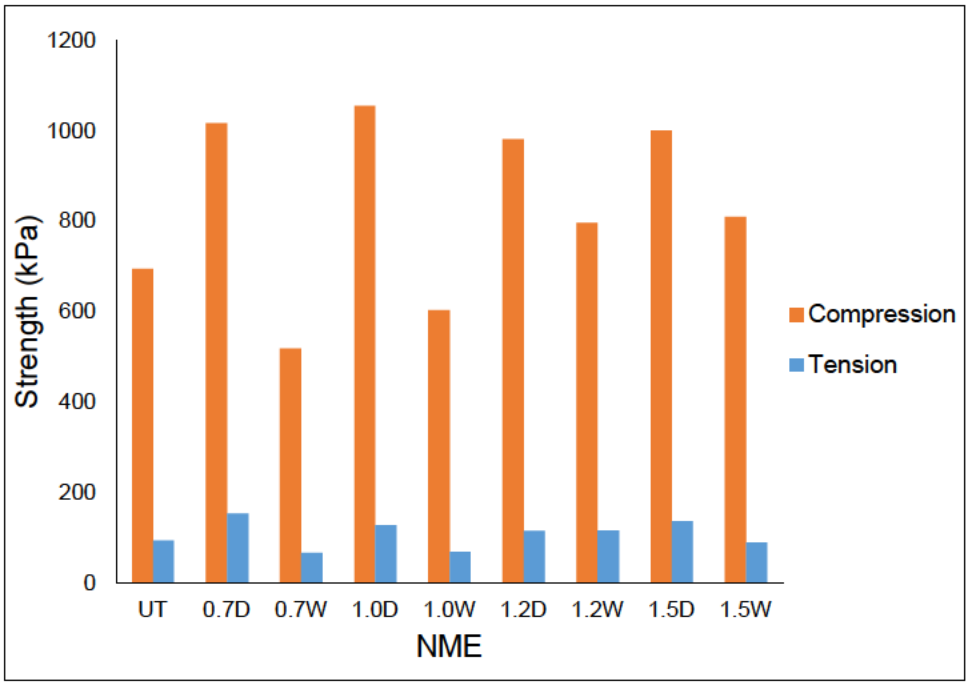

Figure 5-21: Estimated compressive and tensile strengths

Shear strength properties determined from STT provide better understanding of the fundamental properties and behavioural characteristics of granular and equivalent materials. It is for this reason that STT are included in TG2 (2020) as the primary method of characterisation and material optimisation during mix design of bituminous materials.

The results show that the NME acts to increase the shear strength of material by increasing the cohesive strength component while the angle of friction remains virtually unaffected. The range of cohesion of NMESMs (168 to 197 kPa) is considerably lower than the range for BSM2 material provided in TG2 (i.e. 225 to 265 kPa) but well above the range for unbound granular materials (100 – 125 kPa). This clearly indicates that the NMESM is an improvement on the unbound material though it might not be at the level of BSMs. However, as stated earlier, the comparison with BSMs may be unfair considering the inherent quality of the materials designated for stabilisation with the two technologies. The maximum 152 kPa cohesion obtained for the wet test is considerably high compared to a wet conditioned unbound material and exhibits good resistance to moisture damage. This is exemplified by the high RetC values of up to 99%.

According to Thompson and Visser (1996), granular materials exhibit distress through cumulative permanent deformation or inadequate stability. Both forms of distress are related to the ultimate shear strength of the material and to prohibit shear failure or excessive gradual shear deformation in the layer the traffic-generated shear stresses must be limited. SAPEM (2013) provides a method of determining the shear strength of the materials (also known as the safety factor) using the shear parameters obtained from the Mohr-Coulomb model, using Equation 5-7. This is used in a transfer function (Equation 5-8) to estimate the material's structural capacity to a terminal condition of 20 mm of rutting in a pavement layer.

$$F = \frac{\sigma_3\left[k\left(tan^2\left(45\ \frac{\phi}{2}\right)-1\right)\right]+2kCtan\left(45\ \frac{\phi}{2}\right)}{(\sigma_1-\sigma_3)} \quad \text{Equation 5-7}$$

$$N = 10^{(\alpha F+\beta)} \quad \text{Equation 5-8}$$

Where;

F = Shear strength (factor of safety)

σ_1, σ_3= Major and minor principle stresses acting in the middle of the granular

C = Cohesion

Φ = Angle of friction

K = Constant for moisture, 0.8 for moderately wet and 0.95 for normal

α, β = Constants based on road category. Values provided in SAPEM (2013)

N = Number of ESAL to safeguard against shear failure

The two equations are depicted in graphical format in Figure 5-22 for categories of roads from A to D, as defined by SA standards (SAPEM, 2013). The graph was used to determine the structural capacity of a NMESM constructed layer based on obtained results of shear strength tests. Considering a Category D road class, defined as a rural access road with a daily traffic of less than 500 equivalent vehicle units (evu) and a design reliability of 50%, the results show that a layer of NMESM can sustain over a million ESAL in a dry state and more than 0.7 million ESAL in a wet condition. It is observed that the traffic sustainable by the NMESM in the TD condition is well over 220% of what would be sustained in the UT material condition.

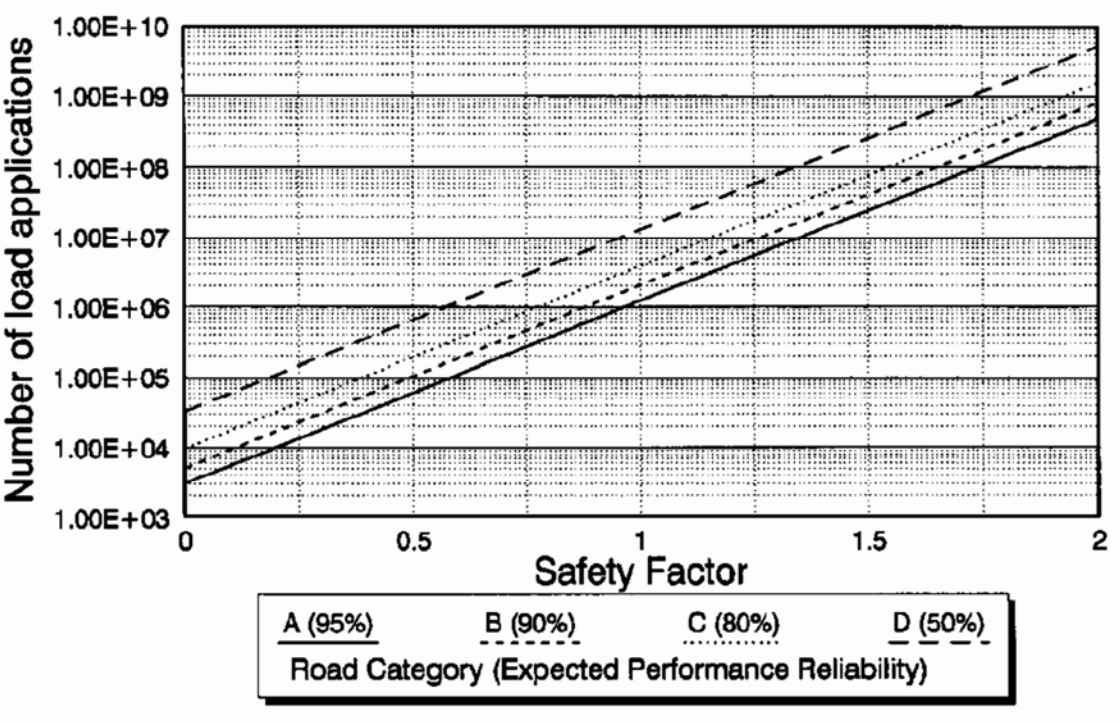

Figure 5-22: Transfer function for granular materials (Theyse et al. 1996)

5.10 Repeated Load Triaxial Test (M_R)

M_R tests were conducted on an unstabilised (control) specimen and on both dry and wet conditioned specimens stabilised at 1.5% NME. As explained in Section 3.4.5.2, the tests were conducted at SRs of 20%, 30%, 40%, 50% and 60% at each of the confining pressures; 20 kPa, 50 kPa, 100 kPa, 150 kPa and 200 kPa. The results of the tests at each confinement pressure were plotted against bulk stress in Figure 5-23.

The results show higher M_R values for the TD results followed by the TW and lastly the UT. This is consistent at all confining stresses. The M_R is observed to vary between 150 to 600 MPa for the UT material condition, 190 to over 900 MPa for the TW condition and 600 to over 1500 MPa for the TD condition, indicating average differences of 92% between TD and TW and 45% between TW and UT material conditions. The results show that M_R increases with increase in confining pressure. This can be attributed to the increase in density resulting in higher material stiffness. Additionally, stress dependency is observed particularly in the results of the UT and TW results. This is typical granular material behaviour, as Jenkins et al. (2007) explain, and can be attributed to stress hardening. However, this behaviour appears to wear down with the TD results as evidenced from the change in slope of the function lines.

Smit et al. (2021) report similar findings. A closer examination of the (TD) results indicates, to some extent, a parabolic behaviour of the material as shown in the plots of the average M_R results against the bulk stress, in Figure 5-24. The M_R reduces to a base point and increases thereafter. This is particularly evident at low confining stresses and the phenomenon wears off as the confining stress increases.

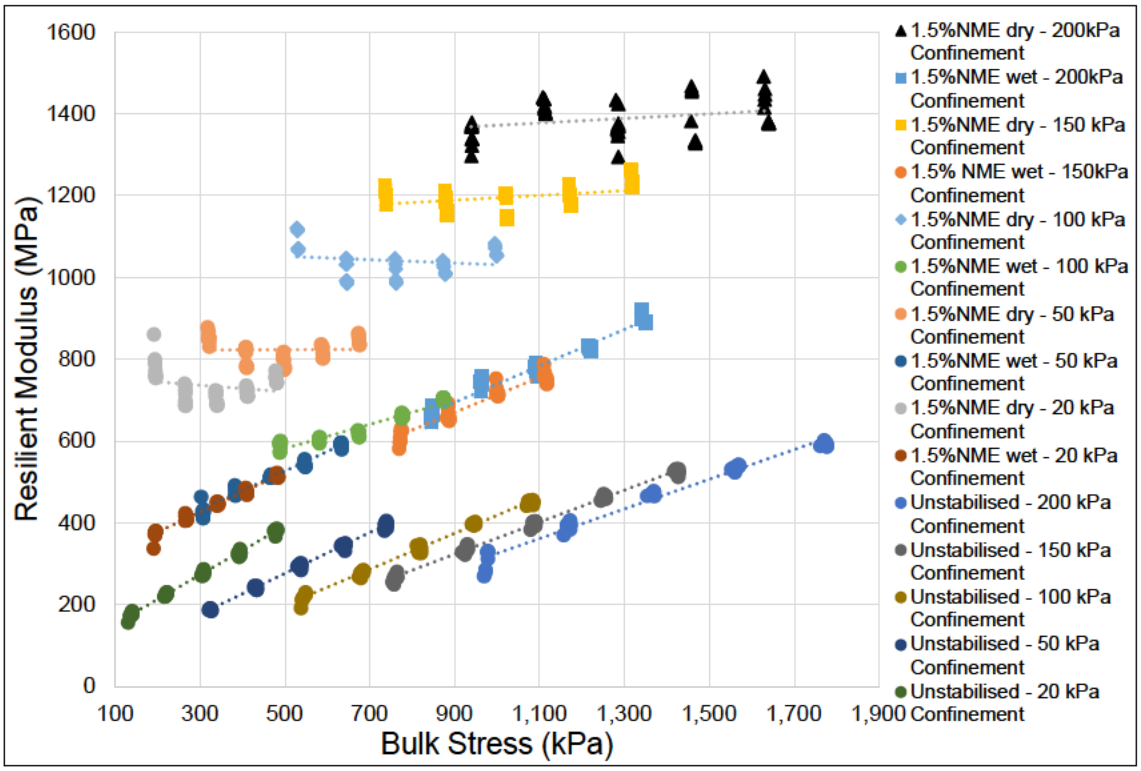

Figure 5-23: Results of resilient modulus tests

The observed behaviour (stress independence) of TD materials can be attributed to the residue stress state of materials after compaction as also observed by Araya (2011) and Uzan (1985). When subjected to compaction, particles of the material are rearranged by translation and/or rotation before locking in position. After removal of the externally applied compaction stress, the material is not in a stress-free state but rather a residual stress state induced by both the effects of confinement and aggregate interlock. When such a specimen is subjected to deviator stresses, under low confining stress, the aggregate interlock is disrupted causing an initial decrease in M_R (softening), before increasing. Jenkins (2000) explains that this phenomenon is associated with strongly bound materials, which explains why the phenomenon is not

observed with the TW and the UT results. The phenomenon has also been associated to inadequate conditioning of specimens, though not in this case.

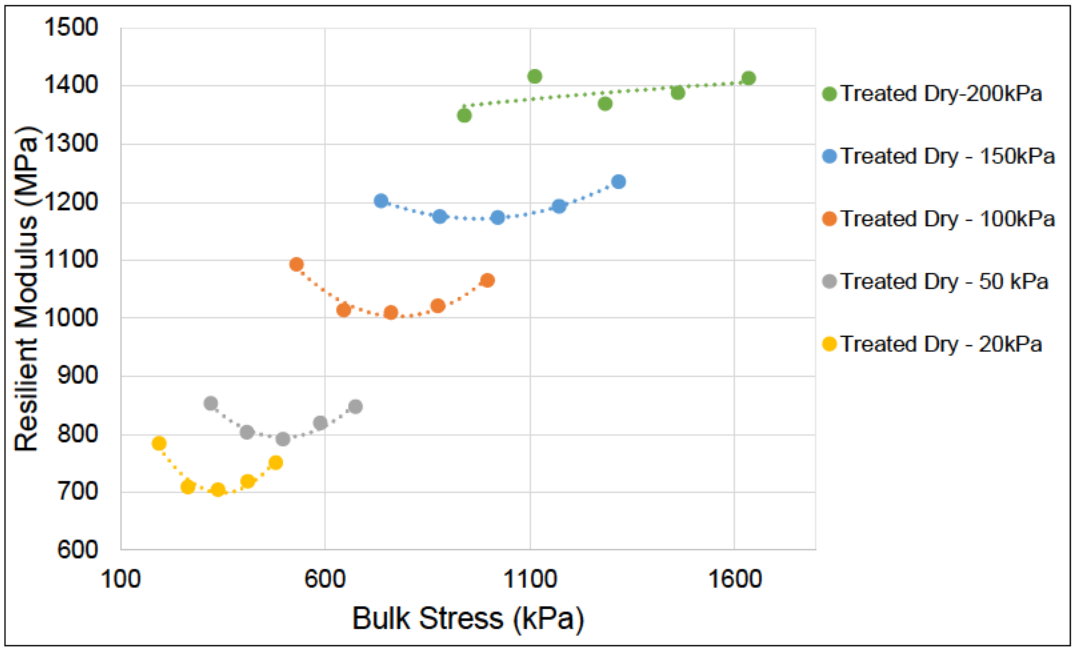

Figure 5-24: Treated dry M_R Vs Bulk stress

5.10.1 Modelling of M_R behaviour

It is discussed in Section 2.11.5.5a that M_R models developed for granular materials can also be used to describe the behavioural patterns of NMESM. Considering that this (NMESM) is a relatively new material, nine models were appraised for their suitability to model the material behaviour of NMESMs. The models were normalized to the experimental data using non-linear regression and the solver function in Excel to determine the coefficient of determination. The method works by obtaining the average of the experimental M_R data and the average of the calculated M_R data for any given model. The difference between the two sets of data is squared and, using the solver function, minimised to calculate the normalized data for the calculated M_R values. Care should be taken to check the practicality of the obtained solutions as the solver function is based on maximising R^2 values. Therefore, manual manipulation of the results may be required, at times, to ensure the solutions are practical, and this may be at the expense of a lower R^2.

A summary of the evaluated models is reproduced in Table 5-8 for easy reference while Figure 5-25 shows typical regression graphs based on the Bulk Stress-Resilient Modulus (M_R-θ) model. The rest of the models are appended in Appendix H and a summary of the results provided in Table 5-9.

Table 5-8: Summary of evaluated M_R models (reproduced from Table 2-3)

No.	Name	Formula	Source
1	M_R-θ	$M_R = k_1\theta^{k_2}$	Jenkins (2000), Ebels (2008)
2	Uzan Model	$M_R = k_1\theta^{k_2}\sigma_d{}^{k_3}$	Uzan (1985)
3	Universal	$M_R = k_1 P_a \left(\frac{\theta}{P_a}\right)^{k_2} \left(\frac{\tau_{oct}}{P_a} + 1\right)^{k_3}$	Wang et al. (2022)
4	Superpave	$M_R = k_1 P_a \left(\frac{\theta - 3k_4}{P_a}\right)^{k_2} \left(\frac{\tau_{oct}}{P_a}\right)^{k_3}$	Hopkins et al. (2001), Wang et al. (2022)
5	M_R-θ-σ_d/σ_{df}	$M_R = k_1\theta^{k_2}\left(1 - k_3\left(\frac{\sigma_d}{\sigma_{df}}\right)^{k_4}\right)$	Jenkins (2000), Kotzé (2022)
6	Parabolic M_R-σ_3-σ_d	$M_R = k_1\sigma_3{}^{k_2}\left(k_3\left(\frac{\sigma_d}{\sigma_{df}}\right)^2 + k_4\left(\frac{\sigma_d}{\sigma_{df}}\right) + k_5\right)$	van Niekerk (2002)
7	M_R-θ-σ_1/σ_{1f}	$M_R = k_1\theta^{k_2}\left(1 - k_3\left(\frac{\sigma_1}{\sigma_{1f}}\right)^{k_4}\right)$	Jenkins (2000), Kotzé (2022)
8	TU Delft M_R-σ_3- σ_1/σ_{1f}	$M_R = k_1\sigma_3{}^{k_2}\left(1 - k_3\left(\frac{\sigma_1}{\sigma_{1f}}\right)^{k_4}\right)$	Jenkins (2000), Kotzé (2022)
9	M_R-σ_3- σ_d/σ_{df}	$M_R = k_1\sigma_3{}^{k_2}\left(1 - k_3\left(\frac{\sigma_d}{\sigma_{df}}\right)^{k_4}\right)$	Jenkins (2000), Kotzé (2022)

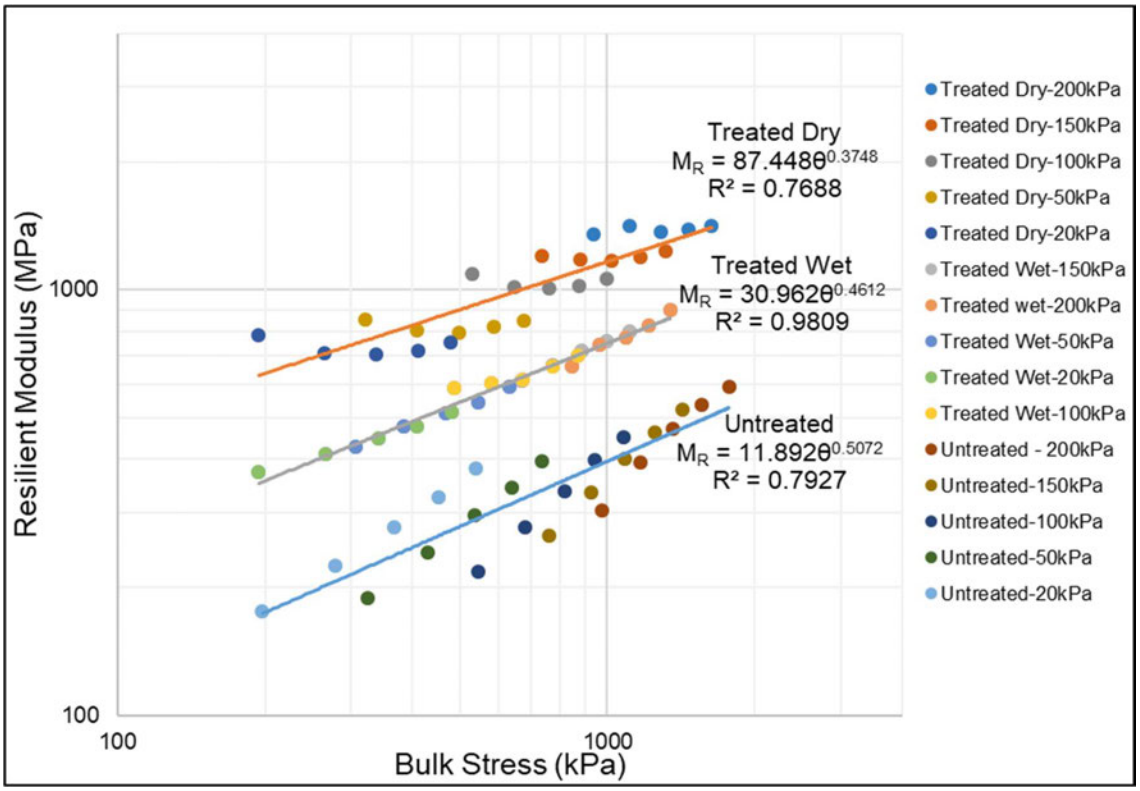

Figure 5-25: M_R-θ fitted model

Relatively varied results of the correlations between the predicted data and the measured data (based on the R^2) are obtained as shown in Table 5-9. The first four models appear to produce relatively inconsistent findings among the three treatment conditions, with one or two material conditions exhibiting good fit while the other(s) is (are) fairly low. Models five to nine appear to provide better fit of the data (among the three treatment conditions) with R^2 above 0.9 for all three material treatments. This is especially so for the TD and the UT materials as can be seen from Figure 5-26, Figure 5-27 and Figure 5-28, which show plots of the predicted vs measured data for TD, TW and UT materials respectively. The first four models are plotted separately from the last five mainly to avoid crowding the plots. Note that models five to nine are only plotted for points with results of σ_{1f} and σ_{df} available from the respective ST tests.

Table 5-9: Summary of regression model coefficients

No	Model	Cond.	k_1	k_2	k_3	k_4	k_5	R^2
1	M_R-θ	TD	87.448	0.3748				0.7688
		TW	30.962	0.4612				0.9809
		UT	11.892	0.5072				0.7927
2	Uzan	TD	75.873	0.3963	0.001			0.7913
		TW	28.173	0.4754	0.0004			0.9825
		UT	8.71	0.001	0.5954			0.9855
3	Universal	TD	4.606	0.7163	-0.5353			0.9203
		TW	2.519	0.4762	-0.001			0.9825
		UT	1.139	0.5478	-0.001			0.8182
4	Superpave	TD	0.478	1.3666	-0.4728	-149.18		0.9905
		TW	1.6004	0.6334	-0.0159	-59.85		0.9859
		UT	0.0151	1.6883	-0.001	-557.09		0.8390
5	Mr-θ-σ_d/σ_{df}	TD	388.3	0.5487	0.9496	0.0225		0.9751
		TW	3.43	0.4782	-7.079	0.001		0.9721
		UT	2.23	0.4815	-7.6792	0.393		0.9958
6	Parabolic	TD	193.28	0.3826	0.788	-0.591	1.035	0.9882
		TW	6.8617	0.3008	19.03	-0.1778	19.922	0.9848
		UT	4.3929	0.3216	-14.42	41.671	4.8321	0.9963
7	Mr-θ-σ_1/σ_{1f}	TD	415.37	0.5795	0.964	0.0225		0.9746
		TW	31.726	0.4891	0.2035	0.1		0.9848
		UT	0.4594	0.4555	-51.061	0.4365		0.9952
8	Mr-σ_3-σ_d/σ_{df}	TD	8.5405	0.3834	-20.351	0.0068		0.9830
		TW	4.7545	0.301	-40.951	0.2365		0.9778
		UT	7.467	0.3213	-19.156	0.678		0.9962
9	Mr-σ_3-σ_1/σ_{1f}	TD	8.054	0.3829	-21.721	0.0093		0.9830
		TW	5.159	0.2755	-43.66	0.3158		0.9765
		UT	6.8724	0.2896	-25.534	0.8177		0.9967

TD – Treated Dry, TW – Treated Wet, UT – Untreated

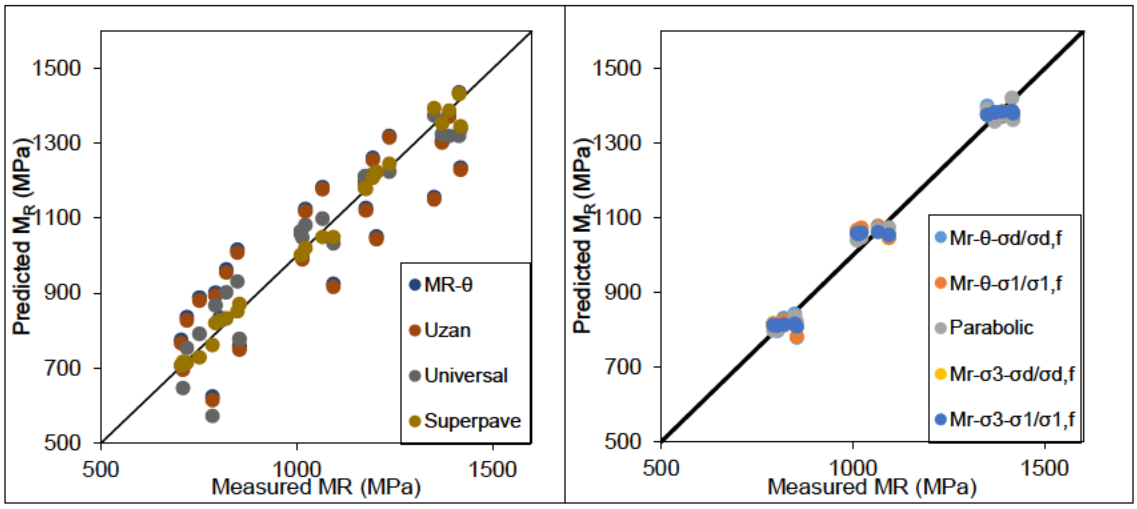

Figure 5-26: Measured vs predicted M_R – TD

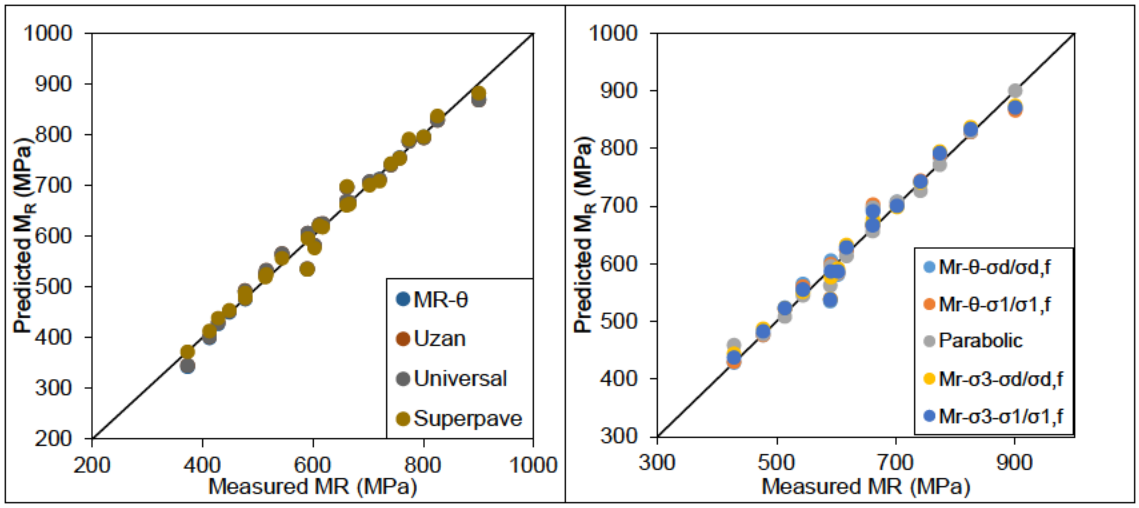

Figure 5-27: Measured vs predicted M_R – TW

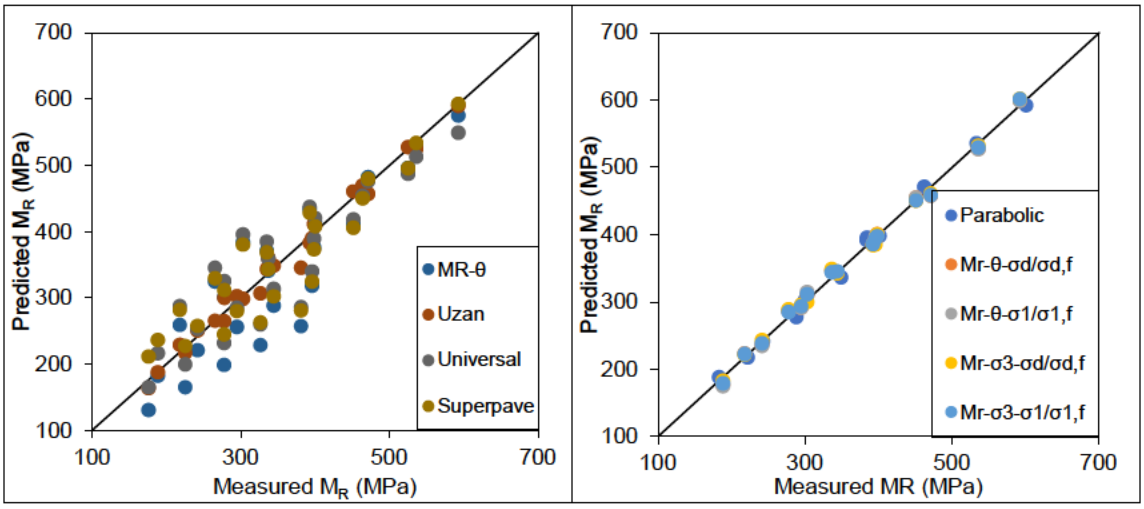

Figure 5-28: Measured vs predicted M_R – UT

5.10.1.1 Optimal M_R prediction model

Additional assessments were conducted on the prediction models to determine the optimum model to be considered for design purposes. Statistical data, other than the R^2 coefficient, were used to quantify the goodness-of-fit of the data from the prediction models and the measured data. Comparisons of the two data sets are made based on the Root Mean Square Error (RMSE) and the Mean Absolute Error (MAE). Other statistics of the predicted data are included to show consistency of the data. Table 5-10 presents the results for all three material conditions, UT, TW and TD.

It is determined that low values of RMSE and MAE are obtained for the UT and TD specimens for models five to nine as established in the preceding section with the R^2 coefficients. This is not the case with the TW specimens, which shows relatively good fit with all the models, particularly the superpave and parabolic. Nonetheless, the results appear to show that factors, θ, P_a and τ_{oct} do not significantly influence the M_R of NMESMs. Instead, it is shown that the principal stress ratio ($\frac{\sigma_1}{\sigma_{1f}}$) and deviator stress ratio ($\frac{\sigma_d}{\sigma_{df}}$) influence the M_R, with the latter appearing to have the most influence. These findings are consistent with the assertion by Jenkins (2000) that the ratio ($\frac{\sigma_d}{\sigma_{df}}$) is a better performance parameter of granular materials. Confining stress also appears to influence the M_R quite significantly as indicated in the models where it is incorporated.

The variance and standard deviation of the predicted data for all the models are comparable while the skewness does not significantly depart from zero, indicating a generally symmetrical distribution. The negative kurtosis for all models means fewer and/or less extreme outliers of the distribution. These factors show consistent distribution of the predicted data.

On consideration of all the factors, the parabolic model is shown to have the best combination of factors and is thus determined to provide the best fit for the three datasets.

Table 5-10: Comparison of statistics of the M_R prediction models evaluated

Model	**Mod MR-θ**			**Uzan**			**Universal**		
Condition	**UT**	**TW**	**TD**	**UT**	**TW**	**TD**	**UT**	**TW**	**TD**
Residual Sum of Squares	66568	8404	303255	4285	8331	301939	53923	8326	116617
Root Mean Square Error	51,60	18,34	110,14	13,09	18,25	109,90	46,44	18,25	68,30
Mean Absolute Error	0,134	0,023	0,096	0,033	0,023	0,095	0,122	0,023	0,058
Variance	14272,9	20174,9	48366,0	12250,4	19676,5	49170,9	10582,3	19681,1	58590,8
St. Deviation	119,47	142,04	219,92	110,68	140,27	221,75	102,87	140,29	242,06
Skewness	0,200	-0,072	-0,069	0,333	-0,077	-0,063	0,078	-0,077	-0,302
Kurtosis	-0.765	-0.819	-0.852	-0.468	-0.816	-0.854	-0.792	-0.817	-1.151
Model	**Superpave**			**Mr-θ-σd/σd,f**			**Parabolic**		
Condition	**UT**	**TW**	**TD**	**UT**	**TW**	**TD**	**UT**	**TW**	**TD**
Residual Sum of Squares	47721	6665	13772	795	6653	20508	698	3629	9675
Root Mean Square Error	43,69	16,33	23,47	7,28	21,06	36,98	6,82	15,56	25,40
Mean Absolute Error	0,115	0,017	0,017	0,021	0,022	0,023	0,018	0,016	0,015
Variance	10353,1	19462,1	59771,9	13391,7	16725,0	57675,3	13331,5	16673,7	58411,9
St. Deviation	101,75	139,51	244,48	115,72	129,33	240,16	115,46	129,13	241,69
Skewness	0,693	0,107	0,154	0,406	0,173	0,158	0,477	0,465	0,204
Kurtosis	-0.201	-0.893	-1.385	-0.144	-0.777	-1.588	-0.112	-0.476	-1.580
Model	**Mr-θ-σ1/σ1,f**			**Mr-σ3-σ1/σ1,f**			**Mr-σ3-σd/σd,f**		
Condition	**UT**	**TW**	**TD**	**UT**	**TW**	**TD**	**UT**	**TW**	**TD**
Residual Sum of Squares	907	6456	20940	612	5600	13991	718	5298	14009
Root Mean Square Error	7,77	20,75	37,36	6,38	19,32	30,54	6,92	18,79	30,56
Mean Absolute Error	0,022	0,021	0,023	0,017	0,021	0,019	0,018	0,022	0,019
Variance	13461,2	16714,6	57556,0	13388,3	16708,2	58269,5	13325,8	16651,9	58272,1
St. Deviation	116,02	129,29	239,91	115,71	129,26	241,39	115,44	129,04	241,40
Skewness	0,374	0,173	0,137	0,436	0,269	0,182	0,483	0,345	0,182
Kurtosis	-0.158	-0.840	-1.602	-0.093	-0.827	-1.615	-0.080	-0.801	-1.615

5.11 Repeated Load Triaxial Test (Plastic Strain)

Due to resource limitations, a constrained study of the plastic strain behaviour of NMESMs was carried out. Tests for UT, TW and TD specimens were conducted at a single SR of 0.2 and a confinement pressure of 100 kPa at 25 ºC as explained in Section 3.4.5.3. The tests were conducted up to 80,000 load cycles, as per CSIR protocol, and the results are plotted against the number of load applications (cycles) on a semi-logarithmic plot in Figure 5-29.

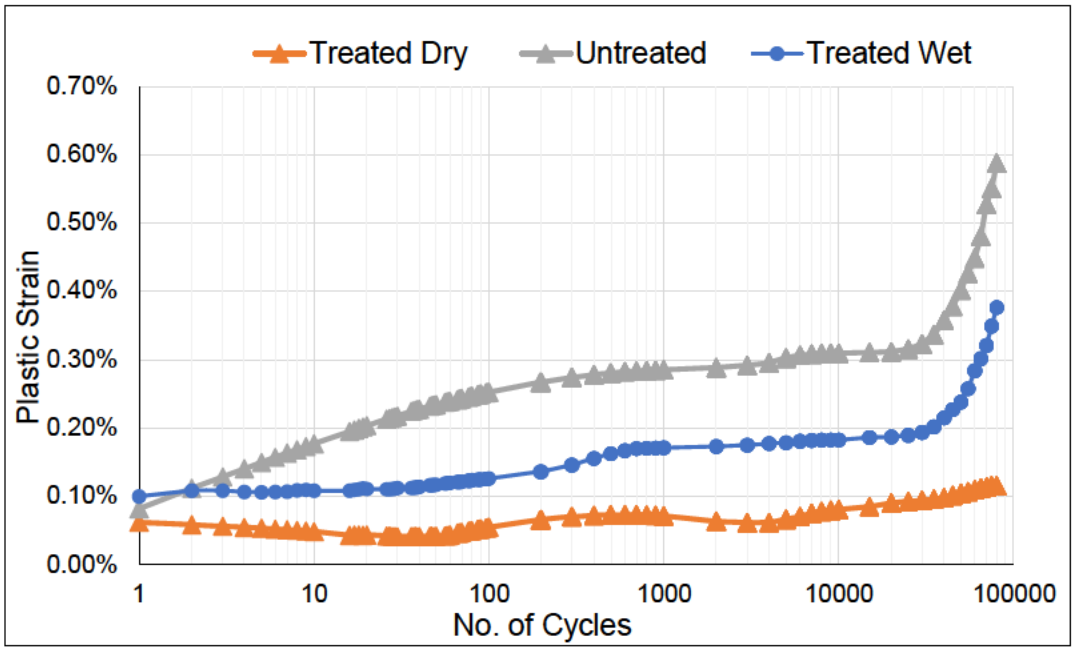

Figure 5-29: Plastic strain plotted against the number of load cycles

The results show that the UT specimen exhibits more deformation compared to the TW and TD specimens. This is consistent with the findings of Smit et al. (2021) and shows the bonding influence of the NME on the material. The deformation of the UT specimen is observed to proceed relatively quickly in the initial phase up to 1000 cycles where it appears to level off. This relatively rapid increase in strain observed with the UT specimens can be attributed to material settlement and particles locking in position. The treated specimens show relatively constant strain for the first 100 cycles after which it picks up, up to around 1000 cycles, then appears to level off. The second phase, exemplified by the roughly linear part of the graph, is characteristic of a relatively constant rate of deformation. The UT and TW specimens transition into the third phase of the material behaviour, tertiary flow, where accelerated deformation is

observed. However, this is not the case with the TD specimen. During the third phase, the material may be considered to be failing in shear under repeated loading. The beginning of the third phase is called the flow-point. Before this point, the rate of strain accumulation is minimal, while after the flow point, strain accumulation accelerates.

Jenkins (2000), Ebels (2008) and Twagira (2010) identify the existence of a critical deviator stress ratio (DSR). When a material is repeatedly loaded above this critical DSR, the permanent deformation behaviour includes a third phase as described above. Repeated loading below this critical stress ratio results in on-going stable second phase behaviour. The results obtained appear to suggest a critical DSR of around 20% for the UT and TW specimens, however, this is worth further investigations as only one SR was considered in this study and the number of load cycles was limited.

5.12 Void content analysis and permeability

The void content of bituminous materials is a critical parameter linked to the performance and durability of the material mix. While a sufficient amount of voids is needed to maintain material stability, high void contents allow for intrusion of air into the mix, which may induce hardening of the binder leading to brittleness and failure of the material. Water intrusion, equivalently, leads to loss of bearing strength of the mix and underlying layers. The intrusion and flow of water through soil voids (called permeability) is governed by Darcy's law, which states that for laminar flow conditions in a saturated soil, the rate of flow of water is directly proportional to the hydraulic gradient.

5.12.1 Voids analysis

The void contents of the NMESMs were evaluated after carrying out tests for the RDv and RDm as detailed in the methodology. The results of the tests, shown in Figure 5-30, indicate that the void content of NMESMs varies within a narrow range, reducing from 22% to 20% for NME applications from 0.7% to 1.5%. This indicates a reduction of up to 10% from the presumed void content of the unstabilised specimen. By comparison, it is noted that BSMs have a void content between 10 and 13% (Twagira, 2010) probably a result of a higher bitumen residue content of more than 2%. Material

grading, compaction level and the physical properties of mineral aggregates also influence the voids content of materials.

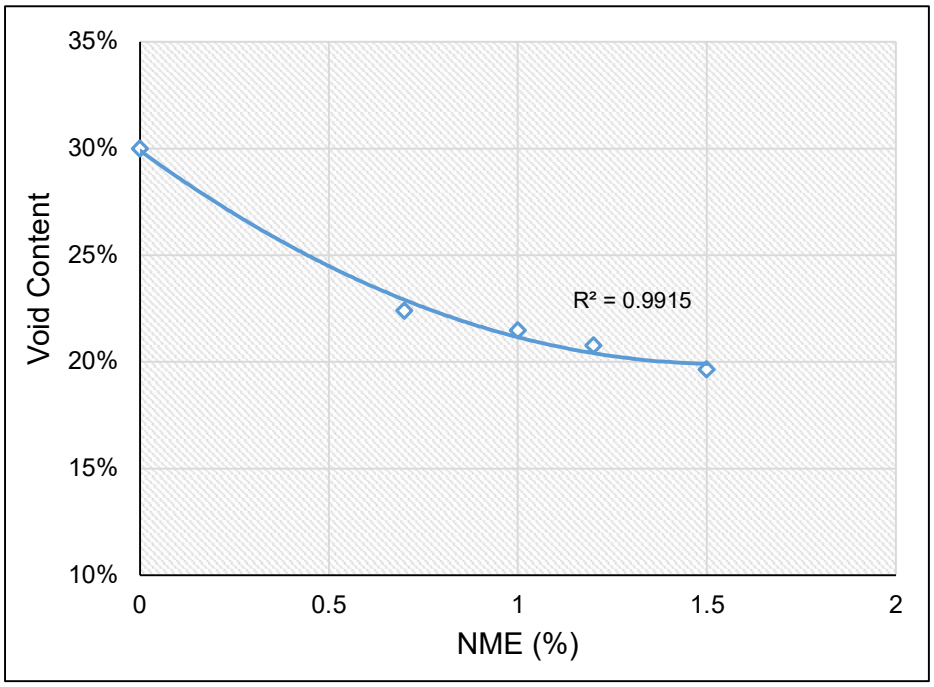

Figure 5-30: Void Content

5.12.2 Permeability

Recognising the narrow range of the void content of NMESM, the permeability was determined at 1% NME only, as well to save on resources. Results, comparing the stabilised and unstabilised specimens, are presented in Appendix I and illustrated in Figure 5-31.

It has been suggested by a number of researchers that permeability increases with increase in the degree of saturation (Dal-Ben, 2014; Trishna, n.d). In unsaturated mixes, the pressure head is negative, meaning that it is lower than atmospheric pressure (soil suction) and some of the void spaces are filled with gas (air). This is not the case with saturated soils and the absence of air in the pore spaces means that water can flow easily without hindrance. Therefore, the specimens were subjected to saturation until steady-state flow through the specimens was achieved before proceeding with the test. Of note was the considerable amount of time (days) needed to saturate the NME sample.

The results show that the material's permeability reduces by more than 85% when treated with NME. This is consistent with the findings of Alsharef et al. (2016), Liu et al. (2021) and Qacha (2022).

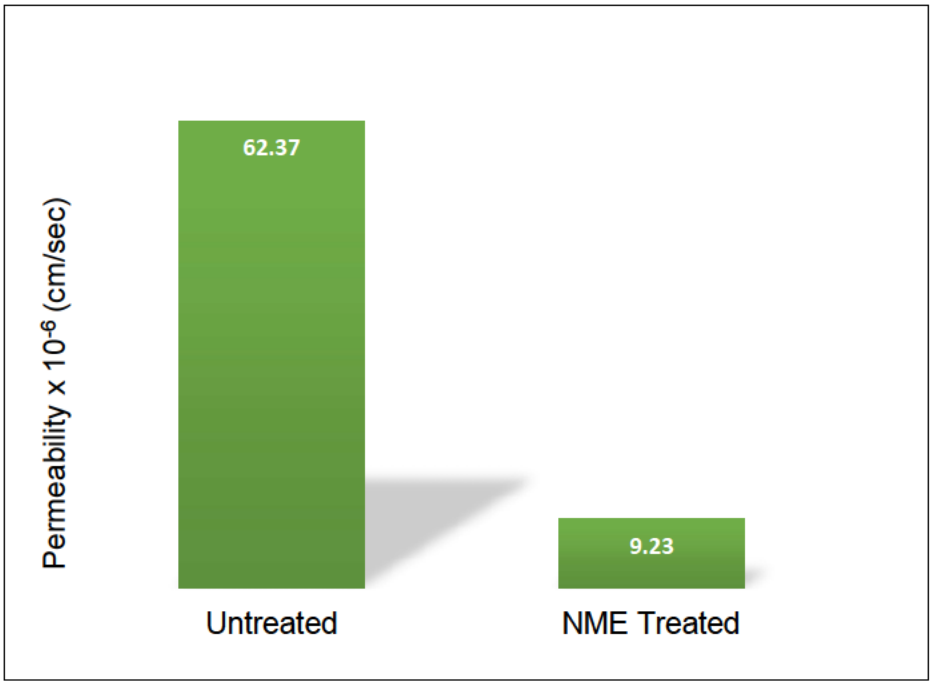

Figure 5-31: Permeability test results

Permeability is dependent on void content in a material mix, and the isolation or interconnectedness thereof. Material mixes with high-interconnected voids allow moisture to permeate from one end to the other, thus have high permeability. The results show that the NME not only reduces the void content of NMESMs but also acts to disrupt the interconnectedness of the voids due to the gels formed by the residue bitumen. This is an invaluable property for a gravel road-wearing course. On the other hand, the possibility of development of isolated voids is worth investigating. These have a propensity to retain pore water, which, under particular load conditions, leads to the build-up of pore pressures that are damaging to the material.

5.13 Scanning Electron Microscopy results

The topography and elemental composition of a control specimen and NME stabilised specimens were assessed using a combination of SEM and EDX analysis. Several images of the specimens were produced, at different magnifications, to observe the

appearance and gelation of the binder in relation to the gravel particles. The images provided in this section are chosen on the basis of clarity, to exemplify the effect of the NME in the material mix.

Figure 5-32 shows an image of the unstabilised sample. It appears as a hard crust, probably quartz, with some loose particles, a result of cleaving from the large specimen. Some voids can be made out as indicated by the ellipses. Arrangements of crystallised morphologies of flaky clay particles, probably kaolinite, are also observed as indicated by the arrows. These are observed more clearly in Figure 5-33, which shows the same image at twice the magnification. The image also shows additional voids on the surface of the specimens.

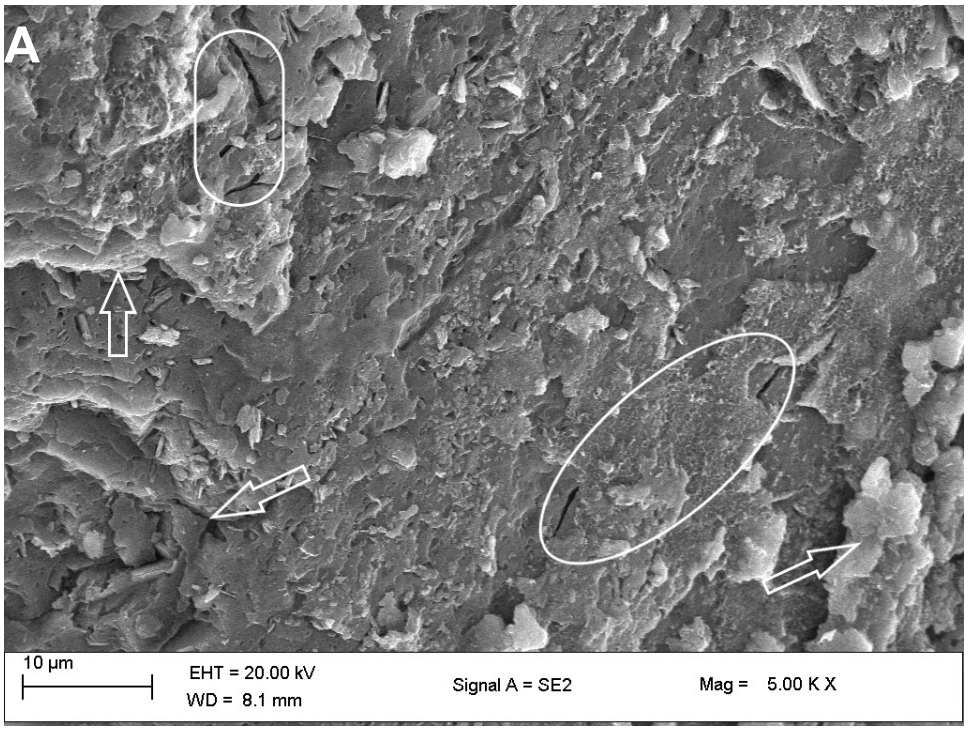

Figure 5-32: SEM micrograph of unstabilised (control) specimen

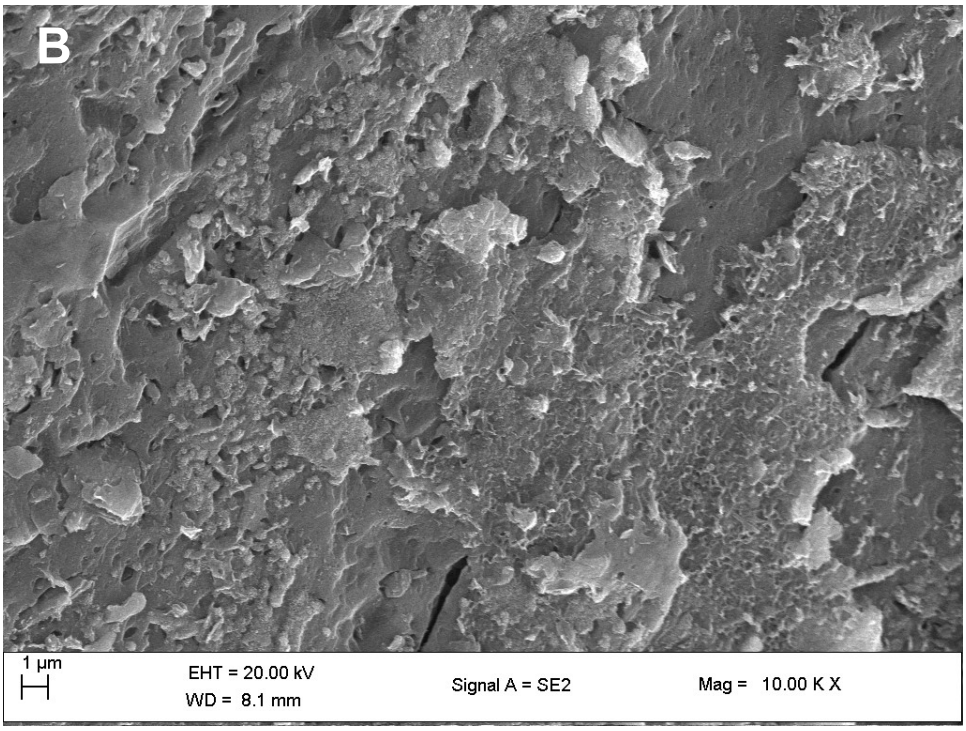

Figure 5-33: SEM micrograph of unstabilised (control) specimen

Figure 5-34 shows elements in the control specimen. It is shown that Silicon (Si), Oxygen (O), Aluminium (Al) and Iron (Fe) are the most abundant elements in the material with relative amounts of 17.47%, 32.58%, 8.22% and 29.6% respectively, at the indicated error percentage level in Table 5-11. The combined total of the said elements makes up more than 87% of the elemental composition of the material. They probably occur as oxides corresponding to Silica (SiO_2), Alumina (Al_2O_3) and Iron (FeO and Fe_2O_3). The high concentration of SiO_2 is typical of this type of material as was indicated by the XRD tests in Section 4.2.6.

Figure 5-35 and Figure 5-36 show stabilised specimens at 1.2 and 1.5% NME. The images appear to show a gel of the NME encapsulating some of the (finer) particles of the material mix. Some tendrils of gel attaching to neighbouring particles can just about be made out as indicated in Figure 5-35. Figure 5-36 appears to show an increased concentration of the gel encapsulating what appears to be loose particles from the mix matrix. Loose particles may be a result of cleaving which is quite a challenge for a granular material, prone to disintegration. This obviously impacts the clarity of images produced.

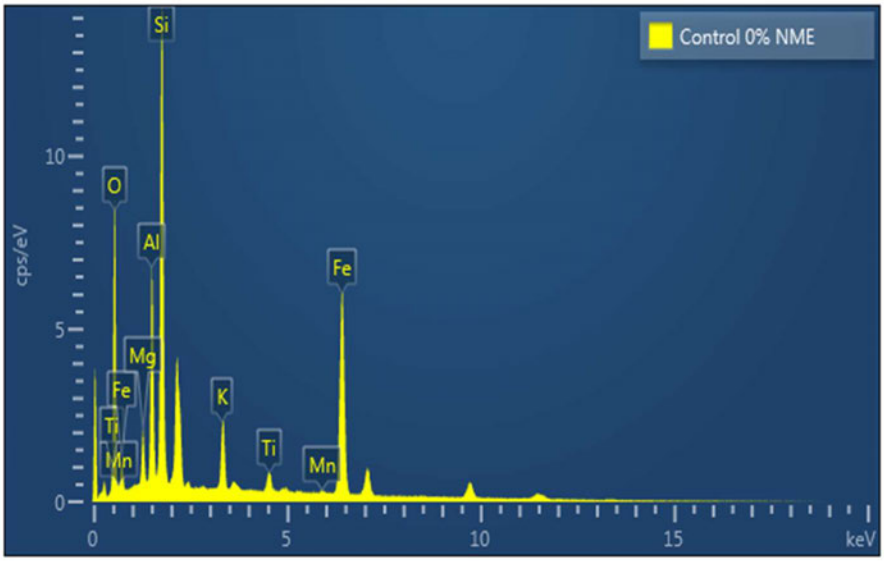

Figure 5-34: EDX element analysis of control)

Table 5-11: Elemental composition of control

Element	C	O	Mg	Al	Si	K	Ti	Mn	Fe	Total
Wt%	4.35	32.58	2.52	8.22	17.47	3.49	1.47	0.3	29.6	100
Wt%Sigma	0.79	0.36	0.07	0.11	0.19	0.07	0.06	0.07	0.31	

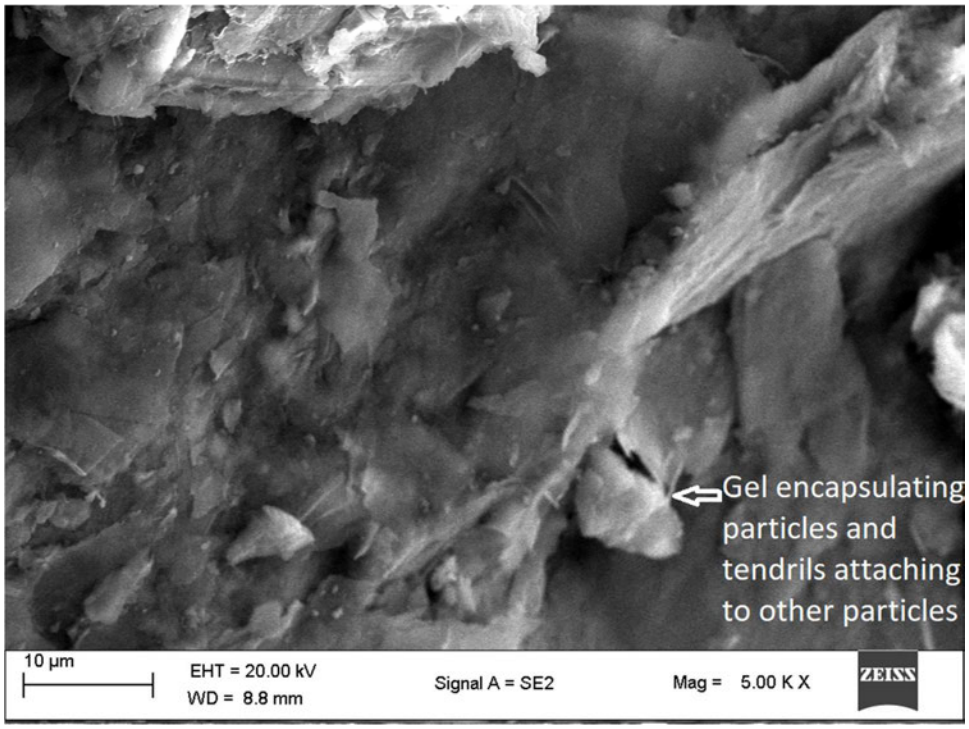

Figure 5-35: SEM micrograph of 1.2% NME specimen

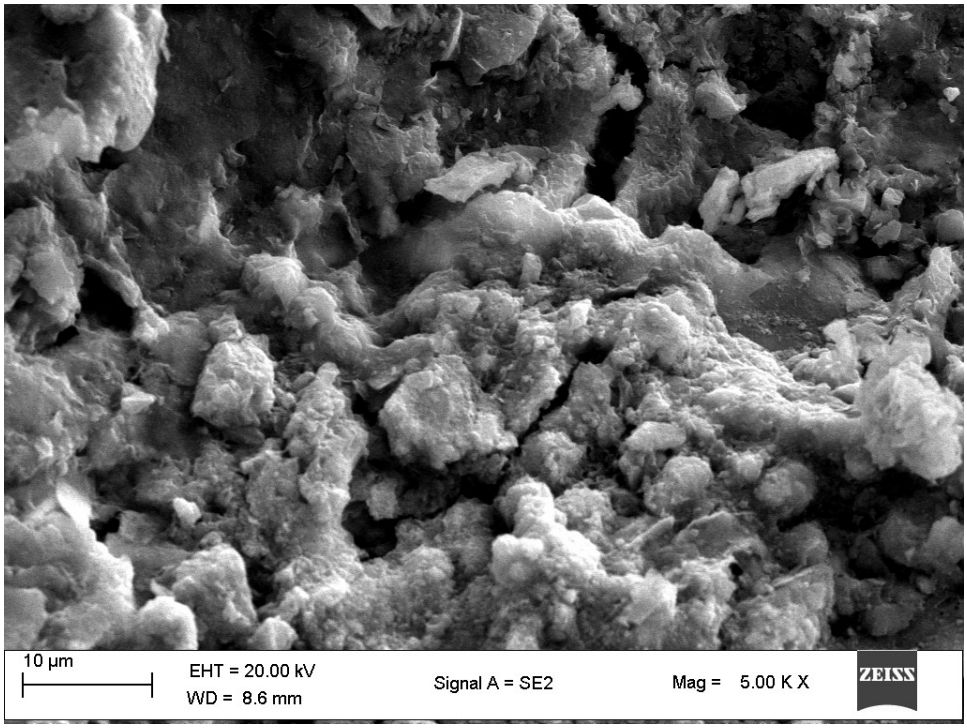

Figure 5-36: SEM micrograph of 1.5% NMESM

Figure 5-37 and Figure 5-38 show EDX analyses of the elemental compositions of the material mixes at 1.2 and 1.5% NME applications, respectively. It is observed that the Si and O peak in both specimens compared to the control.

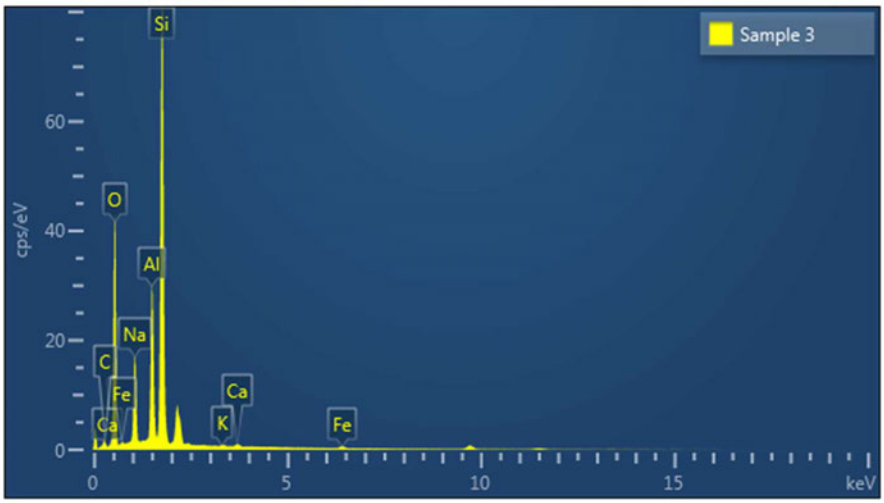

Figure 5-37: EDX elemental analysis (1.2% NME)

Table 5-12 and Table 5-13 show that the weight percentage of Si increases from 17.47 to 26.72 and 28.62 at 1.2 and 1.5% NME respectively with the O increasing by similar

margins. This is an indication of the formation of siloxane (Si-O-Si) bonds in the material mix.

Table 5-12: Elemental composition (1.2 % NME)

Sample 3	C	O	Na	Al	Si	K	Ca	Fe	Total
Wt%	7.64	47.45	7.97	9.21	26.72	0.15	0.26	0.61	100
Wt% Sigma	0.86	0.48	0.11	0.11	0.28	0.03	0.03	0.05	

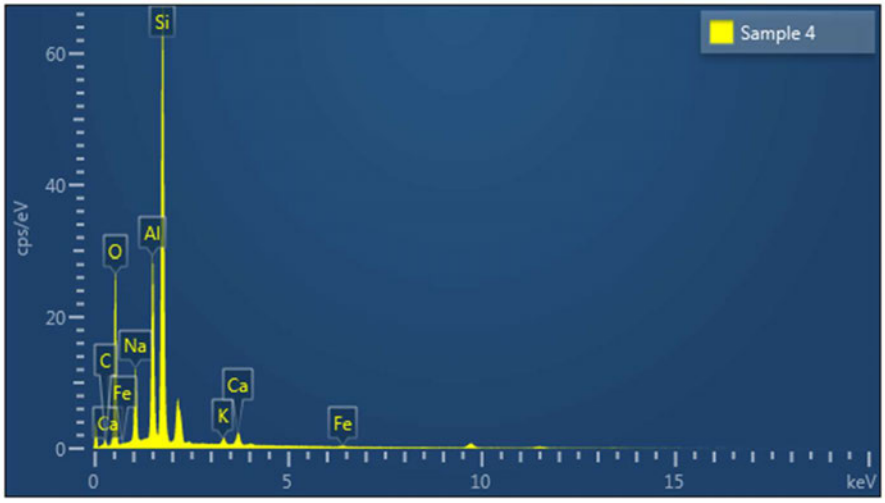

Figure 5-38: EDX element analysis (1.5% NME)

Table 5-13: Elemental composition (1.5% NME)

Sample 4	C	O	Na	Al	Si	K	Ca	Fe	Total
Wt%	7.31	43.54	6.82	11.32	28.62	0.7	1.41	0.28	100
Wt% Sigma	0.92	0.48	0.11	0.14	0.32	0.04	0.04	0.05	

5.14 Summary

This Chapter provided detailed results and analyses of the tests conducted on the NMESMs in line with the objectives of the study. The results generally show and confirm that the NME improves material properties by increasing mechanical strength and improving the materials' resistance to moisture damage. It is observed that minimal application of 0.7% NME increases material strength properties by more than 70% in the case of CBR. The results of ITS, UCS and STT show that increasing the application rate of NME, above 0.7%, does result in significant improvements of the strength of the material. However, wet conditioned test results show that increasing the NME application rate acts to improve the materials' hydrophobicity properties and hence resistance to moisture damage. This is one prominent feature of NME

stabilisation, invaluable for roads that are directly exposed to moisture. Furthermore, based on ITS and UCS test results, it is shown that NMESMs can retain more than 65% of the strength after twenty-four hours of moisture exposure.

Results of STT show that the NME improves the shear strength of material by increasing the cohesive strength component while the angle of friction remains virtually unchanged. The increased shear strength improves the materials' traffic carrying capacity by more than 200% in the dry condition and over 100% in the wet condition as simulated by the four-hour soaking. In the same vein, the resilient response to load and permanent deformation properties are improved such that the material, even in a wet condition, retains significantly superior characteristics than in its UT state.

The improvement of the material properties is extended to permeability, an invaluable property particularly for gravel roads. It is shown that the NME acts to reduce the materials' void content, and the interconnectedness of the voids, thus, reducing permeability of the material. In this way, use of the NMESM as a gravel-wearing course would protect the underlying material (subgrade) from moisture and retain its bearing strength.

6 PAVEMENT MODELLING AND STRUCTURE ANALYSIS

6.1 Introduction

Numerical modelling of pavement performance has become an integral part of modern-day pavement engineering. The availability of various applications that model and simulate pavement performance on a small scale make it easier for engineers to make decisions about the implementation of various interventions on road pavement structures. More so with the advent of mechanistic design methodologies, the iterative manipulations required to converge to a solution, which would otherwise be quite daunting if done manually, can now be done with the aid of various packages that are based on established performance models.

Pavement performance numerical models are based on two different approaches, linear and non-linear. The linear approach uses theory of elasticity to determine structural dynamic properties and response to loading effects while non-linear approach presumes a non-linear relationship between applied forces and responses thereof. Non-linear effects can originate from geometrical non-linearities (i.e. large deformations), material nonlinearities or contact (Femto, 2017). Various linear and non-linear elastic multi-layer programs are available for numerical modelling of pavement performance, such as BISAR (Shell, 1998), KENPAVE (Huang, 1993) or RUBICON (MAS, 2007), however, more accurate models are obtained from models that are based on FE methods.

This Chapter presents results of numerical modelling implemented in this study. A FE based platform, ANSYS 2022 R2, was used to simulate a pavement structure and critical responses to applied loading obtained to indicate pavement performance. A 3-D model was implemented due to its distinctive accuracy in configuration and ability to capture non-linear effects and asymmetrical effects. The pavement structure simulated is based on the Ingweni road identified in Section 3.5.

6.2 Pavement structure and material conditions

Three pavement structures were considered for this study as shown in Figure 6-1. Two structures consisting of a gravel-wearing course material stabilised with NME in the wet and dry condition are compared to the one without the treatment. The wearing

course for all three structures is 150 mm and is supported by a subgrade modelled to a depth of 2500 mm.

Material properties considered are also shown in the figure. The difference of the three structures is the elastic moduli (E) of the wearing courses, which were determined from the M_R tests as 240 MPa for the UT pavement, 500 MPa for the TW pavement and 800 MPa for the TD pavement. A gravel soil was considered for the subgrade with E = 50 MPa, estimated based on DCP tests conducted on the model road. Poisson's ratios (μ) of 0.4 and 0.45 were considered for the wearing course and subgrades respectively.

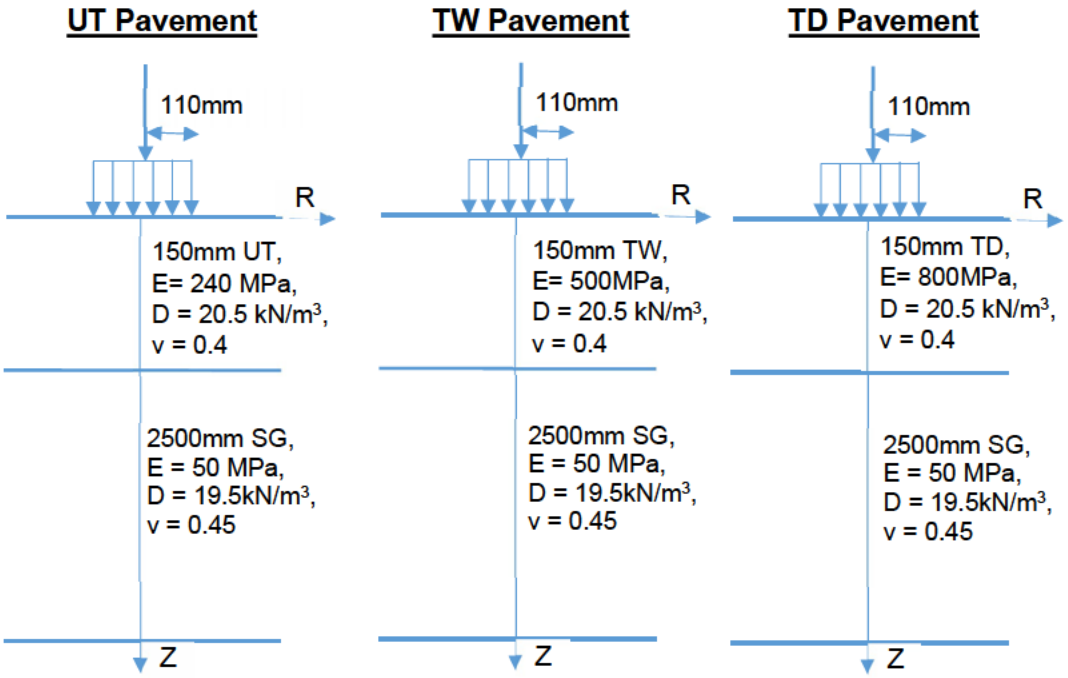

Figure 6-1: Comparison of pavement structures used in the analysis

6.3 Model geometry and loading

Considering conditions of symmetry, a 3-D quarter model of 1500 mm x 1500 mm was developed. The model was constrained at the bottom in all directions while displacements on the four vertical faces was only allowed in the Z direction. A typical FE mesh of 0.6 mm was used in the analysis as shown in Figure 6-2. The loading condition consisted of a super single of 25 kN. The wheel load is modelled as a circular loading area with a radius of 110 mm, recommended for a category D road (De Beer

et al. 1999). Thus, a resulting uniform contact pressure equal to 650 kPa was considered as shown in Figure 6-3.

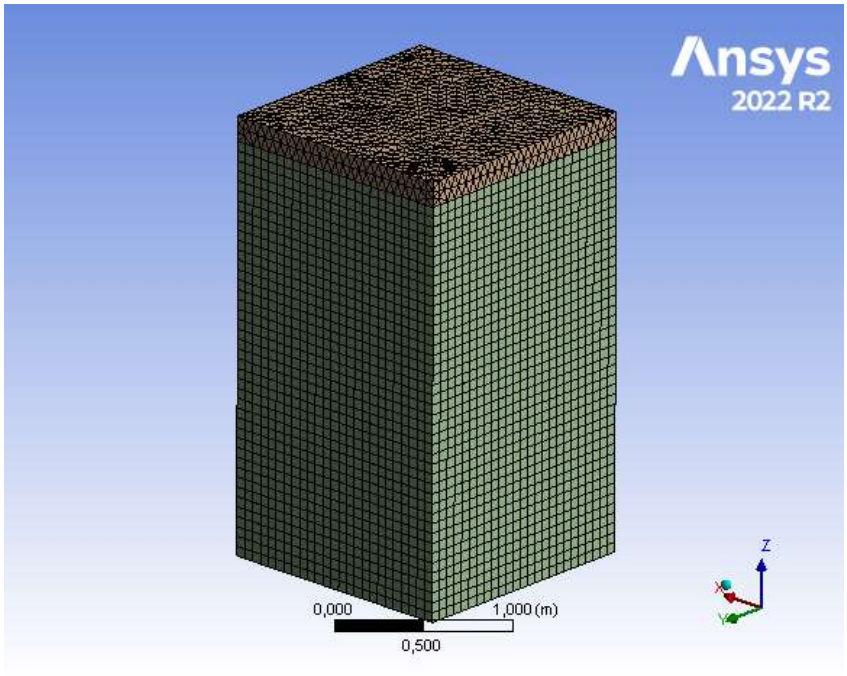

Figure 6-2: FE geometry of model

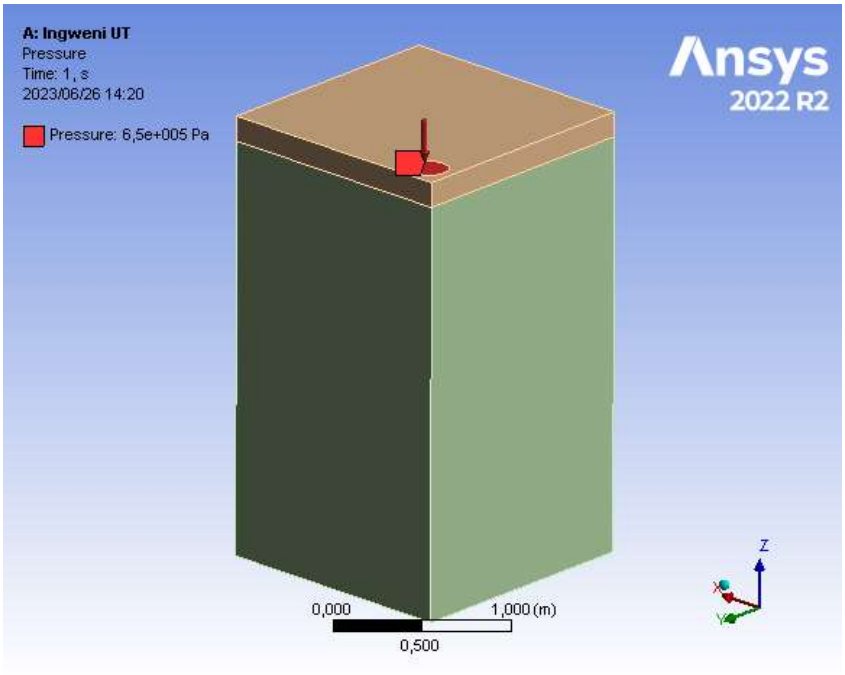

Figure 6-3: Loading condition

6.4 Validation

Validation of the developed model is a key requirement, undertaken to verify and ascertain generated results. The KENPAVE software, a duly calibrated multi-layer computer package for pavement structure analysis and design, was used for this purpose. Thus, a linear elastic analysis of the developed model for the UT pavement structure was undertaken in ANSYS, and the obtained responses to applied loading compared to equivalent responses from a linear analysis of the pavement structure modelled in KENPAVE. The same material properties were considered in both models. A minor difference in geometry was that, while KENPAVE considers a subgrade of infinite depth, the subgrade in ANSYS is modelled to a finite depth of 2500 mm as stated earlier. However, this does not affect the results as indicated below.

Results of the two analyses for governing comparison parameters, strain and stress, show good fit as presented in Figure 6-4 and Figure 6-5 respectively. The developed FE model was therefore deemed valid for use in FE analysis of the modelled pavement structure.

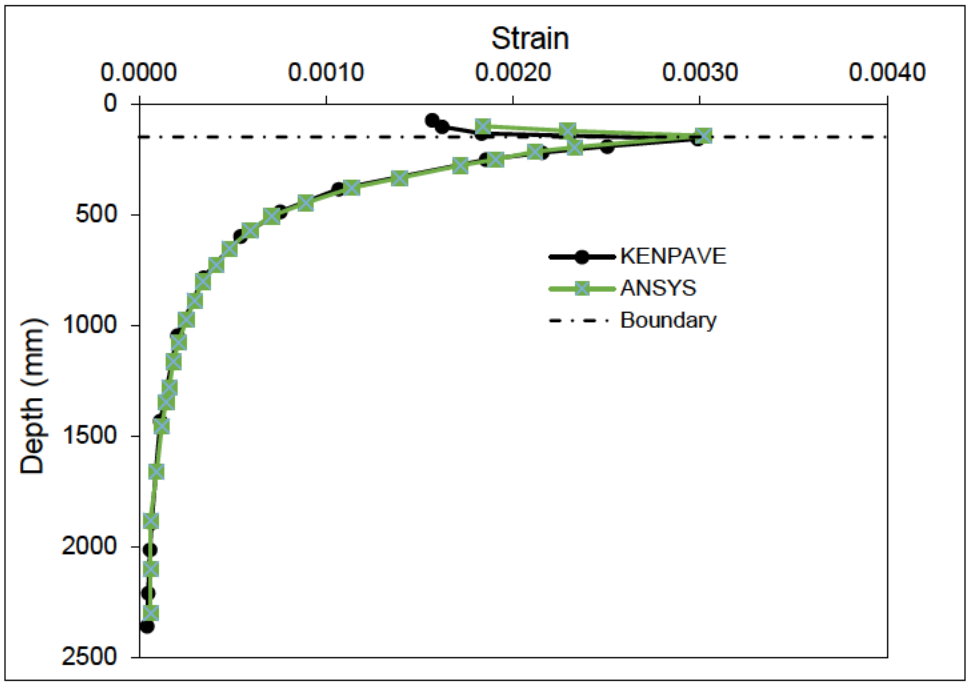

Figure 6-4: Strain responses from KENPAVE and ANSYS

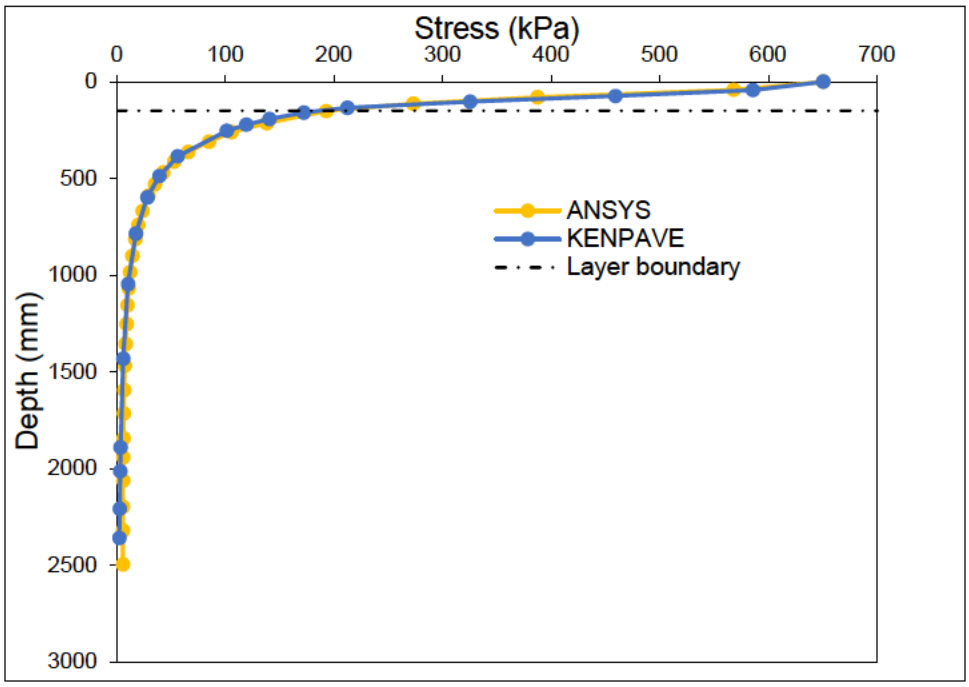

Figure 6-5: Stress responses from KENPAVE and ANSYS

6.5 Geometric non-linearity in ANSYS

The analysis above, for validation, considered linear or elastic behaviour. However, materials rarely behave in a linear manner. Non-linearities occur when the direct proportionality of stress and strain is not tenable as is the case with simple linear elastic behaviour. In such a case, the stiffness of the structure is no longer constant but varies with load. Non-linearities can also be due to large deformations which may occur under traffic loads owing to the elasto-plastic behaviours of materials used for construction of gravel roads. Thus, two cases of non-linearity were considered in this study i.e. geometric non-linearity and material non-linearity. Geometric non-linearity was considered for the UT pavement structure and the software generated deformation results for linear and non-linear analysis are provided in Figure 6-6 and Figure 6-7 respectively.

It is observed that when geometric non-linearity is considered, a slight increase, equivalent to 1.2%, in deformation is recorded. The results therefore indicate stiffness varies with load, brought on by the deformation of the structure. This is taken into account in subsequent analyses.

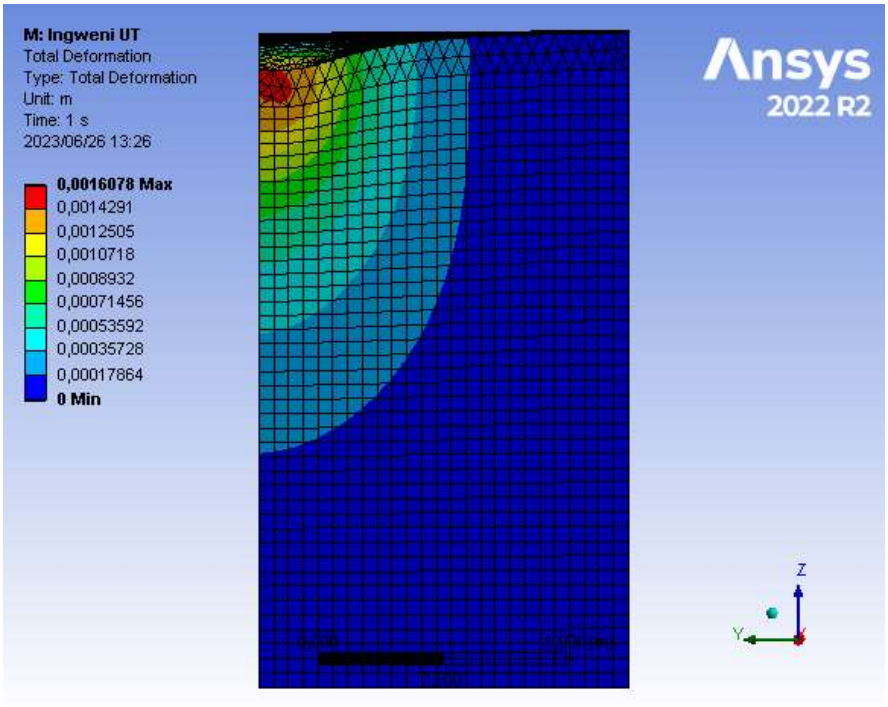

Figure 6-6: Deformation responses of UT pavement to linear analysis

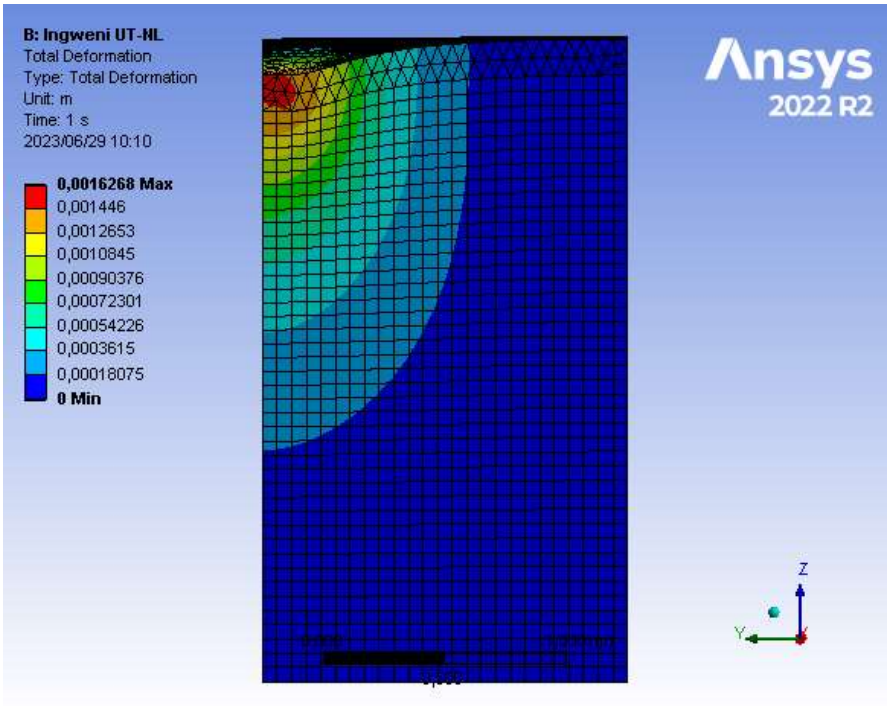

Figure 6-7: Deformation responses of UT pavement to geometric non-linear analysis

6.6 Analysis incorporating material non-linearity

The treated pavement structures (TD and TW) models were developed by duplicating the validated UT model above and inputting/changing material properties for the NMESM wearing courses as indicated in Figure 6-1. Material non-linearities were considered in the wearing course. The ANSYS software provides a number of options for this purpose, one of which is the Drucker-Prager (DP) model. This is a 3-D pressure-dependent model for estimating the stress state at which a material fails or undergoes plastic yielding (Alejano and Bobet, 2012). To use the DP model in ANSYS 2022 R2, linear elastic parameters, E and μ, are augmented with parameters for the DP model; uniaxial compressive strength, uniaxial tensile strength and biaxial compressive strength. These were determined from the ST tests as indicated in Table 6-1.

Table 6-1: Input parameters for DP model

TD, DP Base	
Uniaxial Compressive Strength (MPa)	0.957
Uniaxial Tensile Strength (MPa)	0
Biaxial Compressive Strength (MPa)	1.875
TW, DP Base	
Uniaxial Compressive Strength (MPa)	0.629
Uniaxial Tensile Strength (MPa)	0
Biaxial Compressive Strength (MPa)	1.636

6.6.1 Stress distribution

The equivalent stress distribution models of the UT, TW, and TD pavement structures are presented in Figure 6-8, Figure 6-9 and Figure 6-10 respectively. The UT pavement structure does not include material non-linearity and is only included in the analysis to extend the discernment of the influence of the NMESM. This is on the basis that the strain and deformation responses obtainable, if material non-linearity was included in the UT pavement structure, would be larger.

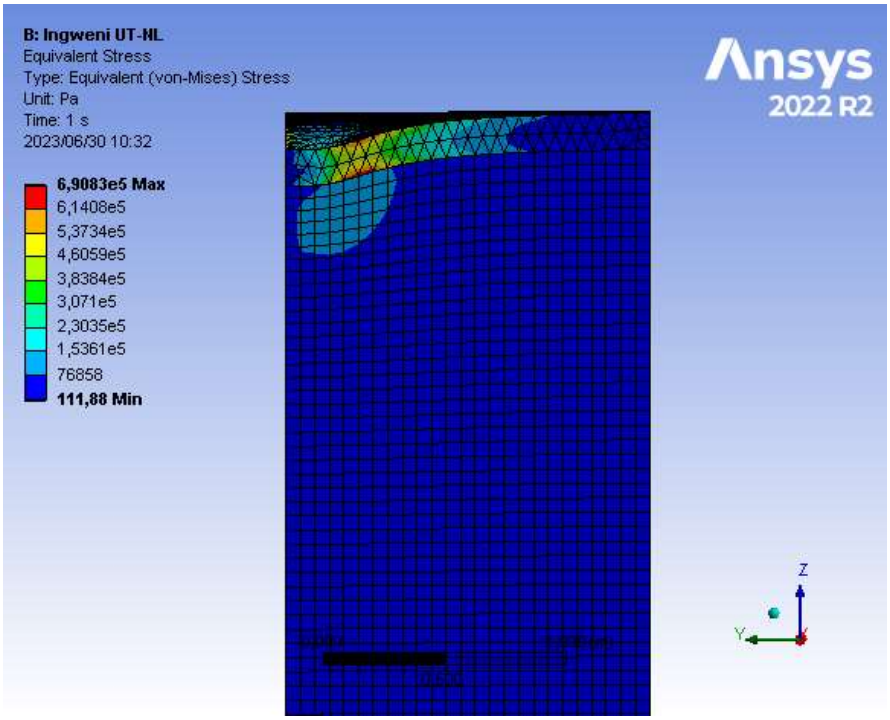

Figure 6-8: Stress distribution of UT pavement structure

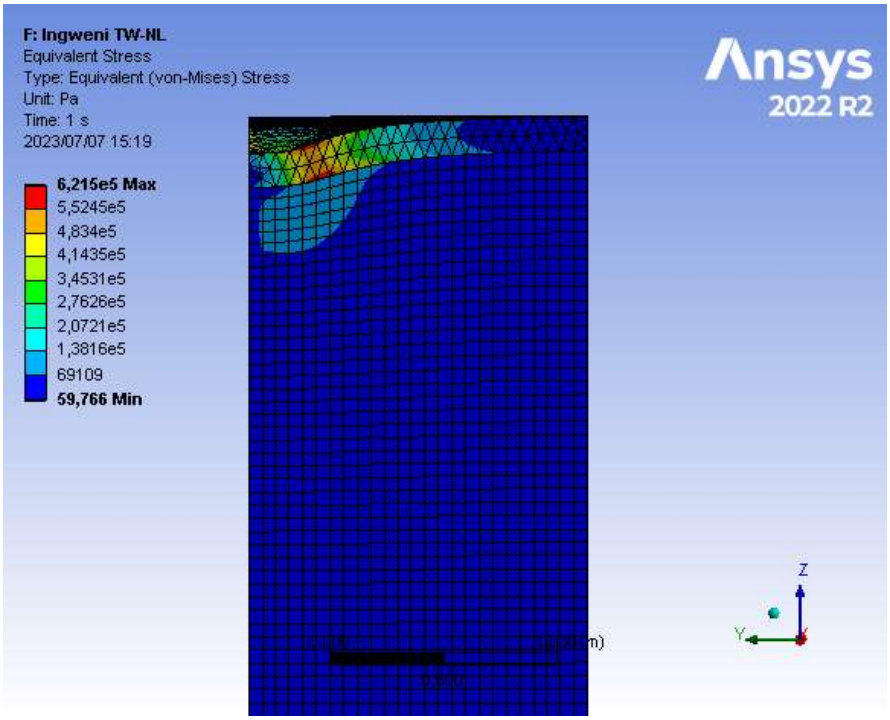

Figure 6-9: Stress distribution of TW pavement structure

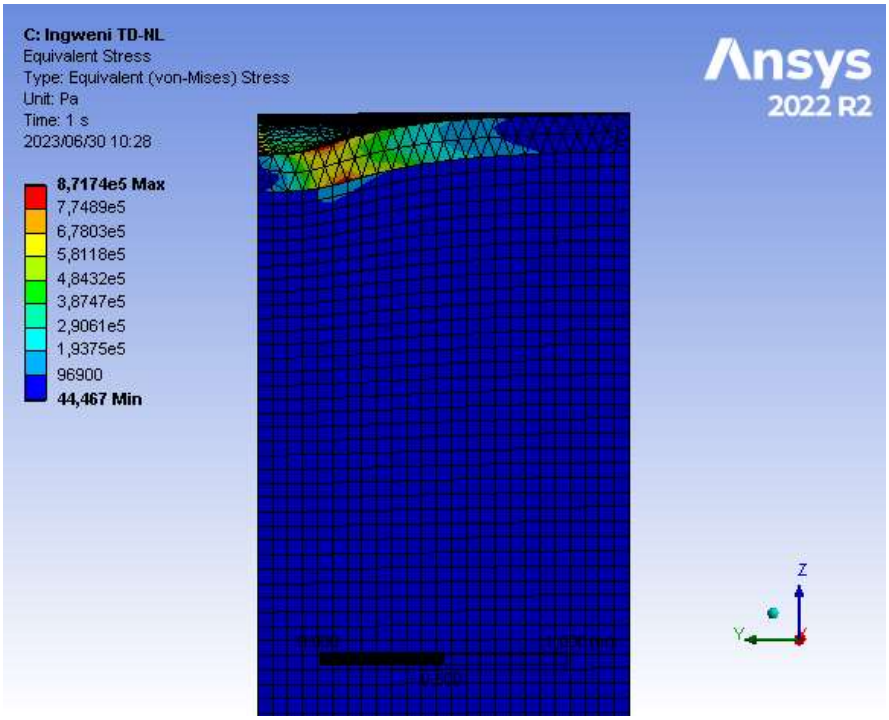

Figure 6-10: Stress distribution of TD pavement structure

It is observed that the influence of stress in the UT pavement structure (Figure 6-8) extends quite significantly into the subgrade. This is comparable to the TW pavement structure but it is not the case with the TD pavement. The NMESM wearing course in TD pavement structure is observed to take the brunt of the stresses, with very limited influence on the subgrade (Figure 6-10). This demonstrates the superiority of the NMESM in terms of load spreading abilities and stress distribution, especially in the dry condition, protecting the subgrade from excessive stresses.

6.6.2 Strain distribution

Figure 6-11 compares the vertical strain responses of the three pavement structures. It is observed that the critical (maximum) strain responses occur in the wearing course, close to the interface with the subgrade. The results also show that introduction of NMESM wearing courses reduces the critical strain by more than 14% and 12% in the dry and wet conditions respectively. Larger differences in critical strain responses would be expected when material non-linearity is considered in the UT wearing course. The influence of stress in the subgrade is also observed from the strain distribution results of the pavement structures. Differences in strain responses are observed to extend up to a depth of about 1500 mm into the subgrade.

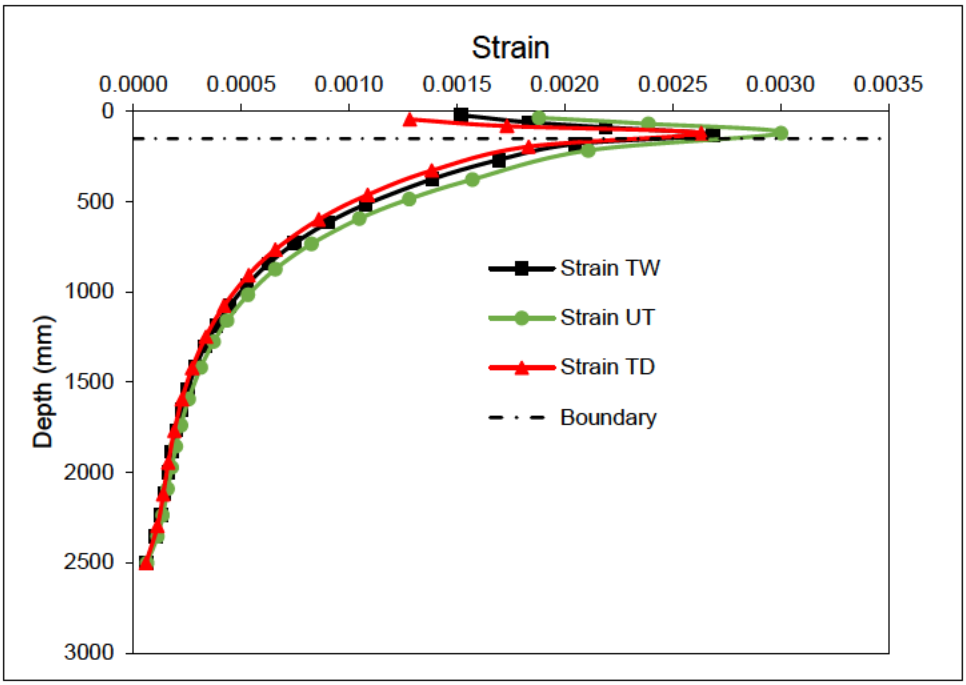

Figure 6-11: Comparison of deformation between UT and TD pavement structures

6.6.3 Deflection distribution

Figure 6-12 compares the distribution of the surface measured deflections of the UT, TW and TD pavement structures. As expected, the deflection is maximum centrally under the load and extends up to about 1.3 m away. This shows the extent of influence of the load. The maximum deflection of the UT pavement structure, recorded at 1.63 mm, is over 15% and 28% higher than that with the NMESM wearing course, in the wet and dry conditions, recorded at 1.41 mm at 1.27 mm respectively.

6.6.4 Sensitivity analysis

6.6.4.1 Effect of reducing thickness

As part of a sensitivity analysis, the effect of reducing the thickness of the wearing course was also investigated. The thickness was reduced to 100 mm and the results of deflection and strain responses of the pavement structures, in the dry condition, are presented in Figure 6-13 and Figure 6-14 respectively. It is observed that deflection of the pavement structure with the 100 mm wearing course, indicated at Def. 100TD, is higher than that with the 150 mm wearing course as expected, but lower than that of

the UT pavement structure. The deflection of the 100 mm NMESM wearing course is 14% lower than the case with the unstabilised 150 mm wearing course.

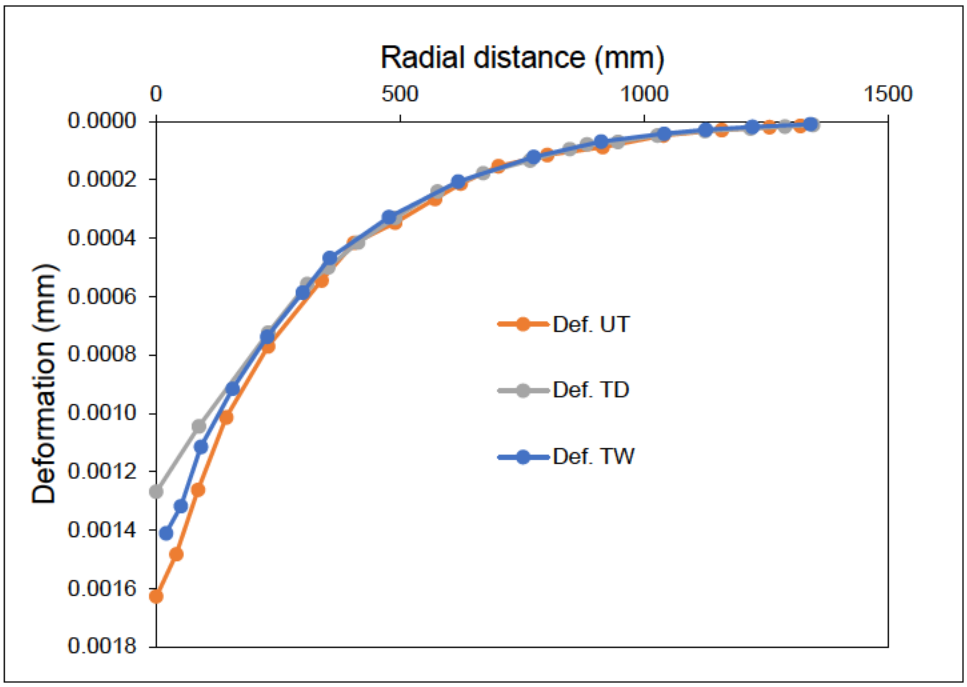

Figure 6-12: Comparison of deformation between UT and TD pavement structures

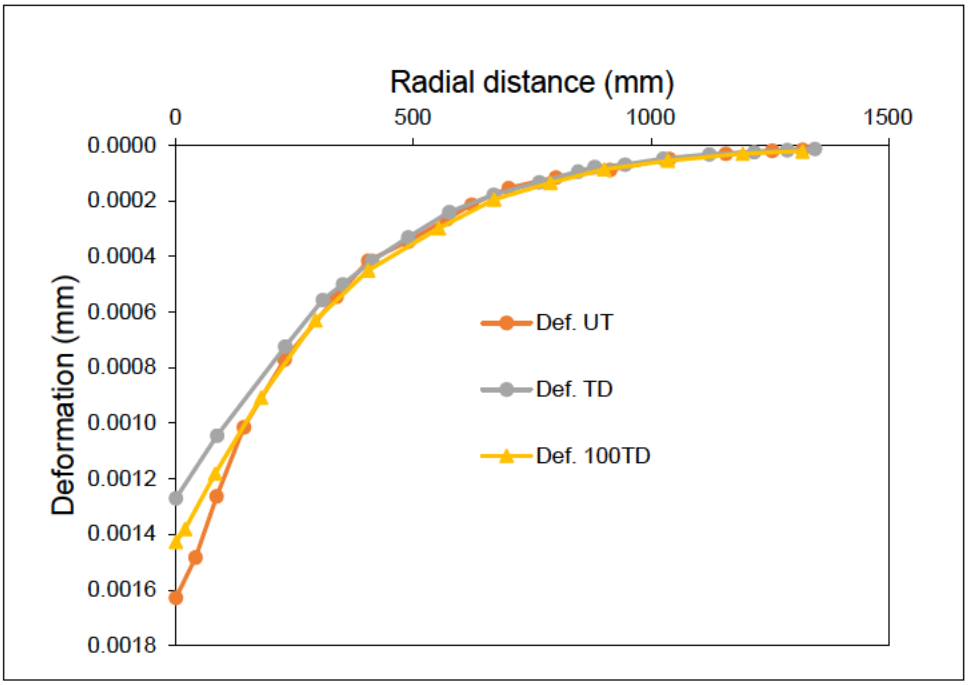

Figure 6-13: Comparison of deformation with reduced thickness of wearing course

The strain response of the 100mm NMESM wearing course is indicated as strain 100TD in Figure 6-14. Results of the analysis show that maximum strain is recorded on the surface of the wearing course. The strain decreases within the layer and increases again at the bottom of the layer. The maximum strain recorded at the surface is higher than that for the 150 mm NMESM wearing course, but lower than the UT wearing course, while the strain recorded at the bottom of the layer is comparable to the 150 mm NMESM wearing course. The influence of the stress in the subgrade of the 100TD is also observed in the strain distribution and is shown to be comparable to that of the UT pavement structure.

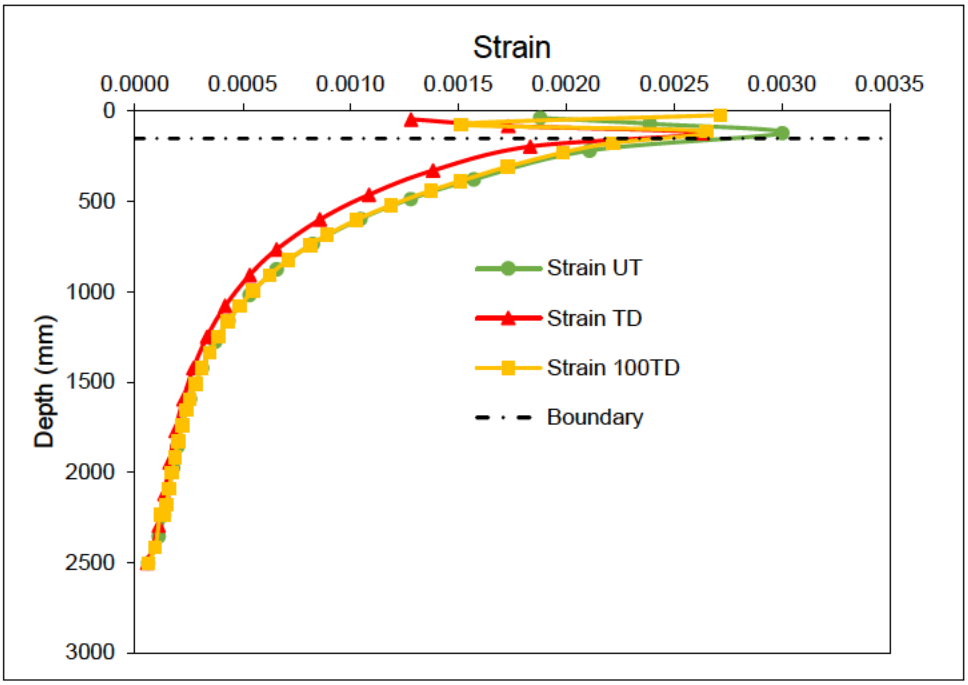

Figure 6-14: Comparison of strain response with reduced thickness of wearing course

6.6.4.2 Effect of subgrade strength

Subgrade strength is known to significantly influence the performance of road pavements and determines, in part, the thickness and strength of the wearing course. Therefore, the influence of the subgrade strength was also investigated as part of the sensitivity analysis. The subgrade resilient modulus was doubled to 100 MPa and results of deflection (indicated as 100subDef) and strain (indicated as 100subStr) compared to the original pavement structure as shown in Figure 6-15 and Figure 6-16 respectively.

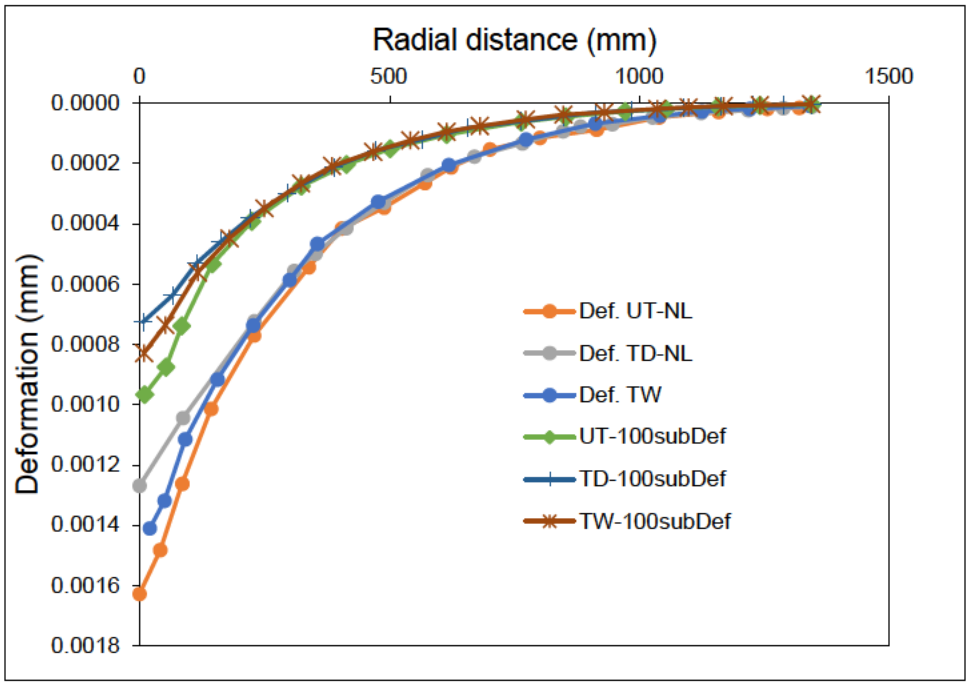

Figure 6-15: Effect of increased subgrade strength on deflection

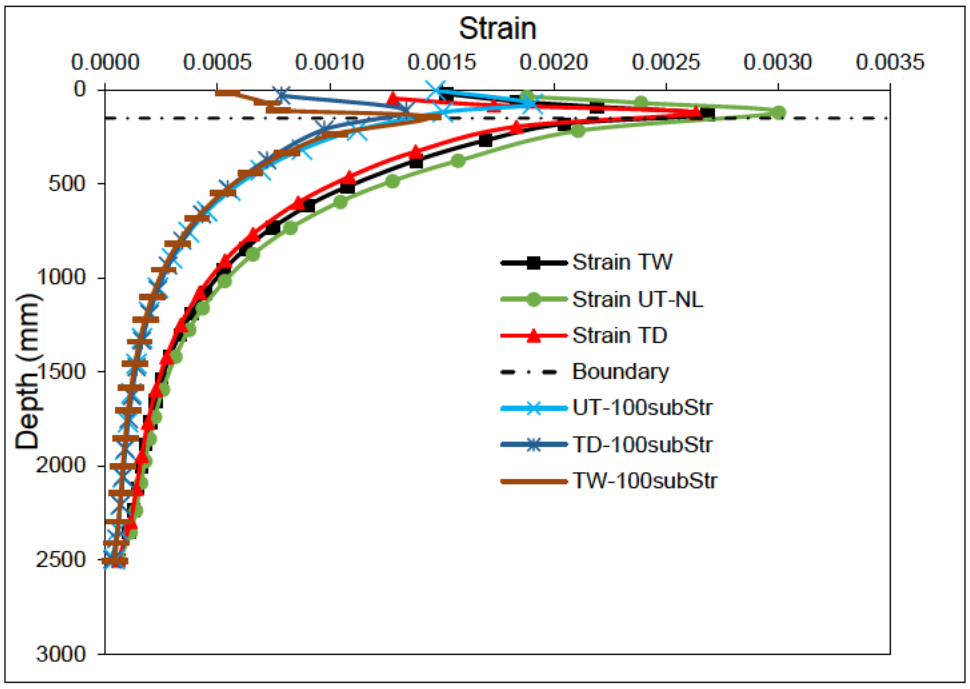

Figure 6-16: Effect of increased subgrade strength on strain

The results show a significant shift of the graphs to the left indicating reductions in both deflections and strains. The maximum deflections are determined to decrease by 70% on average while the strain decreases by more than 88%. It is also observed that

with increased subgrade strength, the difference of the influence of the stress in the subgrade is not very significant as observed from the gaps of the strain distribution curves of the three pavement structures. This indicates that the stress distribution is confined to the upper section of the pavement structure.

6.7 Discussion of results

The results show maximum vertical strains occurring near the bottom of the wearing course. These are not critical strains as failure of the wearing course is governed by the shear safety factor as discussed in Section 5.9. However, the results indicate the propensity of the pavement structure to fail through deformation. More so, the fact that these strains occur near the transition with the subgrade. It is an established fact that failure mechanisms of subgrades is determined by the vertical compressive stress at the surface.

Sensitivity analyses show that reducing the wearing course thickness shifts the maximum strain to the surface. In this case, it is clear that deformation of the wearing course is a key factor. However, results of deflection indicate that the pavement still performs better with the 100 mm NMESM wearing course than the case with the 150 mm UT wearing course.

The subgrade strength is observed to play a significant role in the performance of the pavement structure. This is demonstrated by the reductions in deflection and vertical strain of up to 70% and 88% respectively. It is observed in Figure 6-16 that the increase in subgrade strength does not result in the shifting of the maximum strain locations of the NMESM wearing course, as the case with the UT, where the strain appears to shift towards the centre.

6.8 Summary

This Chapter considered the modelling of pavement structures, implemented on a FE based platform, ANSYS 2022 R2. Pavement structures incorporating NMESM wearing courses in the wet and dry condition are compared to a structure without the stabilised layer, acting as the control. The KENPAVE pavement structural design and analysis software was used to validate the UT pavement structure model. TW and TD models

were developed based on the validated UT model and analysed, taking into account geometric and material non-linearities.

The analysis shows that the use of NMESMs as a wearing course improves the performance of the gravel road, by absorbing most of the stresses applied on the surface, thus protecting the subgrade. Consequently, strain and deflection responses of the pavement structure are improved by as much as 28%. In this regard, the thickness of NMESM wearing course can be reduced, saving costs of materials in the process. It is also observed that even in the wet condition, the NMESM wearing course performs better.

The findings in this study and models developed are only applicable to the test conditions that were used. While care was taken to choose realistic and typical test conditions, actual pavement structural conditions may vary from those selected for numerical modelling. Consequently, the pavement responses determined are hypothetical and show how the material qualities determined in the study may help in pavement modelling.

7 CONCLUSION AND RECOMMENDATIONS

7.1 Introduction

This study hypothesises that advancing sustainable gravel road construction through innovative nano-emulsion treatment of a micaceous gravel is significant. The study investigated the efficacy of NME for gravel material stabilisation by evaluating and characterising the engineering strength and durability properties of NMESMs in the laboratory. The study extends the knowledge on NME efficacy by supplementing routine material strength characterisation tests with advanced testing through STT and RLTT. The investigation of the behavioural trends of NMESMs stabilised at varying NME applications using STT has not been done before and is crucial to optimising the constituent materials, particularly the binder, in mix designs. Equally, very little information is available regarding the resilient response and plastic strain behaviour of NMESMs.

7.2 Conclusions

The findings of the study show that NME has the potential to make a significant impact on the road construction industry. The viscoelastic properties of the residue bitumen are greatly improved by the properties of the nanomaterial, resulting in improved binding abilities. The nanomaterial also allows for the use of minimal quantities of binder, potentially leading to substantial savings of bitumen emulsions. The binder acts at molecular level, protecting the gravel material from secondary weathering effects by limiting the access of moisture. This has been shown to significantly improve the material's durability and bears significant importance in the advent of climate changes. Additionally, because the NMESMs are less permeable, the potential of swelling of pavement layers due to moisture hoarding is reduced. The stabilised material produced remains flexible, and permanent deformation is the most credible failure mechanism. Pavements with flexible layers require far less effort to rehabilitate when the terminal condition is reached, compared to materials that fail due to full-depth cracking. These properties allow naturally available materials to be used in any pavement layer at a low risk. The maintenance of the gravel colour is another advantage of NME stabilisation, particularly for gravel roads. It has functional advantages as it prevents road users from visualising the road as a surfaced road and

applying excessive speeds (as the case may be where gravel surface has a dark outlook).

The following points were also noted:

a) Not all nanosilanes can function as material stabilisers. Only compounds with the ability to form three-dimensional networks and have a minimum of three reactive groups can function as stabilisers. Others are also excluded on account of their toxicity or propensity to produce toxic by-products.
b) The production of a stable NME with a long shelf life can only be achieved if the two media, nanosilane and CBE, are compatible. This requires matching the chemistry of the two materials.
c) The modification of CBE with organofunctional nanosilanes improves many properties of the emulsion including thermodynamic and kinetic stability, size, rheological and stabilisation properties. Additionally, the material is imparted with hydrophobic properties, such that it repels water.
d) The effective stabilisation of gravel materials with NME requires compatibility between the two media. This requires matching of the mineralogy of the gravel materials to the NME. Currently, NMEs are commercially produced and can be tailored to the gravel material considered for stabilisation.
e) In addition to point d), the formation of siloxane bonds between the nanosilane and gravel materials requires the presence and availability of adequate SIO_2. Thus, silicate-based materials are particularly suited for NME stabilisation.
f) The incorporation of active fillers, especially hydrated lime, does not improve the properties of NMESM.

The remainder of this section is organised into six subsections. Subsection 7.2.1 summarises the major findings on the characteristics of the mechanical strength and load bearing capacity of NMESMs while subsection 7.2.2 deals with the major findings on stiffness and deformation characteristics of NMESMs. Subsection 7.2.3 focuses on durability and moisture susceptibility characteristics of NMESMs, while Subsection 7.2.4 presents findings on the permeability and void characteristics. Subsection 7.2.5 presents findings on changes in phase composition and microstructure and Subsection 7.2.6 highlights results from numerical modelling of gravel road structures incorporating NME stabilised layers.

7.2.1 Findings on the characteristics of the mechanical strength and load bearing capacity of NMESMs

The evaluation of the characteristics of the mechanical and load bearing strength properties of NMESMs was done through five test methods, i.e. DCP-DN, CBR, ITS, UCS and STT. Key findings from these tests are itemised below;

a) Improvement in strength properties by over 70% for DCP-DN and CBR, 33% for UCS and 16% for ITS on application of 0.7% NME.
b) Results of UCS and ITS show no significant improvements after application of more than 0.7% NME.
c) Improvement of the shear strength of materials by improving the cohesion parameter by up to 54% while the angle of friction parameter remains virtually unaffected.
d) Improvement of materials' resistance to moisture damage, which improvement is increased with increase in applied NME. Based on ITS and UCS tests, it is shown that NMESMs can withstand up to twenty-four hours of moisture exposure, retaining up to 65% of the original strength.
e) Can be used to functionalise marginal quality materials and the obtainable material properties (after stabilisation) are equivalent to high quality materials usable even as base and subbase layers of flexible pavements.
f) Based on the stress-strain relationships, it is observed that stabilisation with NME results in flexible materials with permanent deformation the main failure mechanism.
g) Based on obtained material shear strength properties and by using established material transfer functions, it is observed that the traffic loading capacity of NMESM increases by over 200% in the dry condition and over 100% in the wet condition compared to the equivalent unstabilised material.

7.2.2 Findings on stiffness and deformation characteristics of NMESMs

The synthesis of collective results of tests for stiffness and deformation characteristics evaluated through RLT tests enabled the following results to be drawn;

a) Significant increase in M_R observed with NME treatment especially for TD specimens. TW specimens are also observed to perform better that UT specimens at all confinement pressures.
b) Results obtained exhibit a combination of stress-dependent and –independent behaviour. For UT and TW, M_R increases with increase in deviator stress but this is not case with TD specimens especially at low confining stress.
c) M_R is also observed to increase with increase in confinement due to the increased stiffness resulting from the density increase.
d) The parabolic model is determined to best describe the resilient behaviour of NMESMs.
e) Based on the limited tests conducted for plastic strain behaviour, lower deformation properties of TD and TW specimens are indicated compared to UT.

7.2.3 Findings on durability and moisture susceptibility characteristics of NMESMs

The MDR concept was utilised to evaluate the durability and moisture susceptibility characteristics of NMESMs. Results of various tests on wet conditioned material specimens were compared to their dry conditioned equivalents to determine the residual strength. Key findings from this aspect of the study are listed below;

a) NME imparts hydrophobic properties on stabilised materials such that they resist wetting by water.
b) Resistance to moisture damage is increased with increased application of NME.
c) At high NME application levels of up to 1.5%, wet conditioned material specimens can retain more that 65% and 75% of UCS and ITS strengths respectively, even after 24 hours of wet conditioning.
d) The resistance to moisture damage is enhanced by the action of residue bitumen in encapsulating fine particles, resisting water access.

7.2.4 Findings on the permeability and void characteristics

Key findings from the tests for permeability and void characteristics include;

a) NME stabilisation results in the reduction in void ratio of the material by up to 33%.

b) Void ratio of NMESMs over 50% higher than typical void ratios of BSMs probably due to the higher residue bitumen in the latter.
c) Over 85% reduction in permeability of gravel material is obtainable due to NME stabilisation.
d) The NME not only acts to reduce voids but also reduces the interconnectedness of the voids thus, the reduction in permeability.

7.2.5 Findings on changes in phase composition and microstructure

SEM tests conducted to evaluate changes in phase composition and microstructure yielded the following findings;

a) NME stabilised specimens appear as gel encapsulating what appears as fine particles in the material. The breaking and crumbling of the materials make it difficult to get clear images.
b) The probable formation of Si-O-Si bonds is indicated by the increase in phase compositions of Si and O after NME stabilisation.

7.2.6 Findings on numerical modelling of a gravel road structure incorporating NME stabilised layers

Numerical modelling and pavement structure analysis was implemented in a FE based modelling software and the key findings from the study include;

a) NMESM wearing course takes up the brunt of the stresses from the traffic loading, thus protecting the subgrade from excessive stresses.
b) Implementation and use of NMESM as a wearing course reduces strain and deflection responses of pavement structure by up to 14% and 28% respectively.
c) The increased performance of the pavement structure resulting from implementation of NMESM makes it possible to reduce the thickness of the wearing course, thus saving on material.
d) The subgrade strength plays a critical role in the performance of the gravel road.

7.3 Study recommendations

As highlighted in Section 2.11.6, the proposed NDPS provides material specifications before and after treatment of the gravel material with NME. It is observed that the

gravel material used in this study meets requirements that would result in a NME2 material. However, after stabilisation, the NMESM falls short of the requirements for NME2 and is instead classified as NME4. Akhalwaya and Rust (2018) make similar observations and propose for the redefining of the NME classes. In this regard, it is the considered view of this author that, despite the fact that the specifications provided for untreated material are minimum specifications, such specification may be a source of confusion. It is recommended that this specification be excluded and, in its place, a minimum material class (e.g. G8 or better) be provided for consideration with NME treatment. Material test requirements for NMESM classes should only be specified after stabilisation.

Additionally, as part of material characterisation and for use in high-level pavement design, the recommendations for range of STT limits in Table 7-1 are proposed. In such a case, a similar assessment would be conducted to determine if STT must be included in the mix design as proposed in TG2 (2020) for BSMs.

Table 7-1: Recommended classification limits for STT

Material Class	Conditioning	Cohesion (kPa)	Angle of Friction (°)
NME3 to NME4	Dry	175 - 190	45 - 50
	Wet	110 - 140	45 - 50

7.4 Recommendations for further studies

This study provides a good understanding of the behavioural characteristics of NMESMs, particularly with regard to mechanical strength properties and durability. It is the considered view of the author that NMESMs would also benefit from further studies in the following areas;

a) Currently NME and similar products are commercial products and, depending on the number of producers, among other factors, their costs may inhibit full implementation. Therefore, a Life-Cycle Cost Analysis (LCCA) is required to quantify the cost-benefit ratio of implementing the product.
b) There is need for further plastic strain tests on the NMESMs at increased cycles and different SRs to ensure tertiary flow behaviour is properly captured.
c) Methods of preparing test specimens for SEM tests should be looked into, to avoid disintegration of specimens and appearance of loose particles on the

surface. SEM tests after a specified period of, say six months or more, be considered to observe the final, equilibrium, distribution of the binder in the material.

d) Consider methods of assessing the short-term and long-term strength aspects of NMESMs that include ageing aspects of NMEs e.g. by analysing cores obtained from in-service roads over a specified period.

e) All tests were conducted at room temperature in the range of 20 to 25 C. The viscosity of the emulsion allows that stabilisation is done at room temperature. However, it may be beneficial to determine how the material behaves in different temperature environments. This is in recognition of the susceptibility of some nanomaterials to temperature effects, especially high temperatures.

REFERENCES

Abdullin, A. I. and Emelyanycheva, E. A. 2020. Water-Bitumen Emulsions Based on Surfactants of Various Types. Journal of Chemical Technology and Metallurgy, 55, 1, 2020, 73-80. Available at: https://dl.uctm.edu/journal/node/j2020-1/10_19-71_p_73-80.pdf (accessed: 12 July 2022)

Akhalwaya I. and Rust F. C. 2018. Laboratory Evaluation of Road Construction Materials Enhanced with Nano-Modified Emulsions (NMEs). Southern African Transport Conference (SATC2018) and International Conference on Transport Infrastructure (ICTI), CSIR Available: https://www.researchgate.net/publication/326480143_laboratory_evaluation construction_materials_enhanced_with_nano-modified_emulsions_nmes (Accessed: 29 April 2020)

Alaswadko N. H. A. 2016. Deterioration Modelling of Granular Pavements for Rural Arterial Roads. PhD Thesis. Faculty of Science, Engineering and Technology. Swinburne University of Technology.

Alejano L. R., Bobet A. 2012. Drucker–Prager Criterion. Rock Mech. Rock Eng 45:995–999. DOI 10.1007/s00603-012-0278-2

Alireza S. G. S., Mohammad M. S., and Hasan B. M. 2013. Application of Nanomaterial to Stabilize a Weak Soil. International Conference on Case Histories in Geotechnical Engineering. Available at: https://scholarsmine.mst.edu/icchge/7icchge/session_06/5 (Accessed: 18 June 2021)

Al-Mohammedawi, A. and Mollenhauer, K. 2022. Current Research and Challenges in Bitumen Emulsion Manufacturing and Its Properties. Materials 2022, 15, 2026. https://doi.org/10.3390/ma15062026

Alsharef J. M. A, Taha M. R., Firoozi A. A., Govindasamy P., 2016. Potential of Using Nanocarbons to Stabilize Weak Soils, Applied and Environmental Soil Science, vol. 2016, ArticleID 5060531. https://doi.org/10.1155/2016/5060531

Alzaidy, F., & Albayati, A. H. K. 2021. A Comparison between Static and Repeated Load Test to Predict Asphalt Concrete Rut Depth. Engineering, Technology & Applied Science Research, 11(4), 7363–7369. https://doi.org/10.48084/etasr.4236

American Association of Petroleum Geology (AAPG) Wiki, 2014. SEM, XRD, CL, and XF methods. Available at: https://wiki.aapg.org/SEM,_XRD,_CL,_and_XF_methods (Accessed: 12 May 2021)

Araya A. 2011. Characterization of unbound granular materials for pavements. PhD Thesis. Delft, Netherlands.

Arkles B., 2006. Hydrophobicity, Hydrophilicity and Silanes. Available at: https://www.gelest.com/wp-content/uploads/technical_library/HydrophobicityHydrophilicityandSilanes.pdf (Accessed: 5 May 2021)

Aswathanarayan J. B., Vittal R. R., 2019. Nano-emulsions and their potential applications in food industry. Front. Sustain. Food Syst., https://doi.org/10.3389/fsufs.2019.00095

Ba M., Fall M., Samb F., Sarr D. and Ndiaye M. 2011. Resilient Modulus of Unbound Aggregate Base Courses from Senegal (West Africa). Open Journal of Civil Engineering. DOI:10.4236/ojce.2011.11001

Bahia, H., Jenkins, K., & Hanz A., 2008. Performance grading of bitumen emulsions for sprayed seals. 1st International sprayed sealing conference. Adelaide, South Australia: Australian Road Research Board (ARRB). ISBN: 1876592559

Baig N., Kammakakam I. and Falath W., 2021. Nanomaterials: a review of synthesis methods, properties, recent progress, and challenges. Mater. Adv., 2021, 2, 1821–1871. Royal Society of Chemistry. DOI: 10.1039/d0ma00807a

Barskale, R.D.; Itani, S.Y. 1989. Influence of aggregate shape on base behavior. Transp. Res. Rec. 1227, 173–182. Available at: https://onlinepubs.trb.org/Onlinepubs/trr/1989/1227/1227-017.pdf (Accessed: 25 July 2022)

Bayda, S., Adeel, M., Tuccinardi, T., Cordani, M., & Rizzolio, F. 2019. The History of Nanoscience and Nanotechnology: From Chemical-Physical Applications to Nanomedicine. Molecules (Basel, Switzerland), 25(1), 112. https://doi.org/10.3390/molecules25010112

Bell T. E., 2006. Understanding Risk Assessment of Nanotechnology. Available at: http://www.nanosmile.org/images/stories/ExternData/understanding_risk_assessment.pdf (Accessed: 22 September 2020)

Bennett H. E., Ducasse K., Payne G. A. and Sewlal S. 2002. Innovative Initiatives in Road Design and Construction, In the Province of KwaZulu-Natal, South Africa. Available at: http://hdl.handle.net/2263/7879 (Accessed: 20 December 22)

Bitumina, 2014. Bitumen Emulsions, Available at: http://www.bitumina.co.uk/bitumenemulsions.html (Accessed: 30 September 2020).

Bondietti, M., Murphy, D., Jenkins, K. and Burger, R. 2004. Research on the stabilisation of two different materials using bitumen emulsion and cement. Proceedings of the 8th Conference on Asphalt Pavements for Southern Africa. Sun City, South Africa.

Boverhof D. R. et al. 2015. Comparative assessment of nanomaterial definitions and safety evaluation considerations. Regulatory Toxicology and Pharmacology. https://doi.org/10.1016/j.yrtph.2015.06.001

BRB, 2021. Silanes for coatings and adhesives. Available at: https://www.brb-international.com/clients/asset_854EB699-0F42-4F14-AFF3-345C27039448/contentms/img/Silicone/pdf/product/silanes/brb-silanes-presentation.pdf (Accessed: 4 August 2021)

Brinker, C. J., and Scherer G. 1990. Sol-Gel Science: The Physics and Chemistry of Sol Gel Processing. London: Academic Press. ISBN-13:978-0-12-134970-7

Buchanan, S. 2007. Resilient Modulus: What, Why, and How? Available at: https://www.vulcaninnovations.com/public/pdf/2-Resilient-Modulus-Buchanan.pdf (Accessed: 14 April 2021)

Caicedo B. and Mendoza C. 2015. Geotechnical behaviour of unpaved roads: understanding the CBR test. Fundamentals to Applications in Geotechnics. Doi: 10.3233/978-1-61499-603-3-95

Chacha, 2014. Method for analysing soil samples for mineral composition using XRD. Available: https://www.worldagroforestry.org/sites/default/files/METH11V01%20XRD.pdf (Accessed: 12 May 2021)

Chakwizira, J. & Mashiri, M., 2009. The Contribution of Transport Governance to Socio-Economic Development in South Africa. Available at: https://researchspace.csir.co.za/dspace/bitstream/handle/10204/3696/Chakwizira_d2_2009.pdf (Accessed: 22 June 2021)

CIVCAL, 2023. Available at: http://civcal.media.hku.hk/airport/investigation/laboratory/permeability/_hidden/fallinghead.jpg (accessed: 18 April 2023)

Committee of Transport Officials (COTO), 2020. Draft Standard Specifications for Road and Bridge Works -Chapter 4: Earthworks and Pavement Layers: Materials. The South African National Roads Agency

Dal Ben M. 2014. Resilient response and performance of bitumen stabilized materials with foam incorporating reclaimed asphalt. PhD dissertation, published at the University of Stellenbosch, South Africa.

De Beer M., Kannemeyer L., and Fisher C., 1999. Towards improved mechanistic design of thin asphalt layer surfacings based on actual tyre/pavement contact stress-in-motion (SIM) data in South Africa. 7th Conference on Asphalt Pavements for Southern Africa.

Deepa V., Eldhose S., Anu V., 2019. Analysis of Material Cost in Road Construction through Lot Sizing Techniques MAT Journals 2019, Page 38-45. e-ISSN: 2457-001X Volume 5 Issue 1

Department of Transport (DoT), 2023. Overview: South Africa's road network. Available at: https://www.transport.gov.za/roads (Accessed: 16 January 2023)

Draft Project Specifications for NME (2021). Part C: Cold In-Situ Stabilisation with a Nano modified Emulsion (NME) Stabilising Agent. Available at: https://www.nelsonmandelabay.gov.za/DataRepository/Documents/annexure-c59-end-product-specifications-for-the-use-of-additives-to-improvematerials-in-road-construction_1i5cR.pdf (Accessed: 15 February 2022)

Dybaiski N., J., 1976. The Chemistry of Asphalt Emulsion, Fifty fifth Annual Meeting Transport Research Board, 1976 available at: https://e-asphalt.com/wp-content/uploads/2019/04/TRB1976_Asphalt_Emulsions.pdf (accessed: 12 July 2022)

Ebels L. 2008. Characterisation of Material Properties and Behaviour of Cold Bituminous Mixtures for Road Pavements. PhD Dissertation. Stellenbosch University. Available at: https://scholar.sun.ac.za/handle/10019.1/1137 (Accessed: 21 December 22)

Ekblad, J. 2008. Statistical evaluation of resilient models characterizing coarse granular materials. Mater Struct. 41, 509–525. https://doi.org/10.1617/s11527-007-9262-9

Engmana, M., Jamesb, A., Needhamc, D., & Ngd, T. 2000. Specifying Slurry Surfacing Emulsion Quality: Particle Size and Size distribution. Available at: https://e-asphalt.com/wp-content/uploads/2019/04/ISSA98particle-size.pdf (Accessed: 2 October 2020)

Federal Highway Administration (FHWA). 2014. Pavement Sustainability. Technical Brief. FHWA-HIF-14-012. Available at: https://www.fhwa.dot.gov/pavement/sustainability/hif14012.pdf (Accessed: 3 March 2022)

Federal Highway Administration (FHWA). 1996. Long-Term Pavement Performance: Protocol P46 - Resilient Modulus of Unbound Granular Base/Subbase Materials and Subgrade Soils. Available at: https://www.fhwa.dot.gov/publications/research/infrastructure/pavements/ltpp/p46/p46.pdf (Accessed: 14 December 2022)

Femto, 2017. In FEA, what is linear and nonlinear analysis? Available at: https://www.femto.eu/stories/linear-non-linear-analysis-explained/ (Accessed: 22 May 2023)

Feng H., Le H. T. N., Wang S., Zhang M. H. 2016. Effects of silanes and silane derivatives on cement hydration and mechanical properties of mortars. Construction and building material. http://dx.doi.org/10.1016/j.conbuildmat.2016.11.004

Ferry, 1998. Unsealed Roads Are Sustainable [online]. Transactions of the Institution of Professional Engineers New Zealand: General Section, Vol. 25, No. 1: 54-61. Available: https://search.informit.com.au/documentSummary;dn=185169763787878;res=IELENG> ISSN: 0114-1562 (Accessed: 24 April 2020).

Firoozi et al., 2017. Fundamentals of soil stabilization. International Journal of Geo-Engineering. https://doi.org/10.1186/s40703-017-0064-9

Fonseca B.S.D., Pinto A.P.F., Piçarra S., M. and Montemor M, 2018. Advanced Materials for the Conservation of Stone, Springer. ISBN: 978-3-319-72260-3

Fraissard M. P. 2012. Rural roads important to global development. World Highways. Available at: https://www.worldhighways.com/feature/rural-roads-important-global-development (Accessed: 24 June 2021)

Franklin R. and Zhou Q., 2018. Polymer stabilisers for bituminous emulsions. EP 3 227 391 B1 Available at: https://patents.google.com/patent/EP3227391B1/en (Accessed: 30 September 2020)

Gallagher P. M. and Mitchell J. K. 2002. Influence of colloidal silica grout on liquefaction potential and cyclic undrained behavior of loose sand. Soil Dyn Earthq Eng 22:1017–1026. https://doi.org/10.1016/S0267-7261 (02)00126-4

Geotechdata.info. 2013. Soil void ratio. Available at: http://geotechdata.info/parameter/soil-void-ratio.html (Accessed: 26 April 2023)

Goddard, W. A., Brenner D. W., Lyshevski S. E., and Iafrate G. J., 2003. Handbook of nanoscience, engineering and technology. CRC Press LLC. ISBN 0-8493-1200-0

Goodarzi, F., & Zendehboudi, S. 2018. A Comprehensive Review on Emulsions and Emulsion Stability. The Canadian Journal of Chemical Engineering, 97, 281-309. https://doi.org/10.1002/cjce.23336

Gourley C. S. and Greening P. A. K. 1999. Environmental damage from extraction of road building materials: Results and recommendations from studies in Southern Africa. Project Report PR/OSC/169/99. Transport Research Laboratory. Available at: https://assets.publishing.service.gov.uk/media/57a08d9940f0b652dd001a7a/R6021.pdf (Accessed: 27 January 2021)

Govindasamy P., Taha M. R., Alsharef J. and Ramalingam K. 2017. Influence of Nanolime and Curing Period on Unconfined Compressive Strength of Soil. Hindawi. Applied and Environmental Soil Science. https://doi.org/10.1155/2017/8307493

Greenwood J. R and Joanne E Norris J. E. 1999. Moisture in the bag – a simplified procedure for the determination of soil moisture content by oven drying. New Civil Engineer. Available at: https://www.newcivilengineer.com/archive/moisture-in-the-bag-a-simplified-procedure-for-the-determination-of-soil-moisture-content-by-oven-drying-01-06-1999/ (Accessed: 10 January 2023)

Gu C. et al. 2020. Resilient and permanent deformation of unsaturated unbound granular materials under cyclic loading by the large-scale triaxial tests. Acta Geotech. 15, 3343–3356. https://doi.org/10.1007/s11440-020-00966-0

Henderson, M.G., & Van Zyl, G.D., 2017. Management of Unpaved Roads: Developing a Strategy and Refining Models. 36th Southern African Transport Conference (SATC 2017) Pretoria, South Africa. ISBN Number: 978-1-920017-73-6

Henning T.F.P., Giummarra G. J. and Roux D. C., 2008. The development of gravel deterioration models for adoption in a New Zealand gravel road management system. Research Report 348, Land Transport New Zealand. ISBN 978-0-478-30977-5

Hicks, R. G. and Monismith, C. L. 1972. Prediction of the resilient response of pavements containing granular layers using nonlinear elastic theory. Proceedings of the 3rd International Conference on the Structural Design of Asphalt Pavements, Grosvenor House, Park Lane, London, UK.

Hopkins, T.C.; Beckham, T.L.; Sun, C.; Ni, B. 2001. Resilient Modulus of Kentucky Soils; Report No. KTC-01-07/SPR163-95-1F; University of Kentucky: Lexington, KY, USA, 2001

Houston M., and Long F. 2004. Correlation between different ITS and UCS test protocol for foamed bitumen treated materials. 8th Conference on asphalt pavements for Southern Africa. Sun City, South Africa.

Huang, Y. H. 1993. Pavement Analysis and Design, published by Prentice Hall, Englewood Cliff, New Jersey, USA.

Hunter R. N., Self A. and John Read J. 2015. The Shell Bitumen Handbook. ICE Publishing. ISBN 978-0-7277-5837-8

Hussain S. A. 2016. Soil Stabilization using Nano-Materials for Rural Roads–A Case Study. IJIRSET. ISSN (Online): 2319 – 8753

Huurman, M., 1997. Permanent deformation in concrete block pavements, in Faculty of Civil Engineering and Geosciences. Delft University of Technology. Delft.

Ignatavicius S. et al. 2021. The use of anionic bitumen emulsions in pavements – A state of the art review. 7th Eurasphalt and Eurobitume congress. Available at: https://www.researchgate.net/publication/352709655 (Accessed 11 January 2023)

James A. 2006. Asphalt Emulsion Technology: Overview of Asphalt Emulsions. TRB. ISSN 0097-8515

Jayakody, S., Gallage, C. and Ramanujam, J. 2019. Performance characteristics of recycled concrete aggregate as an unbound pavement material. Heliyon. Volume 5, Issue 9, ISSN 2405-8440.

Jeevanandam, J., Barhoum, A., Chan, Y. S., Dufresne, A., & Danquah, M. K. 2018. Review on nanoparticles and nanostructured materials: history, sources, toxicity and regulations. Beilstein journal of nanotechnology, 9, 1050–1074. https://doi.org/10.3762/bjnano.9.98

Jenkins K.J. 2000. Mix design consideration for the cold and half-warm bituminous mixes with emphasis on famed bitumen. PhD dissertation, published at the University of Stellenbosch, South Africa.

Jenkins, K. J., Long F. M. and Ebels L.J. 2007. Foamed bitumen mixes = shear performance? International Journal of Pavement Engineering, 8:2, 85 98, DOI: 10.1080/10298430601149718

Jerez L. D., Gomez O. E., Murillo C. A., 2018. Stabilization of Colombian lateritic soil with a hydrophobic compound (organosilane). International Journal of Pavement Research and Technology. https://doi.org/10.1016/j.ijprt.2018.06.001

Jordaan G. J. and Steyn W.J.v.M. 2021c. Constructability of road pavement layers using New-age (Nano) Modified Emulsions (NME) stabilisation of naturally available granular materials in roads varying from highways to local access roads. doi:10.20944/preprints202110.0181.v2

Jordaan G. J., 2019. Understanding New-Age use of “Nano”-Modifications in Road Pavement Design and Construction [Paper under preparation]. Available at: http://www.soilform.co.za/pdf/Understanding-new-age-use-of-Nano-modifications-in-road-pavement-design-and-construction2-1.pdf (Accessed: 2 October 2020)

Jordaan G. J., 2019a. Nanotechnology in Road Pavement Engineering. Available at: http://www.satc.org.za/assets/6.2019_sa-china_nano-technology-in-road-pavement-engineering_70.pdf (Accessed: 27 January 2021)

Jordaan G.J. and Kilian A., 2016. The cost-effective upgrading, preservation and rehabilitation of roads – optimising the use of available technologies. Proceedings of the 35th Southern African Transport Conference (SATC 2016). ISBN Number: 978-1-920017-64-4

Jordaan G.J. and Steyn W.J.V. 2021a. Nanotechnology Incorporation into Road Pavement Design Based on Scientific Principles of Materials Chemistry and Engineering Physics Using New-Age (Nano) Modified Emulsion (NME) Stabilisation/Enhancement of Granular Materials. Appl. Sci. 2021, 11, 8525. Doi: 10.3390/app11188525

Jordaan G.J., A Kilian A., Du Plessis L., and Murphy M, 2017b. The development of cost-effective pavement design approaches using mineralogy tests with new Nano-technology modifications of materials. Available: http://www.satc.org.za/assets/1a_jordaan.pdf (Accessed: 15 April 2020)

Jordaan, G. J. and Steyn W. J. 2019. Testing of granular soil characteristics for the optimisation of pavement designs using reactive stabilising agents including "new-age" nano-technologies. Conference for Asphalt Pavements for Southern Africa (CAPSA 2019).

Jordaan, G. J. and Steyn W.J.v.d.M. 2022. Practical Application of Nanotechnology Solutions in Pavement Engineering: Construction Practices Successfully

Implemented on Roads (Highways to Local Access Roads) Using Marginal Granular Materials Stabilised with New-Age (Nano) Modified Emulsions (NME). Applied Sciences 12, no. 3: 1332. https://doi.org/10.3390/app12031332

Jordaan, G.J. and Steyn, W.J.v. 2021c. Engineering Properties of New-Age (Nano) Modified Emulsion (NME) Stabilised Naturally Available Granular Road Pavement Materials Explained Using Basic Chemistry. Appl. Sci. 2021, 11, 9699. https:// doi.org/10.3390/app11209699

Jordaan, G.J., and Kilian, A. 2016. The cost-effective upgrading, preservation and rehabilitation of roads – optimising the use of available technologies. Proceedings of the 35th SATC conference. ISBN: 978-1-920017-64-4

Jordaan, G.J., Kilian, A., Muthivelli, N. and Dlamini, D., 2017a. Practical Application of Nanotechnology in Roads in Southern Africa. 8th Africa Transportation Technology (T2) Conference, Lusaka, Zambia. Available at: http://www.soilform.co.za/pdf/T2%20conference%20in%20Livinston%20-%20Final%20Paper%2016-05-2017.pdf (Accessed: 21 December 2022)

Jordaan, G.J.; Steyn, W.J.v.d.M. 2021b. Fundamental Principles Ensuring Successful Implementation of New-Age (Nano) Modified Emulsions (NME) for the Stabilisation of Naturally Available Materials in Pavement Engineering. Appl. Sci. 2021, 11, 1745. https://doi.org/10.3390/app11041745

Kambole C. 2018. Characterisation of slags for utilisation in road construction. Thesis for D.Eng. Tshwane University of Technology.

Kashaya A. A., 2013. Surface Run-off Behaviour of Bitumen Emulsions Used for The Construction of Seals. Dissertation submitted for Master of Science in Engineering Available at: https://core.ac.uk/download/pdf/37411501.pdf (Accessed: 12 July 2022)

Kassa G. M., 2015. Modelling of Gravel Loss for Unsealed Roads. MSc Thesis. Addis Ababa Institute of Technology. Available at: http://etd.aau.edu.et/bitstream/handle/123456789/9420/Getahun%20Mekonnen.pdf?sequence=1&isAllowed=y (Accessed: 20 December 2022)

Kidgell M.M., Steyn W.J. and Jordaan G., 2019. Effect of Nano-Modified Emulsions (NME) (Nano-Silanes) Stabilizers on the Properties of Dolomite. Southern Africa Transportation Conference (SATC 2019) Available At: https://www.researchgate.net/publication/334443389 (Accessed: 22 July 2020)

Kiihnl, L. P. 2020. Best Practices for Asphalt Emulsion Particle Size Analyses Using a Coulter Counter. Theses and Dissertations. Available at: https://scholarworks.uark.edu/etd/3657 (Accessed: 21 July 2021)

Klein, C. & Hurlbut, C. S., Jr. 1993. Manual of Mineralogy (after J. D. Dana). New York, NY: John Wiley & Sons, Inc.

Kodaka T, Ohno Y, Takyu T. 2005. Cyclic shear characteristics of treated sand with colloidal silica grout. Proceedings of the International Conference on Soil Mechanics and Geotechnical Engineering, Aa Balkema Publishers, 16(2): 401 Available at: http://civil.meijo-u.ac.jp/lab/kodaka/pdf/icsmge1.pdf (accessed: 19 August 2022)

Kopeliovich, D. 2013. Surfactants. Available at: https://www.substech.com/dokuwiki/doku.php?id=surfactants (accessed: 12 July 2022)

Kotzé J-C. 2022. Performance Characteristics of BitumenEmulsion Stabilized Mine-Haul roads. MSc Dissertation. Stellenbosch University.

Kumar R., Mathur R. and Mishra A. K. 2011. Opportunities & Challenges for Use of Nanotechnology in Cement-Based Materials. Available at: https://www.nbmcw.com/article-report/infrastructure-construction/transportation-metrorail-airways-waterways/use-of-nanotechnology-in-cement-based-materials.html (accessed: 19 May 2023)

Laurie, A. P. 1926. Preservation of Stone. U.S. Patent 1,607,762.

Leon L., Chung E. J. and Rinaldi C. 2020. A brief history of nanotechnology and introduction to nanoparticles for biomedical applications. Nanoparticles for Biomedical Applications. Elsevier Inc. https://doi.org/10.1016/B978-0-12-816662-8.00001-1

Lesueur D. et al., 2008. Bitumen nanoemulsions and their interest for cold recycling of bituminous mix. Available at: https://www.researchgate.net/publication/291759067 (Accessed: 25 May 2021)

Lesueur D., 2011. Polymer Modified Bitumen: Polymer modified bitumen emulsions. Woodhead Publishing, Pages 25-42. https://doi.org/10.1533/9780857093721.1.25

Li C., 2016. Improving performance and sustainability of unpaved roads: Stabilization and testing. Graduate Theses and Dissertations. Iowa State University. 15960. Available: htts://lib.dr.iastate.edu/etd/15960 (Accessed: 28 April 2020)

Li, N.; Ma, B.;Wang, H.; Tang, J.;Wang, X.; Shao, Z. 2021. Influence of loading frequency on mechanical properties of unbound granular materials via repeated load tests. Constr. Build. Mater. 2021, 301, 124098. ISSN 0950-0618

Liu, G.; Zhang, C.; Zhao, M.; Guo, W.; Luo, Q. 2021. Comparison of Nanomaterials with other unconventional materials used as additives for soil improvement in the context of sustainable development: A Review. Nanomaterials, 11, 15. https://dx.doi.org/10.3390/nano1101 0015

Local Road Research Board (LRRB), 2005. To Pave or Not to Pave? Making Informed Decisions on When to Upgrade a Gravel Road. Available: http://www.mnltap.umn.edu/

publications/factsheets/documents/paveornot/paveornot.pdf (Accessed: 4 May 2020)

Maher, M., Uzarowski, L., Moore, G., and Aurilio, V. 2006. Sustainable pavements-making the case for longer design lives for flexible pavements. Proc., 51st Annual Conf. of the Canadian Technical Asphalt Association, CTAA, Charlottetown, Prince Edward Island, Canada, 44–56

Majeed Z. H. and Taha M. R. 2013. A Review of Stabilization of Soils by using Nanomaterials. Australian Journal of Basic and Applied Sciences, 7(2): 576-581, ISSN 1991-8178

Manual 30 (Sabita). 2011. A guide to the selection of bituminous binders for road construction. Sabita. ISBN 978-1-874968-52-8

Manuello, A. B., Grosso B., Ricciu R. & Rizzu D. 2014. Anisotropic and impulsive neutron emissions from brittle rocks under mechanical load. Meccanica. 50. 10.1007/s11012-014-9987-9.

Marr B. 2020. Seven amazing everyday examples of Nanotechnology in action. Available at: https://www.forbes.com/sites/bernardmarr/2020/07/03/7-amazing-everyday-examples-of-nanotechnology-in-action/?sh=e6739413e823 (Accessed: 11 May 2022)

MAS. 2007. Modelling and analysis Systems, Available at: http://www.modsys1.com (Accessed: 11 May 2022)

Materne, T., Buyl, F.D., & Witucki, G. 2012. Organosilane Technology in Coating Applications: Review and Perspectives. Available at: https://www.academia.edu/10140050/Organosilane_Technology_in_Coating_Applications_Review_and_Perspectives (Accessed: 28 September 2020)

Mbaraga A. 2015. Shrinkage Characterisation, Behavioural Properties and Durability of Cement-Stabilised Pavement Materials. PhD Dissertation. Stellenbosch University

McGoldrick, S. 2020. A practical guide to introductory geology. Mount Royal University Library. Available at: https://openeducationalberta.ca/practicalgeology (Accessed: 21 July 2022).

Mealey S. K., Thomas B., 2006. Past, present and future of organosilane treatments for fillers. Available at: https://citeseerx.ist.psu.edu/viewdoc/download?doi=10.1.1.568.2249&rep=rep1&type=pdf (Accessed: 5 May 2021)

Ministry of Works Transport and Communications (MWTC) 2016. Low volume roads manual. Tanzania. ISBN: 978-9976-9974-0-8

Miskovsky, K. 2004. Enrichment of fine mica originating from rock aggregate production and its influence on the mechanical properties of bituminous

mixtures. Journal of Materials Engineering and Performance, Vol 13(5). DOI: 10.1361/15477020420837

Mitchell, J.K. 1993. Fundamentals of soil behaviour, second edition, John Wiley & sons, inc. USA

Mkhize S. 2022. Compatibility of Adhesion Promoter to be used for Cationic and Anionic Emulsions. SATBinder Conference. Available at: https://socsat.co.za/compatibility-of-adhesion-promoters-to-be-used-for-cationic-and-anionic-emulsions/ (accessed: 10 October 2022)

Moloisane, R. J. and Visser A. T., 2014. Evaluation of the strength behaviour of unpaved road material treated with electrochemical-based non-traditional soil stabilisation additives. Available:https://www.researchgate.net/publication/287214812_Evaluation_of_the_strength_behaviour_of_unpaved_road_material_treated_with_electrochemical-based_non-traditional_soil_stabilisation_additives (Accessed: 6 August 2019)

Mshali, M R, & Visser, A T. 2012. Influence of mica on unconfined compressive strength of a cement-treated weathered granite gravel. Journal of the South African Institution of Civil Engineering, 54(2), 71-77. Available at: http://www.scielo.org.za/scielo.php?script=sci_arttext&pid=S1021-20192012000200008&lng=en&tlng=en. (Accessed: 14 April 2022)

Mulusa W.K. 2009. Development of a simple Tri-axial test for characterising Bitumen Stabilised Materials. Dissertation for Master of Science in Engineering, University of Stellenbosch.

Murphy M., Jordaan G. J., Modise T. S., Dryburgh R. C. L., 2019. The influence of characteristics of emulsifying agents on the stabilisation of granular materials using nano-silane modified bitumen emulsions. 12th CAPSA. Available at: https://www.researchgate.net/publication/336614749 (Accessed: 30 September 2020)

Mwaipungu R. R. and Allopi D., 2012. The Use of Gravel Loss Predicting Models for Effective Management of Gravel Roads. Proceedings of the 31st Southern African Transport Conference (SATC 2012). Pretoria, South Africa. ISBN: 978-1-920017-53-8

Mwaipungu R. R. and Allopi D., 2014. The sustainability of gravel roads as depicted by sub Saharan Africa's standard specifications and manuals for road works: Tanzania case study WIT Transactions on The Built Environment, Vol 138 DOI: 10.2495/UT140481

Mwaipungu R. R., 2015. The formulation and application of a gravel loss model in management of gravel roads in Iringa Region, Tanzania. PhD thesis. Durban University of Technology

Nagarajan and Hatton, 2008. Nanoparticles: Synthesis, Stabilization, Passivation, and Functionalization ACS Symposium Series; American Chemical Society: Washington, DC. Doi: 10.1021/bk-2008-0996.ch001

Nanowerk, 2020. Nanotechnology Examples and Applications. Available at: https://www.nanowerk.com/nanotechnology-examples-and-applications.php (Accessed: 31 May 2021)

National Centre for Asphalt Technology (NCAT), 2009. Laboratory evaluation of Zycosil as an anti-stripping agent for Superpave Mixtures – Phase II. Auburn, USA.

National Centre for Asphalt Technology (NCAT), 2011. Effects of Nanotac additive on bond strength and moisture resistance of Tach Coats. Auburn, USA

National Nanotechnology Initiative (NNI), 2021. What It Is and How It Works. Available at: https://www.nano.gov/nanotech-101/what (Accessed: 5 July 2021)

Netterberg F. 2018. Importance of the zero point in DCP testing of structural capacity of flexible pavements. SATC. Pretoria, South Africa. ISBN Number: 978-1-920017-89-7

Obuseng M., 2019. SA's gravel, paved roads will cost an estimated R400 billion. Available at: https://www.sabcnews.com/sabcnews/sas-gravel-paved-roads-will-cost-an-estimated-r400-billion/ (Accessed: 20 April 2020)

Oladele A. S., 2013. Gravel Road Performance Modelling for Optimal Maintenance Interventions of Botswana District Transportation Networks. University of Botswana. DOI: 10.13140/RG.2.1.2552.3604

Osinubi K.J., Eberemu A.O., Bello A.O. and Adzegah A. 2012. Effect of fines content on the engineering properties of reconstituted lateritic soils in waste containment application. Nigerian Journal of Technology (NIJOTECH). Vol. 31, pp. 277–287. ISSN 1115-8443

Oxford University Press (OUP), 2021. Performance Model. Available at: https://www.encyclopedia.com/computing/dictionaries-thesauruses-pictures-and-press-releases/performance model#:~:text=performance%20model%20A%20model%20created,access%20latency%2C%20etc.). (Accessed: 14 April 2021)

Paige-Green P. 2008. A Reassessment of Some Road Material Stabilization Problems. Proceedings of the 27th Southern African Transport Conference (SATC 2008). Pretoria, South Africa. ISBN Number: 978-1-920017-34-7

Paige-Green P. and Du Plessis L. 2009. The use and interpretation of the Dynamic Cone Penetrometer (DCP) test. CSIR Built Environment. Pretoria. Available at: https://rtdcp.co.za/wp-content/uploads/2019/11/The_use_and_interpretation_of_the_Dynamic_Cone_Penetrometer_01.pdf (Accessed: 12 April 2023)

Paige-Green P., and Hongve J., 2003. Alternatives to Conventional Gravel Wearing Courses on Low Volume Roads. Tenth Regional Seminar for Labour-based Practitioners Arusha, Tanzania 13th – 17th October 2003. Available at: https://researchspace.csir.co.za/dspace/bitstream/handle/10204/1993/Paige-Green_2003_1.pdf?sequence=1&isAllowed=y (Accessed: 27 October 2020)

Paige-Green, P. 1999. A comparative study of the grading coefficient, a new particle size distribution parameter. Bull Eng Geol Env 57, 215–223. https://doi.org/10.1007/s100640050039

Paige-Green, P. 2007. Improved material specifications for unsealed roads. Quarterly Journal of Engineering Geology and Hydrogeology, 40, 175 - 179. DOI:10.1144/1470-9236/06-037

Paige-Green, P. and Netterberg F. 2004. Cement stabilization of road pavement materials: Laboratory testing programme Phase 1. CSIR Transportek. Available at: https://researchspace.csir.co.za/dspace/bitstream/handle/10204/3142/Paige-Green_2004.pdf?sequence=1&isAllowed=y (Accessed: 20 April 2023)

Paige-Green, P. and Van Zyl, G.D. 2019. A review of the DCP-DN pavement design method for low volume sealed roads: development and applications. Journal of Transportation Technologies, 9, 397-422. https://doi.org/10.4236/jtts.2019.94025

Paige-Green, P. and Visser, A.T. 1991. Comparison of the Impact of Various Unpaved Road Performance Models on Management Decisions. Transp. Res. Rec. 1991, 2, 137–142

Paige-Green, P., Pinard, M. and Netterberg, F. 2015. A review of specifications for lateritic materials for low volume roads. Transportation Geotechnics, vol. 5, pp. 86–98

Papadimitropoulos V. C., Karatzas S. K., Chassiakos A. P., 2018. Applications of Nanomaterials in Pavement Engineering: A Review. The Tenth International Conference on Construction in the 21 st Century (CITC-10) July 2nd-4th, 2018, Colombo, Sri Lanka. Available at: https://www.researchgate.net/publication/323831350 (Accessed: 28 July 2020)

Partl M.N., Gubler R. and Hugener M., 2004. Nano-science and technology for asphalt pavements", In Special publication-Royal Society of Chemistry, Cambridge, UK, 343-356. https://doi.org/10.1039/9781847551528-00343

Pavement Design Manual (PDM), 2013. Volume I – Flexible Pavements. Ethiopia Roads Authority.

Persoff P., Apps J., Moridis G., Whang J. M. 1999. Effect of dilution and contaminants on sand grouted with colloidal silica. J Geotechn Geoenviron Eng 125(6):461–469. https://doi.org/10.1061/(ASCE)1090-0241(1999)125:6(461)

PIARC (World Road Association), 2021. Deterioration Models for Lifecycle Planning. Available at: https://road-asset.piarc.org/en/data-and-modeling-lifecycle-planning/deterioration-models (Accessed: 14 April 2021)

Pinard M I, Hongve J. Infra Africa (Pty) Ltd (2020). Pavement Design of Low Volume Roads Using the DCP-DN Method. London: ReCAP for UK aid.

Pinard M. et al., Infra Africa (Pty) Ltd (2019). Low Volume Roads Manual Volume 1: Pavement Design. Ministry of Housing and Infrastructure Development. Zambia. ISBN: 978-9982-70-970-5

Platypus Technologies, LLC. 2022. Material Characterization Techniques: Microscopy and Spectroscopy. AZoNano. Available at: https://www.azonano.com/article.aspx?ArticleID=6026 (Accessed: 29 September 2022)

Plotnikova, I., 1993. Control of the interaction process between emulsion and mineral aggregate by means of physiochemical modification of their surfaces, First World Congress on Emulsion, Paris.

Puppala, A. J., Chomtid, S., & Bhadriraju, V. 2005. Using Repeated-Load Triaxial Tests to Evaluate Plastic Strain Potentials in Subgrade Soils. Transportation Research Record, 1913(1). https://doi.org/10.1177/0361198105191300109

Qacha, B. 2022. Improving mine haul road performance through innovative material treatment using Nano-Modified Emulsions (NME's). Dissertation for MSc. Stellenbosch University.

Rahman F. 2021. Types of bitumen emulsions – uses, advantages and manufacture. Available at: https://theconstructor.org/transportation/bitumen-emulsion-types-uses-advantages/16375/ (Accessed: 25 May 2021)

Raj P.P. 2008. Soil Mechanics and Foundation Engineering. Dorling Kindersley Ltd. ISBN 81-317-1177-3

Ray, P. C., Yu, H., & Fu, P. P. 2009. Toxicity and environmental risks of nanomaterials: challenges and future needs. Journal of environmental science and health. Part C, Environmental carcinogenesis & ecotoxicology reviews, 27(1), 1–35. https://doi.org/10.1080/10590500802708267

ReCAP, 2023. Dynamic Cone Penetrometer – Low volume roads design software. Available at: https://dcp-dn.csir.co.za/ (Accessed: 12 April 2023)

Reeb J. and Milota M. 1999. Moisture Content by the Oven-Dry Method for Industrial Testing. Oregon State University. Available at: https://ir.library.oregonstate.edu/downloads/jm214q048 (Accessed: 10 January 2023)

Republic of South Africa (RSA), 1996. National Transport Policy White Paper. Available at: https://www.gov.za/documents/national-transport-policy-white-paper (Accessed: 25 April 2021)

Roads Authority (RA), 2014. Materials Manual. Roads Authority of Namibia. Available at: https://www.ra.org.na/Documents/Maintenance/MATERIALS%20MANUAL_oct%202014.pdf (Accessed: 4 January 23)

Rolt J., Mukura K. and Otto A., 2020. Development of a Simplified Agency Life-Cycle Costing Tool for Gravel Roads. Sustainability 2020, 12, 4512; doi: 10.3390/su12114512

Rosales J., Agrela F., Marcobal J., Diaz-López J., Moyano G., Caballero A. and Cabrera M. 2020. Use of Nanomaterials in the Stabilization of Expansive Soils into a Road Real-Scale Application. Materials, 13, 3058; doi:10.3390/ma13143058

Ross D. and Field K. 2007. South African road surfacing policy, international oil price changes, and the shadow pricing of costs and benefits. Available at: https://www.sabita.co.za/documents/Don%20Ross%20report%20surfacing%20gravel%20roads.pdf (Accessed: 20 January 2022)

Ross D. and Field K. 2007. South African road surfacing policy, international oil price changes, and the shadow pricing of costs and benefits http://www.sabita.co.za/documents/Don%20Ross%20report%20surfacing%20gravel%20roads.pdf (Accessed: 28 October 2020)

Rust F. C., Akhalwaya I., Jordaan G. J. and du Plessis L., 2019. Evaluation of a nano-silane modified emulsion stabilised base and subbase under HVS traffic, Conferencence on Asphalt Pavements for Southern Africa (CAPSA'19), Sun City, South Africa. Available at: http://hdl.handle.net/10204/11220 (accessed: 5 August 2020)

Rust, F.C.; Smit M. A., Akhalwaya, I., Jordaan, G.J., Du Plessis, L. 2020. Evaluation of two nano-silane-modified emulsion stabilised pavements using accelerated pavement testing. International Journal of Pavement Engineering. https://doi.org/10.1080/10298436.2020.1799210

Sağlik A., and Gungor A. G. 2012. Resilient Modulus of unbound and bituminous bound road materials. 5th Eurasphalt & Eurobitume Congress, Istanbul. Available at: https://www.researchgate.net/publication/318865503 (Accessed: 25 Apr. 2020)

Saha P. and Ksaibati K. 2017. Developing an Optimization Model to Manage Unpaved Roads. Hindawi Journal of Advanced Transportation, Volume 2017, Article ID 9474838, https://doi.org/10.1155/2017/9474838

Saidi T. and Douglas T. S. 2017. Nanotechnology in South Africa - Challenges in evaluating the impact on development. S. Afr. j. sci. vol.113. http://dx.doi.org/10.17159/sajs.2017/a0217

Shell Global Solutions. 1998. BISAR 3.0 Software and User Manual, CD-ROM, Shell International Oil Products B.V., Bitumen Business Group, Amsterdam, the Netherlands.

Sherwood, P. 1993. Soil stabilization with cement and lime. State of the Art Review. London: Transport Research Laboratory, HMSO. ISBN 9780115511714

Smit M. A, Akhalwaya I. and Rust F. C. 2021. Laboratory evaluation of alternative cost-effective pavement materials. Virtual Southern African Transport Conference. http://hdl.handle.net/10204/12110

Smita, S. et al. 2012. Nanoparticles in the environment: assessment using the causal diagram approach. Environ Health 11 (Suppl 1), S13. https://doi.org/10.1186/1476-069X-11-S1-S13

Solà N. Q. 2013. Highly concentrated bitumen emulsions - A state of the art, review of experimental results. Master Dissertation. Universitat de Lleida. Available at: https://repositori.udl.cat/bitstream/handle/10459.1/46663/nquerols.pdf?sequence=1&isAllowed=y (Accessed: 21 July 2021)

South African Institution of Civil Engineering (SAICE), 2022. Infrastructure report card. ISBN 978-0-6397-4193-2

South African Nanotechnology Initiative (SANI). 2003. The National Nanotechnology Strategy. Department of Science and Technology. ISBN 0-621-36395-2

South African National Roads Agency Ltd (SANRAL), 2020. Annual performance plan for the financial year 2021 /22 – 2023/24. Available: https://www.nra.co.za/publications/strategic-plan/ (Accessed: 27 February 2022)

South African Pavement Engineering Manual (SAPEM), 2013. Chapter 10: Pavement Design. South African National Roads Agency Ltd. ISBN 978-1-920611-10-1

Southern Africa Bitumen Association (SABITA), n.d. Advancing the public interest a case for surfacing gravel roads Available at: http://www.sabita.co.za/documents/InformationSeriesNo2.pdf (Accessed: 20 April 2020)

Southern African Transport and Communications Commission (SATCC). 1998. Code of Practice for the Design of Road Pavements. Division of Roads and Transport Technology, CSIR.

Steyn W. J. 2008. Research and application of nanotechnology in transportation. Proceedings of the 27th Southern African Transport Conference (SATC 2008). Pretoria, South Africa. ISBN Number: 978-1-920017-34-7

Steyn W.J., 2009. Potential applications of Nanotechnology in pavement engineering. Journal of Transportation Engineering. DOI: 10.1061/(ASCE)0733-947X(2009)135:10(764)

Taha, M. R. 2009. Geotechnical properties of soil–ball milled soil mixtures. 3rd symposium on nanotechnology in construction (berlin; heidelberg: springer–verlag), 377–382. doi: 10.1007/978-3-642-00980-8_51

Tak S., Kim S. and Yeo H. 2013. Large-Scale Maintenance Optimization Problems for Civil Infrastructure Systems. https://doi.org/10.1016/B978-0-12-398364-0.00022-X

Tamiri T. and S. Zitrin S. 2013. Explosives: Analysis. Encyclopaedia of Forensic Sciences (Second Edition). Academic Press. Pages 64-84. ISBN 9780123821669.

Taniguchi, N. 1974. On the Basic Concept of Nanotechnology. Proceedings of the International Conference on Production Engineering, Tokyo, 18-23

Tarrer A.R. and Wagh V. 1991. The effect of the physical and chemical characteristics of the aggregate on bonding. SHRP-A/UIR-91-507, contract A-003B. Available at: https://onlinepubs.trb.org/onlinepubs/shrp/shrp-91-507.pdf (Accessed: 26 Aug. 2022)

Technical Guideline (TG2). 2020. Bitumen Stabilised Materials: A guideline for design and construction of bitumen emulsion and foamed bitumen stabilised materials. Sabita. ISBN 978-1-874968-77-1

Technical Recommendations for Highways (TRH13). 1986. Cementitious stabilisers in road construction. Pretoria, South Africa. ISBN: 0 7988 3647 4.

Technical Recommendations for Highways (TRH14). 1985. Guidelines for Road Construction Materials. Pretoria, South Africa. ISBN: 0 7988 3311 4.

Technical Recommendations for Highways Draft (TRH12), 1997. Flexible pavement rehabilitation investigation and design. Department of Transport, Pretoria, SA.

Technical Recommendations for Highways Draft (TRH20), 1990. The structural design, construction and maintenance of unpaved roads. Department of Transport, Pretoria, SA. ISBN 0 908381 87 5

Technical Recommendations for Highways Draft (TRH24), 2022. Upgrading of Unpaved Roads. COTO. The South African National Roads Agency SOC Limited.

Technical Recommendations for Highways Draft (TRH4), 1996. Structural design of flexible pavements for interurban and rural roads. Department of Transport, Pretoria, SA. ISBN 1-86844-218-7

Technical Recommendations for Highways Draft (TRH7), 1994. The use of bitumen emulsions in the construction and maintenance of roads. Department of Transport, Pretoria, SA. ISBN 1-86844-150-4

Theyse H. L. De Beer M. and Rust F. C. 1996. Overview of South African Mechanistic Pavement Design Method. Transportation Research Record Journal of the Transportation Research Board. DOI: 10.3141/1539-02

THEYSE, H.L. 2008. The Classical South African Mechanistic-Empirical Design Method. Pavement Modelling Corporation, Pretoria. Flexible pavement design

course. Session 2: Structural capacity analysis. Module 3: Mechanistic-empirical design.

Thompson R. J. and Visser A. T. 1996. Towards a mechanistic structural design method for surface mine haul roads. SAICE Journal. Available at: https://journals.co.za/doi/pdf/10.10520/AJA10212019_23878 (accessed: 10 June 2023)

TMH1. 1986. Standard Methods of Testing Road Construction Materials, 2nd Edition ISBN 0-7988-3653-9 pp. 1-232

Tolochko N.K., 2009. History of Nanotechnology. Encyclopedia of Life Support Systems (EOLSS). Available at: http://www.eolss.net/sample-chapters/c05/E6-152-01.pdf (Accessed: 28 July 2020)

Toole T., Rice Z., Latter L. & Sharp K., 2018. Appropriate Use of Marginal and Non-Standard Materials in Road Construction and Maintenance. Austroads, AP-T335-18, Sydney, NSW, Australia. ISBN 978-1-925671 -63-6

Toole, T 1987. The use of calcrete in unpaved roads in Botswana. MPhil thesis, University of Birmingham, UK.

Toole, T, Morosiuk, G, Petts, RC & Done, S. 2001. Management guidelines for unsealed roads, project report PR/INT/230/00, Transport Research Laboratory, Crowthorne, Berkshire, UK.

Transport (official guide to SA). 2019. Available at: https://www.gcis.gov.za/sites/default/files/docs/resourcecentre/pocketguide/2012/22-Transport-2018-19%28print%29.pdf (accessed: 23 January 2022)

Twagira E. M. 2010. Influence of Durability Properties on Performance of Bitumen Stabilized Materials. PhD Dissertation. Stellenbosch University. Available at: https://scholar.sun.ac.za/handle/10019.1/3993 (Accessed: 26 December 2020)

Ugwu O. O., Ogboin A. S. and Nwoji C. U. 2018. Characterization of Engineering Properties of Active Soils Stabilized with Nanomaterial for Sustainable Infrastructure Delivery. Front. Built Environ. 4:65. Doi: 10.3389/Fbuil.2018.00065

Ugwu O., Arop J.B., Nwoji C.U., Osadebe N.N., 2013. Nanotechnology as a Preventive Engineering Solution to Highway Infrastructure Failures. J. Constr. Eng. Manage. 2013.139:987-993. DOI: 10.1061/(ASCE)CO.1943-7862.0000670

University of Pretoria (UP), n.d. Chapter 4 – Mechanistic-Empirical design models in pavement engineering. Available at: https://repository.up.ac.za/bitstream/handle/2263/25951/04chapter4.pdf?sequence=5&isAllowed=y (Accessed: 4th April 2023)

Uzan, J. 1985. Characterization of Granular Material. in Transportation Research Records 1022. Washington DC: Transportation Research Board. Available at:

https://onlinepubs.trb.org/Onlinepubs/trr/1985/1022/1022-007.pdf (accessed: 20 January 2022)

Van Niekerk, A.A. 2002. Mechanical behaviour and performance of granular bases and sub-bases in pavements, PhD dissertation, Delft University of Technology.

van Niekerk, AA., van Scheers, J., & Galjaard, JC. 2000. Resilient deformation behaviour of coarse-grained mix granulate base course materials from testing scaled gradings at smaller specimen sizes. In Wegbouwkundige werkdagen, deel 2 (pp. 251-268). CROW. ISBN: 90-6628-314-9

van Wijk I., Williams D. J. and Serati M. 2019. Use of gravel loss prediction models in the design and management of unsealed road pavements. Transportation Research Board. Doi: 10.1177/0361198119854081

Van Zyl, G., Henderson, M., & Uys, R. 2007. Applicability of existing gravel-road deterioration models questioned. Transportation Research Record, 1989–1(1), 217–225. https://doi.org/10.3141/1989-25

Verhaenghe, B., Maina J., Paige-Green, P., de Beer, M. and Du Plessis L. 2010. The CSIR's contribution to the development of innovative technologies and solutions for enhanced road system performance. Science real and relevant conference, South Africa. Available at: https://researchspace.csir.co.za/dspace/handle/10204/4251 (Accessed: 20 December 22)

Wacker, 2015. Organofunctional silanes –for powerful connections. Available at: https://www.wacker.com/h/medias/7082-EN.pdf (Accessed: 5 January 2023)

Wang, M.; Yu, Q.; Xiao, Y.; Li, W. 2022. Resilient Modulus Behavior and Prediction Models of Unbound Permeable Aggregate Base Materials Derived from Tunneling Rock Wastes. Materials 2022, 15, 6005. https:// doi.org/10.3390/ma15176005

Weinert H.H. 1980. The natural road construction materials of Southern Africa. Academia. Cape Town.

Weiss, N.R.; Slavid, I.; Wheeler, G. 2000. Development and assessment of a conversion treatment for calcareous stone. In Proceedings of the Ninth International Congress on Deterioration and Conservation of Stone, Venice, Italy, 19–24 June 2000; Volume 2, pp. 533–540.

Wendler, E., L. Sattler, S. Simon, H. Ettl, and F. Heckmann. 1999. Untersuchungen zur Wirksamkeit von Konsolidierungmitteln an Tuffeaustein von Kathedrale St. Gatien in Tours. In Monuments historiques et environments, 244-61. Colloquium on Recherches Franco-Allemandes sur la pierre el le vitrail 1988-1996. Paris: Exe Productions.

Wheeler G., 2005. Alkoxysilanes and the Consolidation of Stone. The Getty Conservation Institute. Los Angeles, California, USA, 2005. Available at:

https://www.getty.edu/conservation/publications_resources/pdf_publications/pdf/alkoxysilanes_vl.pdf (Accessed: 7 December 2020)

Wypych F., Bergaya F. and Schoonheydt R. A. 2018. From polymers to clay polymer nanocomposites. Developments in Clay Science. Elsevier. Volume 9. Pages 331-359. ISSN 1572-4352. ISBN 9780081024324.

Xu F., Zeng W., and Li D. 2019. Recent advance in alkoxysilane-based consolidants for stone. Progress in Organic Coatings. DOI: 10.1016/j.porgcoat.2018.11.003

Yaacob H. et al. 2013. Bitumen Emulsion in Malaysia–A Conspectus. Jurnal Teknologi. DOI: 10.11113/jt.v65.2153

Zhu W., Bartos P.J.M and Porro A. 2004. Application of nanotechnology in construction Summary of a state-of-the-art report. Materials and Structures, Vol. 37, pp 649-658. http://dx.doi.org/10.1007/BF02483294

APPENDICES

Appendix A – DCP-DN Results

DCP Summary Report - Single Mould Analysis

Job Ref. no	Giba Gorge		
Project date:	14 September, 2021	**Analysis date:**	10 January, 2023
Compactive Effort	Heavy		
Design DN (mm/blow):	13	**Moisture Content:**	OMC
Borrow Pit #:		**OMC (%):**	5.6
Test Pit #:		**Layer Depth in Test Pit (mm):**	0 - 0
Single Mould Run:	Sample no 1 Mould no 1		

Average equivalent strength (Existing Mould)

Depth (mm)	W. Ave. DN. (mm / blow)	Best Fit DN (mm / blow)	Blows	Ave. E-Moduli (MPa)
15 - 99	5.15	4.61	17	196

Average equivalent strength (Redefined-EasyDCP Mould)

Depth (mm)	W. Ave. DN. (mm / blow)	Blows	Ave. E-Moduli (MPa)
0 - 114	5.56	22	180

DCP Laboratory Curve Profile

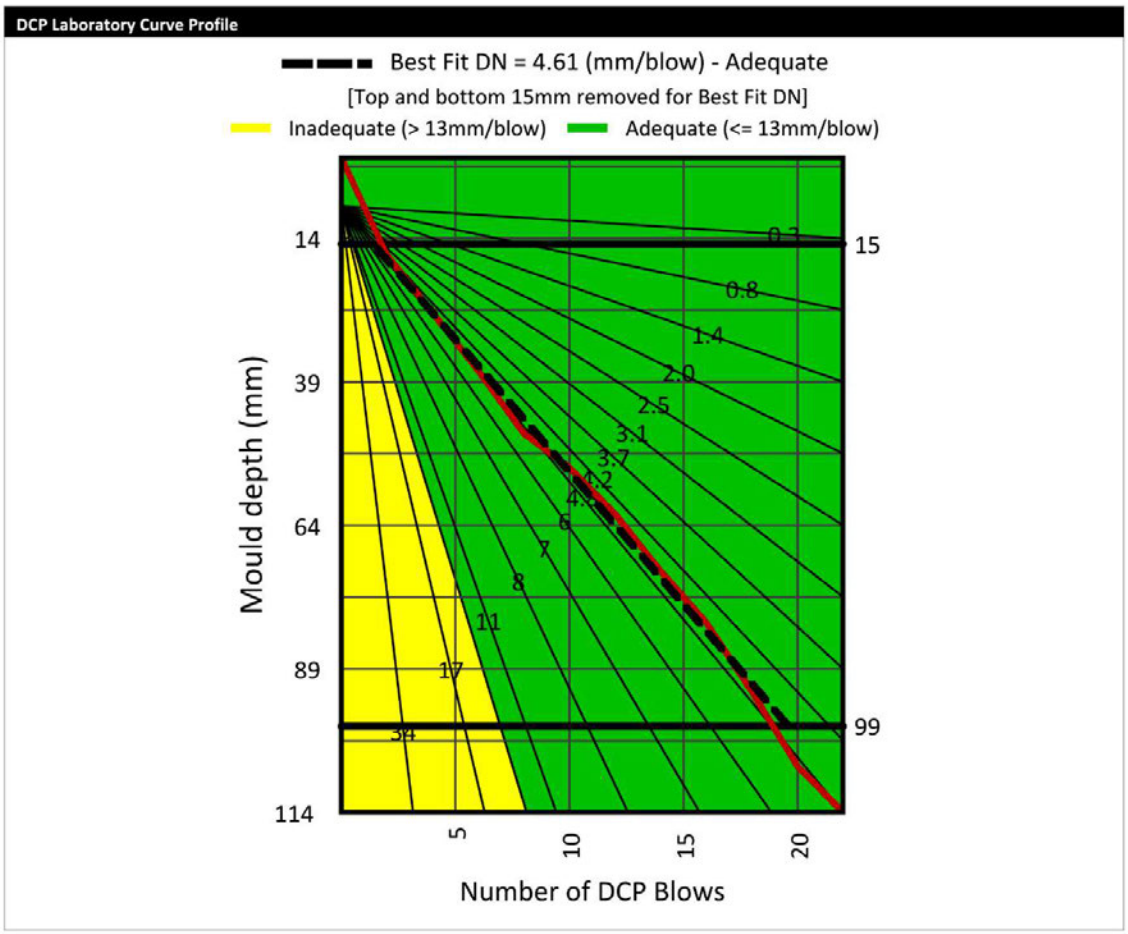

Appendix A 1: DCP-DN untreated 1

DCP Summary Report - Single Mould Analysis

Job Ref. no	Giba Gorge				
Project date:	14 September, 2021		**Analysis date:**		10 January, 2023
Compactive Effort	Heavy				
Design DN (mm/blow):	13		**Moisture Content:**	SOAKED	
Borrow Pit #:			**OMC (%):**	0	
Test Pit #:			**Layer Depth in Test Pit (mm):**	0 - 0	
Single Mould Run:	Sample no 2 Mould no 2				

Average equivalent strength (Existing Mould)

Depth (mm)	W. Ave. DN. (mm / blow)	Best Fit DN (mm / blow)	Blows	Ave. E-Moduli (MPa)
15 - 101	5.36	4.52	18	188

Average equivalent strength (Redefined-EasyDCP Mould)

Depth (mm)	W. Ave. DN. (mm / blow)	Blows	Ave. E-Moduli (MPa)
0 - 116	5.89	22	170

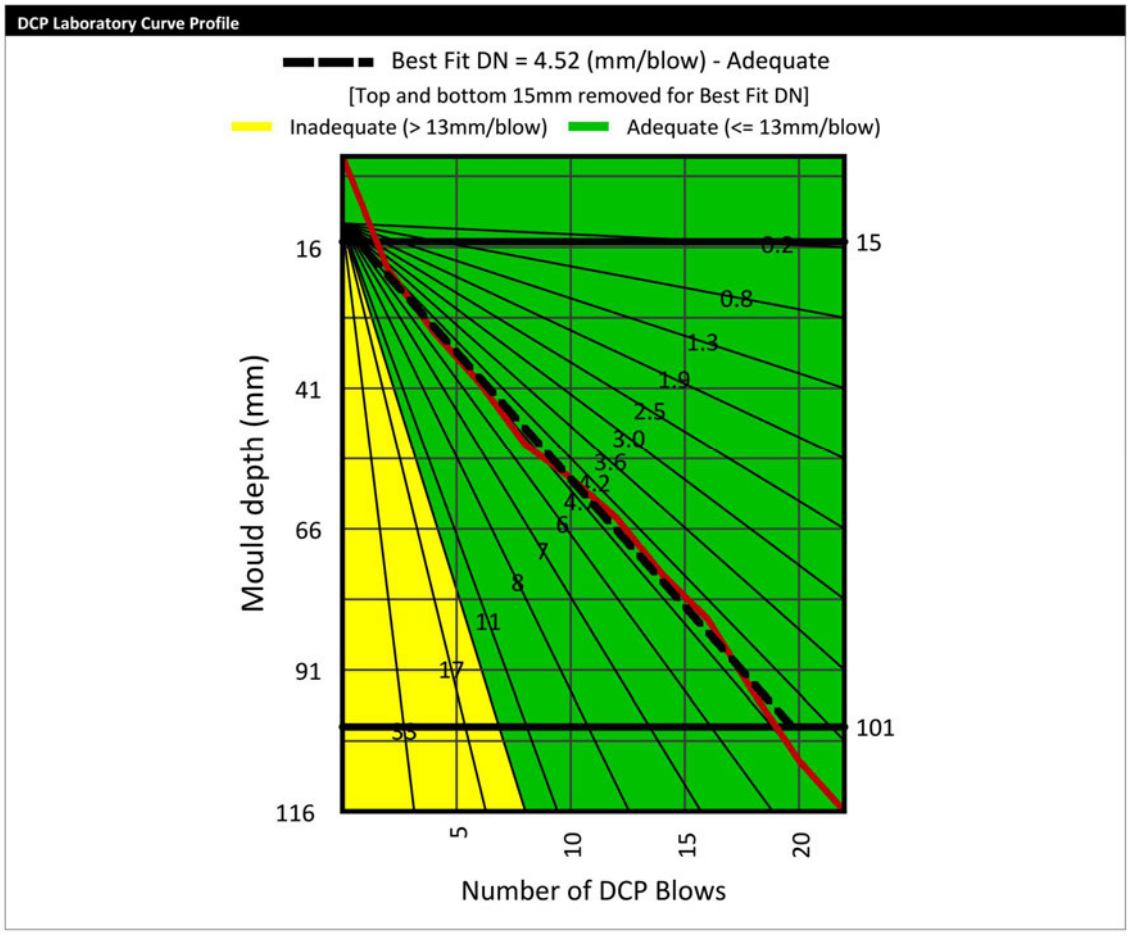

Appendix A 2: DCP-DN untreated 2

DCP Summary Report - Single Mould Analysis

Job Ref. no	Giba Gorge		
Project date:	14 September, 2021	**Analysis date:**	10 January, 2023
Compactive Effort	Heavy		
Design DN (mm/blow):	13	**Moisture Content:**	SOAKED
Borrow Pit #:		**OMC (%):**	0
Test Pit #:		**Layer Depth in Test Pit (mm):**	0 - 0
Single Mould Run:	Sample no 3 Mould no 0.7-1		

Average equivalent strength (Existing Mould)

Depth (mm)	W. Ave. DN. (mm / blow)	Best Fit DN (mm / blow)	Blows	Ave. E-Moduli (MPa)
15 - 96	3.06	2.71	29	340

Average equivalent strength (Redefined-EasyDCP Mould)

Depth (mm)	W. Ave. DN. (mm / blow)	Blows	Ave. E-Moduli (MPa)
0 - 34	4.68	8	217
34 - 111	2.58	32	408

DCP Laboratory Curve Profile

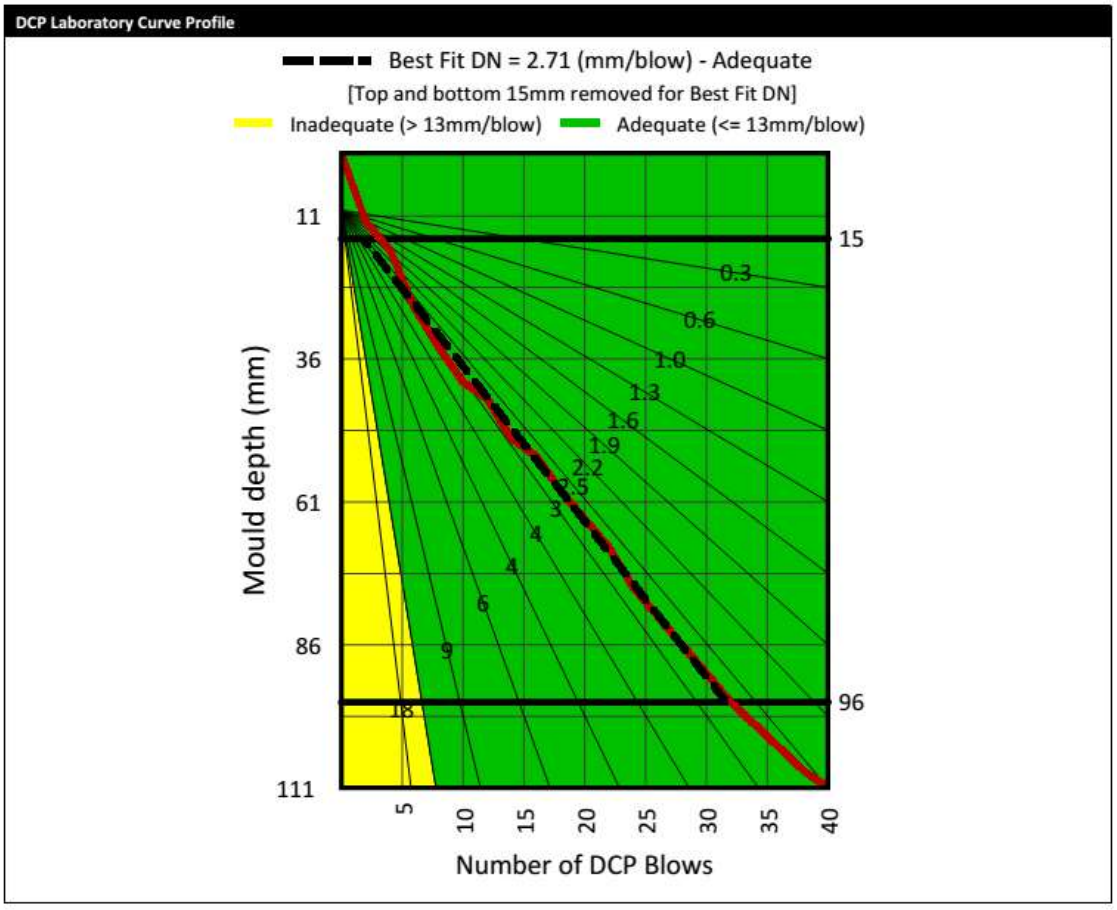

Appendix A 3: 0.7NME DCP-DN 1

DCP Summary Report - Single Mould Analysis

Job Ref. no	Giba Gorge		
Project date:	14 September, 2021	**Analysis date:**	10 January, 2023
Compactive Effort	Heavy		
Design DN (mm/blow):	13	**Moisture Content:**	SOAKED
Borrow Pit #:		**OMC (%):**	0
Test Pit #:		**Layer Depth in Test Pit (mm):**	0 - 0
Single Mould Run:	Sample no 3 Mould no 0.7-2		

Average equivalent strength (Existing Mould)

Depth (mm)	W. Ave. DN. (mm / blow)	Best Fit DN (mm / blow)	Blows	Ave. E-Moduli (MPa)
15 - 89	2.51	2.34	31	421

Average equivalent strength (Redefined-EasyDCP Mould)

Depth (mm)	W. Ave. DN. (mm / blow)	Blows	Ave. E-Moduli (MPa)
0 - 30	3.36	9	309
30 - 104	2.32	33	456

DCP Laboratory Curve Profile

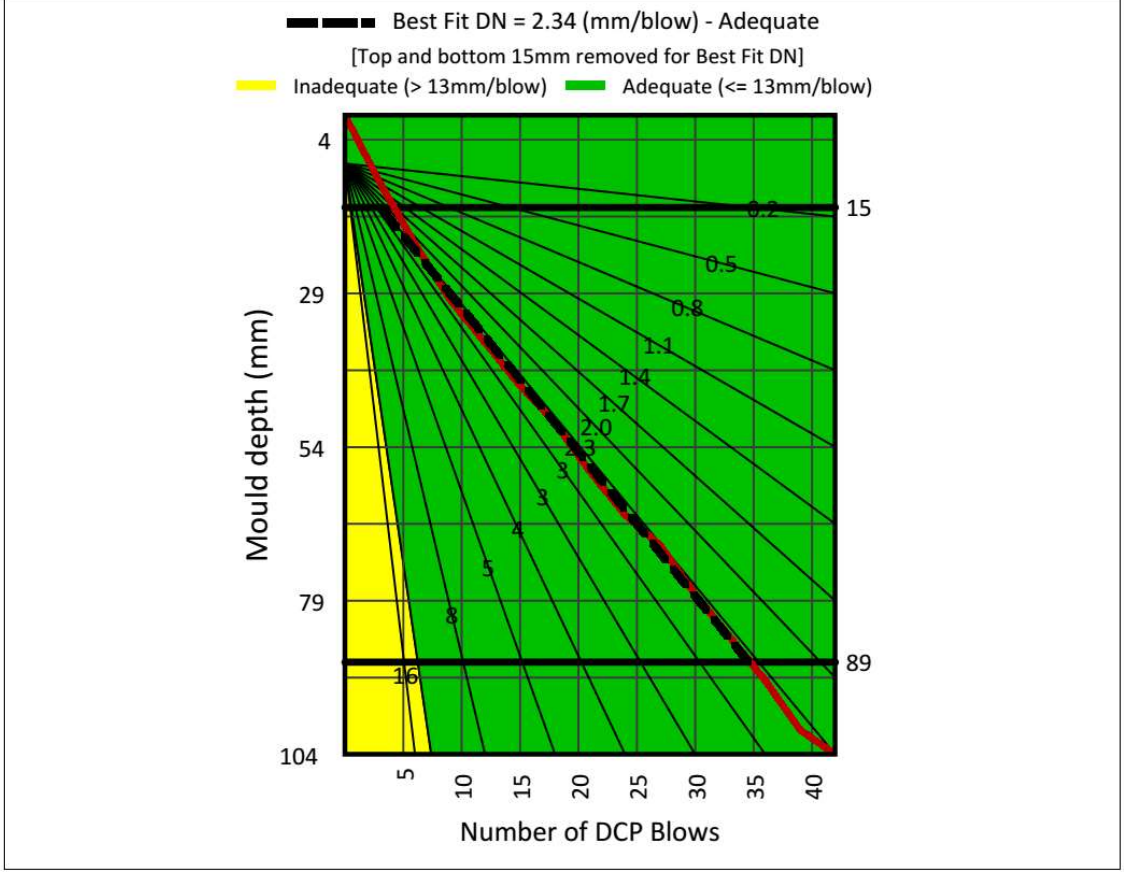

Appendix A 4: 0.7NME DCP-DN 2

DCP Summary Report - Single Mould Analysis

Job Ref. no	Giba Gorge		
Project date:	14 September, 2021	**Analysis date:**	10 January, 2023
Compactive Effort	Heavy		
Design DN (mm/blow):	13	**Moisture Content:**	SOAKED
Borrow Pit #:		**OMC (%):**	0
Test Pit #:		**Layer Depth in Test Pit (mm):**	0 - 0
Single Mould Run:	Sample no 3 Mould no 0.7-3		

Average equivalent strength (Existing Mould)

Depth (mm)	W. Ave. DN. (mm / blow)	Best Fit DN (mm / blow)	Blows	Ave. E-Moduli (MPa)
15 - 104	2.92	2.77	32	357

Average equivalent strength (Redefined-EasyDCP Mould)

Depth (mm)	W. Ave. DN. (mm / blow)	Blows	Ave. E-Moduli (MPa)
0 - 119	2.94	42	355

DCP Laboratory Curve Profile

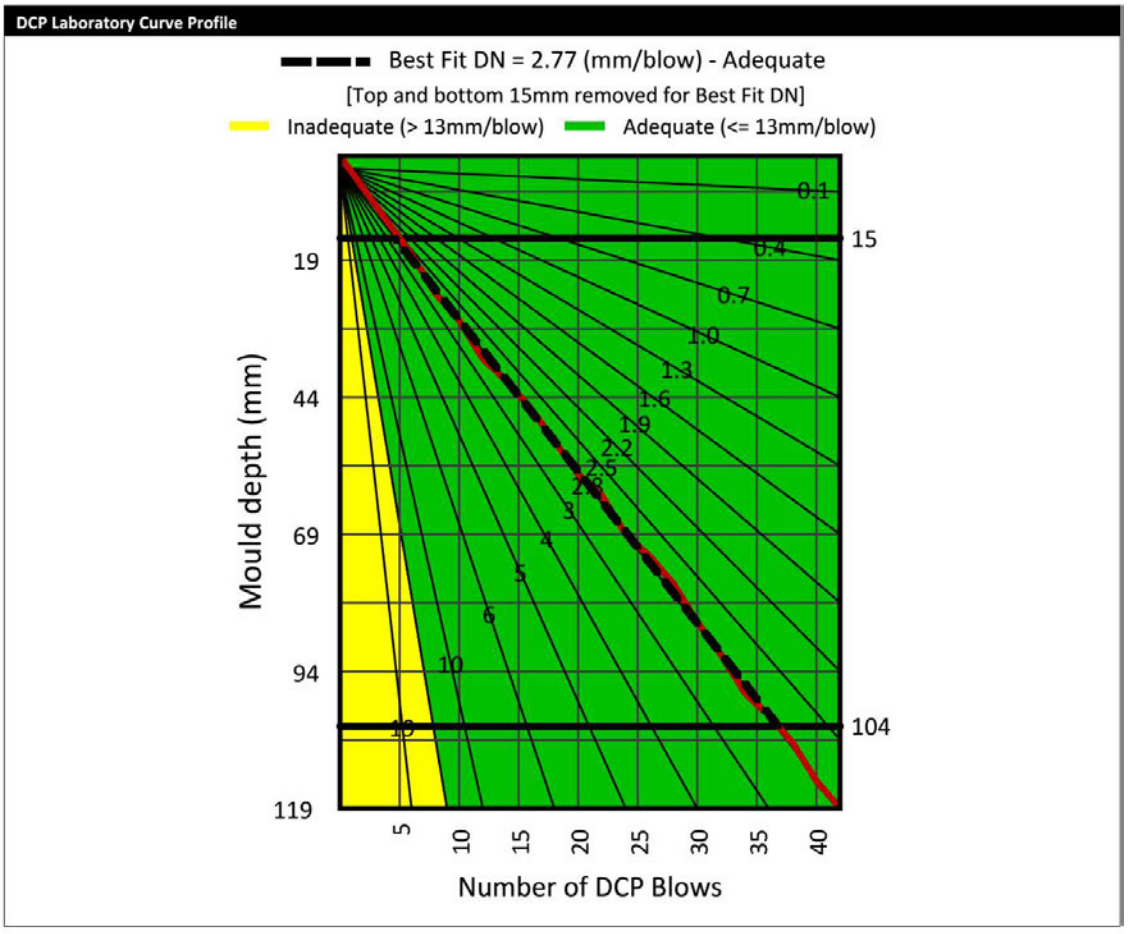

Appendix A 5: 0.7NME DCP-DN 3

DCP Summary Report - Single Mould Analysis

Job Ref. no	Giba Gorge				
Project date:	14 September, 2021		**Analysis date:**		10 January, 2023
Compactive Effort	Heavy				
Design DN (mm/blow):	13		**Moisture Content:**	SOAKED	
Borrow Pit #:			**OMC (%):**	0	
Test Pit #:					
Single Mould Run:	Sample no 4 Mould no 1-1				

Average equivalent strength (Existing Mould)

Depth (mm)	W. Ave. DN. (mm / blow)	Best Fit DN (mm / blow)	Blows	Ave. E-Moduli (MPa)
15 - 85	2.24	2.02	36	474

Average equivalent strength (Redefined-EasyDCP Mould)

Depth (mm)	W. Ave. DN. (mm / blow)	Blows	Ave. E-Moduli (MPa)
0 - 30	3.36	9	309
30 - 100	1.89	42	567

DCP Laboratory Curve Profile

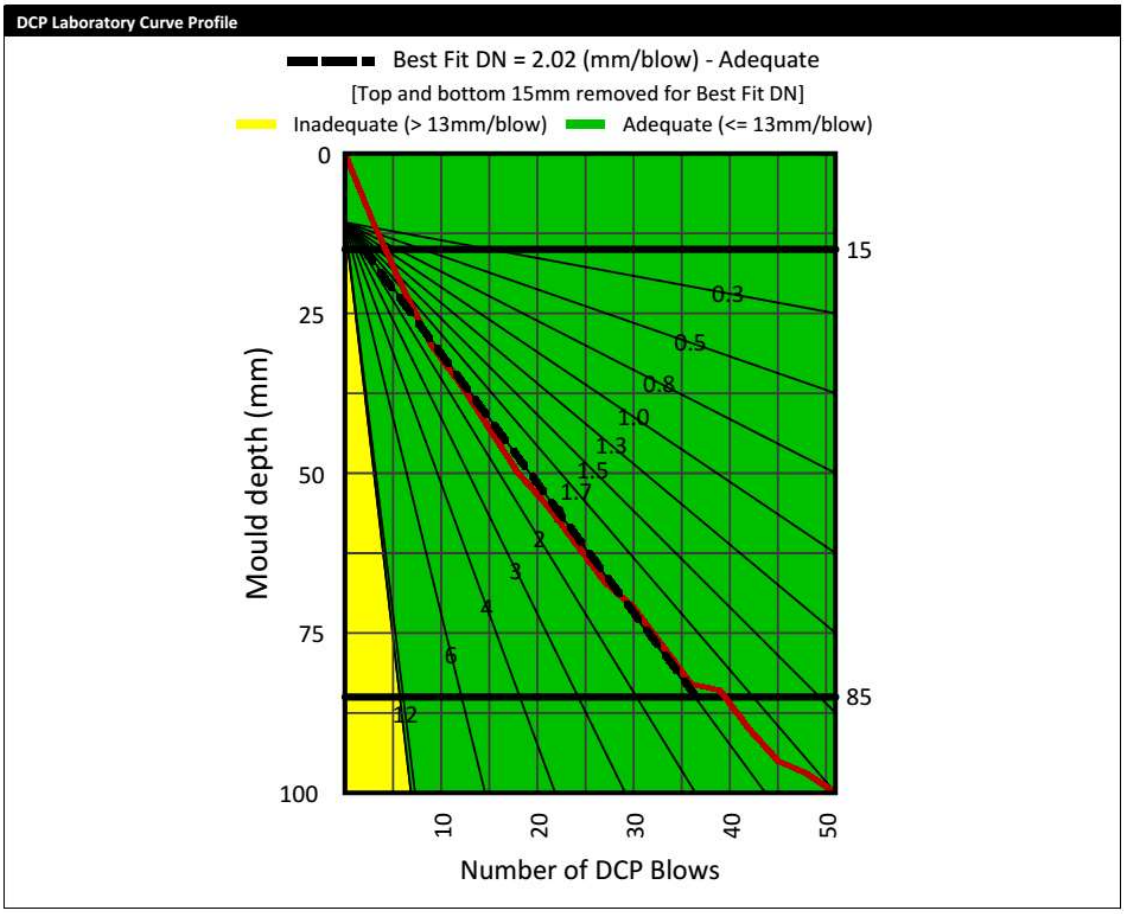

Appendix A 6: 1.0NME DCP-DN 1

DCP Summary Report - Single Mould Analysis

Job Ref. no	Giba Gorge		
Project date:	14 September, 2021	**Analysis date:**	10 January, 2023
Compactive Effort	Heavy		
Design DN (mm/blow):	13	**Moisture Content:**	SOAKED
Borrow Pit #:		**OMC (%):**	0
Test Pit #:		**Layer Depth in Test Pit (mm):**	0 - 0
Single Mould Run:	Sample no 2 Mould no 1-2		

Average equivalent strength (Existing Mould)

Depth (mm)	W. Ave. DN. (mm / blow)	Best Fit DN (mm / blow)	Blows	Ave. E-Moduli (MPa)
15 - 85	1.73	1.49	46	623

Average equivalent strength (Redefined-EasyDCP Mould)

Depth (mm)	W. Ave. DN. (mm / blow)	Blows	Ave. E-Moduli (MPa)
0 - 45	2.66	18	395
45 - 100	1.36	43	807

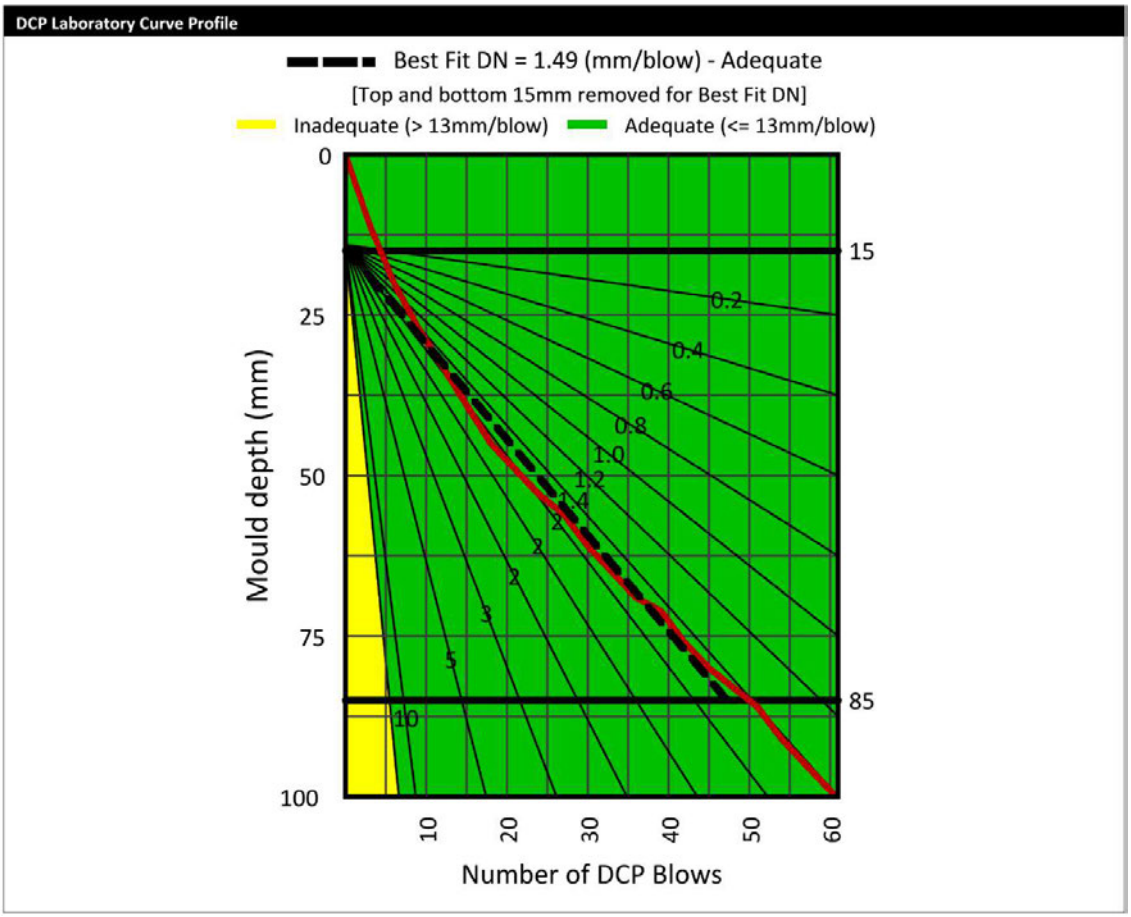

Appendix A 7: 1.0NME DCP-DN 2

DCP Summary Report - Single Mould Analysis

Job Ref. no	Giba Gorge		
Project date:	14 September, 2021	**Analysis date:**	10 January, 2023
Compactive Effort	Heavy		
Design DN (mm/blow):	13	**Moisture Content:**	SOAKED
Borrow Pit #:		**OMC (%):**	0
Test Pit #:		**Layer Depth in Test Pit (mm):**	0 - 0
Single Mould Run:	Sample no 3 Mould no 1-3		

Average equivalent strength (Existing Mould)

Depth (mm)	W. Ave. DN. (mm / blow)	Best Fit DN (mm / blow)	Blows	Ave. E-Moduli (MPa)
15 - 96	2.22	2.09	39	479

Average equivalent strength (Redefined-EasyDCP Mould)

Depth (mm)	W. Ave. DN. (mm / blow)	Blows	Ave. E-Moduli (MPa)
0 - 90	2.44	39	433
90 - 111	1.52	15	718

DCP Laboratory Curve Profile

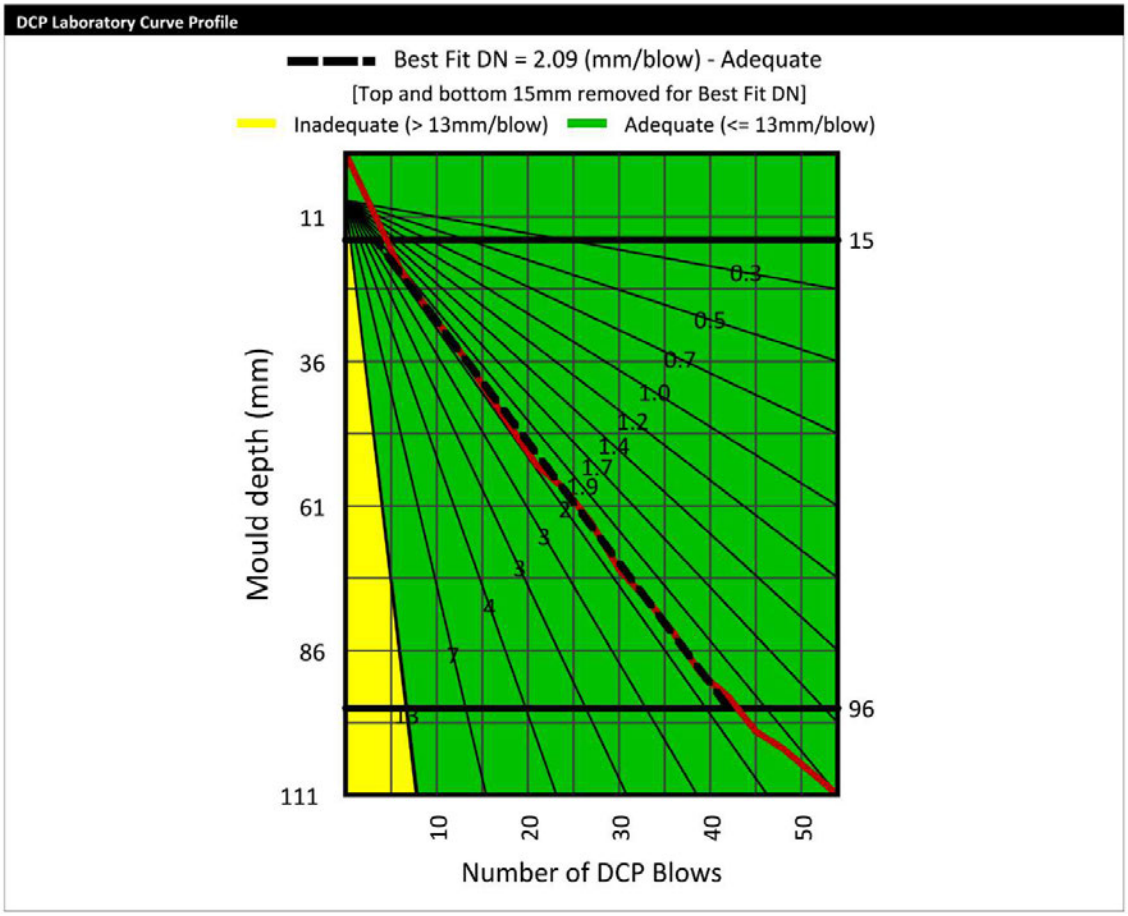

Appendix A 8: 1.0NME DCP-DN 3

DCP Summary Report - Single Mould Analysis

Job Ref. no	Giba Gorge		
Project date:	14 September, 2021	**Analysis date:**	10 January, 2023
Compactive Effort	Heavy		
Design DN (mm/blow):	13	**Moisture Content:**	SOAKED
Borrow Pit #:		**OMC (%):**	0
Test Pit #:		**Layer Depth in Test Pit (mm):**	0 - 0
Single Mould Run:	Sample no 2 Mould no 1.2-1		

Average equivalent strength (Existing Mould)

Depth (mm)	W. Ave. DN. (mm / blow)	Best Fit DN (mm / blow)	Blows	Ave. E-Moduli (MPa)
15 - 85	1.60	1.41	50	679

Average equivalent strength (Redefined-EasyDCP Mould)

Depth (mm)	W. Ave. DN. (mm / blow)	Blows	Ave. E-Moduli (MPa)
0 - 44	2.27	21	467
44 - 100	1.37	47	800

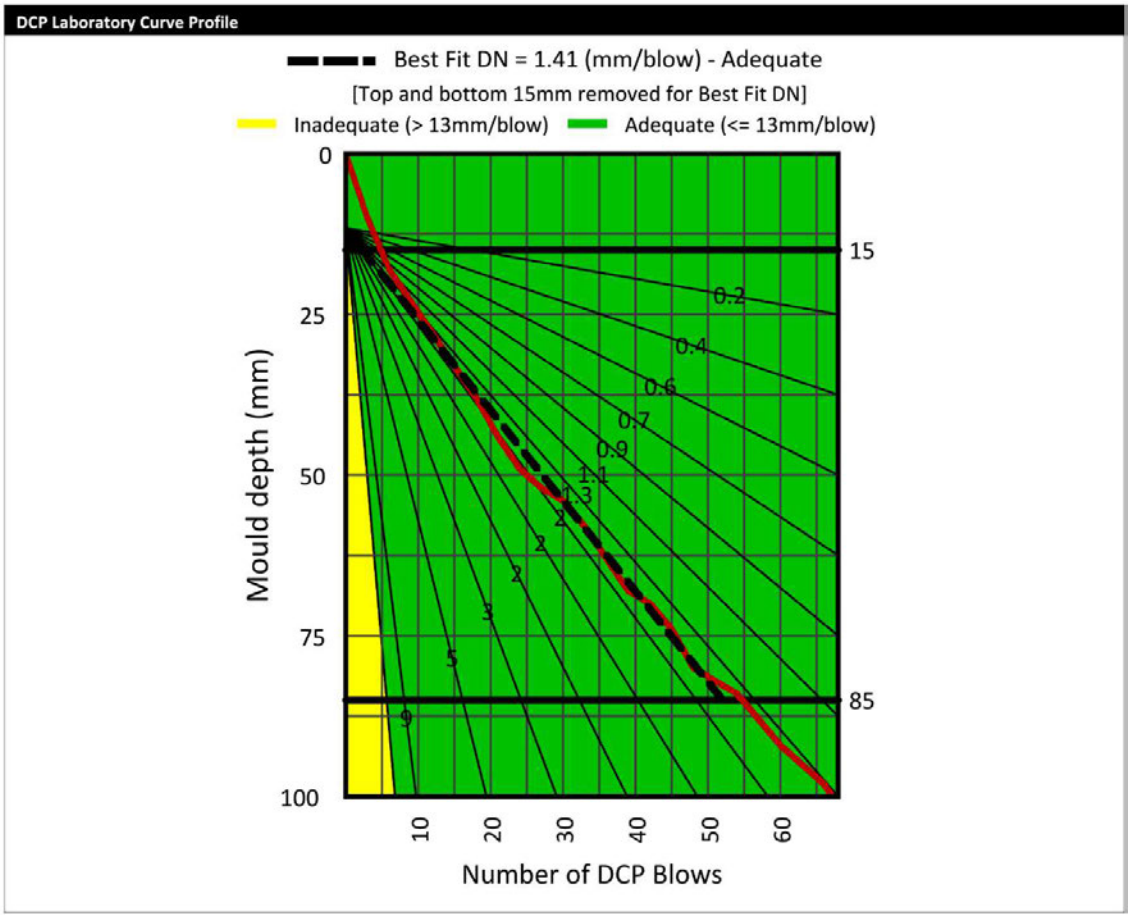

Appendix A 9: 1.2NME DCP-DN 1

DCP Summary Report - Single Mould Analysis

Job Ref. no	Giba Gorge		
Project date:	14 September, 2021	**Analysis date:**	10 January, 2023
Compactive Effort	Heavy		
Design DN (mm/blow):	13	**Moisture Content:**	SOAKED
Borrow Pit #:		**OMC (%):**	0
Test Pit #:		**Layer Depth in Test Pit (mm):**	0 - 0
Single Mould Run:	Sample no 1 Mould no 1.2-1		

Average equivalent strength (Existing Mould)

Depth (mm)	W. Ave. DN. (mm / blow)	Best Fit DN (mm / blow)	Blows	Ave. E-Moduli (MPa)
15 - 80	1.65	1.63	41	655

Average equivalent strength (Redefined-EasyDCP Mould)

Depth (mm)	W. Ave. DN. (mm / blow)	Blows	Ave. E-Moduli (MPa)
0 - 95	1.65	63	658

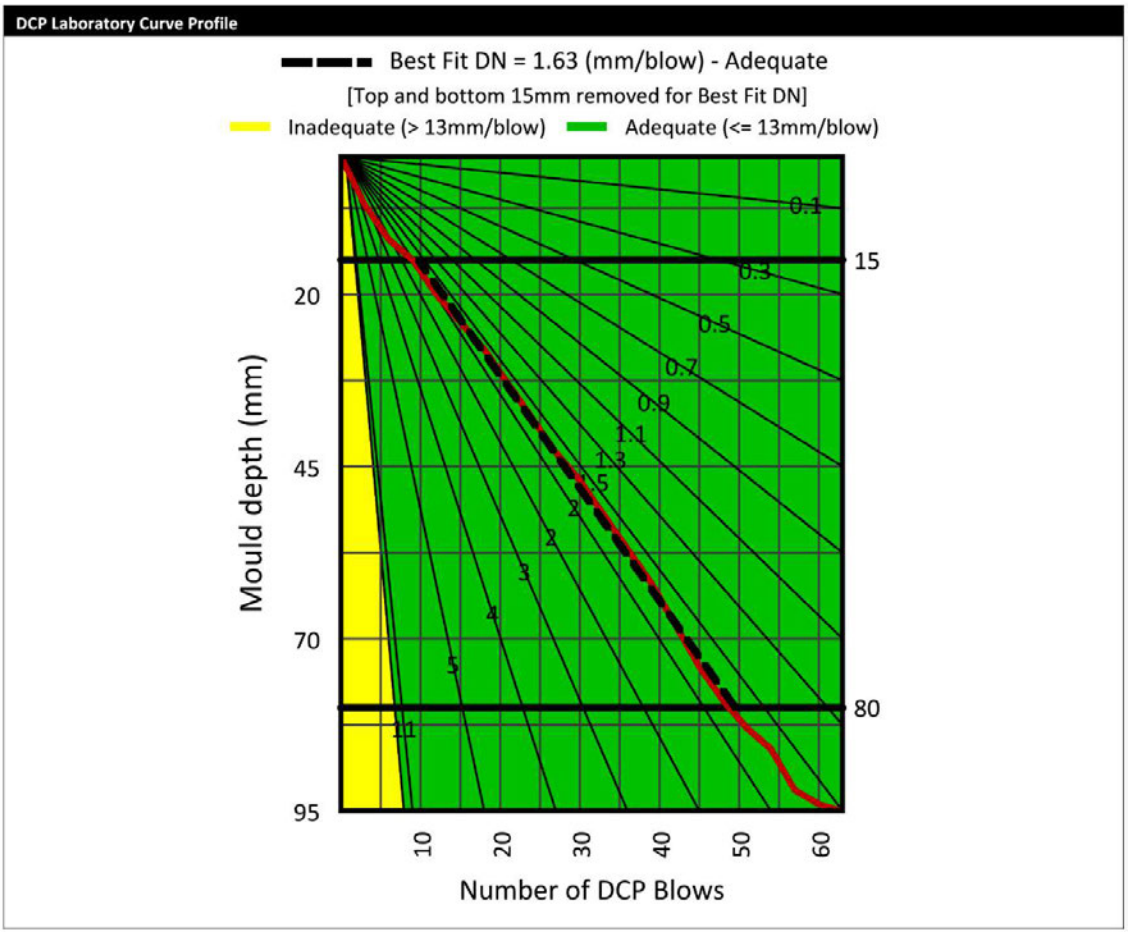

Appendix A 10: 1.2NME DCP-DN 2

DCP Summary Report - Single Mould Analysis

Job Ref. no	Giba Gorge				
Project date:	14 September, 2021		**Analysis date:**		10 January, 2023
Compactive Effort	Heavy				
Design DN (mm/blow):	13		**Moisture Content:**	SOAKED	
Borrow Pit #:			**OMC (%):**	0	
Test Pit #:					
Single Mould Run:	Sample no 6 Mould no 1.5-2				

Average equivalent strength (Existing Mould)

Depth (mm)	W. Ave. DN. (mm / blow)	Best Fit DN (mm / blow)	Blows	Ave. E-Moduli (MPa)
15 - 35	1.48	1.03	19	738

Average equivalent strength (Redefined-EasyDCP Mould)

Depth (mm)	W. Ave. DN. (mm / blow)	Blows	Ave. E-Moduli (MPa)
0 - 35	1.48	30	738
35 - 50	0.37	46	3161

DCP Laboratory Curve Profile

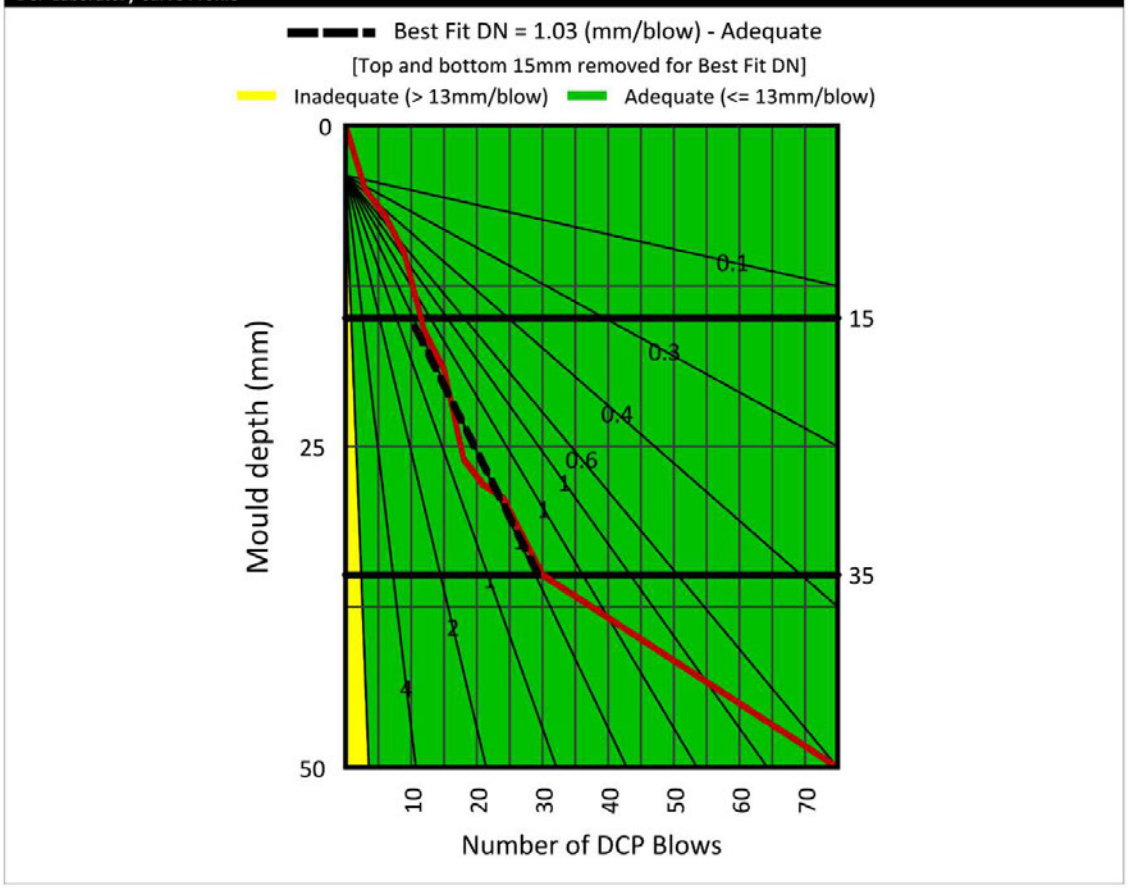

Appendix A 11: 1.5NME DCP-DN 1

Appendix B – CBR Results

UT1 -CBR Test Results

Comp	1927	1924	1873	Client	
mm	Test 1	Test 2	Test 3	Reference	
0.00	0.00	0.00	0.00	Date Tested	01 Jul 2022
0.64	0.18	0.04	0.03		
1.27	0.69	0.23	0.18		
1.91	1.59	0.61	0.45		
2.54	2.51	1.23	0.92		
3.18	3.35	2.05	1.54		
3.81	4.11	2.92	2.19		
4.45	4.83	3.77	2.82		
5.08	5.49	4.51	3.38		
5.72	6.09	5.15	3.87		
6.35	6.64	5.80	4.35		
6.99	7.15	6.40	4.80		
7.62	7.63	6.97	5.23		
8.26	8.07	7.49	5.62		
8.89	8.57	7.99	5.99		
9.53	9.01	8.43	6.32		
CBR	18.8%	9.2%	6.9%	@ 2.54mm	
	27.4%	22.5%	16.9%	@ 5.08mm	
	30.1%	27.5%	20.6%	@ 7.62mm	

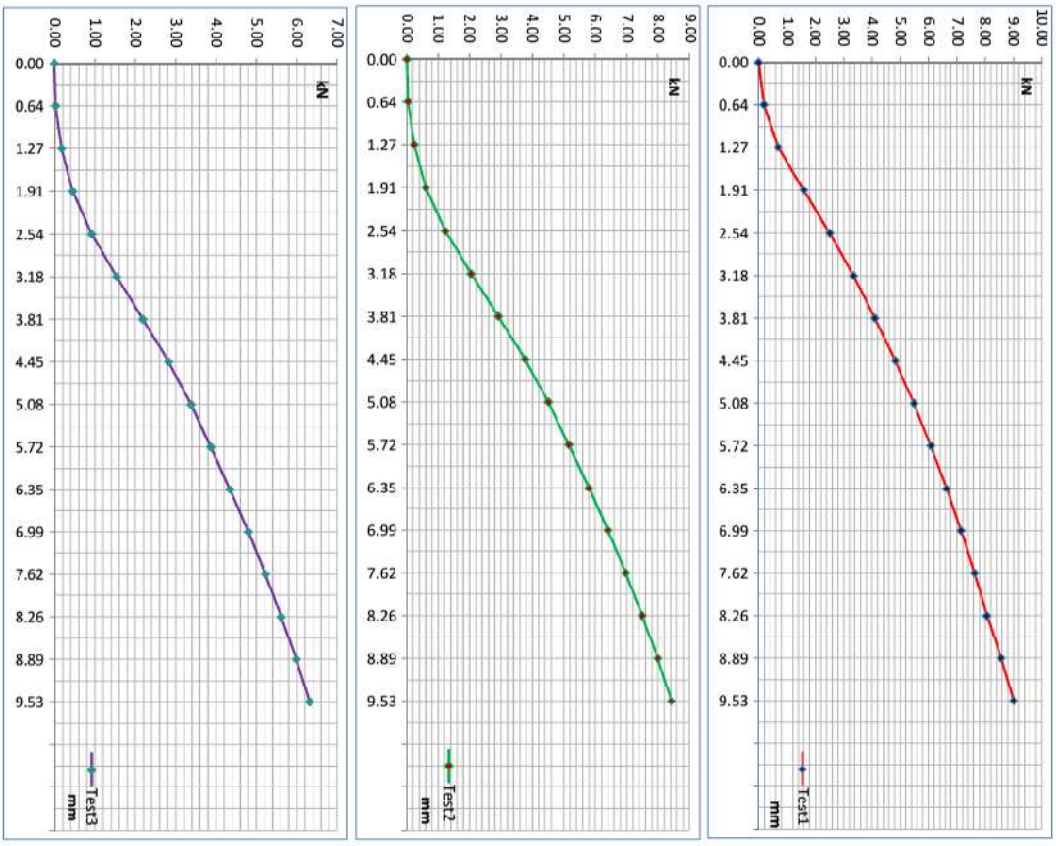

Appendix B 1: CBR UT1

UT2-CBR Test Results

Comp	1946	1956	1906	Client	
mm	Test 1	Test 2	Test 3	Reference	
0.00	0.00	0.00	0.00	Date Tested	01 Jul 2022
0.64	0.08	0.21	0.07		
1.27	0.51	0.81	0.46		
1.91	1.34	1.87	1.20		
2.54	2.39	2.95	2.15		
3.18	3.44	3.94	3.10		
3.81	4.37	4.83	3.93		
4.45	5.18	5.66	4.67		
5.08	5.89	6.46	5.30		
5.72	6.54	7.16	5.88		
6.35	7.16	7.81	6.45		
6.99	7.76	8.41	6.98		
7.62	8.26	8.96	7.43		
8.26	8.70	9.49	7.83		
8.89	9.12	10.08	8.21		
9.53	9.53	10.60	8.58		
CBR	17.9%	22.1%	16.1%	@ 2.54mm	
	29.4%	32.3%	26.5%	@ 5.08mm	
	32.6%	35.4%	29.3%	@ 7.62mm	

Appendix B 2: CBR UT2

CBR Test Results

Comp	1990	2001	1975	Client	
mm	Test 1	Test 2	Test 3	Reference	
0.00	0.00	0.00	0.00	Date Tested	01 Jul 2022
0.64	0.07	0.20	0.24		
1.27	0.41	0.82	0.93		
1.91	1.06	1.92	2.15		
2.54	2.15	3.94	3.39		
3.18	3.58	6.58	4.53		
3.81	5.11	8.89	5.55		
4.45	6.59	10.93	6.53		
5.08	7.89	12.70	7.43		
5.72	9.03	14.31	8.23		
6.35	10.15	15.88	8.98		
6.99	11.20	17.35	9.67		
7.62	12.19	18.61	10.33		
8.26	13.10	19.72	10.91		
8.89	13.98	20.77	11.59		
9.53	14.75	21.79	12.19		
CBR	16.1%	29.5%	25.4%	@ 2.54mm	
	39.4%	63.4%	37.1%	@ 5.08mm	
	48.1%	73.4%	40.7%	@ 7.62mm	

Appendix B 3: CBR UT3

0.7 NME CBR Test Results

Comp	1991	2017	1998	Client	
mm	Test 1	Test 2	Test 3	Reference	
0.00	0.00	0.00	0.00	Date Tested	07 Jun 2022
0.64	0.13	0.28	0.22		
1.27	0.87	1.64	1.34		
1.91	2.20	3.51	2.72		
2.54	4.03	6.34	4.41		
3.18	6.45	9.70	6.15		
3.81	9.01	13.02	7.80		
4.45	11.60	16.07	9.42		
5.08	13.98	18.73	10.86		
5.72	16.23	21.21	12.21		
6.35	18.35	23.41	13.48		
6.99	20.32	25.37	14.69		
7.62	22.16	27.22	15.80		
8.26	23.81	28.75	16.86		
8.89	25.31	30.29	17.88		
9.53	26.69	31.70	18.83		
CBR	30.2%	47.5%	33.1%	@ 2.54mm	
	69.8%	93.8%	54.2%	@ 5.08mm	
	87.4%	107.4%	62.3%	@ 7.62mm	

Appendix B 4: 0.7NME CBR

1.0NME -CBR Test Results

Comp	1952	1959	2057	Client	
mm	Test 1	Test 2	Test 3	Reference	
0.00	0.00	0.00	0.00	Date Tested	07 Jun 2022
0.64	0.32	0.23	0.27		
1.27	1.62	1.54	1.78		
1.91	3.23	2.97	3.42		
2.54	5.45	4.86	5.61		
3.18	8.11	7.46	8.61		
3.81	11.16	10.45	12.05		
4.45	14.35	13.93	16.07		
5.08	17.26	17.60	20.30		
5.72	19.97	21.19	24.44		
6.35	22.34	24.55	28.32		
6.99	24.48	27.54	31.77		
7.62	26.47	30.09	34.71		
8.26	28.25	32.36	37.33		
8.89	29.90	34.49	39.78		
9.53	31.43	36.34	41.92		
CBR	40.8%	36.4%	42.0%	@ 2.54mm	
	86.2%	87.9%	101.4%	@ 5.08mm	
	104.4%	118.7%	136.9%	@ 7.62mm	

91.9%
1990

Appendix B 5: 1.0NME CBR

1.2NME -CBR Test Results

Comp	2010	2032	2017	Client	
mm	Test 1	Test 2	Test 3	Reference	
0.00	0.00	0.00	0.00	Date Tested	10 Jun 2022
0.64	0.17	0.20	0.44		
1.27	1.04	0.70	3.14		
1.91	3.55	2.89	6.97		
2.54	6.86	5.61	11.26		
3.18	11.07	9.12	15.68		
3.81	15.66	13.56	19.76		
4.45	20.30	19.13	23.55		
5.08	24.44	24.57	26.75		
5.72	28.07	29.73	29.72		
6.35	31.31	34.20	32.41		
6.99	34.18	38.25	34.92		
7.62	36.74	41.90	37.35		
8.26	39.04	45.11	39.49		
8.89	41.15	48.17	41.48		
9.53	43.06	50.90	43.37		
CBR	51.4%	42.0%	84.4%	@ 2.54mm	
	122.1%	122.7%	133.6%	@ 5.08mm	
	144.9%	165.3%	147.3%	@ 7.62mm	

Appendix B 6: 1.2NME CBR

CBR Test Results

Comp	2033	2049	2026	Client	
mm	Test 1	Test 2	Test 3	Reference	
0.00	0.00	0.00	0.00	Date Tested	13 Jun 2022
0.64	0.43	0.27	0.81		
1.27	0.87	2.24	3.12		
1.91	2.54	4.52	7.74		
2.54	5.45	8.14	11.79		
3.18	9.05	12.95	15.94		
3.81	13.29	18.38	18.84		
4.45	18.16	24.10	21.41		
5.08	22.84	29.37	23.83		
5.72	27.13	34.15	26.13		
6.35	30.85	38.40	28.18		
6.99	33.97	42.00	30.16		
7.62	36.75	45.31	31.73		
8.26	39.17	48.07	33.46		
8.89	41.50	50.60	35.20		
9.53	43.58	52.98	36.71		
CBR	40.8%	61.0%	88.4%	@ 2.54mm	
	114.1%	146.7%	119.0%	@ 5.08mm	
	145.0%	178.7%	125.2%	@ 7.62mm	

Appendix B 7: 1.5NME CBR

Appendix C – UCS Results

UCS Test Results					
Comp %	1990	1998	1996	Client	
Maximum kN	Test 1	Test 2	Test 3	Reference	
	30.05	34.09	32.71	Date	04 Jul 2022

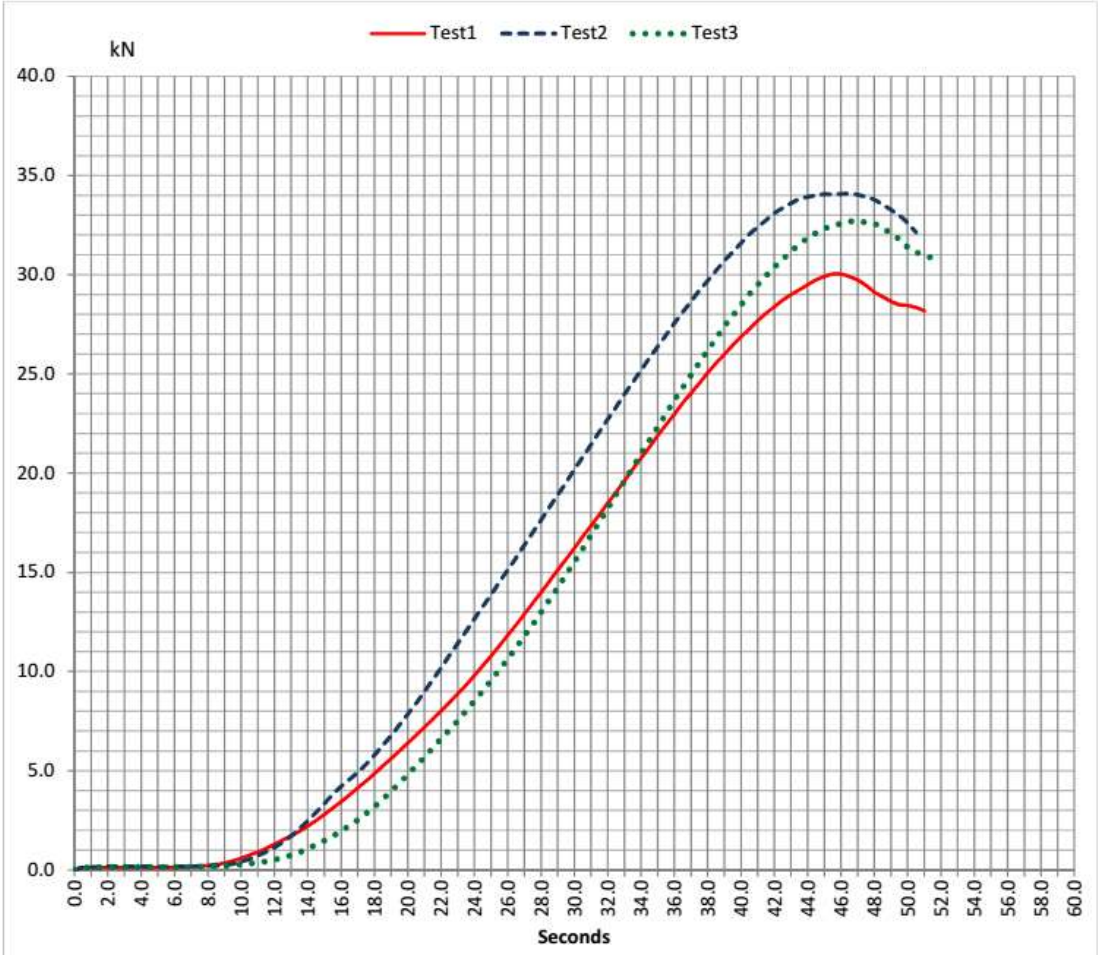

Appendix C 1: UCS UT

UCS Test Results					
Comp	1978	1994	1982	Client	
Maximum kN	Test 1	Test 2	Test 3	Reference	
	41.47	47.75	42.52	Date	22 Jun 2022

Appendix C 2: 0.7NME UCS D

UCS Test Results					
Comp	1978	2001	1988	Client	
Maximum kN	Test 1	Test 2	Test 3	Reference	
	10.25	19.33	15.32	Date	22 Jun 2022

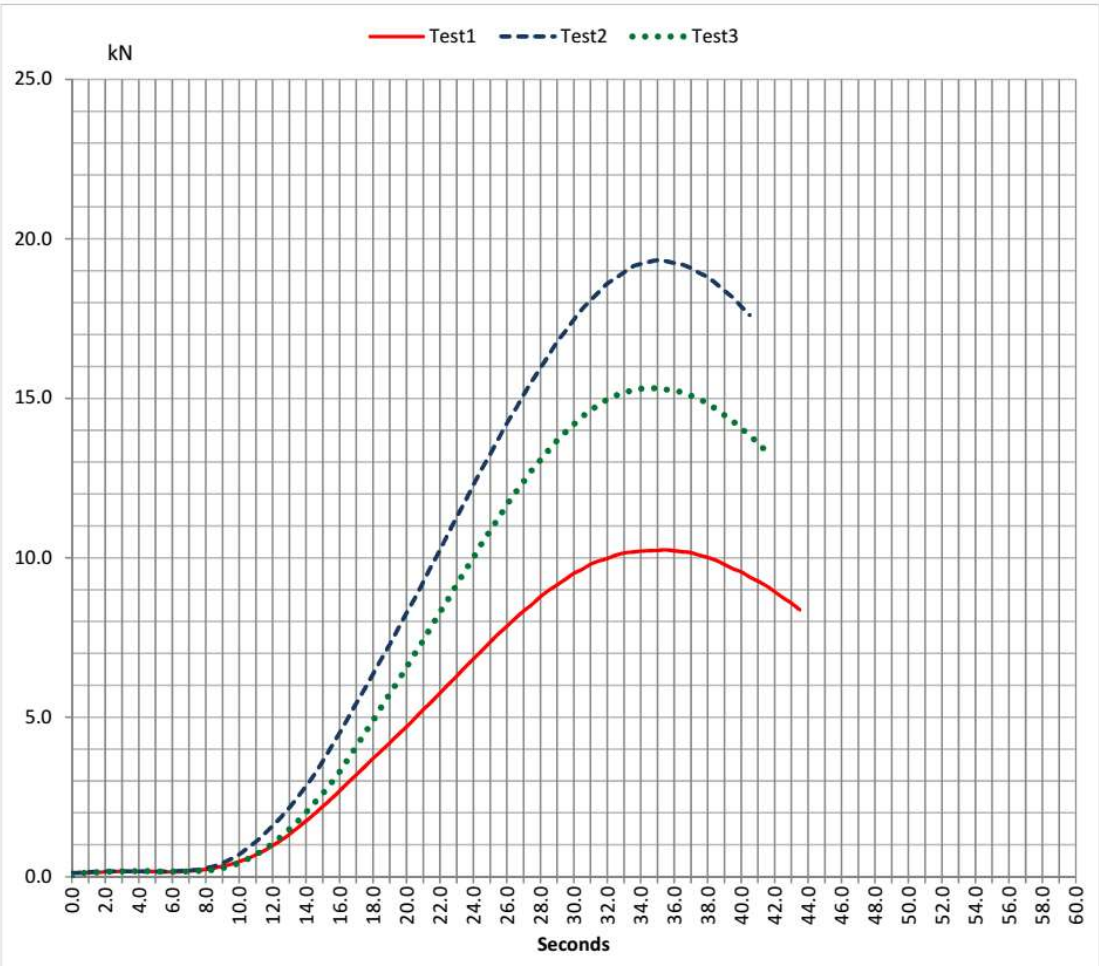

Appendix C 3: 0.7NME UCS W

UCS Test Results					
Comp	1987	1994	2008	Client	
Maximum kN	Test 1	Test 2	Test 3	Reference	
	42.63	43.44	48.19	Date	27 Jun 2022

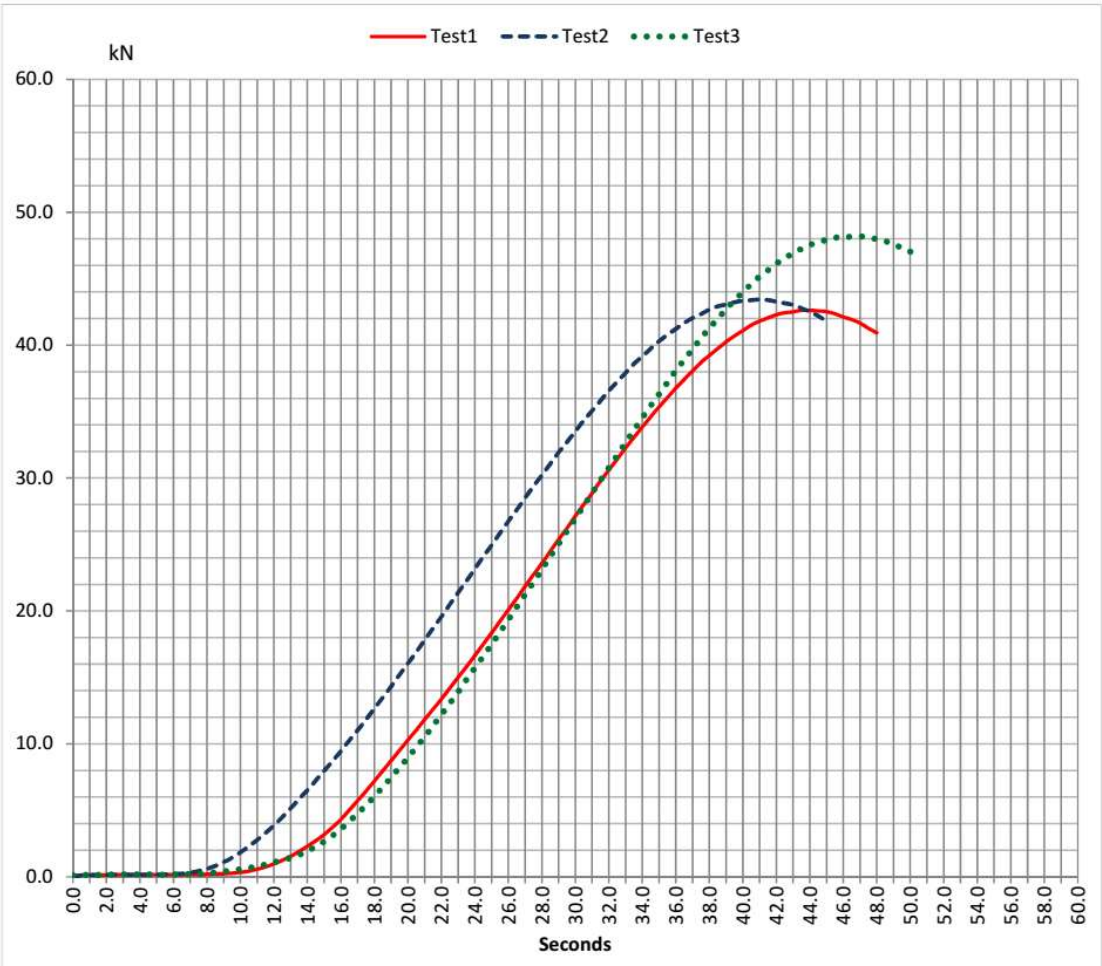

Appendix C 4: 1.0NME UCS D

UCS Test Results					
Comp	1991	1995	1992	Client	
Maximum kN	Test 1	Test 2	Test 3	Reference	
	29.66	30.75	29.86	Date	27 Jun 2022

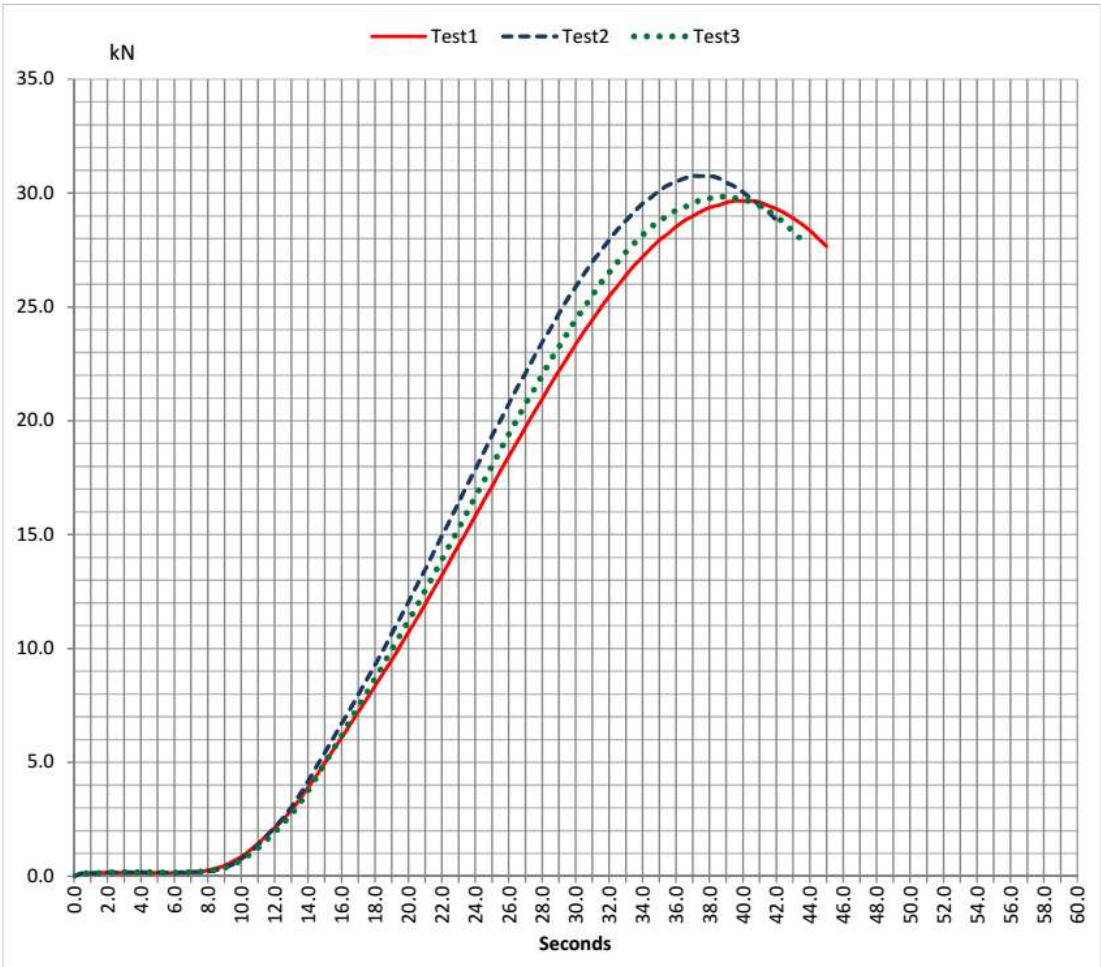

Appendix C 5: 1.0NME UCS W

UCS Test Results					
Comp	1997	1997	2002	Client	
Maximum kN	Test 1	Test 2	Test 3	Reference	
	41.77	42.37	48.17	Date	29 Jun 2022

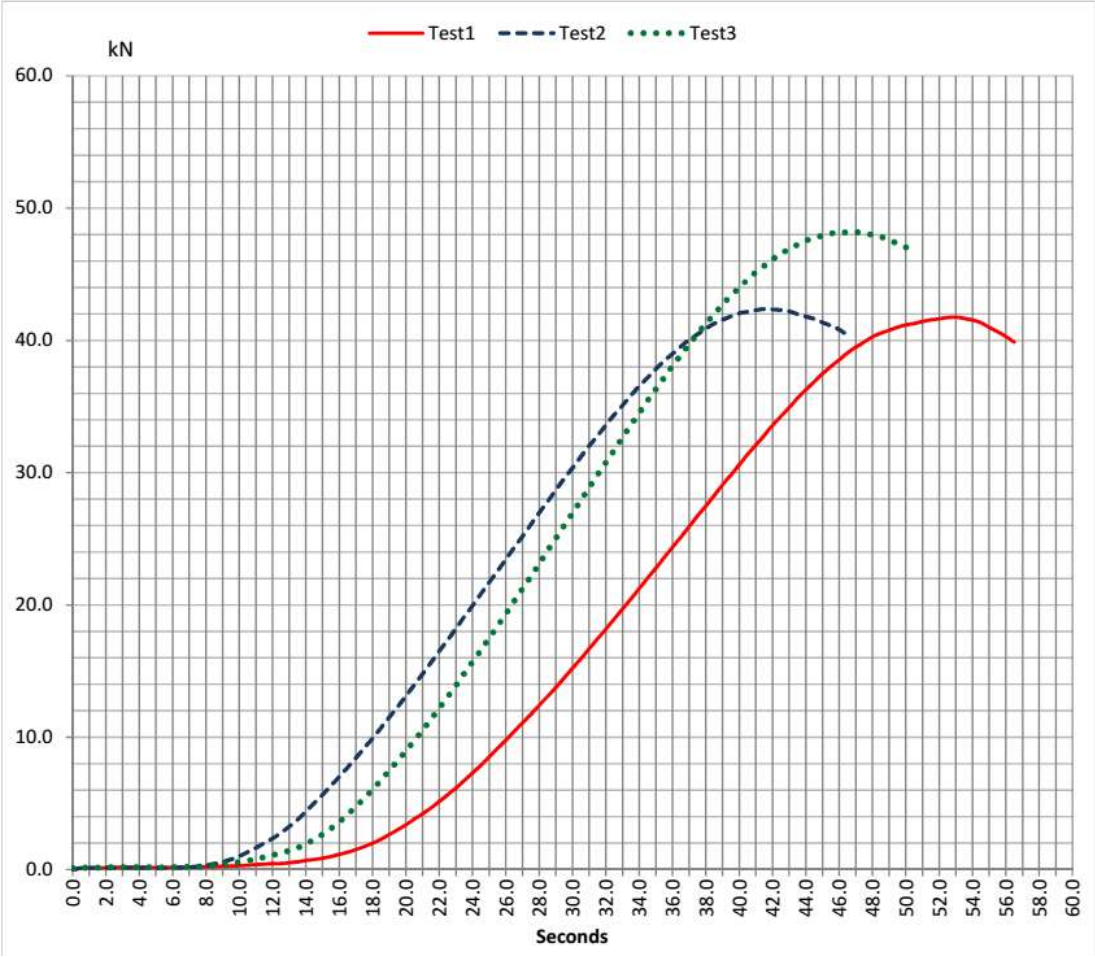

Appendix C 6: 1.2NME UCS D

UCS Test Results					
Comp	2009	2008	2013	Client	
Maximum kN	Test 1	Test 2	Test 3	Reference	
	26.04	32.91	38.06	Date	29 Jun 2022

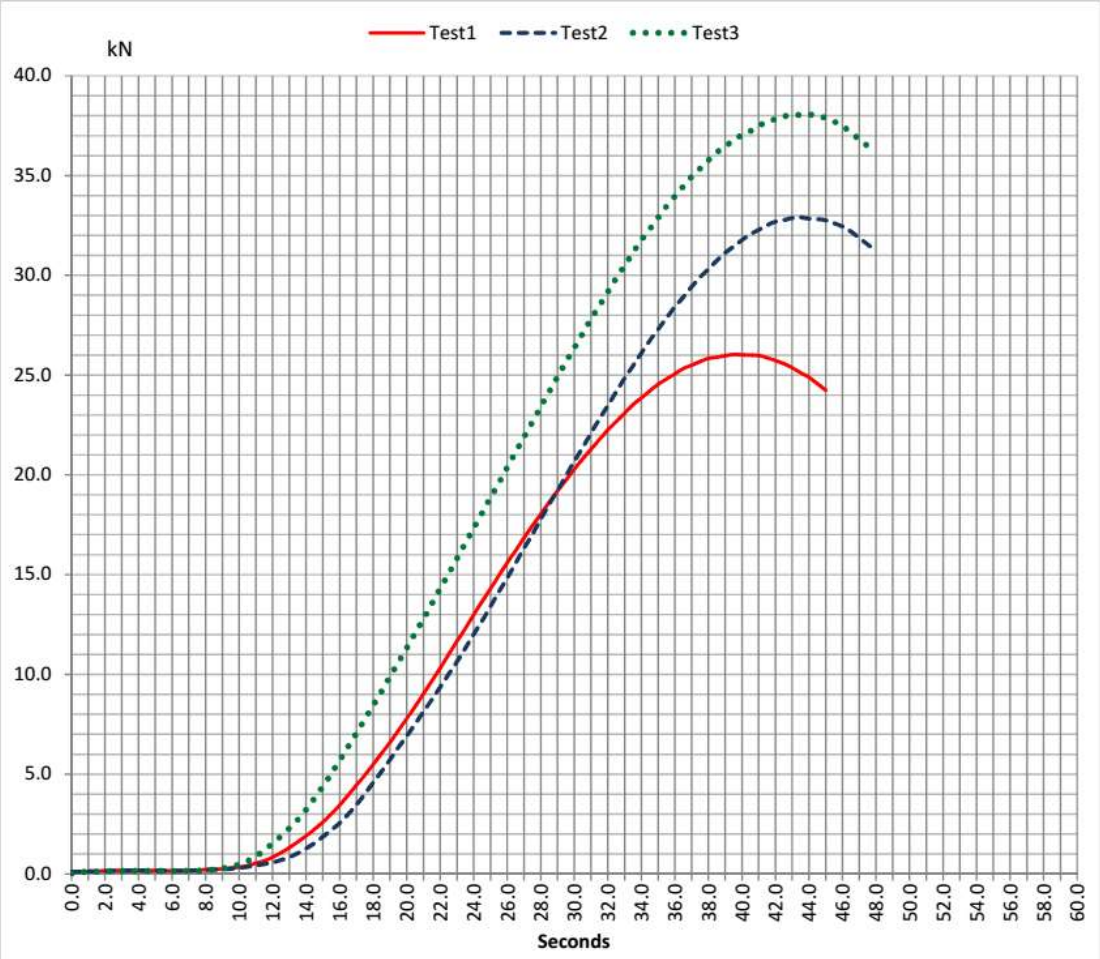

Appendix C 7: 1.2NME UCS W

UCS Test Results					
Comp	2005	1999	1997	Client	
Maximum kN	Test 1	Test 2	Test 3	Reference	
	48.39	48.69	42.72	Date	5 October 2022

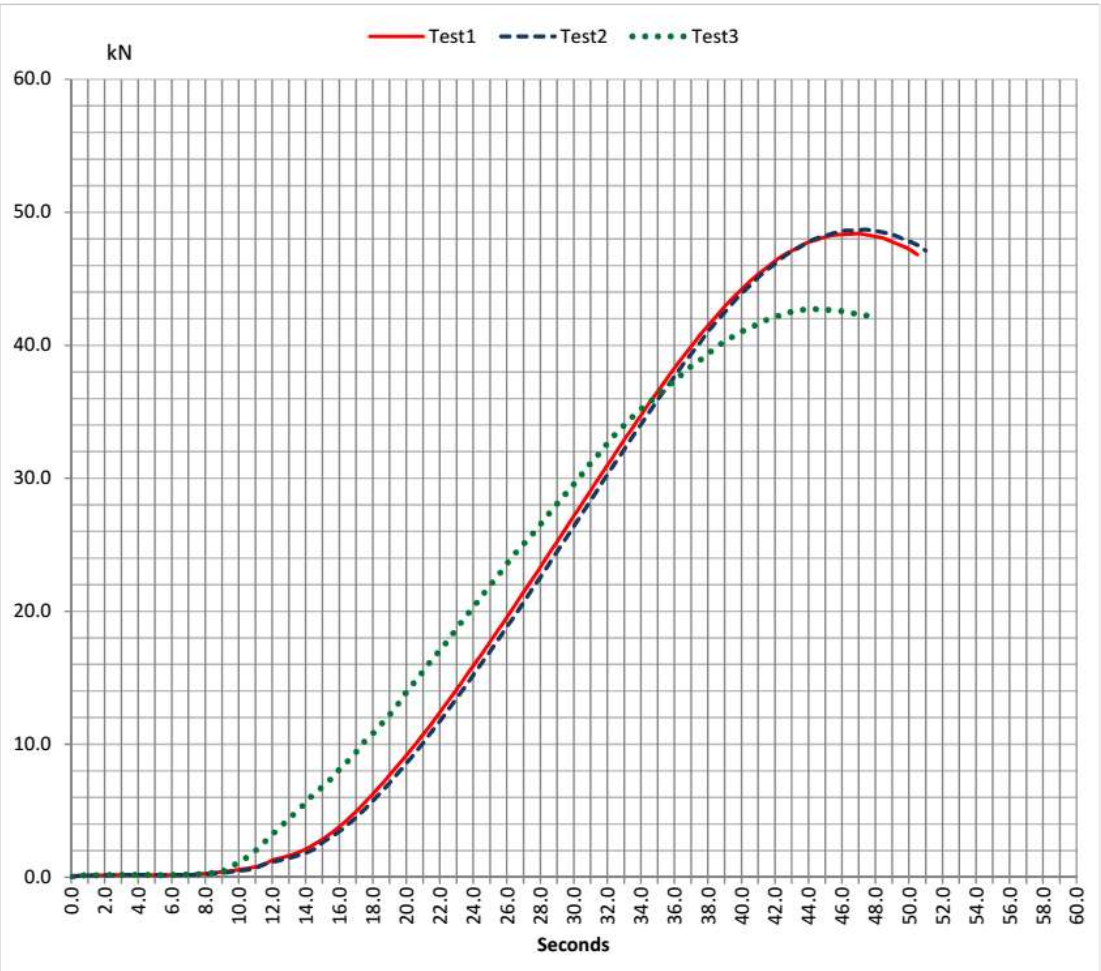

Appendix C 8: 1.5NME UCS D

UCS Test Results					
Comp	1989	1996	2002	Client	
Maximum kN	Test 1	Test 2	Test 3	Reference	
	32.64	35.7	40.7	Date	5 October 2022

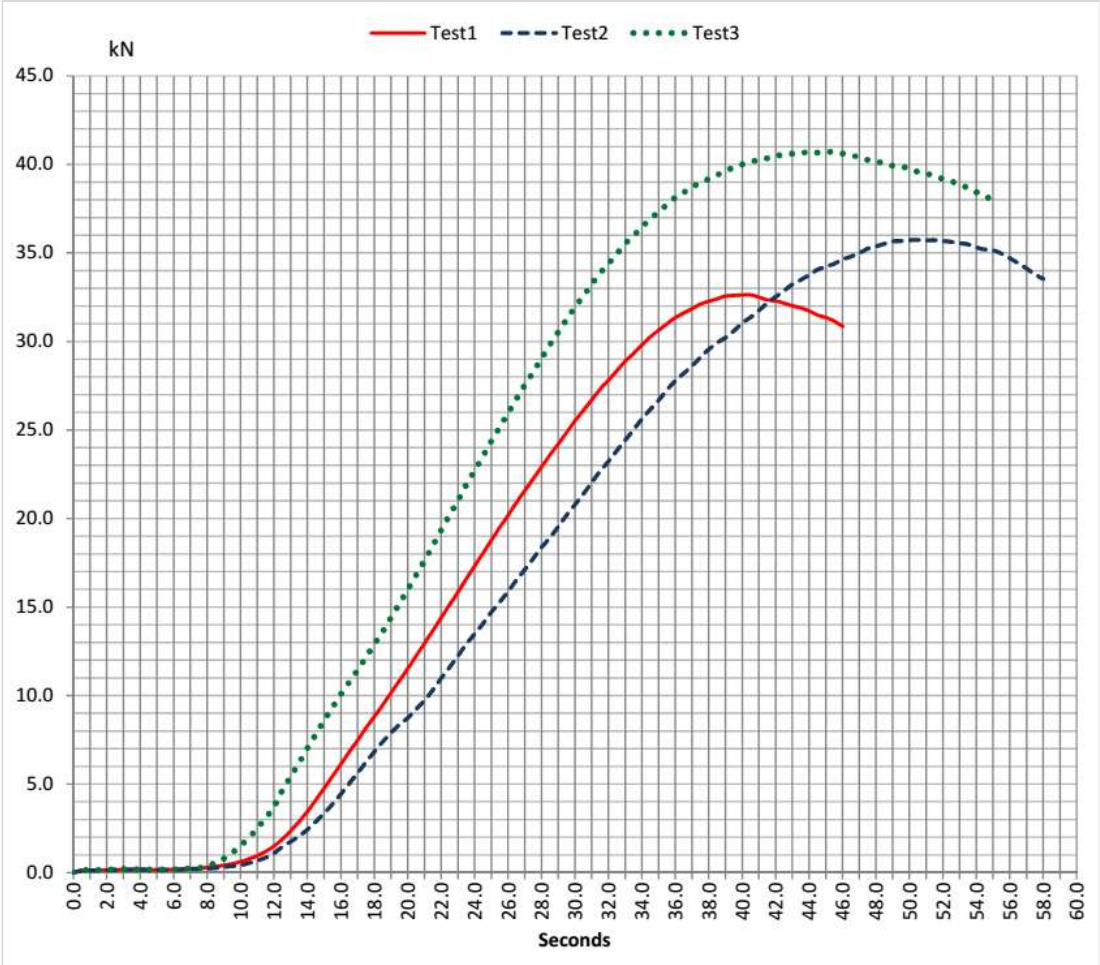

Appendix C 9: 1.5NME UCS W

Appendix D – ITS Results

ITS Test Results					
Comp %	1995	2002	2011	Client	
Maximum kN	Test 1	Test 2	Test 3	Reference	
	3.77	3.78	3.99	Date	04 Jul 2022

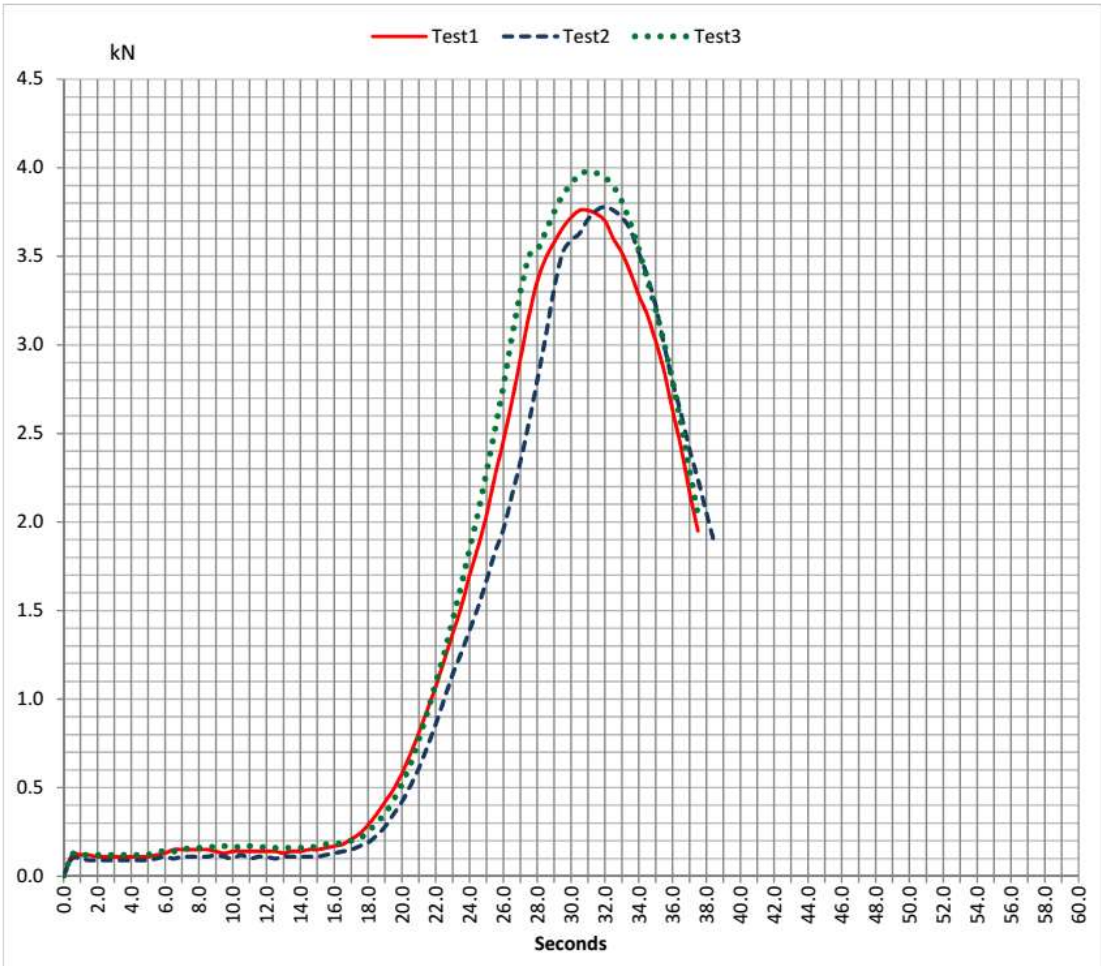

Appendix D 1: ITS UT

ITS Test Results					
Comp	1984	2011	2004	Client	
Maximum kN	Test 1	Test 2	Test 3	Reference	
	4.15	4.77	4.25	Date	22 Jun 2022

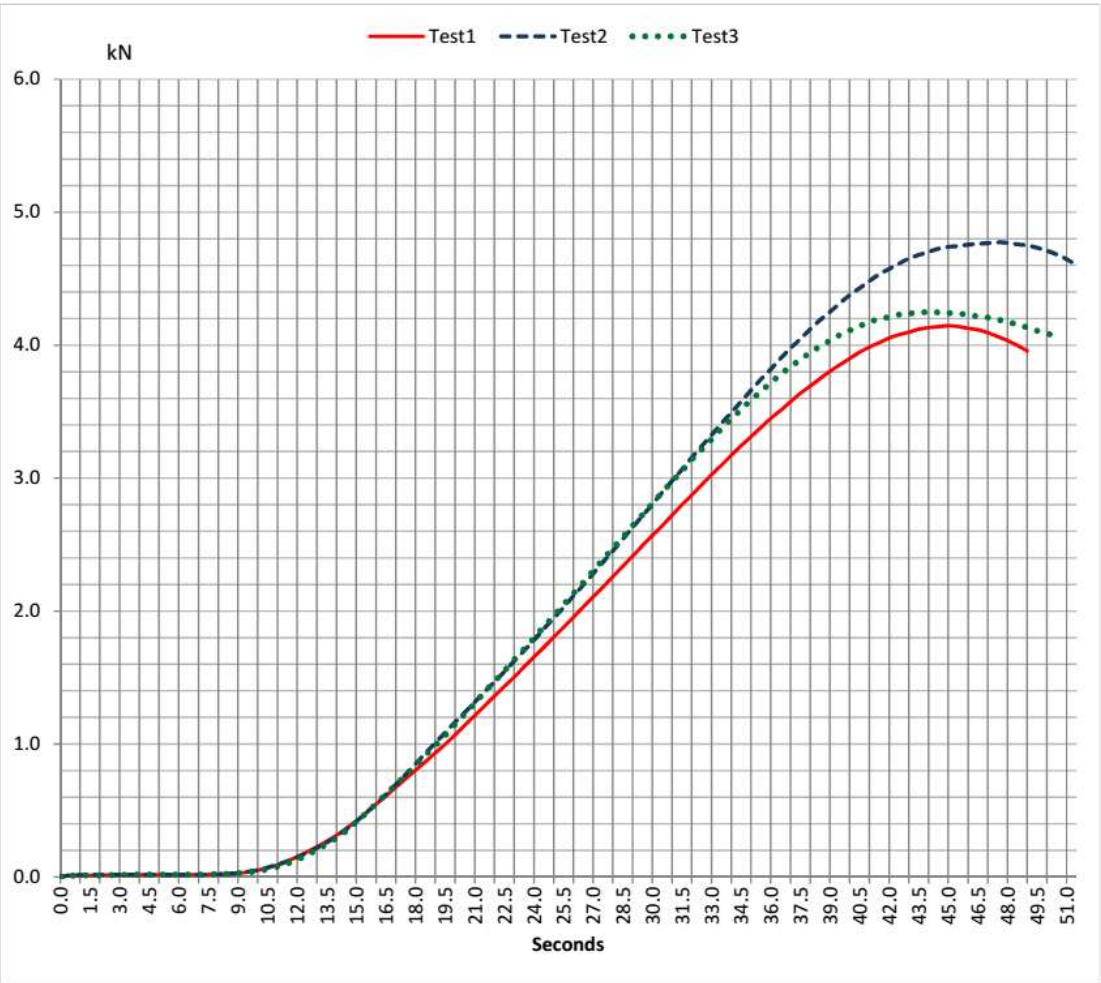

Appendix D 2: 0.7NME ITS D

ITS Test Results					
Comp	1999	2014	2000	Client	
Maximum kN	Test 1	Test 2	Test 3	Reference	
	2.34	2.75	2.07	Date	22 Jun 2022

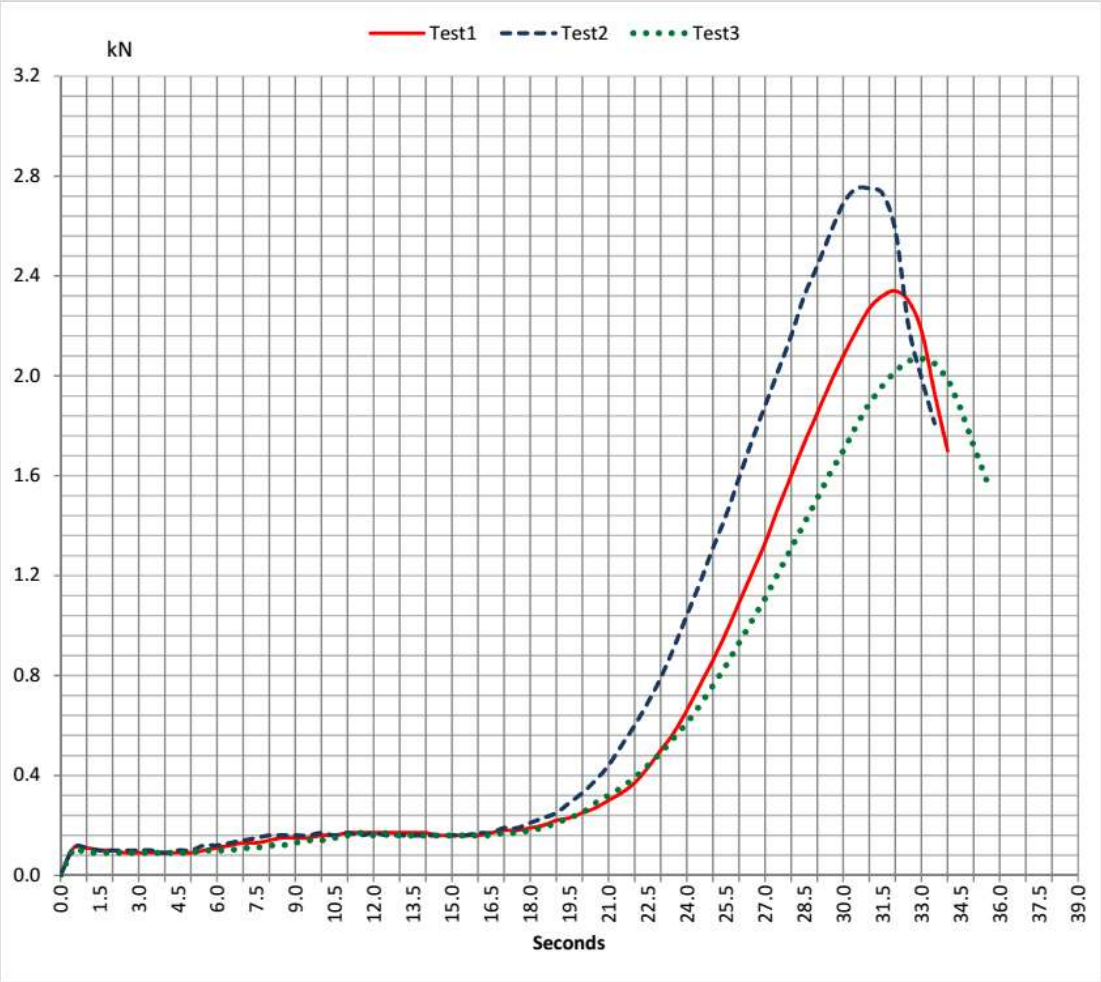

Appendix D 3: 0.7NME ITS W

ITS Test Results					
Comp	2003	2021	1986	Client	
Maximum kN	Test 1	Test 2	Test 3	Reference	
	4.62	4.72	3.6	Date	27 Jun 2022

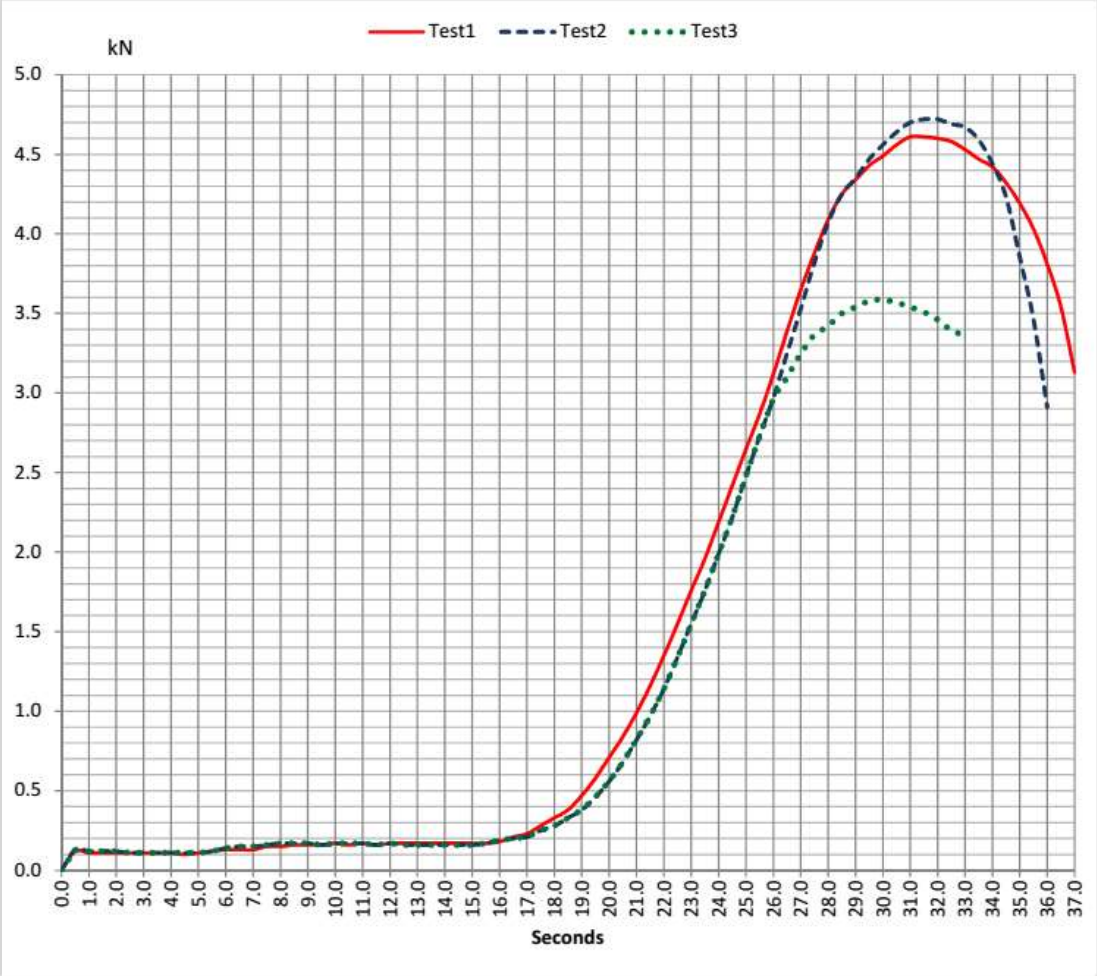

Appendix D 4: 1.0NME ITS D

ITS Test Results					
Comp %	1986	1997	1991	Client	
Maximum kN	Test 1	Test 2	Test 3	Reference	
	3.33	3.51	3.51	Date	27 Jun 2022

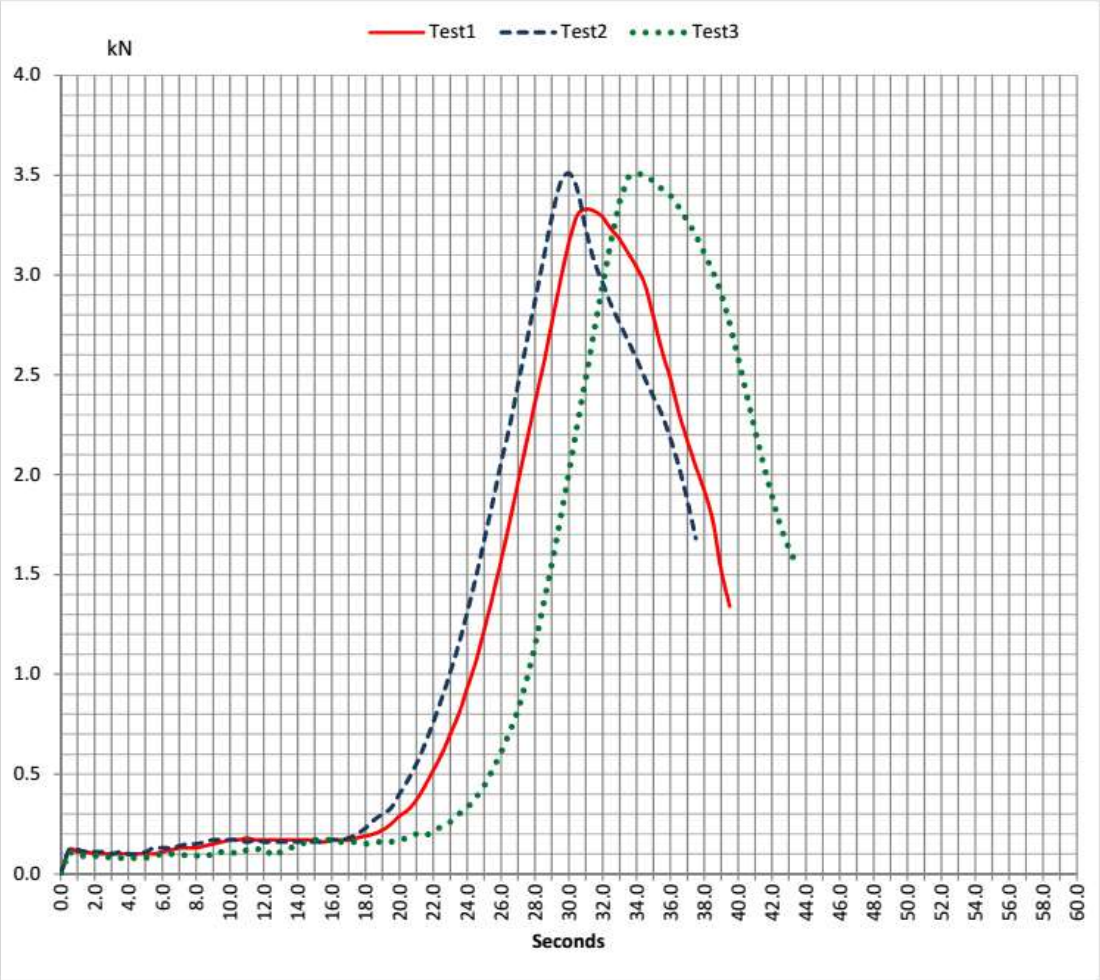

Appendix D 5: 1.0NME ITS W

ITS Test Results					
Comp	2013	2000	2025	Client	
Maximum kN	Test 1	Test 2	Test 3	Reference	
	4.52	4.39	4.73	Date	29 Jun 2022

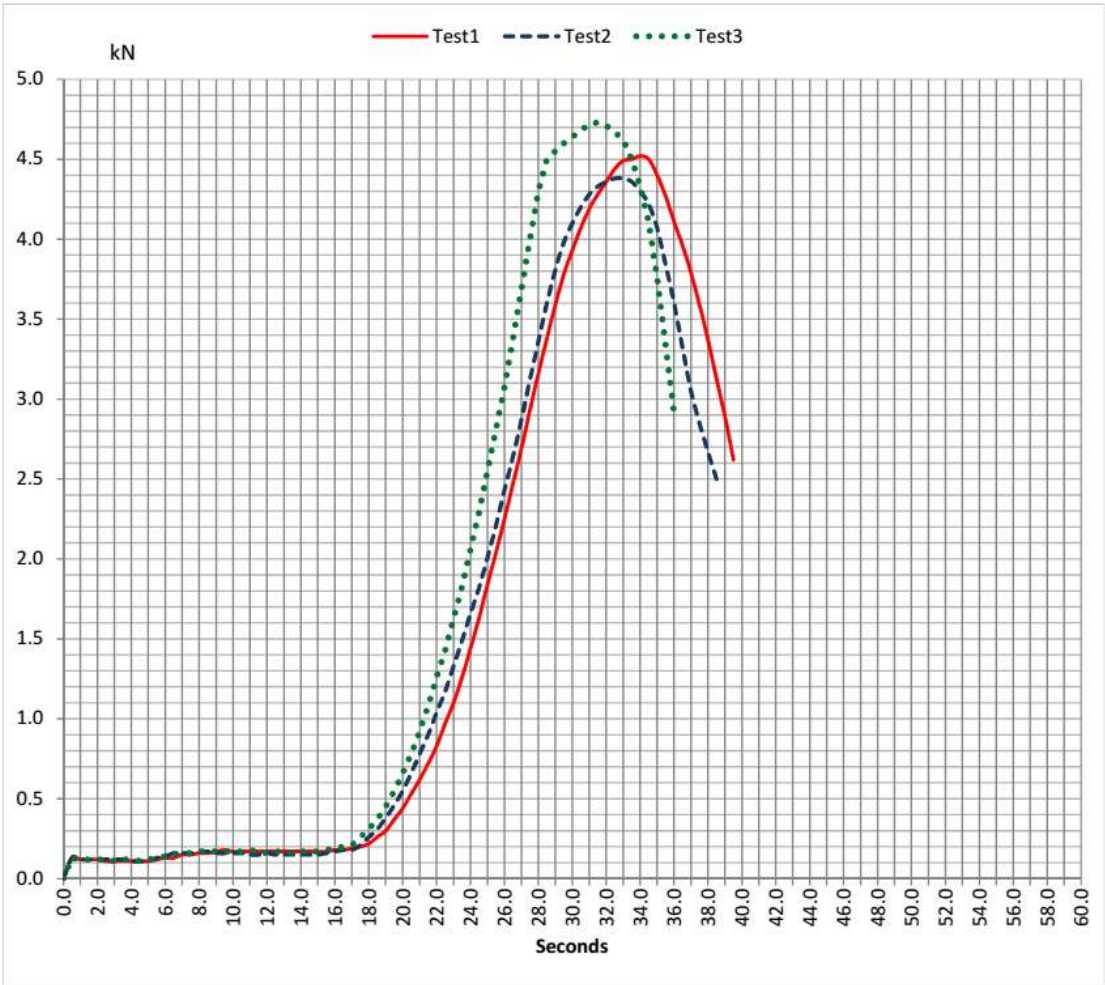

Appendix D 6: 1.2NME ITS D

ITS Test Results					
Comp %	2012	1986	2018	Client	
Maximum kN	Test 1	Test 2	Test 3	Reference	
	4.79	3.45	4.99	Date	29 Jun 2022

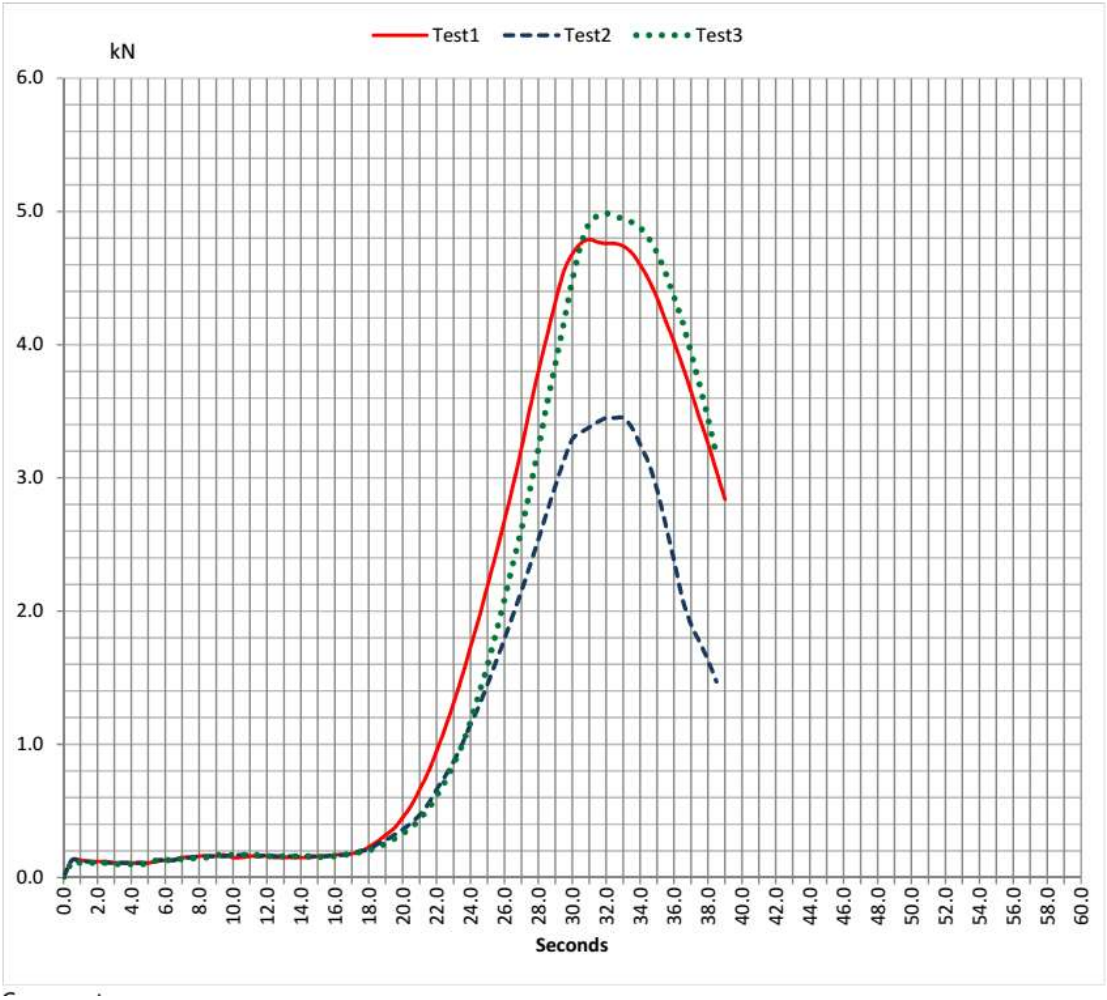

Appendix D 7: 1.2NME ITS W

ITS Test Results					
Comp	2005	2001	2016	Client	
Maximum kN	Test 1	Test 2	Test 3	Reference	
	4.25	4.59	4.93	Date	29 Jun 2022

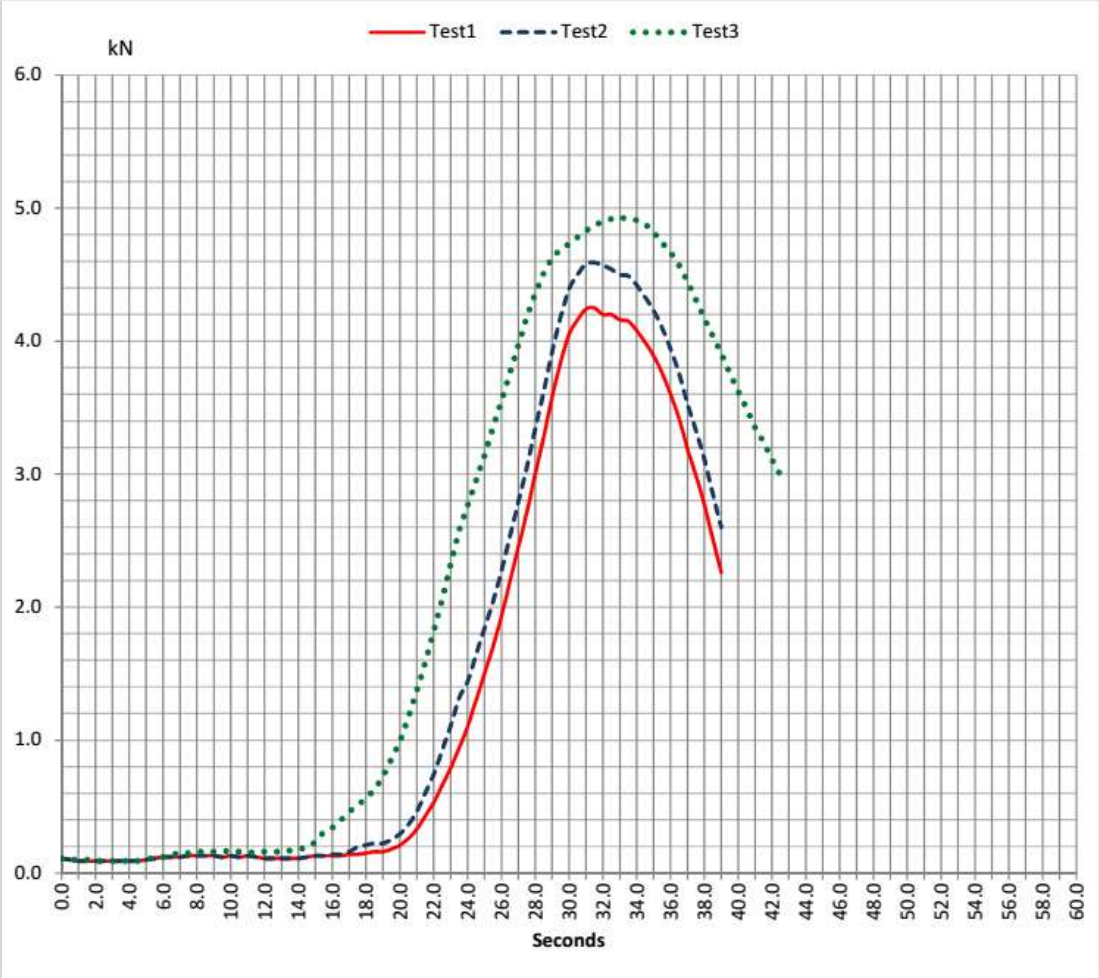

Appendix D 8: 1.5NME ITS D

ITS Test Results					
Comp	1995	2031	2004	Client	
Maximum kN	Test 1	Test 2	Test 3	Reference	
	4.47	4.57	4.36	Date	29 Jun 2022

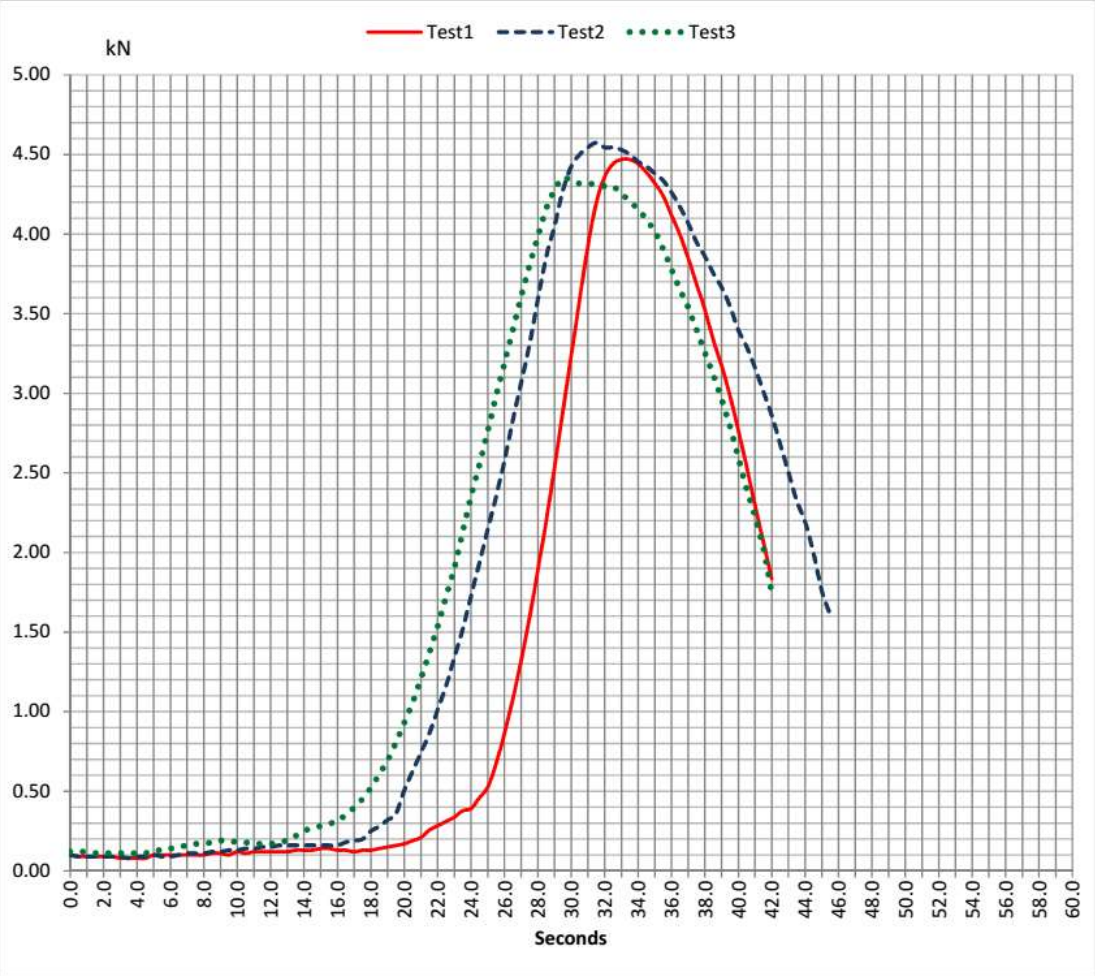

Appendix D 9: 1.5NME ITS W

Appendix E – Moisture Conditioning

12hrs - UCS Test Results					
Comp	1988	1996	2005	Client	
Maximum kN	Test 1	Test 2	Test 3	Reference	
	33.97	32.50	35.09	Date	01 Aug 2022

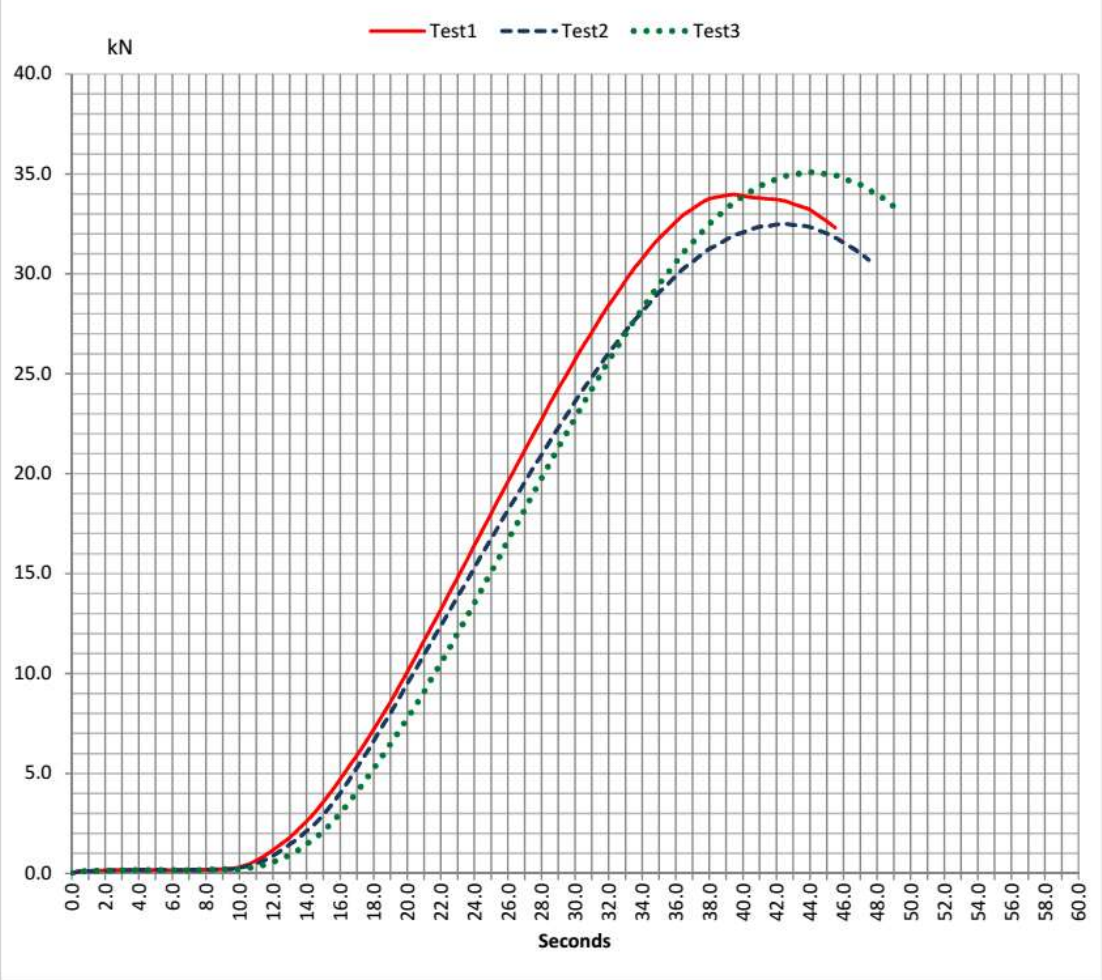

Appendix E 1: UCS – 12 hrs

24hrs - UCS Test Results					
Comp	2007	2006	1993	Client	
Maximum kN	Test 1	Test 2	Test 3	Reference	
	31.94	30.92	27.51	Date	01 Aug 2022

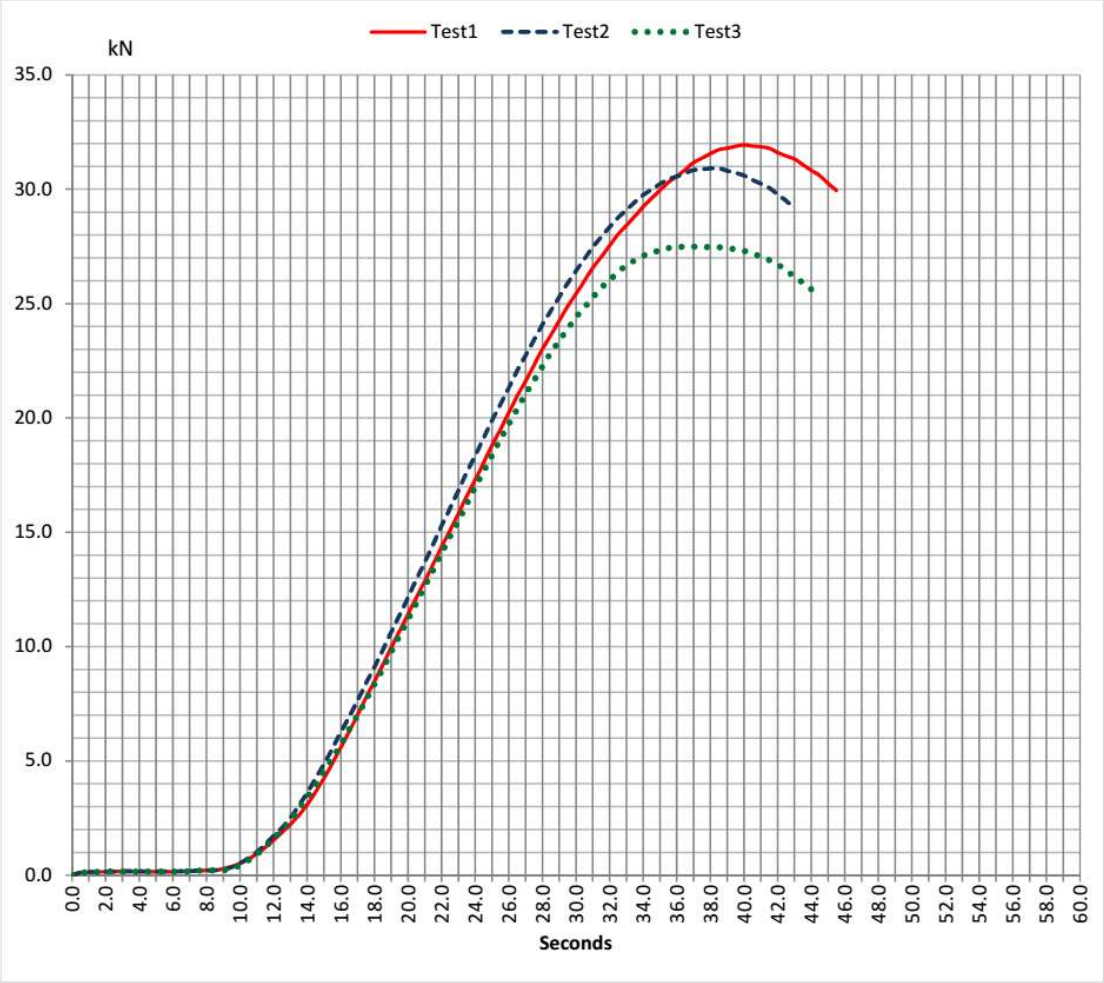

Appendix E 2: UCS – 24 hrs

12hrs -ITS Test Results					
Comp	2011	2001	1989	Client	
Maximum kN	Test 1	Test 2	Test 3	Reference	
	3.80	3.53	3.44	Date	01 Aug 2022

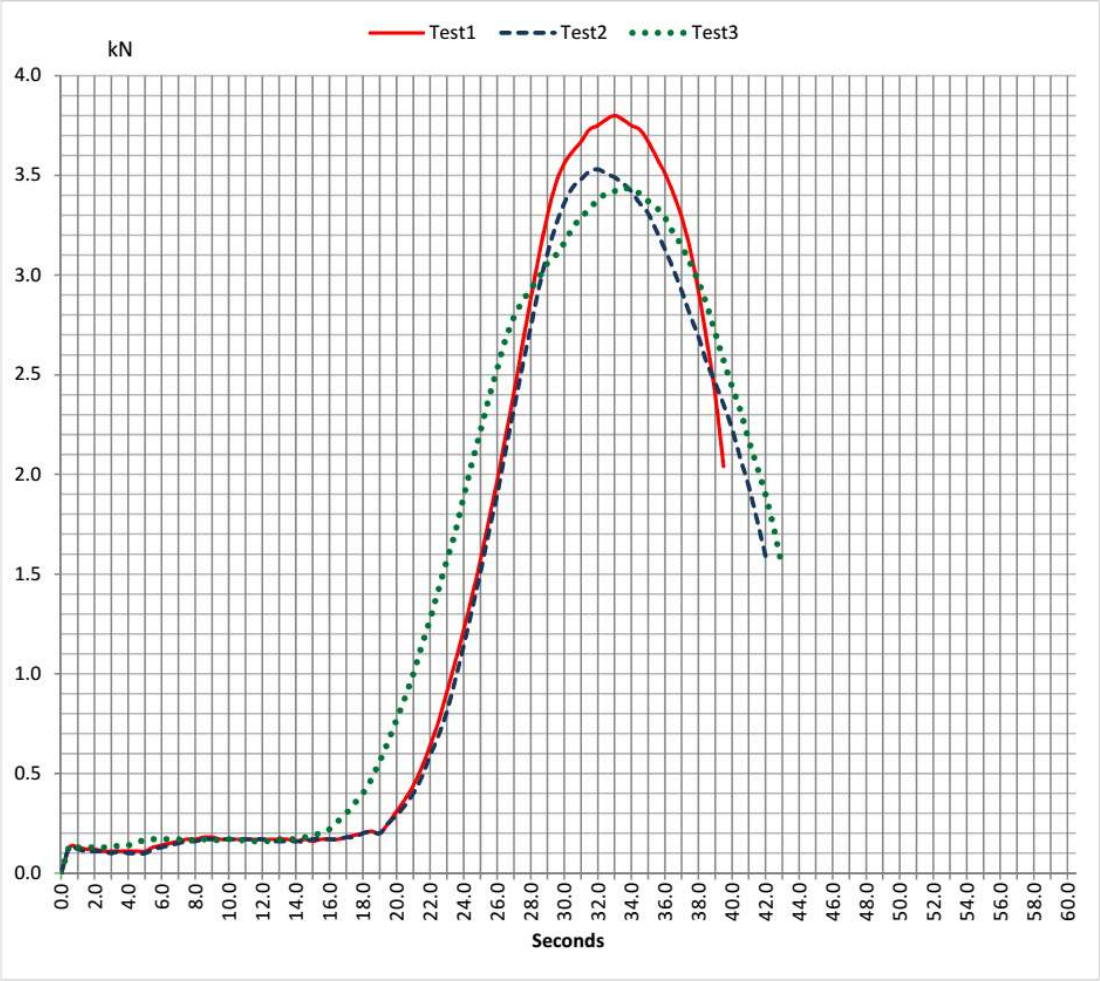

Appendix E 3: ITS – 12 hrs

24hrs - ITS Test Results					
Comp	1991	1997	2003	Client	
Maximum kN	Test 1	Test 2	Test 3	Reference	
	3.73	3.84	3.74	Date	01 Aug 2022

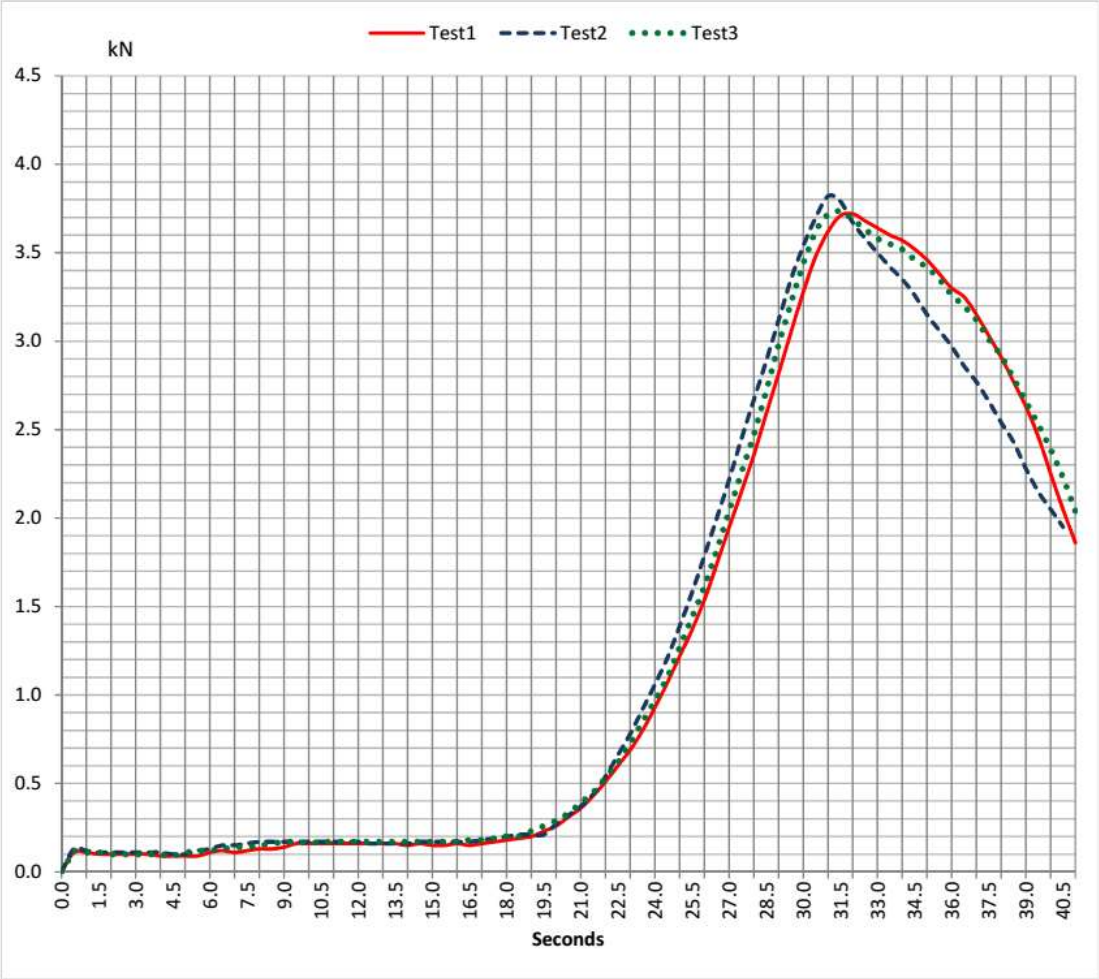

Appendix E 4: ITS – 24 hrs

Appendix F – CBE Results

ITS Test Results					
Comp	2016	2009	2001	Client	
Maximum kN	Test 1	Test 2	Test 3	Reference	
	2.53	3.41	3.17	Date	15 Aug 2022

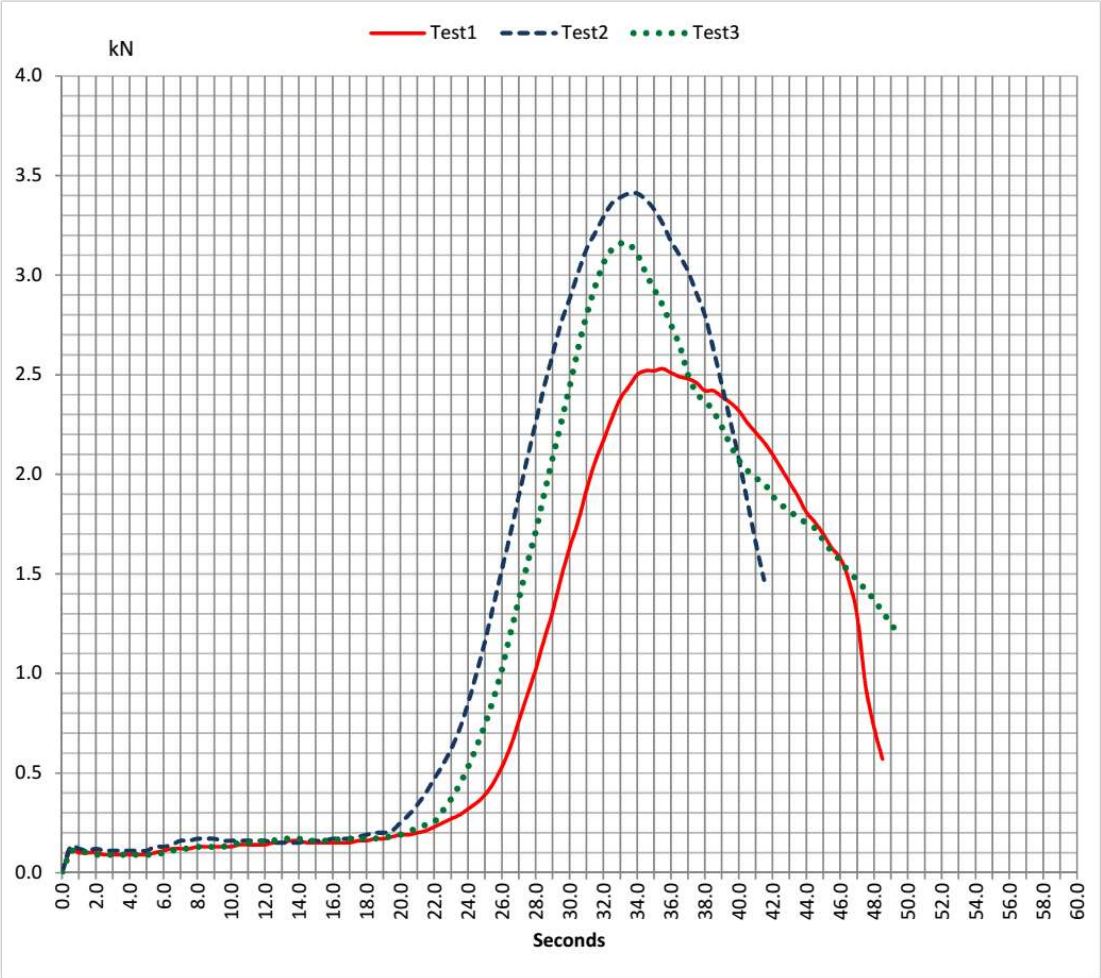

Appendix F 1: ITS – CBE

UCS Test Results					
Comp	2000	1986	1993	Client	
Maximum kN	Test 1	Test 2	Test 3	Reference	
	38.76	36.08	38.15	Date	15 Aug 2022

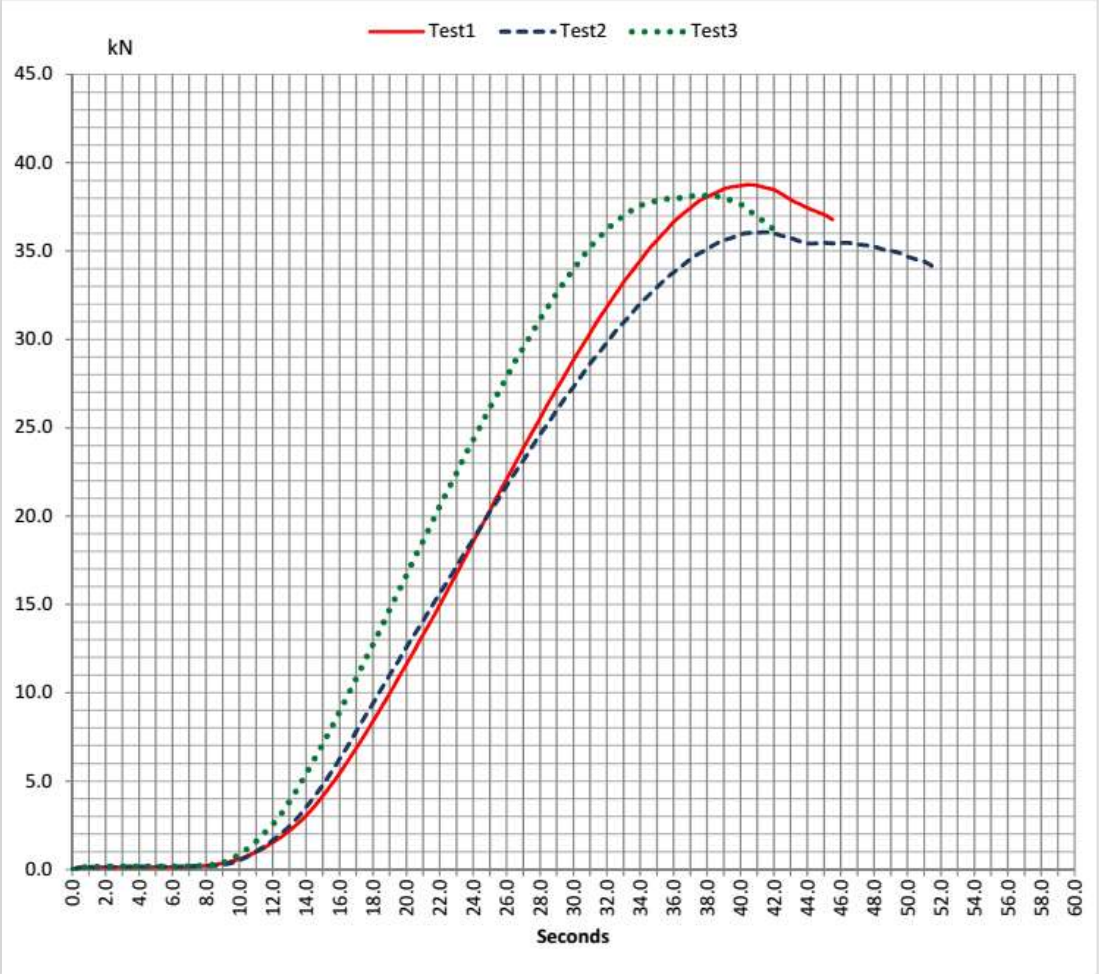

Appendix F 2: UCS – CBE

UCSwet Test Results					
Comp	1997	1986	2004	Client	
Maximum kN	Test 1	Test 2	Test 3	Reference	
	16.99	16.26	10.06	Date	15 Aug 2022

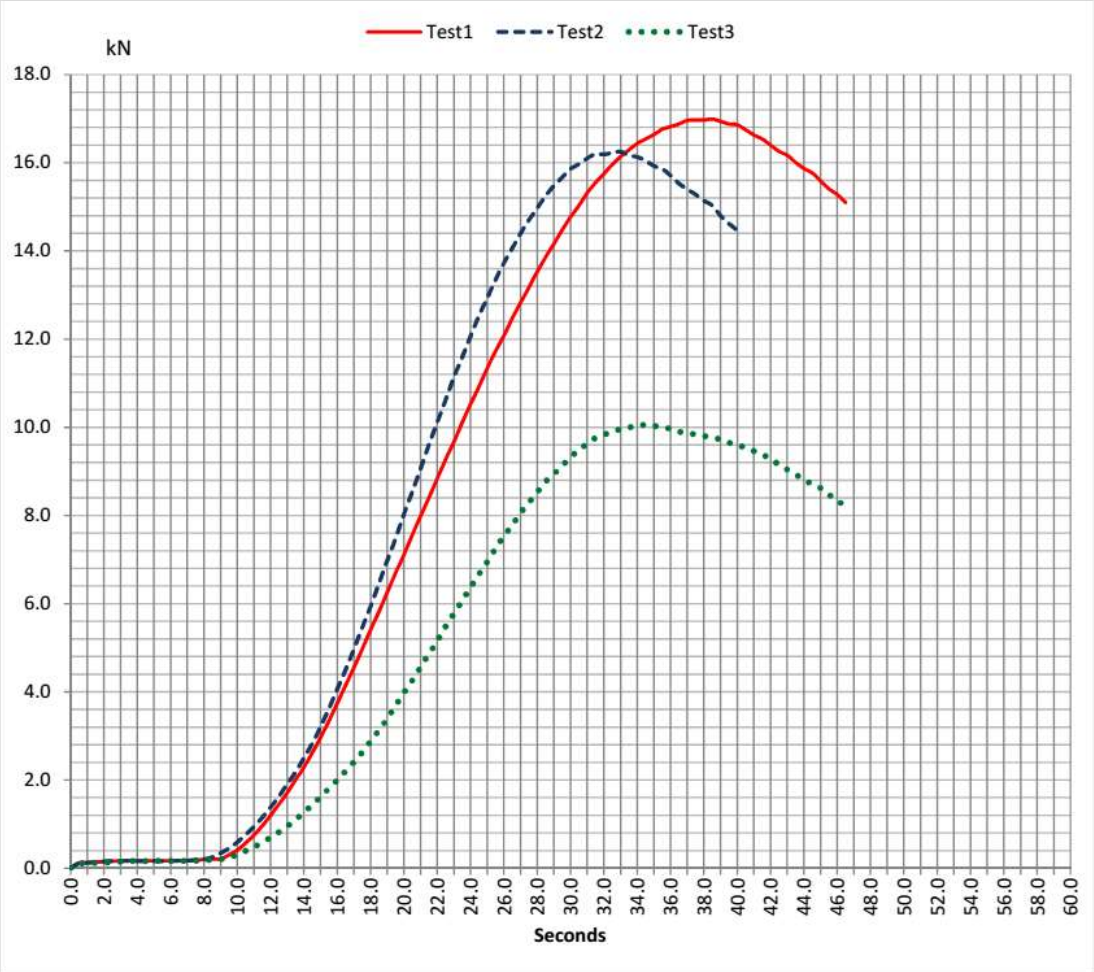

Appendix F 3: UCS – CBE_W

Appendix G – Shear Strength Results

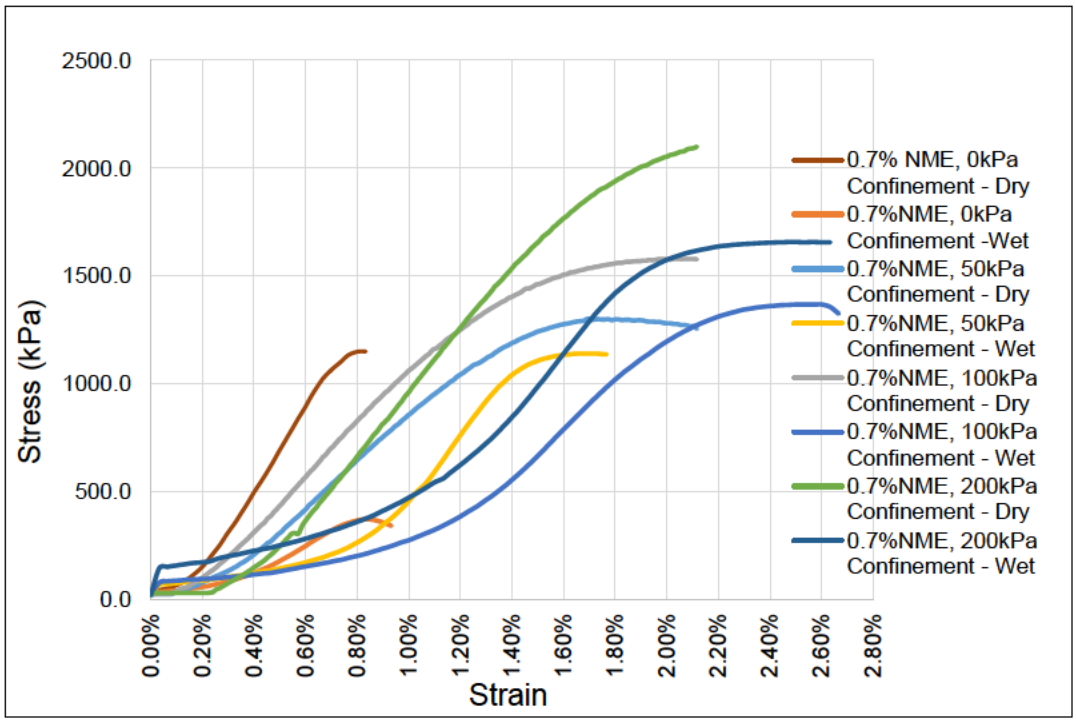

Appendix G1: Stress-strain diagram (0.7% NME)

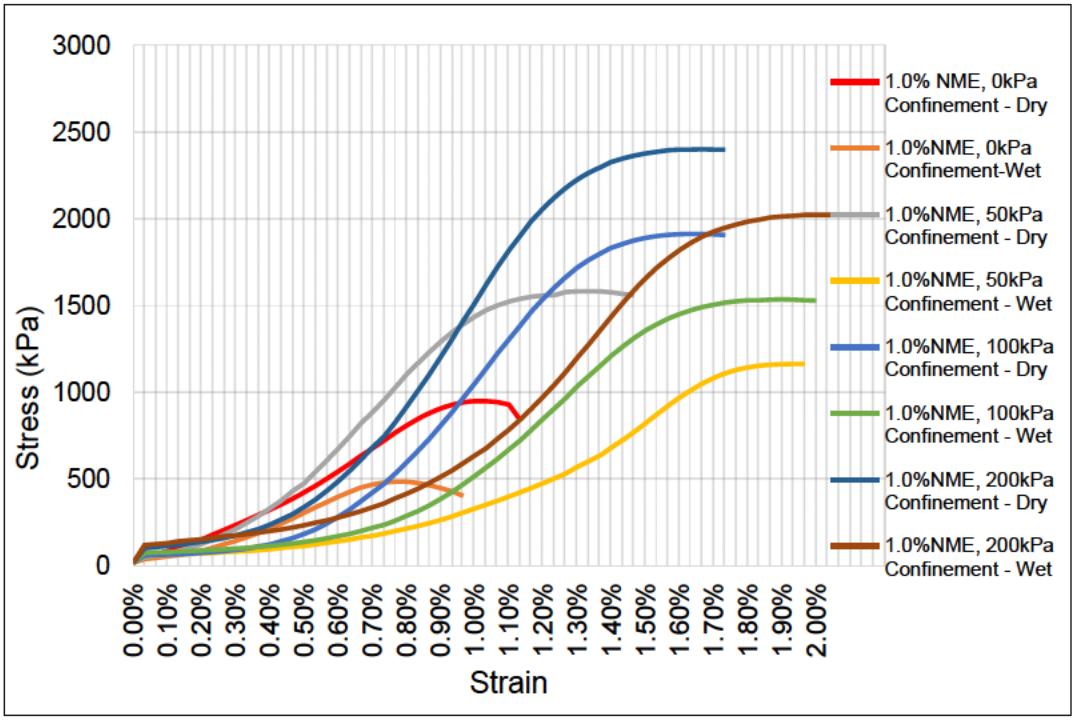

Appendix G 2: Stress-strain diagram (1.0% NME)

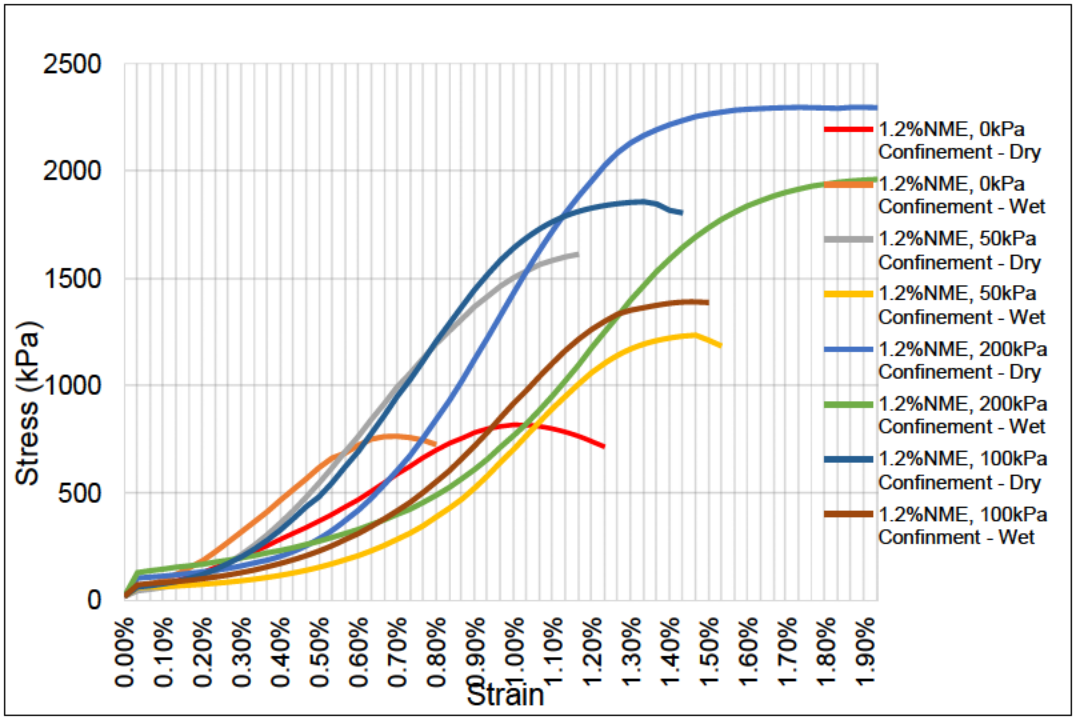

Appendix G 3: Stress-strain diagram (1.2% NME)

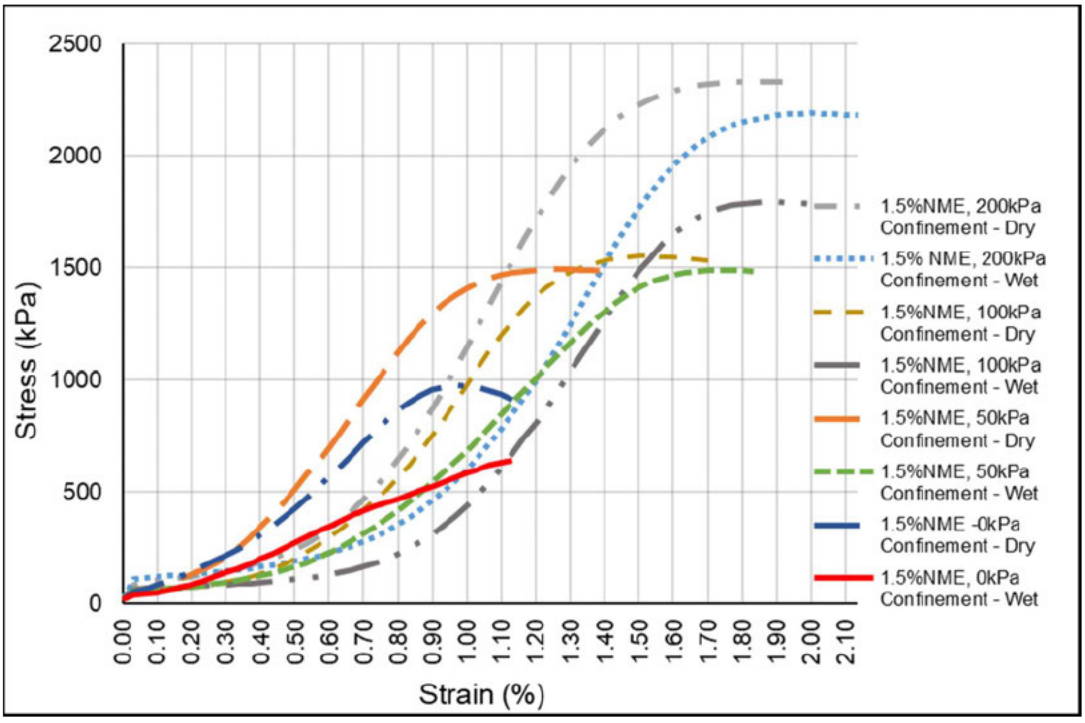

Appendix G 4: Stress-strain diagram (1.5% NME)

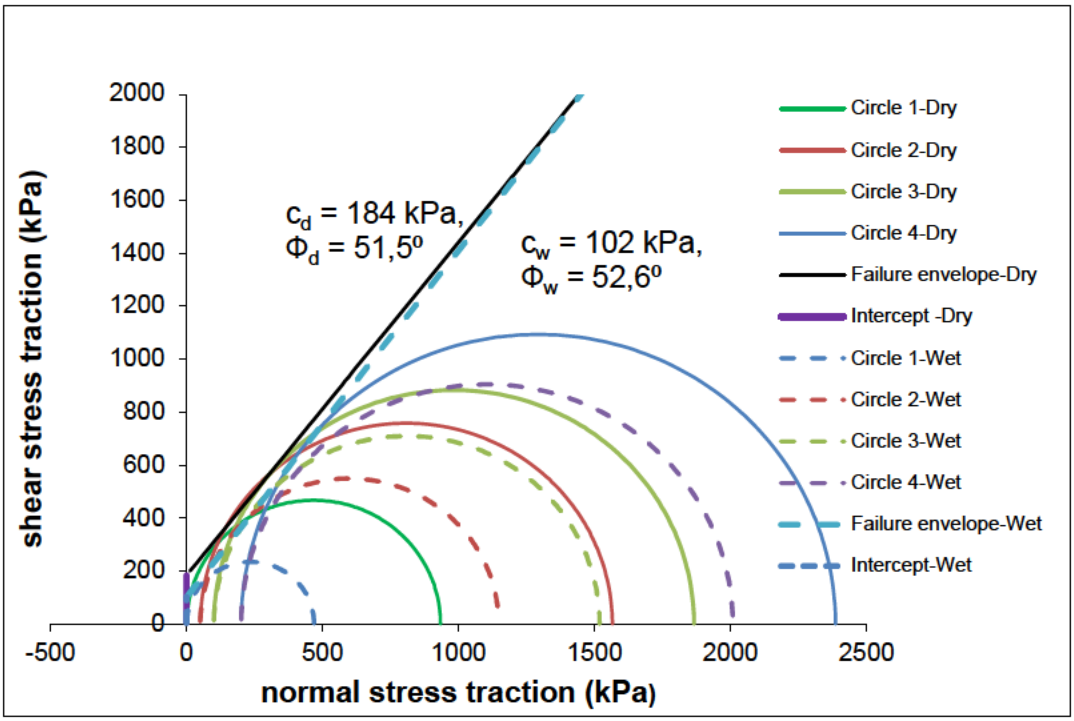

Appendix G 5: Shear Strength Properties – 1.0%NME

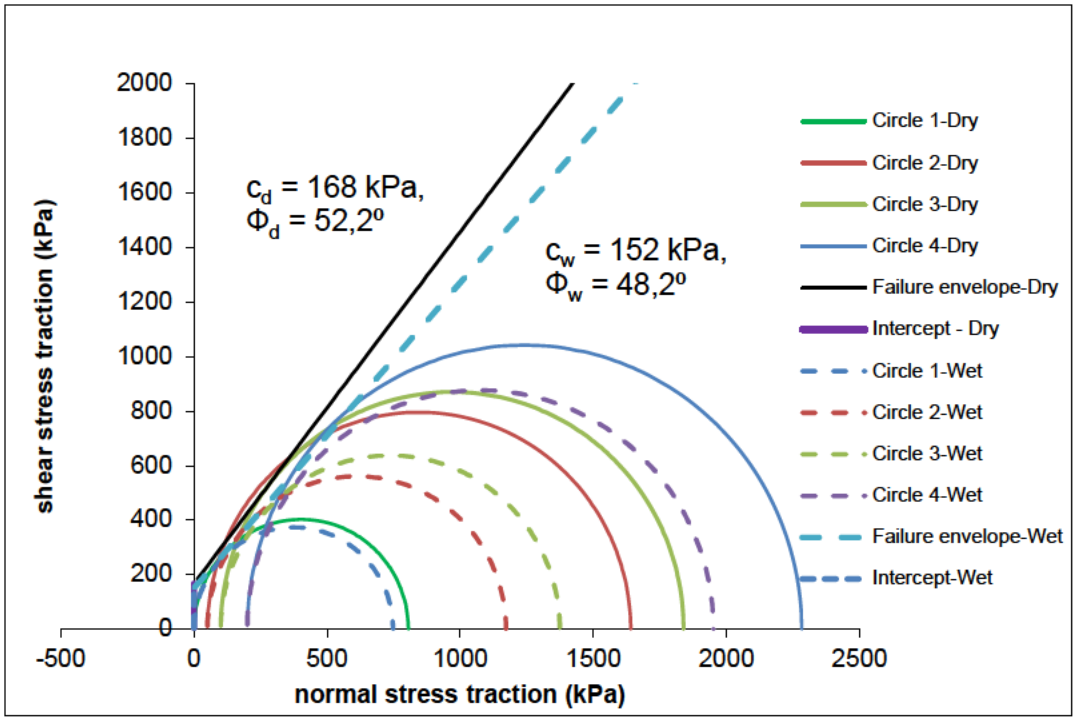

Appendix G 6: Shear Strength Properties – 1.2%NME

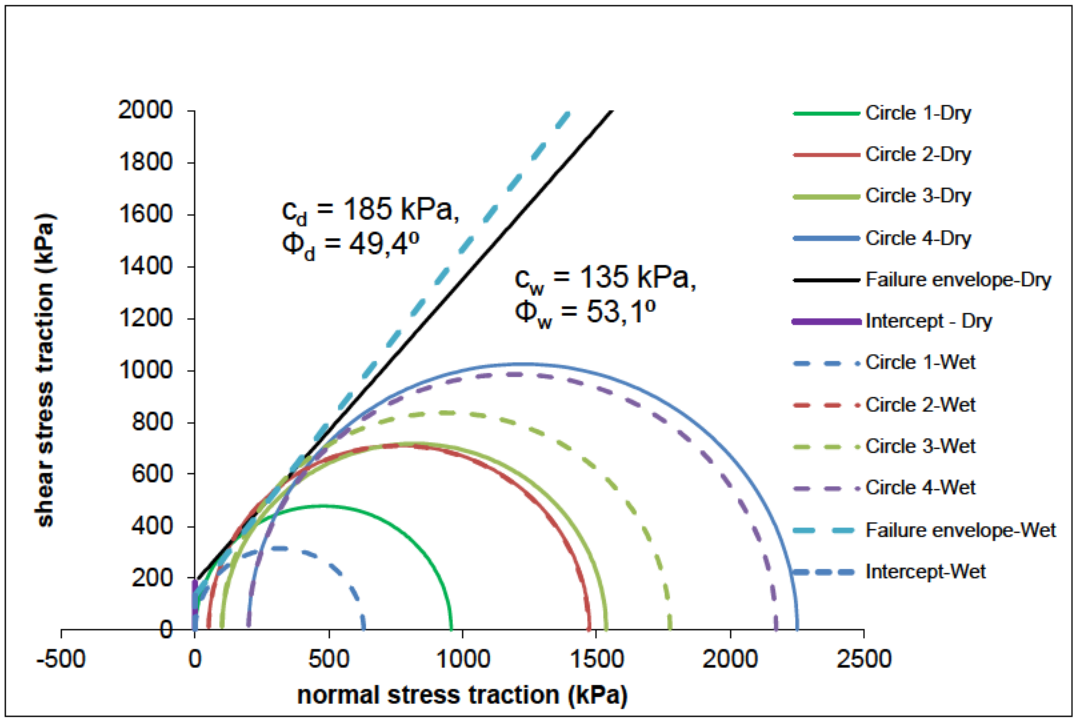

Appendix G 7: Shear Strength Properties – 1.5%NME

Appendix H – M_R Modelling

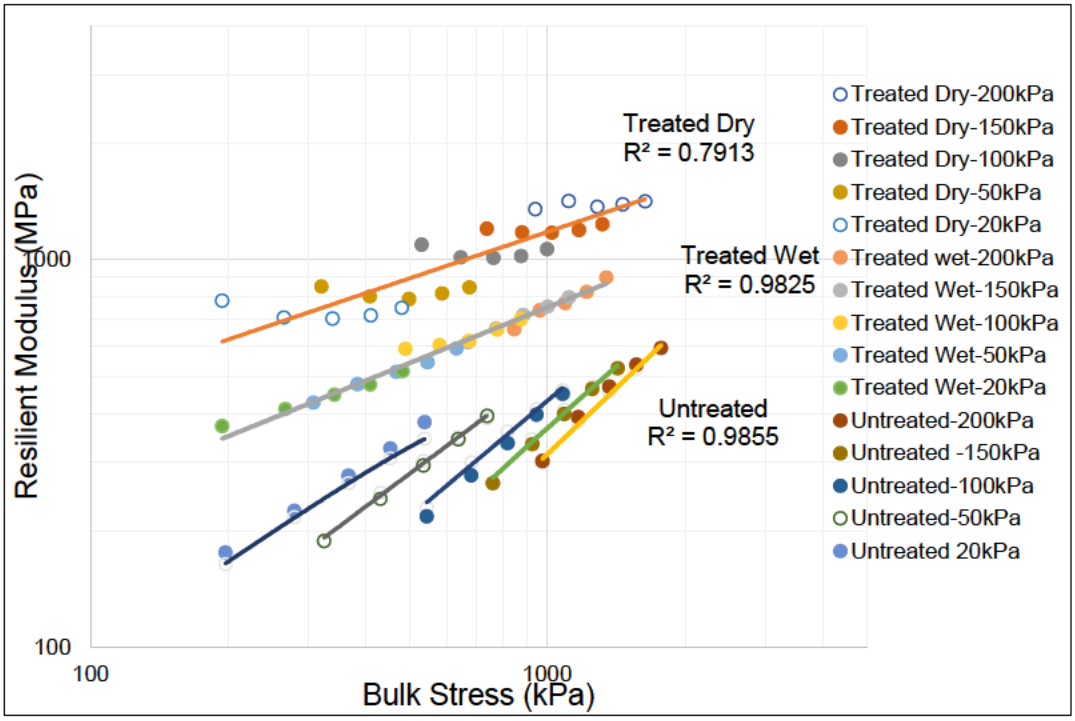

Appendix H 1: Uzan fitted model

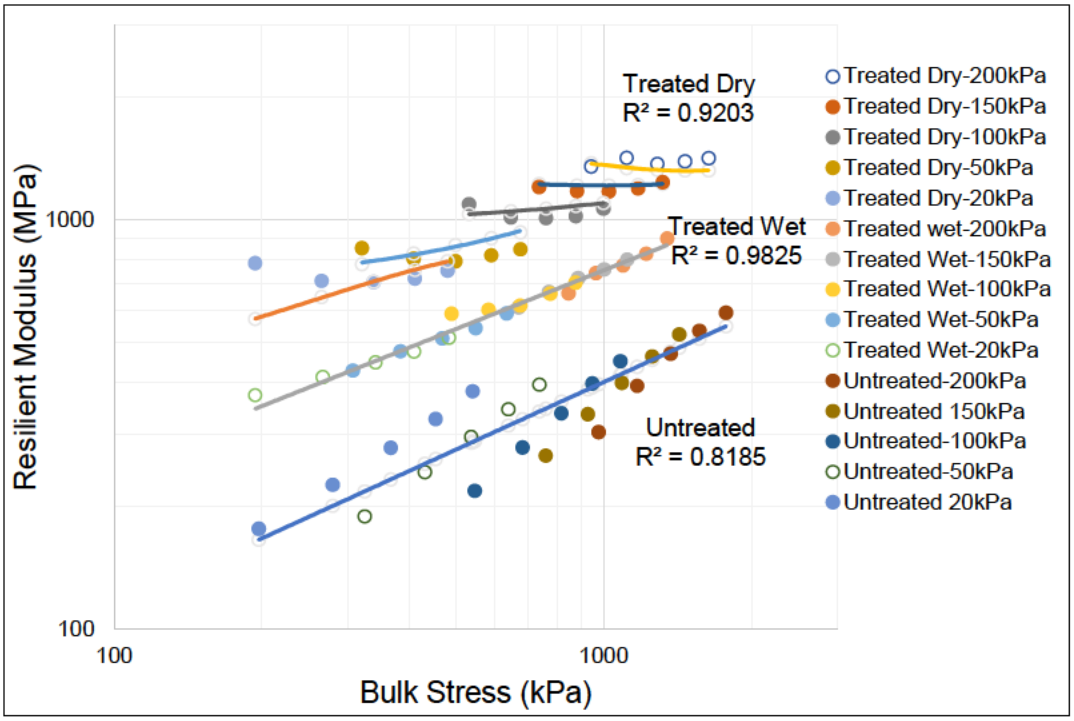

Appendix H 2: Universal fitted model

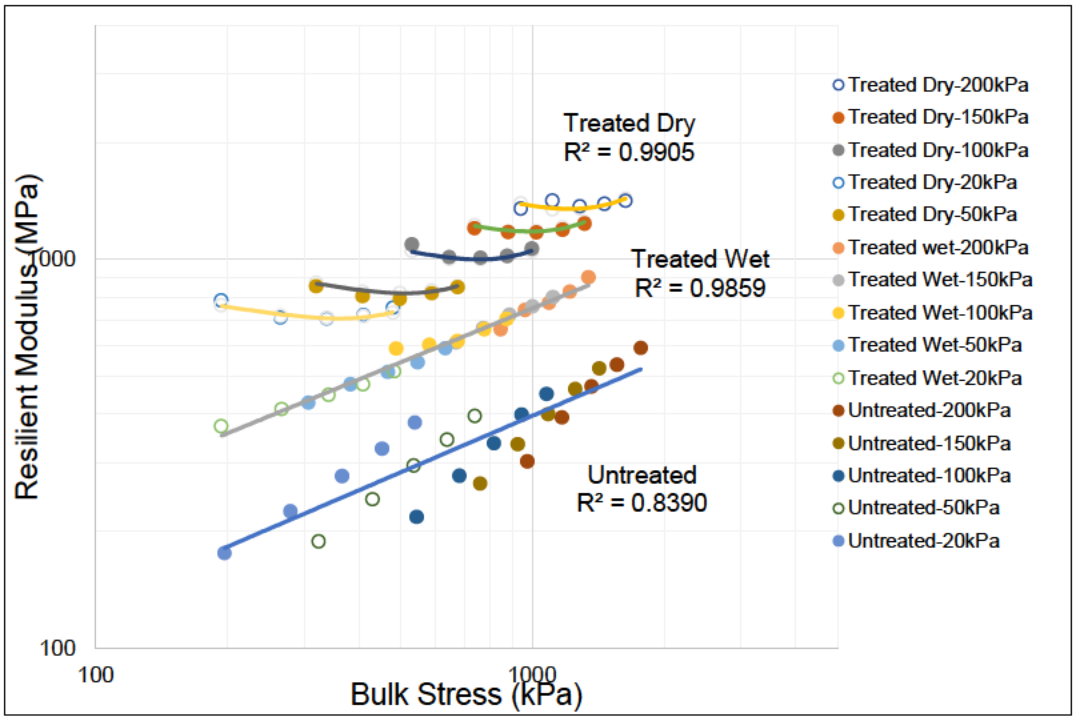

Appendix H 3: Superpave fitted model

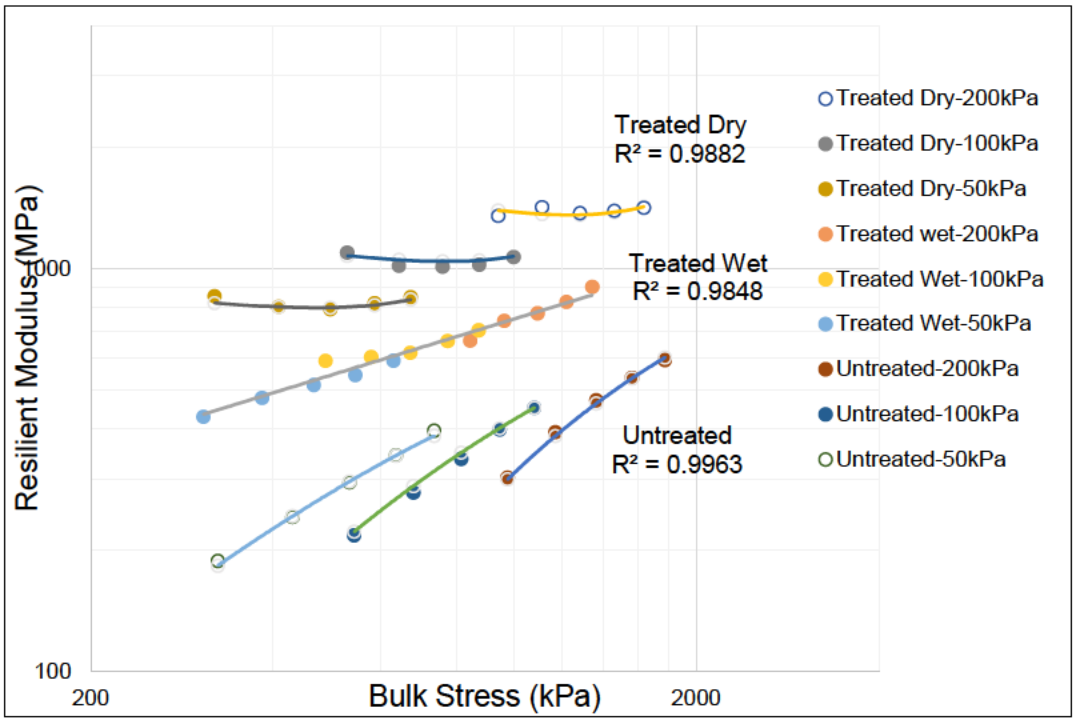

Appendix H 4: Parabolic fitted model

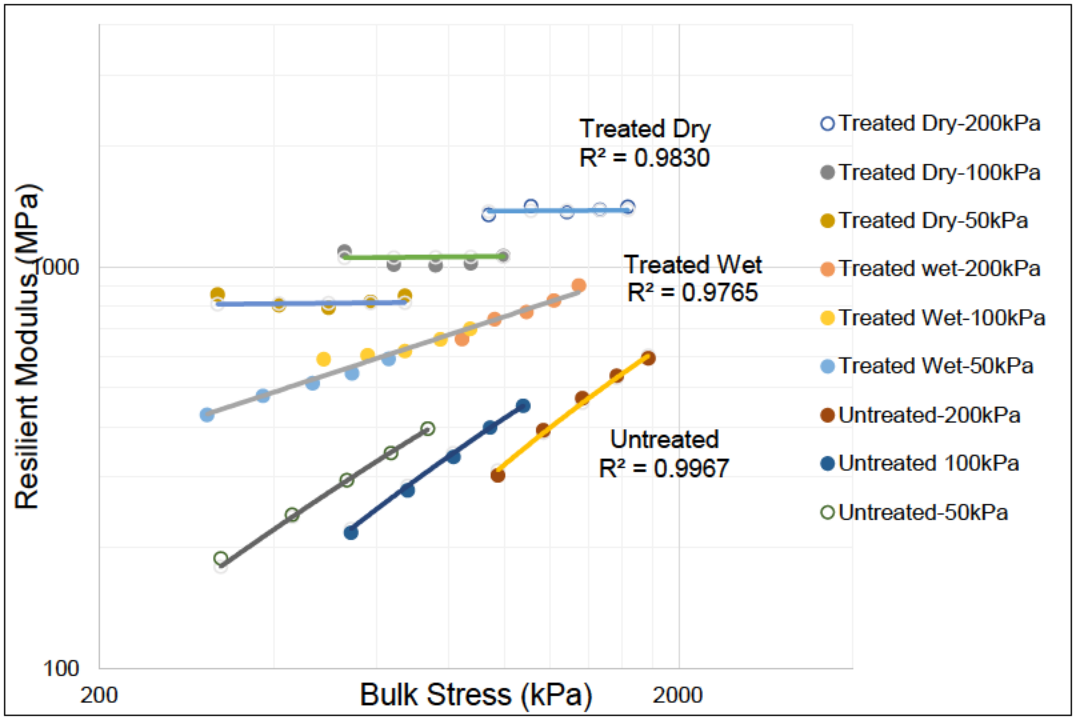

Appendix H 5: TU Delft fitted Model

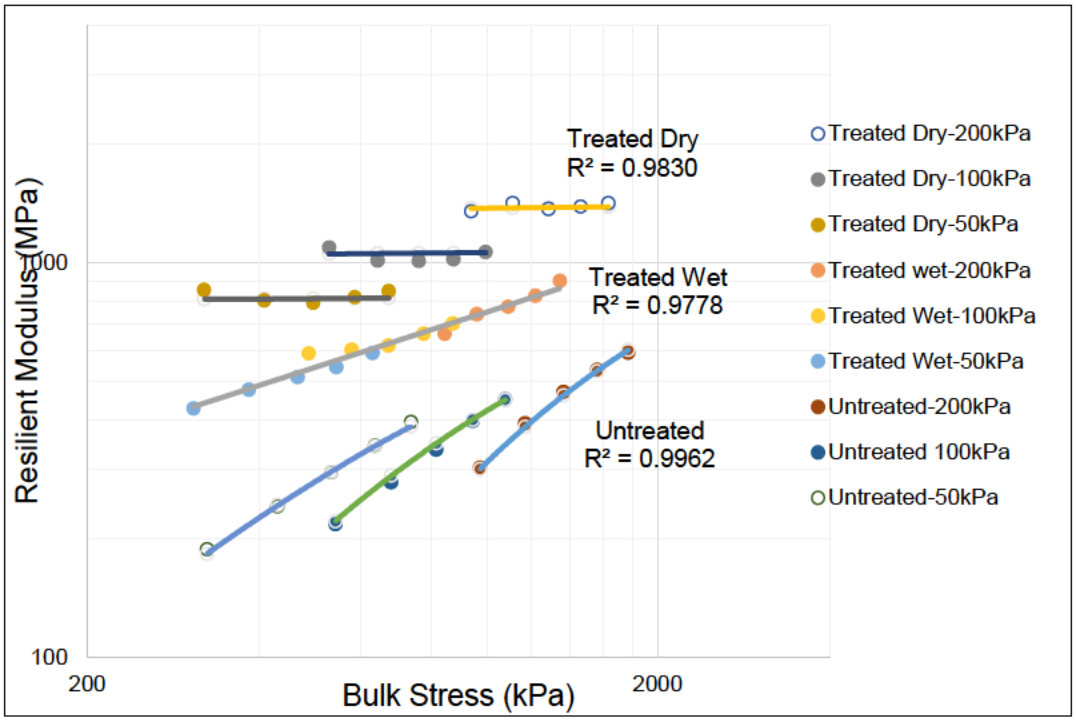

Appendix H 6: M_R-σ_3-σ_d/σ_{df} fitted model

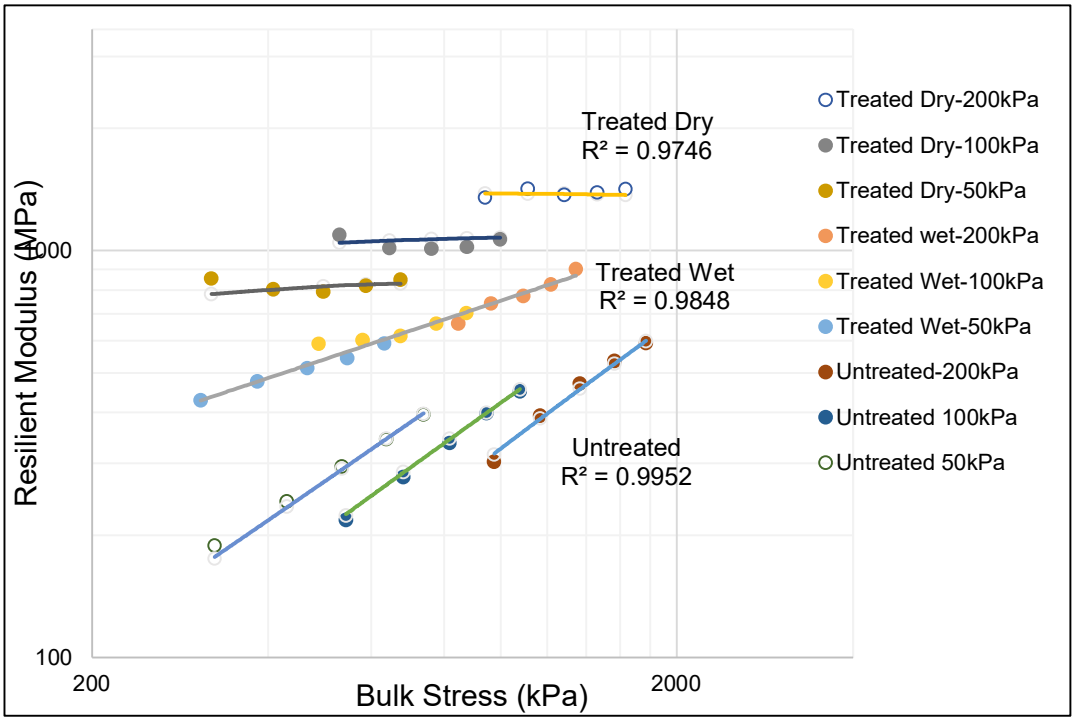

Appendix H 7: MR-θ-σ_1/σ_{1f} fitted model

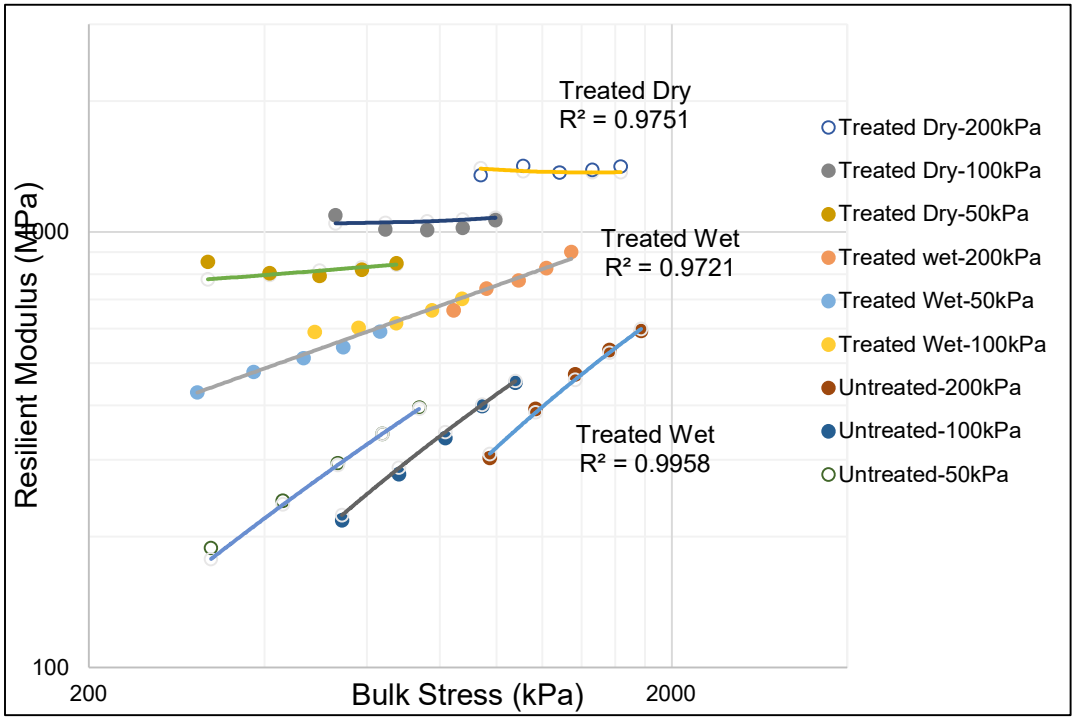

Appendix H 8: MR-θ-σ_d/σ_{df} fitted model

Appendix I – Permeability Results

Falling Head Permeability

THEKWINI SOILS LAB. CC

Date : 30-09-2021

Ref : 9332

Client : Nathan Chilukwa

Project : UKZN

Laboratory Number	Sample Type	Depth	Dry Density Kg/m^3	Permeability k = cm/sec
06012	Natural	-	2093	$6{,}237 \times 10^{-5}$
06012	1% NME	-	2093	$9{,}234 \times 10^{-6}$

Appendix I 1: Perm.